ROBUST NONLINEAR FINITE SHELL ELEMENT ANALYSIS OF CIVIL ENGINEERING STRUCTURES

TANG YIQUN

Ph.D

The Hong Kong Polytechnic University

2018

The Hong Kong Polytechnic University

Department of Civil and Environmental Engineering

ROBUST NONLINEAR FINITE SHELL ELEMENT ANALYSIS OF CIVIL ENGINEERING STRUCTURES

TANG YIQUN

A Thesis Submitted in
Partial fulfilment of the Requirements for
the Degree of Doctor of Philosophy

October 2017

CERTIFICATE OF ORIGINALITY

I hereby declare that this thesis is my own work and that, to the best of my knowledge and belief, it reproduces no material previously published or written, nor material that has been accepted for the award of any other degree or diploma, except where due acknowledgement has been made in the text.

_____(Signed)

TANG YIQUN (Name of student)

To my family

for their love and support

ABSTRACT

Finite shell elements are widely used in prediction of the structural behaviour of civil engineering structures. Over the past decades, many shell elements based on different theories and assumptions have been developed either for general or special shell structures. However, there still exists a need to develop or improve shell elements so that they can capture the critical effects of shell structures with high computational efficiency. For example, accurate and efficient shell elements for civil engineering structures such as walls, floors, roofs of buildings and thin-walled structures are urgently required to consider both the geometric and material nonlinearities. With the recently significant improvement of computer hardware, it is possible to perform nonlinear analysis and design of structures with thousands of degrees of freedom in personal computers even laptops. For building structures, it is vital to develop robust shell elements with good convergence to link to advanced beam-column elements for second-order direct analysis, so that a safer and more economical design can be achieved. Thus, this research project aims to propose high performance flat triangular and quadrilateral shell elements with advanced techniques for nonlinear finite element analysis. The assumption of large displacements, large rotations, but small strains, well accepted in geometrically nonlinear analysis and applicable to most civil engineering structures, is adopted in this study. The main contributions of this research project are summarised in the following.

First, a novel pure deformational method is proposed to simplify the shell element formulations and as a result the associated quantities and the computational cost are significantly reduced. The pure deformational method has been widely utilized in the

derivation of both displacement-based and force-based beam-column elements. However, the application of this technique in shell elements is not popular as beam-column elements due to increasing complexity in shell elements. Thus, narrowing the gap will make a significant contribution to the development and improvement of finite shell elements. It should be pointed out that the proposed pure deformational method has a wide application range since it is independent of the element type which may be derived with different assumptions and theories, once the element shape (triangle or quadrangle) is known. Also, the pure deformational method can contribute to a novel element-independent co-rotational (EICR) formulation, which is a well-accepted formulation for geometrically nonlinear finite element analysis. The EICR formulation is different from the traditional total Lagrangian (TL) and updated Lagrangian (UL) formulations based on the Green-Lagrangian strains.

Further, the thesis proposes a novel EICR formulation for triangular and quadrilateral shell elements based on the proposed pure deformational method. In the EICR formulation, the geometrically nonlinear analysis procedure for flat quadrilateral shell elements is more complicated than the one for flat triangular shell elements, because of the warping phenomenon that the 4 corner nodes of quadrilateral shell element being not coplanar may occur during the analysis process. Thus, unlike flat triangular shell elements, the warping effect should be considered in the derivation of geometrically nonlinear quadrilateral shell elements. In addition, different from the traditional EICR formulation, the proposed EICR formulation is simpler by using pure deformational method and therefore enhances the numerical efficiency of geometrically nonlinear analysis.

Based on the proposed EICR formulations, a nonlinear triangular shell element and a

nonlinear quadrilateral shell element are developed. The elastoplastic behaviour of shells is considered based on the layered approach in which a shell will be divided into several layers through the thickness. The proposed elements allow for the transverse shear effect and the drilling rotations and therefore can be used to analyse various civil engineering structures. The inclusion of drilling rotation allows the shell elements to effectively connected in-plane to beam-column elements. These numerical examples show that the proposed shell elements can analyse thin shell structures without locking problems.

Finally, the proposed nonlinear shell elements based on the simplified EICR method are implemented in the program NIDA. A number of benchmark problems are provided to verify the proposed shell elements. The present results compared well with other elements in commercial software and literature illustrate that the proposed nonlinear shell elements are robust, accurate and efficient.

PUBLICATIONS

Journal Papers

Tang, Y. Q., Zhou, Z. H. & Chan, S. L. (2015). Nonlinear beam-column element under consistent deformation. *International Journal of Structural Stability and Dynamics*, *15*(05), 1450068.

Tang, Y. Q., Zhou, Z. H., & Chan, S. L. (2016). Geometrically nonlinear analysis of shells by quadrilateral flat shell element with drill, shear and warping. *International Journal for Numerical Methods in Engineering*, *108*(10), 1248-1272.

Tang, Y. Q., Zhou, Z. H., & Chan, S. L. (2017). A simplified co-rotational method for quadrilateral shell elements in geometrically nonlinear analysis. *International Journal for Numerical Methods in Engineering* 112(11), 1519-1538.

Tang, Y. Q., Liu, Y. P., & Chan, S. L. (2018). Element-independent pure deformational and co-rotational methods for triangular shell elements in geometrically nonlinear analysis. *International Journal of Structural Stability and Dynamics*, *18*(05).

Tang, Y. Q., Liu, Y. P., & Chan, S. L. (2018). A co-rotational framework for quadrilateral shell elements based on the pure deformational modes. *International Journal of Advanced Steel Construction*, *14*(4).

Tang, Y. Q., Liu, Y. P., & Chan, S. L. A flat triangular shell element for geometrically nonlinear elastoplastic analysis based on a novel simplified element-independent co-rotational formulation. (*To be submitted*)

Conference Papers

Tang, Y. Q., Zhou, Z. H. & Chan, S. L. Nonlinear beam-column element under consistent deformation. *The Eighth International Conference on Advances in Steel Structures,* July 21-24, 2015, Lisbon, Portugal.

Tang, Y. Q., Chan, S. L. A simplified co-rotational approach for triangular shell elements based on the pure deformational mode. *The 11th International Conference "Shell Structures: Theory and Applications".* October 11-13, 2017, Gdansk, Poland.

ACKNOWLEDGEMENTS

First, I would like to express my sincere gratitude to my supervisor, Prof. S. L. Chan, for giving me the opportunity to pursue my Ph.D. study in The Hong Kong Polytechnic University, which is a great challenge and achievement in my life. I deeply appreciate not only for his expert guidance, continuous support and invaluable suggestions, but also for providing me with a versatile platform in which I can obtain practical engineering experience and learn advanced academic knowledge. Towards job and research, Prof. Chan is always practical, precise and devoted, which encourages me to complete my Ph.D. study.

I would also like to express my profound appreciation to Dr. Z. H. Zhou and Dr. Y. P. Liu for their continuous care and encouragement. Their positive attitude and extraordinary experience in research inspired me. I would also like to express my special appreciation to my master degree supervisor, Prof. Z. X. Li. Her encouragement and guidance is important to my Ph.D. study, further career and life.

Getting through my Ph.D. study required more than academic support, I would like to thank all the NIDA team members who accompanied me over these years in Hong Kong. I cannot begin to express my gratitude and appreciation for their friendship.

I would like to thank the Department of the Civil and Environment Engineering, The Hong Kong Polytechnic University for providing the financial support during my Ph.D. study.

Finally, and most importantly, I am deeply grateful to my grandmothers, my parents and my girlfriend for their patience, unconditional love and support all the time.

CONTENTS

LIST OF FIGURES

LIST OF TABLES

CHAPTER 1

INTRODUCTION

1.1 Background

In structural engineering, shells refer to a type of structural elements which are defined by their geometries as three-dimensional solids with small thickness relatively to other dimensions. In addition, its deformations should not be greater than the thickness. The primary difference between a shell structure and a plate structure is that, in the unstressed state, the former has a curvature opposed to the latter which is assumed to be initially flat. The membrane action in a surface is caused by in-plane forces. In a shell structure, these forces may be the primary forces caused by applied edge loads or edge deformation, or the secondary forces resulting from flexural deformations. In a plate, the membrane action due to secondary forces is neglected due to small deflection assumption (Chen, 2005). Thus, a plate can be regarded as a special case of a flat shell.

The in-plane membrane stiffness and the out-of-plane bending stiffness of a shell can resist the transverse loads together, which is different from the case of a plate based on small deflection theory. Thus, shell structures are widely used in various fields of civil, mechanical, architectural, aeronautical, and marine engineering. The common applications in civil and architectural engineering are varieties of concrete shell roofs, liquid retaining structures and water tanks, concrete silos, cooling towers, containment shells of nuclear power plants, concrete arch dams, etc. In mechanical

engineering, shell structures are applied to piping systems, curved panels, pressure vessels, etc. In aeronautical and marine engineering, shell structures can be used for aircrafts, spacecrafts, missiles, ships, submarines, etc (Farshad, 2013). Due to these wide and important applications of shell structures in various engineering, the development of analysis method for shell structures is vital to provide economical design and to ensure the safety either in construction stage or in their whole design life.

The finite element method (FEM) is the preferred numerical procedure for the analysis of shell structures, and therefore many different types of finite shell elements have been developed based on different theories and assumptions. For example, the axisymmetric shell elements can be used in the analysis of axisymmetric shell structures, which are efficient and accurate for shell structures with large curvatures, even using coarse meshes of shell elements. However, this kind of shell elements cannot be used in the unsymmetrical shell structures and, as a result, their application is limited and it is adopted only in special structural forms. Alternatively, the flat shell elements based on plate/shell theory are applicable for general shell structures. Flat shell elements can be used to simulate curved surfaces which are divided into many facets. A flat shell element consists of a membrane part and a plate part, in which the former reflects the membrane or in-plane effects while the latter simulates the bending or out-of-plane effects. Although finer meshes of flat shell elements should be used in the simulation of shell structures with large curvatures, they have simpler formulations and need less modelling efforts. Therefore, they are widely adopted in practical shell structures with different shapes and have been extensively implemented in commercial finite element software. Another practical type of shell

element is the isoparametric elements based on the degenerated three-dimensional stress conditions. Their detailed introduction and pertaining literature reviews are presented in the next section. In addition to the basic classification method based on the different fundamental theories, there exist other classification methods for shell elements according to element shapes (i.e. triangle or quadrangle), number of nodes, displacement interpolations, variational principles, etc.

In history, many research topics on shell elements concerning element performance were carried out, including locking phenomenon, shear deformation, spurious zero energy modes due to the reduced integration, warping effect, drilling rotations, invariance of node ordering, incompatible displacement functions, insensitivity to irregular mesh and so on. They attracted great attention with numerous solutions provided by researchers worldwide. These problems may interact with each other and consequently make shell element formulations more complicated, especially in nonlinear analysis. Because of the problems mentioned above, the development of a shell element is more difficult than the other finite elements such as beam-column and solid elements.

The selection of a shell element from numerous element types in literature to simulate a shell structure may confuse engineers, and worse, a poor or unsuitable shell element may bring unsafe design. Chapelle and Bathe (2010) stated that “with the multitude of different shells encountered, and the peculiarities in their behaviours, it is difficult, but a great intellectual challenge, to develop finite element techniques effective for general shell analysis”. Bucalem and Bathe (1997) also suggested that the development of finite shell elements should satisfy the following requirements: (1) the elements should be reliable, with no spurious zero energy mode, no membrane or

shear locking phenomenon, insensitivity to geometric distortions; (2) the elements should be computationally effective; (3) the element formulation should be general, with being applicable to nonlinear analysis, thin and thick plate/shell situations and any shell geometry; (4) the formulation of the elements should be mechanistically clear and sufficiently simple to render the element suitable for engineering analysis. In addition, as computers become more powerful, performing nonlinear analysis and design of large-scale engineering structures is possible. The use of nonlinear analysis can get real and accurate responses of structures under design loads, which contributes to safe and economical construction and utilization of structures. Thus, the development of robust shell elements with simplicity and a wide range of applications and pertaining nonlinear analysis schemes with efficiency and accuracy are not only challenging but also urgent in civil engineering structures.

1.2 Problem statements

This thesis aims to develop several advanced technologies for shell elements in the linear and nonlinear analysis of shell structures in civil engineering on the basis of the finite element program which is named as nonlinear integrated design and analysis (NIDA, 2015) and coded specially for simple and handy nonlinear analysis of practical and slender structures. The final goal is to improve the accuracy and efficiency of finite element analysis of plate/shell structures. Thus, it is essential to identify the assumptions and theories which are consistent with the features of civil engineering structures. The robust finite shell elements used in NIDA should have the following functions and features according to the common civil engineering

structures.

1. The shell element should be able to cooperate with the beam-column element for the analysis of building structures without any inconsistent issues. The beam-column element can be used to simulate beams and columns, whereas the shell element can be used to model roofs, slabs and walls. The flat shell element derived based on stress resultants and classical plate/shell theory is more suitable than the other types of shell element, since the roofs, slabs and walls of building structures usually are flat, while the curved roofs can be simulated by a large number of flat elements. In addition, as mentioned early, the flat shell element has the membrane and plate parts, and therefore the shear walls are generally modelled by the membrane part while the floor slabs and roofs can be simulated by the plate part.

2. The flat shell element should be able to connect with the beam-column element. Like finite shell element, there are also many beam-column elements developed in literature for different purposes. The NIDA software adopts an advanced nonlinear beam-column element which is a pointwise equilibrating polynomial (PEP) element proposed by Chan and Zhou (1994) for nonlinear analysis of frames. The unique feature is that one PEP element per member modelling is adequate in most cases. To connect with this kind of beam-column element, the proposed shell element should have the rotational degrees of freedom without numerical problems. Besides the bending rotations provided by plate element, the in-plane rotations (drilling degrees) should be considered in the membrane element.

3. In the NIDA software, the PEP element allows for large displacements and large rotations using the element-independent co-rotational (EICR) formulation for geometrically nonlinear analysis but is restricted to moderate strains due to the

consideration of bowing (P-δ) effect in the local coordinate system. For nonlinear analysis and design, the continuous updating of node coordinates by nodal displacements reflects the P-△ effects while the local element deformations containing the P-δ effect, and as a result, the PEP element is able to capture the structural behaviours by one-element-per-member modelling. Technically, the local second-order effect (P-δ effect) can be handled by splitting a member into several beam-column elements. However, this is an ineffective modelling method and will significantly increase the computational cost. In some cases, this method may even bring a numerical divergence problem. The small and moderate strains have an identical assumption that the local element configuration is constant. For example, the beam-column element has the same cross-section and length after deformation, while the shell element has the constant thickness, facet and area after deformation. The difference between these two strains is that the small one adopts the linear strain-displacement relationship (i.e. engineering strains) whereas the moderate one uses the nonlinear relationship (i.e. the Green-Lagrangian strains and the von Kármán strains). The strain field of a shell element is similar to the beam-column element, but a simple shell structure (such as a piece of plate or wall) cannot be accurately simulated by only one shell element, since the boundary conditions are very complicated and the accuracy of displacement interpolations even being high order are inadequate to describe these complicated situations. Compared with the small strain assumption, the moderate strain assumption can improve the accuracy of the shell element and simulate shell structures using coarser meshes. However, for nonlinear analysis of general building structures with flat walls, roofs and slabs, the flat shell element using the assumption of large displacements and small strains is generally adequate and efficient.

4. Both triangular and quadrilateral flat shell elements are effective in the simulation of engineering structures and essential in the finite element software such as NIDA to cater for different shapes of shell structures. In general, two triangular elements can be replaced by a quadrilateral element with saving of computational cost. With the same order interpolation functions, quadrilateral elements have higher accuracy. However, a mesh of triangular shell elements can be generated more easily and used for sharp corners and irregular shell structures.

1.3 Objectives

Through the problems discussed in the last section, the research scope of the shell element can be determined and focussed. The motivation of this research project is to propose high-performance finite shell elements for nonlinear analysis of shell structures with improvements in terms of efficiency and accuracy. The detailed objectives are summarized as follows.

1. Propose an innovative pure deformational method for shell elements. This new method will decrease element quantities and simplify element formulation. The pure deformational method, also called the natural method, is often used for the derivations of the beam-column elements. For example, the two-node beam-column element in a plane has three degrees of freedom (two rotations and one translation) per node, and therefore it produces a 6×6 singular stiffness matrix. However, if it is simplified by the pure deformational method, it only has three degrees of freedom (two rotations and one translation) and gives a 3×3 non-singular matrix with simpler expression. The benefits of the pure deformational method are noticeable. This novel method also can

be regarded as the extension of an efficient technology used in beam-column elements to flat shell elements but results in more complicated derivations.

2. Propose a new element-independent co-rotational (EICR) formulation for shell elements in geometrically nonlinear analyses based on the proposed pure deformational method. Compared with the traditional EICR method, the proposed one can be derived more easily with simpler expressions, since it is derived based on the physical meanings, unlike the traditional one based strictly mathematic derivation.

3. Propose a simplified element-independent co-rotational formulation on the basis of the small strains assumption. With this method, the flat shell elements allowing for drilling rotations and transverse shear deformation are adopted and implemented the geometrically nonlinear analysis of shell structures in the software NIDA.

4. Extend the geometrically nonlinear shell analysis into the geometrically nonlinear elastoplastic analysis and implement it in the software NIDA. The elastoplastic behaviour of the shell elements is modelled by the layered approach, in which shell thickness is divided into several layers, with using the plane stress description for each layer.

5. Verify the accuracy and efficiency of the proposed shell elements in nonlinear analysis through a batch of benchmark examples. The results obtained by the proposed shell elements show good agreement with those from the other commercial finite element software and literature.

1.4 Organization

To achieve these objectives, this thesis is divided into eight chapters and organized in the following.

Chapter 1 presents the background of finite shell elements. The functions and assumptions of shell elements suitable for civil engineering structures and the NIDA software are discussed. The research objectives and the layout of the thesis are introduced as well.

Chapter 2 reviews the development of finite shell elements, key issues and the technologies to improve the performance of shell elements. The geometrically nonlinear algorithms based on the Lagrangian kinematic description and the methods used for elastoplastic analysis are also reviewed in brief in this chapter.

Chapter 3 presents an innovative pure deformational method for shell elements, which is element-independent and suitable for any triangular or quadrilateral shell element. The pure deformational method can decrease quantities of an element and simplify an element formulation. And the derivation processes for triangular and quadrilateral shell elements are detailed respectively, in which the basic coordinate system with fewer element quantities is given.

Chapter 4 proposes a novel element-independent co-rotational formulation, which is simpler and can be derived more easily than the traditional one. The method is consistent to and can be derived based on the presented pure deformational method in Chapter 3. Also, the three-dimensional large rotation formulation used in the computational procedure is briefly introduced. Further, a simplified co-rotational

formulation with element-independence technique is proposed on the basis of the former method and the small strains assumption. The situations for both triangular and quadrilateral shell elements are discussed respectively.

Chapter 5 presents a novel nonlinear triangular shell element named as the SCRT3 element based on the simplified co-rotational formulation. A linear triangular membrane element considering drilling rotations and a plate element allowing for shear deformation are combined into the triangular shell element. The proposed pure deformational method is applied to simplify the formulations of these triangular elements. The method used for elastoplastic analysis is introduced. The computation procedures using the SCRT3 element for geometrically nonlinear analysis and geometrically nonlinear elastoplastic analysis used in the NIDA software are detailed respectively.

Chapter 6 proposes a novel nonlinear quadrilateral shell element named as the SCRQ4 element based on the simplified co-rotational formulation. The local quadrilateral shell element consists of a membrane shell element with drilling rotations derived on the basis a mixed type variational formulation and a plate element considering shear deformation. Different from the simplified co-rotational formulation for quadrilateral shell elements introduced in Chapter 3, this chapter adopts another local coordinate system and gives a new co-rotational formulation for geometrically nonlinear analysis. This local coordinate system makes the SCRQ4 element is invariant to the nodal ordering and insensitive to irregular geometries. Also, the novel co-rotational updated Lagrangian formulation is introduced and compared with the simplified co-rotational formulation, demonstrating the advantages of the latter formulation. Finally, the computation procedures using the SCRQ4 element for

geometrically nonlinear analysis and geometrically nonlinear elastoplastic analysis coded in the program NIDA are detailed respectively.

Chapter 7 analyses several benchmark problems involved with geometrically nonlinear elastic and elastoplastic analysis using the SCRT3 and SCRQ4 elements. The results and convergence rates obtained by the proposed shell elements are given and discussed, against those from the shell elements in the other commercial finite element software and literature to verify the accuracy and efficiency of the proposed shell elements.

Finally, Chapter 8 summarizes the contributions and finding of this study. Suggestions and recommendations based on the proposed methods for future studies are also provided.

CHAPTER 2

LITERATURE REVIEW

The research and recent development of finite shell elements and relevant methods for nonlinear analysis are reviewed in this chapter. A large amount of literature concerning finite shell elements has been published during the past decades, and therefore, to the best of the author's knowledge, only the references widely cited and adopted in commercial finite element software are introduced and discussed here. Specifically, the review covers shell element types based on different theories, common shell element issues and pertaining solving techniques, Lagrangian kinematic descriptions used for finite element analysis of geometrically nonlinear shell structures, effective approaches for consideration of elastoplasticity behaviour.

2.1 Shell element

In this section, the literature on the development and discussion of shell elements are reviewed. Although many shell elements have already been proposed, there are two basic approaches to develop shell elements for analysis of general shell structures and received extensive attentions of researchers during the past decades. The first one is the degenerated solid approach based on three-dimensional stress and strain conditions. The second one is the classical shell/plate theory (Bathe and Ho, 1981; Bathe *et al.*, 1983; Dvorkin and Bathe, 1984). Four kinds of finite shell elements often

used for analysis of general shell structures are derived based on these two basic theories. Specifically, the degenerated solid approach leads to the degenerated shell element and the solid-shell element, in which the former containing the translational and rotational degrees of nodes at mid-surface and the latter has the same nodes and only translations as the solid element. Based on the classical shell theory, the geometrically exact shell model using curvilinear coordinates can be formulated entirely in stress resultants (Simo and Fox, 1989), while the flat shell element combined with a membrane element and a plate element is a special case with a more simpler formulation (Arciniega and Reddy, 2007).

2.1.1 Degenerated shell element

For isoparametric shell elements based on the degenerated three-dimensional stress and strain conditions, the original version was proposed by Ahmad *et al.* (1970) for linear analysis of moderate thick and thin shells, whose displacement interpolations are described by three translations of the mid-surface and two rotations about the local axes at each node. This type of shell elements is still one of the fundamental methods for modern finite element analysis of shell structures (Dvorkin and Toscano, 2013). The original formulation was afterwards extended and applied to nonlinear analysis under the assumption of small strains (Bathe and Bolourchi, 1980; Krakeland, 1978; Ramm, 1977).

Although this element proposed by Ahmad et al. (1970) was a breakthrough in the field of finite shell element and is applicable to any shell geometry with thin and thick thickness, it has the shear locking problem as well as the classical Timoshenko beam

element. The shear locking problem describes that the element becomes too stiff when the thickness tends to zero. This is due to the incompatibility between the displacement and rotation interpolations making the shear deformation incorrect for the thin element (Bathe, 2006; Zienkiewicz and Taylor, 2000). A simple method is the use of the reduced or selective integration schemes. These two techniques can be used to solve many different locking problems for different types of finite elements, while the relevant literature is rich. The early works on the reduced integration method can be found in references (Hughes *et al.*, 1978; Pawsey and Clough, 1971; Zienkiewicz *et al.*, 1971). Although the reduced integration method is simple with saving of computation cost, it may lead to spurious zero energy modes causing the rank deficiency of the global stiffness matrix and the global mechanism. Moreover, a near-mechanism might be activated which leads to unacceptable answers, whereas very low convergence rates could occur in some cases (Bucalem and Bathe, 1997). Aforementioned, the locking phenomenon is due to the incompatibility between the displacement and rotation interpolations, so the reduce integration can fix the locking problem through reducing the order of rotation interpolations. Thus, it decreases element accuracy and induces a problem that more elements are needed to simulate a shell structure.

The mixed interpolation of tensorial components (MITC) approach is deemed to be a valid and successful technique to remove the locking problem, by incorporating the displacement and rotation interpolations in the element (Ahmad et al. 1970). It was originally proposed for a 4-node and an 8-node shell elements (the MITC4 and MTIC8 elements) by Dvorkin and Bathe (Bathe and Dvorkin, 1986; Dvorkin and Bathe, 1984) and then was successfully used to reduce both the shear and membrane

locking problem for triangular and high order finite shell elements including the MITC3, MITC6, MITC7, MITC9 and MITC16 shell elements (Bathe *et al.*, 1989; Bathe *et al.*, 2000a, 2000b; Bathe *et al.*, 2003; Bucalem and Bathe, 1993; Bucalem and Da Nóbrega, 2000; Da Veiga *et al.*, 2007; Kim and Bathe, 2009; Lee and Bathe, 2004). Different from the reduced integration method, the MITC family of shell elements has a strong mathematical foundation that assures the convergence of discretization without causing any spurious zero energy modes, and they are relatively insensitive to geometric distortions.

Recently, based on the MITC3 element, Lee *et al.* (Jeon *et al.*, 2015; Lee *et al.*, 2015; Lee *et al.*, 2014) presented a new effective 3-node triangular shell element which is called MITC3+ element and extended into modal analysis and geometrically nonlinear analysis. Ko *et al.* (2016) proposed a new 4-node quadrilateral shell element, called MITC4+ element, to improve the performance of the MITC4 element.

2.1.2 Solid-shell element

Another class of finite elements for analysis of general shell structures is the solid-shell element, which is also generally derived based on the degenerated three-dimensional stress and strain conditions. However, different from the degenerated shell element introduced in Section 2.1.1, they have the same nodes and freedom configurations of solid elements, with containing only three translational degrees of freedom per node. The early studies on the solid-shell element can be found in References (Hauptmann and Schweizerhof, 1998; Hauptmann *et al.*, 2000; Miehe, 1998; Parisch, 1995).

The solid-shell element can not only account for shell-like behaviour in the thickness direction but also connect to solid elements directly. Also, they do not have rotational degrees of freedom, so they can avoid the complex procedures for updating rotation vectors in geometrically nonlinear analyses. In turn, the lack of rotations is a disadvantage in some practical cases. For example, when moments are required to apply at nodes and solid-shell elements need to connect with beam-column elements with rotational degrees of freedom. For these reasons, solid-shell elements are rarely adopted in structural design software.

Like the aforementioned degenerated shell element, the solid-shell element also has several locking problems causing the numerical results to diverge from the analytical solutions. There have been a number of studies to find their causes and address these locking problems. For example, the Poisson's thickness locking is due to Poisson's ratio coupling of the in-plane and transverse normal stresses (Hauptmann and Schweizerhof, 1998; Parisch, 1995; Schwarze and Reese, 2009). The shear and membrane locking can be solved by the enhanced assumed strain (EAS) method (Alves De Sousa *et al.*, 2003; Andelfinger and Ramm, 1993; Areias *et al.*, 2003; Valente *et al.*, 2004) and assumed natural strain (ANS) method (Cardoso *et al.*, 2008; Hauptmann and Schweizerhof, 1998; Kim *et al.*, 2005; Mostafa *et al.*, 2013; Norachan *et al.*, 2012; Schwarze and Reese, 2009; Sze and Yao, 2000). The trapezoidal locking occurs when the element sides in the thickness direction are not perpendicular to the element mid-surface and can be addressed with ANS method (Betsch and Stein, 1995; Bischoff and Ramm, 1997; Schwarze and Reese, 2009). The volumetric locking occurs when the material is nearly incompressible and can be

solved by the EAS method (Simo and Armero, 1992; Simo *et al.*, 1993; Simo and Rifai, 1990).

Recently, Mostafa (2016) presented an eight-node nonlinear solid-shell element for static problems, in which the ANS and EAS approaches are used to remedy the locking problems while the geometrically nonlinear procedure adopts the co-rotational approach. Flores (2016) developed a hexahedral solid-shell element to the analysis with moderate and large strains based on the total Lagrangian formulation. Cho *et al.* (2017) proposed a geometrically nonlinear quadratic solid-shell element based on the co-rotational formulation.

2.1.3 Flat shell element

The degenerated shell element once dominated shell analysis since it was first proposed by Ahmad et al. (1970). Then, the shell element based on the classical shell theory has been increasingly used in the last decades, excited by a series of publications of Simo *et al.* (Simo, 1993; Simo *et al.*, 1989; Simo *et al.*, 1990a, 1992b; Simo and Fox, 1989; Simo *et al.*, 1990b; Simo and Kennedy, 1992). The kinematic assumptions underlying the variational formulation are essentially the same for both elements, but the reduction to stress resultants is carried out numerically in the former and analytically in the latter (Betsch *et al.*, 1996). A comparison between both element formulations discussed by Buechter and Ramm (1992) reveals that they are very close to each other. The only difference remains in the kind of discretization (Arciniega and Reddy, 2007).

As a special case of the shell element based on the classical shell theory, the flat shell element adopts the facet surface rather than the curved surface, and as a result, the coupling between the membrane and bending effect disappears. In a flat shell element, the stress resultants are directly formulated by superimposing a membrane element and a bending element. This assumption makes its formulation much simpler than the other kinds of shell element. For a flat shell element, the membrane stiffness and the plate bending stiffness can be treated separately when the assumption of small strains is adopted. There is no coupling between these two parts consistently in geometrically nonlinear analyses. A membrane element is derived based on the classical theory of plane stress, while a plate bending element is derived based on the classical plate theories. Generally, the Kirchhoff-Love theory is used to thin plates (Timoshenko and Woinowsky-Krieger, 1959) and the Mindlin-Reissner plate theory which is an extension of the former theory and considers transverse shear deformation through the plate thickness (Mindlin, 1951) is for thick plates. Further, based on the theories of nonlinear strains, such as the Green-Lagrangian strains and the von Kármán strains (degenerated Green-Lagrangian strains), the membrane element and the bending element are coupled, and then the shell element can be regarded as the shallowly curved shell element. For a shallowly curved shell element, it is still derived with direct use of stress resultants and has a simpler formulation than the two types of shell elements. The pertaining literature on these topics is extremely large, and therefore only the representative works are reviewed according to the author's best knowledge.

2.1.3.1 Membrane element

The membrane element can also be called the plane stress element or the 2D solid element. It can be used to simulate the structures which are subjected to in-plane

forces and exhibits no stress normal to the surface, such as shear walls, stiffened sheet construction and membrane action in shells (Kansara, 2004).

The simplest membrane element is the constant strain triangle (CST) element for the plane stress problem, in which each node has two translational degrees of freedom. The displacements of CST are assumed to be linear functions over the element. For quadrilateral membrane elements, the simplest one is the four-node isoparametric quadrilateral element, in which the displacements are bilinear functions over the element. The isoparametric technique is an essential development of the finite element method, which can map the simple geometric shape of the element in the natural coordinate system into the distorted shape in the local Cartesian coordinate system, with making the element can be used for more general shapes. Wilson (1996) believed that the introduction of the isoparametric element formulation proposed by Irons and Zienkiewicz (1969) was the single most significant contribution to the field of finite element analysis and allowed very accurate, higher-order elements of arbitrary shape to be developed and programmed with a minimum of effort.

The simple four-node isoparametric element has the shear locking when the element is subjected to pure bending in its plane. This is because its displacement interpolations cannot accurately describe the deformation under in-plane pure bending. To overcome this problem, Wilson *et al.* (1973) added incompatible displacement modes to the isoparametric element for describing constant curvature modes. However, these modes may cause that the edge of two adjacent elements have different curvatures, and then the displacement fields of two elements along this edge are not incompatible. So, these elements are called incompatible mode elements or

nonconforming elements. Similarly, the classical plate being elements demanding C_1 continuous interpolation functions are also incompatible.

To validate a finite element whether violates compatibility requirements or not, the patch test can be used as a quality indicator. The original works was introduced by Irons *et al.* (Bazeley *et al.*, 1966; Irons, 1971; Irons and Razzaque, 1972), in which a patch of elements with a constant strain was checked whether it reproduced exactly the constitutive behaviour of the material and resulted in correct stresses when it became infinitesimally small. If it did, it could then be argued that the finite element model can get the exact behaviour of the real structure as the size of the elements decreased, even the finite element model was non-conforming (Zienkiewicz *et al.*, 2013). In addition, the patch test also can be used to check the accuracy of the computer program.

As a part of the flat shell element, the membrane element has another problem that the absence of drilling (in-plane rotation) degrees of freedom produces a shell element with five degrees of freedom per node and leaves null values in the stiffness matrix. Thus, the singularity of the assembled global stiffness matrix arises in shell analysis if all shell elements are co-planar. The treatment of drilling rotations in the membrane element is another hot issue and has been received several solutions from researchers. The simplest technique is to add an artificial drilling stiffness which is a very small value in general to the shell element stiffness matrix at the stiffness terms associated with the drilling rotations to remove rank deficiency (Zienkiewicz *et al.*, 1967). The similar methods also can be found in the references (Bathe and Ho, 1981; Knight, 1997; Zienkiewicz, 1971), but the suggested values for the stiffness terms associated drilling degrees of freedom may be different. Crisfield and Moita (1996) pointed out

that, in a non-linear environment, there may be problems with this approach when the artificial stiffness is related to the real stiffness of the adjacent elements, especially with plasticity involved. Yang *et al.* (2000) reported that the artificial drilling stiffness may render the numerical method inconsistent and degrade convergence properties, although the problem of singularity is solved by it. This phenomenon was also confirmed by Battini and Pacoste (2006) that the geometrically nonlinear flat shell element using the artificial drilling stiffness based on an element-independent co-rotational formulation cannot compute the whole equilibrium paths of some problems.

A popular and widely accepted solution for the above problem is the inclusion of drilling degrees of freedom in a membrane element with approximations. The singularity problem mentioned before can be solved by this method. Also, the shell elements formed by this kind of membrane elements can get real drill rotational stiffness and accurate results and connect with the beam-column elements with rotational degrees of freedom in-plane to do some practical engineering analyses. Allman (1984) and Bergan and Felippa (1985) are the pioneers to this method and achieved a level of success not previously attained. Their efforts inspired numerous works on this subject (Allman, 1987, 1988a; Carpenter *et al.*, 1985; Cook, 1986, 1987; Macneal, 1987a, 1987b; Macneal and Harder, 1988; Taylor and Simo, 1985; Taylor, 1987). However, these early works concentrated solely on the choice of the finite element interpolation fields in which the drilling rotation is taken as an independent degree of freedom with still based on the conventional displacement-based variational principle of minimum potential energy. To pursue this subject mathematically and improve the performance of the membrane elements with drilling degrees of freedom,

Hughes and Brezzi (1989) proposed an approach based on a mixed variational formulation employing an independent rotation field which was firstly introduced by Reissner (1965) where the skew-symmetric part of the stress tensor was used as a Lagrange multiplier to enforce the equality of independent rotations with the skew-symmetric part of the displacement gradient. Ibrahimbegovic *et al.* (1990) successfully combined the mixed variational formulation by Hughes and Brezzi (1989) and an Allman-type interpolation for the displacement field with an independently interpolated rotation field and therefore proposed a robust quadrilateral membrane element with drilling rotations. The related studies and applications extending the membrane elements with drilling degrees of freedom into nonlinear and dynamic analyses were described in the references (Hughes *et al.*, 1995a; Hughes *et al.*, 1995b; Ibrahimbegović, 1994; Ibrahimbegović and Frey, 1994a, 1994c; Simo *et al.*, 1992a).

A series of 3-node, 9-DOF triangular membrane elements with drilling rotations were proposed by Felippa *et al.* (Alvin *et al.*, 1992; Felippa, 2003; Felippa and Alexander, 1992; Felippa and Militello, 1992) on a unified basis, including the free formulation (FF), the extended free formulation (EFF) and the assumed natural deviatoric strain (ANDES) formulation. In the derivations, the element response was separated into the basic and higher orders, with the former taking care of consistency and the latter considering stability (rank sufficiency) and accuracy. Based on ANDES formulation, the ANDES template for triangular membrane elements, carrying along a set of free numerical parameters, was proposed by Felippa (2003), in which the Optimal ANDES template (OPT membrane element) was proved to perform well in a constant-moment in-plane bending test with high aspect ratio. Also, the ANDES formulation has been used to develop plate bending and shell elements (Militello and Felippa, 1991), while

the OPT membrane element was commonly used to construct flat triangular shell elements and extended to the geometrically nonlinear analysis of shell structures (Battini and Pacoste, 2006; Khosravi *et al.*, 2007).

Besides, a very special approach for drilling rotation problem was proposed by using a single rotation about an element side. This method was originally applied in a linear context by Herrmann (1967) and in relation to a displacement formulation by Morley (1971). Then, these elements were extended to nonlinear shell analysis by many researchers (Baecklund, 1973; Kolahi and Crisfield, 2001; Chen, 1979; Peng and Crisfield, 1992; Providas and Kattis, 1999; Van Keulen *et al.*, 1993). However, they cannot be easily matched with other types of elements in the modelling of complex structures.

Recently, Madeo *et al.* (2014) proposed a new simple and efficient four-node quadrilateral membrane element with drilling rotations based on the strain approach. Zouari *et al.* (2016) presented two four-node quadrilateral membrane elements with drilling rotations based on a plane adaptation of the space fibre rotation concept.

2.1.3.2 Plate bending element

As the other part of the flat shell element, the plate bending element represents the bending behaviour of the shell element and has two out-of-plane rotations and one transverse displacement per node. The development of plate bending elements can be tracked back to the 1960s (Melosh, 1961) and has received an enormous amount of effort from researchers. A large number of plate bending elements using various interpolations, theories and variational principles have been developed in the past a half century. The development and history of plate bending elements were reviewed

by many researchers at different times, such as Batoz *et al.* (1980a), Hrabok and Hrudey (1984) and Cen and Shang (2015). The literature on this topic is extensive and therefore only some popular displacement-based formulations are introduced in this section. Most plate bending elements are generally formulated by two theoretical bases: the Kirchhoff-Love plate theory neglecting transverse shear deformation for thin plates and the Mindlin-Reissner plate theory considering transverse shear deformation for thick plates. In analogy to beams, the Kirchhoff plate theory can be regarded as an extension of the Euler-Bernoulli beam theory, while the Mindlin-Reissner plate theory corresponds to the Timoshenko beam theory. For this reason, some plate elements were derived and extended on the basis of beam elements.

The early plate elements were presented based on the Kirchhoff-Love thin plate theory in which the straight lines are normal to the mid-surface remain straight and normal to the mid-surface after deformation, with neglecting the effects due to transverse shear deformation. Traditional displacement-based plate bending elements generally assume the transversal displacements as polynomial functions over the element. And the bending rotation interpolations are the partial derivatives of the displacement interpolations, which is called the C_1 continuity requirement on the interpolation functions and may lead to incompatible elements. Based on the displacement-type formulations, one of the most common approaches for deriving thin plate elements is the discrete Kirchhoff technique proposed by Baton *et al.* (Batoz, 1982; Batoz et al., 1980a; Batoz and Tahar, 1982). Different from the other displacement-based methods, it initially assumes a cubic variation of the transversal displacement along the sides and quadratic variations of the bending rotations over

the element, including nodal values at the corners and mid-nodes. Thus, when the formulation is applied to a one-dimensional beam element, the exact stiffness matrix of an Euler-Bernoulli beam element with a cubic polynomial displacement can be obtained. Through Kirchhoff hypothesis and simple geometric relationships, the bending rotations can be expressed with only the nodal values at the corners and used to derive the stiffness matrix of the plate bending element. In this derivation, there is no need to define an interpolation function for the displacement of the element, except for the assumption of a cubic variation of the transversal displacement along the sides. The plate bending elements constructed through this technique have been proved to provide high accuracy and good convergence rate for plate bending problems, such as the discrete Kirchhoff triangular (DKT) element with 3 nodes and 9 degrees of freedom (Batoz, 1982; Batoz et al., 1980a) and the discrete Kirchhoff quadrilateral (DKQ) element with 4 nodes and 12 degrees of freedom (Batoz and Tahar, 1982). They are also widely used to construct flat shell elements and implemented in commercial finite element software due to simplicity and reliability.

On the other hand, the Mindlin-Reissner plate theory for thick plates assumes that the normal to the mid-surface remains straight, but not perpendicular to the mid-surface due to transverse shear deformation. Many plate elements based on this theory have been developed like the Kirchhoff plate elements. A simple displacement-based method adopts independent interpolation functions for transversal displacement and rotations over the element, and only C_0 continuity is required. However, the lower order elements using this method without special treatments have the shear locking phenomenon for thin plates, and the mechanism has been introduced in Section 2.1.1. In analogous to the degenerated shell elements, the Mindlin-Reissner plate elements

can also overcome this difficulty using the reduced integration (Pugh *et al.*, 1978; Zienkiewicz *et al.*, 1971) and the selected reduced integration (Hughes et al., 1978; Malkus and Hughes, 1978). Although these two methods eliminate or alleviate the shear locking problem and save computational cost, they cannot always ensure the absence of shear locking. Most importantly, they may lead to rank insufficiency of element stiffness matrices and the spurious zero energy modes under some situations. In order to keep rank sufficiency of element stiffness matrices on the basis of the reduced integration, Belytschko *et al.* (Belytschko *et al.*, 1984; Belytschko *et al.*, 1981; Belytschko and Tsay, 1983) proposed the stabilization method where a stabilizing stiffness matrix is superimposed to the element stiffness matrix obtained using the reduced integration.

An alternative approach to remedy the shear locking problem is the assumed natural strain (ANS) method firstly proposed by Hughes and Tezduyar (1981) for the four-node bilinear isoparametric element based on the Mindlin-Reissner plate theory. The ANS method assumes the shear strains independent of the displacement interpolations, and the shear strains are determined by the strain-displacement relationship at certain discrete points of the element. Thus, the accuracy of the ANS method highly depends on the selection of discrete points. The successful Mindlin-Reissner plate elements using this method can be found in the references (Sze and Zhu, 1998; Sze *et al.*, 1997; Tessler and Hughes, 1983, 1985). A well-known variation of the ANS method is the mixed interpolated tensorial components (MITC) method proposed by Bathe *et al.* (Bathe and Dvorkin, 1985; Brezzi et al., 1989) for the Mindlin-Reissner plate elements, in which the covariant tensor shear strain components were defined and independent of the displacement interpolations. The

MITC method was also applied to the degenerated shell elements (Bathe and Dvorkin, 1986; Dvorkin and Bathe, 1984) as introduced in Section 2.1.1.

Following the discrete Kirchhoff technique by Batoz et al. (1980a) for thin plates, many researchers adopted similar derivation procedures and extended this method to thick plates based on the Mindlin-Reissner plate theory. For example, Chen and Cheung (2000, 2001) used the exact displacement function of the Timoshenko's beam to derive the displacement interpolations of plate elements, and the re-constituting shear-strain technique was used to derive a 3-node triangular and a 4-node quadrilateral Mindlin-Reissner plate element, respectively named RDKTM and RDKQM. The similar works also can be found in the references (Aalto, 1988; Batoz and Lardeur, 1989; Batoz and Katili, 1992; Cai *et al.*, 2011; Ibrahimbegović, 1993; Katili, 1993a, 1993b). These plate elements can converge towards the discrete Kirchhoff plate bending elements when the plate thickness is very thin.

2.2 Geometrically nonlinear shell element

In contrast to the geometrically linear analysis assuming infinitesimally small displacements and strains, the geometrically nonlinear analysis is based on the assumption of large deflections in which the element maintains equilibrium after deformation. In continuum mechanics, there are two basic kinematic descriptions to determine how the body moves. One is the Lagrangian kinematic description where all physical quantities are expressed with initial coordinates, and the other one is the Eulerian kinematic description which uses current coordinates. For solid and structural mechanics problems, both descriptions can be used. However, the

Lagrangian description is more suitable and widely used in commercial finite element software. On the other hand, the Eulerian description is commonly used in fluid mechanics problems. In terms of the strain measures, except for the engineering strain which is a linear strain measure, the other nonlinear strain measures for nonlinear structural and solid mechanics problems are the Green strain, Almansi strain and logarithmic strain. The Green strains are referred to the initial coordinates and used with the Lagrangian kinematic description, while the Almansi strains are referred to the current coordinates and used with the Eulerian kinematic description. Thus, several different geometrically nonlinear analysis schemes can be developed based on the different descriptions and measures.

Generally, there are two types of geometrically nonlinear analyses: (1) large displacements, large rotations, but small strains; (2) large displacements, large rotations, and large strains. The difference between these two types of analyses is whether the strains are assumed to be large or small. In the former type, displacements and rotations of fibres are large, but fibre extensions and angle changes between fibres are small, while large strains mean that fibre extensions and angle changes between fibres are large (Bathe, 2016). The latter analysis type is more general and can be applied to problems of small strains, but the former type is computationally more effective and may also provide more insight into the response prediction. The assumption of large displacements, large rotations, but small strains is suitable for the design and analysis of most civil engineering structures. Thus, this section only reviews the geometrically nonlinear analysis formulations based on the small strains assumption.

The common formulations in present used in the geometrically nonlinear analysis of structural and solid mechanics problems with small strains are the total Lagrangian (TL) and updated Lagrangian (UL) formulations based on the Green strains and the co-rotational (CR) formulation. The published literature on geometrically nonlinear shell elements based on these formulations is reviewed in the following.

2.2.1 Total and Updated Lagrangian formulations

The total and updated Lagrangian formulations use the Green-Lagrangian strains and the 2nd Piola Kirchhoff stresses. Both formulations are based on the same process, except that the only theoretical difference is the choice of reference configurations. The total Lagrangian (TL) formulation is referred to the initial configuration, while the updated Lagrangian (UL) formulation is referred to the last calculated configuration. Indeed, identical results can be obtained if appropriate constitutive tensors are adopted in the numerical solution. The choice of using either the TL or the UL formulation in a finite element solution depends on their relative numerical effectiveness. In general, the strain displacement matrix is more complicated in the TL formulation than in the UL formulation, since the initial strain effect is contained in the TL formulation.

Early geometrically nonlinear shell elements using the TL and UL formulations were proposed by Bathe *et al.* (Bathe and Bolourchi, 1980; Bathe et al., 1983; Dvorkin and Bathe, 1984) based on the degenerated shell approach where the shell element is formulated by three-dimensional stress and strain conditions. However, Surana (1983) pointed out that these formulations are restricted to small rotations between two load

increments since the element displacement field is linearized with respect to nodal rotations. Thus, Surana (1983) adopted general nonlinear functions of nodal rotations in the element displacement field and enabled the element to allow for large load steps and permit large rotations between successive load increments with good convergence based on the previous works. But the nonlinear functions of nodal rotations have three cases according to the sequence of rotations, and therefore the element must determine the rotation sequence, which brings inconvenience to practical applications. Thus, developing an effective and accurate formulation of large rotations in three-dimensional space for geometrically nonlinear finite element analysis was an imperative task.

There are numerous formulations to deal with large rotations in geometrically nonlinear finite element analysis and need not to determine the rotation sequence, such as the references (Ibrahimbegovic, 1997; Ibrahimbegović *et al.*, 1995). The most popular one was proposed by Argyris (1982), in which any spatial rotation vector in a Cartesian system can be assumed as a rotation about an axis and expressed as a rotation matrix. The formulation of finite rotations is computationally convenient and has been widely used in geometrically nonlinear analysis schemes for beam and shell elements containing rotational degrees of freedom. For example, using the rotation formulation, Dvorkin et *al.* (1995) developed a finite strain elastoplastic formulation based on the MITC4 shell element; recently, Jeon et al. (2015) presented the MITC3+ finite shell element for geometrically nonlinear analysis; Ko *et al.* (2017) presented geometrically nonlinear formulation of the MITC4+ shell element. At present, the TL and UL formulations combined with the vector-like parameterization of finite rotations have become basic geometrically nonlinear analysis schemes and

extensively used by researchers to develop novel geometrically nonlinear shell elements, reviewed by Bathe (2016).

The TL and UL formulations are also widely used in the shell elements based on the classical shell theory since the works by Simo and Fox (1989). For example, Ibrahimbegović *et al.* (Ibrahimbegović, 1994; Ibrahimbegović and Frey, 1994a, 1994b) presented a consistent theoretical framework for a novel stress resultant geometrically nonlinear shell theory considering the drilling rotations around the shell normal; Arciniega *et al.* (Arciniega and Roman, 2006; Arciniega and Reddy, 2007) proposed a tensor-based shell element formulation to describe the mathematical model of a shell in a natural and simple way by using curvilinear coordinates. Gruttmann and Wagner (2006) developed a shell element for geometrically nonlinear analysis of thin composite structures based on a Hu-Washizu variational function with independent displacements, stress resultants and shell strains.

The co-rotational procedure can be incorporated into the TL and UL formulations, in which the total deformations of an element are divided into rigid body motions and pure deformations. When the rigid body motion part is removed from the total deformations, the deformational part is always small relative to the local element system which is attached to the element. In the general TL and UL formulations, the displacement interpolations and the variational functions using the TL or UL descriptions are directly formulated in the global coordinate system. However, in the co-rotational procedure, the formulations are established in the local element system firstly and then transformed into the global coordinate system. Thus, the co-rotational TL and UL formulations are simpler than the general formulations, while the tangent stiffness and the internal force in these formulations are not exactly consistent, which

may lead to numerical problems in some cases. An early co-rotational UL formulation is proposed by Hsiao (1987) based the geometrically nonlinear flat triangular shell element proposed by Bathe and Ho (1981) which is restricted to small rotations between two load steps. Hsiao (1987) used the co-rotational procedure to eliminate the rigid body motions and get the element internal nodal forces, therefore removing the restriction. The other applications of the co-rotational TL or UL formulations can be found in the references (Alves De Sousa *et al.*, 2006; Hsiao and Hung, 1989; Hsiao, 1987; Jiang *et al.*, 1994; Kebari and Cassell, 1992; Khosravi et al., 2007, 2008; Kim *et al.*, 2007; Kim and Lomboy, 2006; Kim *et al.*, 2003; Masud *et al.*, 2000; Norachan et al., 2012). In addition, it should be noted that the co-rotational TL and UL formulations are different from the element-independent co-rotational formulation which is introduced and discussed in the following section.

2.2.2 Element-independent co-rotational formulation

In addition to the total Lagrangian (TL) and updated Lagrangian (UL) formulations based on the Green-Lagrangian strains for geometrically nonlinear analysis, another well-accepted method is the element-independent co-rotational (EICR) formulation which is the latest one and attracted extensive discussion recently. The basic idea of the co-rotational method is that the total motions of an element can be divided into rigid body movements and deformational motions. For the decomposition, a local frame is attached to the element and consistently co-rotating with the element. Then, the translations and rotations of the local frame can be regarded as the rigid body movements, while the motions of the element producing in the local frame can be

taken as the deformational motions. In the following, some respective works involved with this formulation are reviewed.

The co-rotational procedure was firstly introduced by Wempner (1969), and then by Belyschko and his co-workers (Belytschko and Hsieh, 1973; Belytschko *et al.*, 1977). As far as the development of the co-rotational approach, there are many different versions proposed for different kinds of finite elements, such as treatment of large rotations, simplification of procedure, derivation of geometric stiffness, selection of the local coordinate system, consideration of large strains etc. The co-rotational TL and UL formulations mentioned before also belong to this procedure.

For geometrically nonlinear analysis with large displacements, large rotations but small strains, a family of co-rotational procedure called element-independent co-rotational (EICR) algorithm was first proposed and named by Rankin and Brogan (1986). Through this procedure, existing linear finite elements can be upgraded to geometrically nonlinear analysis allowing for arbitrarily large rotations. Basically, the property of the element-independence comes from that the geometric stiffness formulated by the nodal internal forces rather than the stresses at integration points in the TL and UL formulations. Thus, the geometric stiffness matrix in the EICR algorithm is explicit and there is no need to conduct the numerical integration, which makes the geometric stiffness matrix is independent of the local element formulation and any geometrically linear element can be upgraded to realize geometrically nonlinear analysis with the EICR algorithm. Generally, due to the omission of the numerical integration of the geometric stiffness, the EICR formulation is more efficient than the TL and UL formulations.

After Rankin and Brogan (1986) presented the EICR algorithm as a general framework, Nour-Omid and Rankin (1991) and Rankin and Nour-Omid (1988) improved this algorithm and pointed out that the EICR formulation presented in the previous work (Rankin and Brogan, 1986) cannot keep equilibrium of the element internal force vector, so the projector operator was proposed to improve the finite element performance. In addition, due to the non-additivity of large rotations in three-dimensional space, a pertaining transformation matrix was also presented. Detailed introduction of the EICR approach is also presented by Felippa and Haugen (2005) in a great review article where the authors discussed several related techniques used in the EICR algorithm, such as mathematics of finite rotations, fitting methods to satisfy invariance to nodal ordering, etc. Following this standard EICR formulation, the pertaining studies for shell elements in geometrically nonlinear analysis also can be found in the publications (Almeida and Awruch, 2011; Areias *et al.*, 2011; Battini, 2007, 2008; Battini and Pacoste, 2006; Battini and Pacoste, 2004; Dal Cortivo *et al.*, 2009; Eriksson and Pacoste, 2002; Pacoste, 1998; Pajot and Maute, 2006; Skallerud and Haugen, 1999).

A similar co-rotational procedure used with a flat triangular shell element was proposed by Levy and co-workers (Gal and Levy, 2005; Gal and Levy, 2006; Levy and Gal, 2001, 2003, 2006; Levy and Spillers, 2013), whose derivation of the geometric stiffness matrix is somewhat different but consistent with the EICR algorithm. The formulation in these papers is based on the load perturbation of the linear equilibrium equations for a flat triangular shell element in the local coordinate system. The flat shell element consists of the constant stress triangular (CST) membrane element described by Zienkiewicz *et al.* (1977) and the discrete Kirchhoff

flat triangular (DKT) plate element proposed by Batoz et al. (1980a). In the derivation, the local geometric stiffness matrix of the flat triangular shell element is derived as the gradient of the nodal force vector and divided into three parts: the in-plane geometric stiffness matrix of a membrane element, the in-plane geometric stiffness matrix of a plate element and the out-of-plane geometric stiffness matrix of a shell element. Specifically, the first two parts represent the changes of the element dimensions respectively, whereas the out-of-plane geometric stiffness matrix of the shell element is due to the rigid body rotations of the element. The drawback of this formulation compared with the standard EICR formulation introduced in the last paragraph is that the first two parts of the geometric stiffness matrices are not element-independent since they are related to the formulations of the membrane and the plate elements. However, the formulation provides another thought to derive the geometric stiffness, with taking the gradients of the nodal internal forces in the local coordinate system directly. So, it is easier to visualize through physical interpretation than the standard formulation.

Crisfield and Moita (1996) presented a unified co-rotational framework for solids, shells and beams, which has strong links with the work by Nour-Omid and Rankin (1991) and inherits the properties of element-independence. It is a simplified formulation since some terms are omitted in the derivation of the internal forces and the tangent stiffness. In addition, Crisfield *et al.* (1995) pointed out that the co-rotational technique cannot be restricted in the local element with small strains, while it can be extended to the analysis of large strains, in which the Biot-stress formulation describing large strains was used in the local element. Similar to the simplified co-rotational framework, Izzuddin (2005) defined a new local co-rotational

system and used vectorial rotations for quadrilateral shell elements, not only the invariance to nodal ordering but also a symmetric tangent stiffness matrix can be achieved. Following this thought, some studies for geometrically nonlinear analysis of shell structures were presented in the references (Izzuddin and Liang, 2016; Li *et al.*, 2008; Li *et al.*, 2011a; Li and Vu-Quoc, 2007; Li *et al.*, 2015; Li *et al.*, 2013; Li *et al.*, 2011b; Li and Vu-Quoc, 2007; Li *et al.*, 2013; Liang and Izzuddin, 2015, 2016).

An alternative approach for geometrically nonlinear shell elements was proposed by Argyris *et al.* (Argyris *et al.*, 2003; Argyris *et al.*, 2002a; Argyris *et al.*, 1997; Argyris *et al.*, 1998; Argyris *et al.*, 2000b; Argyris *et al.*, 2002b). The methodology is based on the physical inspirations of the natural-mode finite element method (NM-FEM) which shares the same concept with the co-rotational method that the total motions of an element can be divided into rigid body movements and natural motions. Also, in this method, the geometric stiffness is nearly generated by the rigid body motions of the element, so the geometric stiffness includes only natural forces which produce rigid body moments. This characteristic is close to the EICR formulation rather than the TL and UL formulations. Thus, the method can be regarded as an alternative simplified EICR method.

2.3 Elastoplastic analysis for shell structures

2.3.1 Basic concepts of elastoplasticity

Material nonlinearity where the stress-strain relationship is nonlinear is essential to the nonlinear analysis of practical shell structures because it significantly influences

ultimate loads and buckling behaviours of structures. Elastoplasticity belongs to material nonlinearity, in which material follows a linear stress-strain relationship for low-stress levels and has a decrease in stiffness as the stress increases when exceeding yield strength. Also, unloading of the elastoplastic material initiates a new branch on the stress-strain curve where the material is again elastic until exceeding yield strength, often with a stiffness equal to the initial elastic stiffness.

In addition to these basic characteristics, the mathematical theory of elastoplastic models has some the fundamental concepts: the yield criterion determining when the material becomes plastic, the flow rule describing the relationship between stresses and strains once the material has become plastic, and the hardening rule establishing conditions for subsequent yielding from the previous plastic straining history (Krabbenhøft, 2002; Marques, 1984).

The yield function depends on stresses and plastic strains and may be related to the past material history via the hardening parameter. There are four common yield criteria used in the current elastoplastic analysis, including Tresca (Tresca, 1869), von Mises (Mises, 1913), Mohr-Coulomb (Coulomb, 1773; Mohr, 1900) and Drucker-Prager (Drucker and Prager, 1952), in which the first two are applied to ductile material such as steel and aluminium, while the last two can describe the response of brittle material such as concrete and soils. The flow rule relates stress to plastic strain increments and is generally established by using the plastic potential. When the flow rule is associated with a particular yield criterion it is an associated flow-rule, otherwise, it is a non-associated flow rule. The hardening rule has two basic modes, including the isotropic hardening where the yield surface is assumed to expand uniformly about the stress space origin during plastic flow and kinematic

hardening which corresponds to a translation preserving the initial shape. Also, the two models can be combined and become a more complex hardening rule (Marques, 1984).

2.3.2 Finite element implementation

The implementation of the elastoplastic constitutive relations in a finite element context has two different levels, including the global level and the material level. On the global level, the equilibrium must be satisfied in any other linear or nonlinear finite element computation, whereas on the material level the elastoplasticity relations must be satisfied (Krabbenhøft, 2002; Zienkiewicz and Taylor, 2000). In analyses, the elastoplastic constitutive model is considered at each numerical integration point of the element. From the global level, the displacement increments corresponding to the applied load vector can be obtained and then the strains can be computed. Since the constitutive matrix depends on the current state of stress, the stiffness matrix is nonlinear and iterative procedures should be used at the global level. In addition, on the material level, the stresses should be determined via the elastoplastic constitutive relationship after a global iterative procedure.

For a given strain increment, there are many procedures to update the current stress state, relating to the integration of the constitutive relations which are rate equations. For instance, a forward-Euler scheme can be used when the stress and strain increments are small and a return to the yield surface is needed to avoid the stresses lying outside the yield surface. However, the stress and strain increments are not infinitesimal and errors would accumulate. To address the problem of increment sizes,

a backward-Euler return-mapping scheme can be employed to evaluate the elastoplastic stress state (Crisfield, 1991).

For the elastoplastic analysis of shell elements, two approaches are usually used by researchers. One is the layered approach, also referred to as "through-the-thickness-integration", while the other one is the non-layered approach. In the following, some articles regarding these two methods are reviewed.

2.3.3 Layered approach

In the layered approach, a shell element can be divided into any desired number of layers. To represent the actual behaviour of the shell, increasing the number of layers can reduce the error due to the approximation that each layer is assumed to be in a state of plane stress. Strains and stresses are calculated and the elastoplastic analysis is performed for each layer separately. Then, the element material stiffness, nodal forces and moments are calculated by integration through the thickness. The layered approach can provide very accurate results when the number of layers is sufficient, but it is demanding on computation compared with the non-layered approach.

An early work regarding shells with large displacements including elastoplastic material behaviour was performed by (Parisch, 1981) based on the degenerated shell element, in which both the TL and UL formulations were used to considered large deflections and a layered approach was proposed for the treatment of elastoplastic behaviour. The similar studies using the layered approach can also be found in the references (Argyris et al., 2002b; Bathe and Dvorkin, 1985; Dal Cortivo et al., 2009;

Dvorkin and Bathe, 1984; Dvorkin et al., 1995; Kebari and Cassell, 1992; Li et al., 2013; Montag *et al.*, 1999).

In addition, the layered approach is also extensively used in analysis of laminated composite shell structures, which can be found in the references (Argyris et al., 1997; Cinefra and Carrera, 2013; Ferreira *et al.*, 2011; Han *et al.*, 2008; Hossain *et al.*, 2004; Khosravi et al., 2008; Kim et al., 2003; Liang and Izzuddin, 2015, 2016; Sessa *et al.*, 2017; Zallo and Gaudenzi, 2003).

2.3.4 Non-layered approach

The non-layered approach, also called the stress resultant approach, which avoids the integration over shell thickness and saves computational cost. However, the yield function and the rate equation should be formulated with the stress resultants and become more complicated than those in a state of plane stress used in the layered approach. Moreover, the non-layered approach is less accurate than the layered approach, since the yield function formulated with the stress resultants is approximate and hard to accurately describe the plastic zone spreading process through the shell thickness. Thus, proposing a more accurate stress resultant yield function suitable for more general cases of shell structures has received a lot of attention from researchers.

An early attempt was presented by Ilyushin (1956) where a complicated yield function formulated directly in terms of stress resultants was proposed based on the thin shell theory and the von Mises yield criterion. After that, Robinson (1971) examined the yield function proposed by Ilyushin (1956) and found that it is very close to the exact one in all cases and should prove useful for practical application,

whereas a modification to consider the effect of transverse shear was presented. Crisfield (1981) and Bieniek and Funaro (1976) also modified the Ilyushin yield function to accurately capture the progressive development of the plastic curvatures across the shell thickness. Shi and Voyiadjis (1992) further modified the yield function to account for the effect of transverse shear forces based on the Mindlin-Reissner plate theory.

The geometrically nonlinear elastoplastic analysis of shell structures using the non-layered approach can be found in the references (Simo et al., 1989; Simo et al., 1990a, 1992b; Simo and Fox, 1989; Simo et al., 1990b; Simo and Kennedy, 1992; Skallerud and Haugen, 1999).

CHAPTER 3

A PURE DEFORMATIONAL METHOD FOR SHELL ELEMENTS

The pure deformational method, also called the natural mode method, was firstly proposed by Argyris *et al.* (1979), in which the pure deformation modes are separated from the rigid body movements of the element. This method has substantial computational advantages, compared with the conventional finite element formulations. This is because the variables based on the pure deformational mode are less and the corresponding formulation is simpler when the rigid body movements are removed. The associated applications of this method for shell elements in nonlinear analysis are introduced by Argyris and his co-workers in the references (Argyris *et al.*, 2000a; Argyris et al., 2003; Argyris et al., 2002a; Argyris et al., 1997; Argyris et al., 1998; Argyris et al., 2002b). However, the pure deformations of the element in this method are different from the general local deformations in the co-rotated local system, and Argyris did not extend this method to be an element-independent method that can be used to any finite element.

In this chapter, a pure deformational method commonly used in beam-column elements is extended into triangular and quadrilateral shell elements. Different from the method presented by Argyris and his co-workers, the proposed method uses the local coordinate system as the basic coordinate system, and the corresponding pure deformations are easier to be extracted and identical to the local deformations.

Moreover, the proposed method is element-independent and can be used for any finite element.

The pure deformational method has been extensively used in the derivation of beam-column elements, but it has not been used for shell elements. The geometric displacement relationships of shell elements are more complicated than beam-column elements and for this reason, the pure deformational method faces more difficulties when applying it to shell elements. The simplicity for derivation and formulation of an element with computational efficiency by the pure deformational method motivate the author to extend it to shell elements.

3.1 A pure deformational method for beam-column elements

To fully illustrate the merits of the pure deformational method, the derivations for a 2D beam-column element using the general method and the pure deformational method are presented respectively in this section. The beam-column element consists of the linear column element and the cubic beam element (Hermit beam element) based on the Euler-Bernoulli hypotheses.

3.1.1 General derivation

For the general derivation of an element, there is no constraint applied on it and the rigid body movements should be considered. Thus, the displacement interpolations

must be able to describe the rigid body movements of the element. Figure 3.1 shows that a 2D beam-column element has two nodes and six degrees of freedom, in which the axial displacement interpolation is linear, and the transverse displacement interpolation is cubic, then we have

$$u = a_0 + a_1 x \tag{3.1a}$$

$$v = \sum_{i=0}^{3} b_i x^i \tag{3.1b}$$

To solve the coefficients, taking advantage of the Euler-Bernoulli hypothesis $\theta = \frac{dv}{dx}$ and substituting the boundary conditions into Eqs. (3.1) give

$$u = (1-\xi)u_1 + \xi u_2 \tag{3.2a}$$

$$\begin{aligned} v = {} & (1-3\xi^2+2\xi^3)v_1 + (\xi - 2\xi^2 + \xi^3)L\theta_1 \\ & + (3\xi^2 - 2\xi^3)v_2 + (\xi^3 - \xi^2)L\theta_2 \end{aligned} \tag{3.2b}$$

in which $\xi = \frac{x}{L}$.

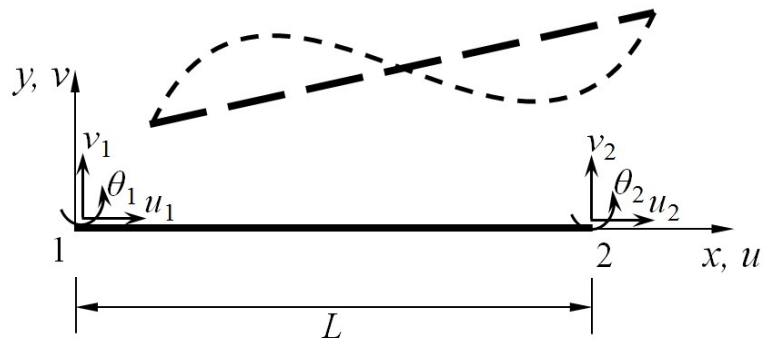

Figure 3.1 A 2D beam-element element

Based on the principle of minimum potential energy, the functional of the beam-column element can be given by

$$\Pi = \frac{1}{2} EA \int_0^L \left(\frac{du}{dx} \right)^2 dx + \frac{1}{2} EI \int_0^L \left(\frac{d^2 v}{dx^2} \right)^2 dx - \boldsymbol{d}^T \boldsymbol{f} \tag{3.3}$$

in which E is the elastic Young's modulus, A is the cross-sectional area, I is the second moment of the cross section, $\boldsymbol{d} = \{u_1 \ v_1 \ \theta_1 \ u_2 \ v_2 \ \theta_2\}^T$ is the displacement vector and $\boldsymbol{f}$ is the external force vector corresponding to $\boldsymbol{d}$.

Substituting Eqs. (3.2) into Eq. (3.3) and using the condition $\delta\Pi = 0$, the stiffness matrix can be obtained as follows,

$$\boldsymbol{K}\boldsymbol{d} = \boldsymbol{f} \tag{3.4a}$$

$$\boldsymbol{K} = \begin{bmatrix} \frac{EA}{L} & 0 & 0 & -\frac{EA}{L} & 0 & 0 \\ 0 & \frac{12EI}{L^3} & \frac{6EI}{L^2} & 0 & -\frac{12EI}{L^3} & \frac{6EI}{L^2} \\ 0 & \frac{6EI}{L^2} & \frac{4EI}{L} & 0 & -\frac{6EI}{L^2} & \frac{2EI}{L} \\ -\frac{EA}{L} & 0 & 0 & \frac{EA}{L} & 0 & 0 \\ 0 & -\frac{12EI}{L^3} & -\frac{6EI}{L^2} & 0 & \frac{12EI}{L^3} & -\frac{6EI}{L^3} \\ 0 & \frac{6EI}{L^2} & \frac{2EI}{L} & 0 & -\frac{6EI}{L^2} & \frac{4EI}{L} \end{bmatrix} \tag{3.4b}$$

This formulation is very classical and can be found in so many publications. It can be seen that $\boldsymbol{K}$ is a 6×6 singular stiffness matrix and its rank is 3, which means that the pure deformational beam-column element only has 3 degrees of freedom.

3.1.2 Derivation based on the pure deformational method

Figure 3.2 shows a pure deformational beam-column element, in which three degrees of freedom are restrained. Thus, the rigid body motions are removed and the rest of deformations $\tilde{\boldsymbol{d}} = \left\{\tilde{u}_2 \;\; \tilde{\theta}_1 \;\; \tilde{\theta}_2\right\}^T$ are pure. Thus, the displacement interpolations become

$$\tilde{u} = \xi \tilde{u}_2 \tag{3.5a}$$

$$\tilde{v} = (\xi - 2\xi^2 + \xi^3)L\tilde{\theta}_1 + (\xi^3 - \xi^2)L\tilde{\theta}_2 \tag{3.5b}$$

Compared with Eqs. (3.2) in the general derivation, Eqs. (3.5) are simpler and can be obtained by directly removing the terms involving the restrained degrees of freedom in Eqs. (3.2). By the principle of minimum potential energy, the stiffness matrix for the pure deformational element can be given by

$$\tilde{\boldsymbol{K}}\tilde{\boldsymbol{d}} = \tilde{\boldsymbol{f}} \tag{3.6a}$$

$$\tilde{\boldsymbol{K}} = \begin{bmatrix} \dfrac{EA}{L} & 0 & 0 \\ 0 & \dfrac{4EI}{L} & \dfrac{2EI}{L} \\ 0 & \dfrac{2EI}{L} & \dfrac{4EI}{L} \end{bmatrix} \tag{3.6b}$$

where the stiffness matrix $\tilde{\boldsymbol{K}}$ is a 3×3 non-singular matrix.

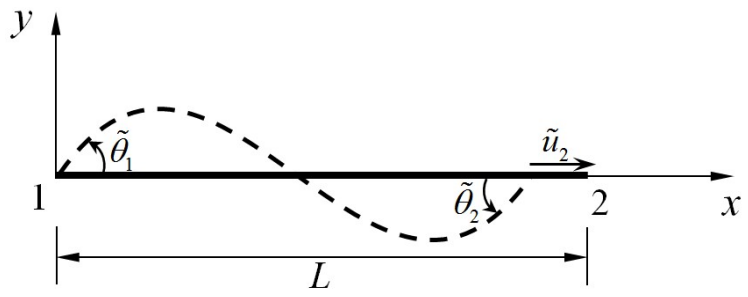

Figure 3.2 A pure deformational 2D beam-element element

Although the stiffness matrix $\tilde{\boldsymbol{K}}$ is simpler, it should be transformed into the one obtained by the general derivation, $\boldsymbol{K}$, to assemble the global stiffness matrix of the whole structure. Thus, the relationship between the pure deformational element in the basic coordinate system and the general element in the local coordinate system should be established. The pure deformations are identical to the corresponding local deformations, but their variations are different. The variations of the pure deformations can be given by

$$\delta\tilde{u}_2 = \delta u_2 - \delta u_1 \tag{3.7a}$$

$$\delta\tilde{\theta}_1 = \delta\theta_1 - \frac{\delta v_2 - \delta v_1}{L} \tag{3.7b}$$

$$\delta\tilde{\theta}_2 = \delta\theta_2 - \frac{\delta v_2 - \delta v_1}{L} \tag{3.7c}$$

Then, the basic-to-local transformation matrix can be obtained as follows,

$$\boldsymbol{L} = \frac{\partial \tilde{\boldsymbol{d}}}{\partial \boldsymbol{d}^T} = \begin{bmatrix} -1 & 0 & 0 & 1 & 0 & 0 \\ 0 & \frac{1}{L} & 1 & 0 & -\frac{1}{L} & 0 \\ 0 & \frac{1}{L} & 0 & 0 & -\frac{1}{L} & 1 \end{bmatrix} \tag{3.8}$$

Thus, the relationship between these two systems can be given by

$$\partial \tilde{\boldsymbol{d}} = \boldsymbol{L} \partial \boldsymbol{d} \tag{3.9a}$$

$$\boldsymbol{f} = \boldsymbol{L}^T \tilde{\boldsymbol{f}} \tag{3.9b}$$

$$\boldsymbol{K} = \boldsymbol{L}^T \tilde{\boldsymbol{K}} \boldsymbol{L} \tag{3.9c}$$

The derivation of the 2D beam-column element can be conducted in the basic coordinate system and makes the formulation simpler. Also, this pure deformational method is element-independent and can be used for any beam-column element with different displacement interpolations, even for the elements considering second order effect and material nonlinearity. For example, Chan (Chan, 1992) investigates the cubic beam-column element with second order effect in the large deflection analysis based on the co-rotational method; Chan and Zhou (Chan and Zhou, 1994) propose a fifth-order polynomial beam-column element with second order effect; Tang *et al*. (Tang *et al.*, 2015) propose a cubic beam-column element allowing for shear deformation and second order effect simultaneously; also, the stability function can be derived by the pure deformational element model as investigated by Chan and Gu (Chan and Gu, 2000).

Additionally, the pure deformational method can be naturally integrated into the element-independent co-rotational (EICR) formulation for geometrically nonlinear

analysis, as shown in the work by Meek (Meek and Tan, 1983) and Crisfield (Crisfield, 1991b). The co-rotational method decomposes the total element deformations into the large rigid body movements and the small pure deformations, which is consistent with the concept of the pure deformational method. Thus, the pure deformational method is very efficient for the derivations of novel elements and it is very significant to extend this method to shell elements.

3.2 A pure deformational method for triangular shell elements

Generally, a flat shell element consists of a membrane element and a plate element. Thus, this section is divided into two parts to discuss the proposed pure deformational methods for triangular membrane and plate elements respectively.

3.2.1 Triangular membrane elements

The pure deformational methods for triangular membrane elements with and without drilling rotations are presented respectively. Similar to the pure deformational method for beam-column elements, the crucial step is to derive the basic-to-local transformation matrix to transfer the quantities from the basic coordinate system corresponding to the pure deformational element model to the local coordinate system.

3.2.1.1 Triangular membrane elements without drilling rotations

As shown in Figure 3.3, a triangular membrane element is defined in the basic coordinate system with a simple support on one side and its rigid body movements are removed.

The coordinates of the three corner nodes in the basic and local coordinate systems are identical and can be given by

$$\boldsymbol{x}_1 = \{0 \;\; 0\}^T, \quad \boldsymbol{x}_2 = \{x_2 \;\; 0\}^T, \quad \boldsymbol{x}_3 = \{x_3 \;\; y_3\}^T \tag{3.10a, b, c}$$

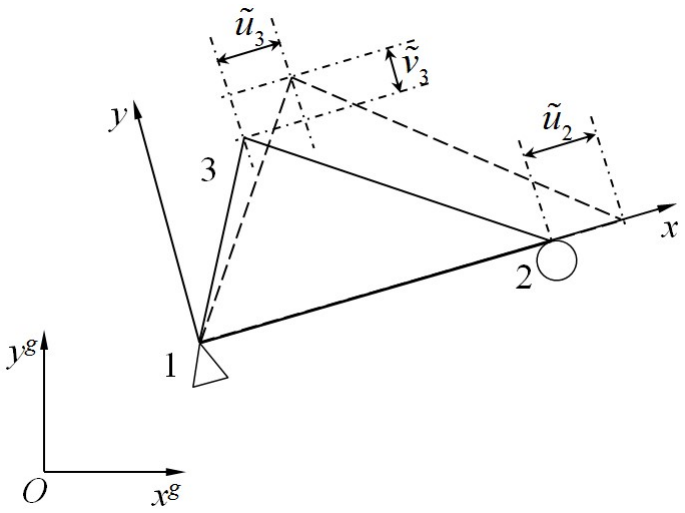

Figure 3.3 A triangular membrane element with a simple support on one side

The basic internal force and displacement vectors are denoted by

$$\tilde{\boldsymbol{f}}_m = \left\{\tilde{f}_{x2} \;\; \tilde{f}_{x3} \;\; \tilde{f}_{y3}\right\}^T \tag{3.11a}$$

$$\tilde{\boldsymbol{d}}_m = \left\{\tilde{u}_2 \;\; \tilde{u}_3 \;\; \tilde{v}_3\right\}^T \tag{3.11b}$$

$$\delta \tilde{\boldsymbol{f}}_m = \tilde{\boldsymbol{K}}_m \delta \tilde{\boldsymbol{d}}_m \tag{3.11c}$$

where the tilde "~" means that the variables belong to the pure deformational element model in the basic coordinate system, and $\tilde{\boldsymbol{K}}_m$ is the stiffness matrix of a triangular membrane element without drilling rotations in the basic coordinate system.

Besides, the displacement and internal force vectors defined in the local coordinate system containing the rigid body movements are denoted by

$$\boldsymbol{f}_m = \left\{ f_{x1} \;\; f_{y1} \;\; f_{x2} \;\; f_{y2} \;\; f_{x3} \;\; f_{y3} \right\}^T \tag{3.12a}$$

$$\boldsymbol{d}_m = \left\{ u_{x1} \;\; u_{y1} \;\; u_{x2} \;\; u_{y2} \;\; u_{x3} \;\; u_{y3} \right\}^T \tag{3.12b}$$

$$\delta \boldsymbol{f}_m = \boldsymbol{K}_m \delta \boldsymbol{d}_m \tag{3.12c}$$

To construct the relationship between the basic and local coordinate systems, the variation of the rigid body rotation about the local *z*-axis $\delta\omega_z$ of a membrane element is need. And $\delta\omega_z$ can be expressed with the variations of the local displacements as follows,

$$\delta\omega_z = \frac{\delta u_{y2} - \delta u_{y1}}{x_2} \tag{3.13}$$

Then, the variations of the pure deformations can be given by

$$\delta\tilde{u}_2 = \delta u_{x2} - \delta u_{x1} \tag{3.14a}$$

$$\delta\tilde{u}_3 = \delta u_{x3} - \delta u_{x1} + y_3 \delta\omega_z \tag{3.14b}$$

$$\delta\tilde{v}_3 = \delta u_{y3} - \delta u_{y1} - x_3\delta\omega_z \tag{3.14c}$$

Through Eqs. (3.13) and (3.14), we have

$$\delta\tilde{\boldsymbol{d}}_m = \boldsymbol{L}_m\delta\boldsymbol{d}_m \tag{3.15a}$$

in which

$$\boldsymbol{L}_m = \begin{bmatrix} -1 & 0 & 1 & 0 & 0 & 0 \\ -1 & -y_3/x_2 & 0 & y_3/x_2 & 1 & 0 \\ 0 & -1+x_3/x_2 & 0 & -x_3/x_2 & 0 & 1 \end{bmatrix} \tag{3.15b}$$

By the principle of virtual work, the relationship of the force vectors between these two different systems can be given by

$$\boldsymbol{f}_m = \boldsymbol{L}_m^T\tilde{\boldsymbol{f}}_m \tag{3.16}$$

in which the basic internal forces $\tilde{\boldsymbol{f}}_m$ can be seen as the action forces at the free degrees of freedom of a pure deformational triangular membrane element. And it can be noticed that $\tilde{f}_{x1} = f_{x1}$, $\tilde{f}_{x2} = f_{x2}$, $\tilde{f}_{x3} = f_{x3}$ from Eq. (3.16). In addition, the other forces in the vector $\boldsymbol{f}_m$ can be regarded as the reaction forces at the restrained degrees of freedom of a pure deformational triangular membrane element, which can also be obtained by the equilibrium equations of a membrane element. Thus, the equilibrium equations can verify the basic-to-local transformation matrix $\boldsymbol{L}_m$.

Taking a variation of Eq. (3.16) gives

$$\delta\boldsymbol{f}_m = \boldsymbol{L}_m^T\delta\tilde{\boldsymbol{f}}_m = \boldsymbol{L}_m^T\tilde{\boldsymbol{K}}_m\delta\tilde{\boldsymbol{d}}_m = \boldsymbol{L}_{m1}^T\tilde{\boldsymbol{K}}_m\boldsymbol{L}_m\delta\boldsymbol{d}_m \tag{3.17a}$$

$$\boldsymbol{K}_m = \boldsymbol{L}_m^T \tilde{\boldsymbol{K}}_m \boldsymbol{L}_m \tag{3.17b}$$

in which $\boldsymbol{K}_m$ is a 6×6 singular stiffness matrix in the local coordinate system, whereas $\tilde{\boldsymbol{K}}_m$ is a 3×3 non-singular stiffness matrix in the basic coordinate system. The relationship in Eqs. (3.17) is applicable to any triangular membrane element without drill rotations, since it is not related to displacement interpolations.

The constant stress triangular (CST) plane element (Zienkiewicz *et al.*, 1977) with linear displacement interpolations over the element area is used for demonstration herein. The stiffness matrix of the triangular membrane element without rigid body movements in the basic coordinate system can be given by

$$\tilde{\boldsymbol{K}}_m = \frac{Et}{4(1-v^2)} \begin{bmatrix} (1-v)x_3^2 / x_2 y_3 + 2y_3 / x_2 & -(1-v)x_3 / y_3 & 2v \\ -(1-v)x_3 / y_3 & (1-v)x_2 / y_3 & 0 \\ 2v & 0 & 2x_2 / y_3 \end{bmatrix} \tag{3.18}$$

in which E is the elastic Young's modulus, t is the thickness of membrane and v is the Poisson's ratio. It can be seen that the expression of this stiffness matrix is much simpler than the traditional derivation.

To assemble the global stiffness matrix of the whole structure, the 3×3 non-singular matrix in Eq. (3.18) needs to be transformed into the 6×6 singular matrix by the basic-to-local transformation matrix in Eqs. (3.17). However, in terms of coding, the former matrix is more concise. Moreover, when the stiffness matrix needs numerical integration, the 3×3 stiffness matrix can save computational cost.

3.2.1.2 Triangular membrane elements with drilling rotations

As a part of a shell element, a membrane element should allow for the in-plane drilling rotations, so that a shell element has six degrees of freedom per node. An usual method is to introduce fictitious stiffness at the drilling degrees of freedom. However, the magnitude of this fictitious stiffness is questionable and induces numerical problems very often. An advanced technique is to contain the drilling rotations in the displacement interpolations, such as the element presented by Allman (1988b), whereas the relevant application is discussed in Chapter 5.

When the drilling rotations are considered, the basic internal force and displacement vectors for a pure deformational membrane element can be denoted by

$$\tilde{\boldsymbol{f}}_m = \left\{ \tilde{f}_{x2} \;\; \tilde{f}_{x3} \;\; \tilde{f}_{y3} \;\; \tilde{m}_{z1} \;\; \tilde{m}_{z2} \;\; \tilde{m}_{z3} \right\}^T \tag{3.19a}$$

$$\tilde{\boldsymbol{d}}_m = \left\{ \tilde{u}_{x2} \;\; \tilde{u}_{x3} \;\; \tilde{v}_{y3} \;\; \tilde{\theta}_{z1} \;\; \tilde{\theta}_{z2} \;\; \tilde{\theta}_{z3} \right\}^T \tag{3.19b}$$

The internal force and displacement vectors in the local coordinate system containing rigid body movements are

$$\boldsymbol{f}_m = \left\{ f_{x1} \;\; f_{y1} \;\; m_{z1} \;\; f_{x2} \;\; f_{y2} \;\; m_{z2} \;\; f_{x3} \;\; f_{y3} \;\; m_{z3} \right\}^T \tag{3.20a}$$

$$\boldsymbol{d}_m = \left\{ u_{x1} \;\; u_{y1} \;\; \theta_{z1} \;\; u_{x2} \;\; u_{y2} \;\; \theta_{z2} \;\; u_{x3} \;\; u_{y3} \;\; \theta_{z3} \right\}^T \tag{3.20b}$$

To establish the relationship of the displacement vectors between the basic and local coordinate systems, Eqs. (3.13) and (3.14) are still valid here and we also have

$$\delta\tilde{\theta}_{z1} = \delta\theta_{z1} - \delta\omega_z \tag{3.21a}$$

$$\delta\tilde{\theta}_{z2} = \delta\theta_{z2} - \delta\omega_z \tag{3.21b}$$

$$\delta\tilde{\theta}_{z3} = \delta\theta_{z3} - \delta\omega_z \tag{3.21c}$$

Though Eqs. (3.13), (3.14) and (3.21), the basic-to-local transformation matrix for a triangular membrane element with drilling rotations can be given by

$$\boldsymbol{L}_m = \begin{bmatrix} -1 & 0 & 0 & 1 & 0 & 0 & 0 & 0 & 0 \\ -1 & -y_3/x_2 & 0 & 0 & y_3/x_2 & 0 & 1 & 0 & 0 \\ 0 & -1+x_3/x_2 & 0 & 0 & -x_3/x_2 & 0 & 0 & 1 & 0 \\ 0 & 1/x_2 & 1 & 0 & -1/x_2 & 0 & 0 & 0 & 0 \\ 0 & 1/x_2 & 0 & 0 & -1/x_2 & 1 & 0 & 0 & 0 \\ 0 & 1/x_2 & 0 & 0 & -1/x_2 & 0 & 0 & 0 & 1 \end{bmatrix} \tag{3.22}$$

3.2.2 Triangular plate elements

The basic-to-local transformation matrix for triangular plate elements is derived in this section. To exclude rigid body movements from a triangular plate element, the vertical displacements in the local coordinate system are restrained, while all of the bending rotations are free in this pure deformational element model, as shown in Figure 3.4. Besides, the definition of local coordinate system and the local node coordinates are the same as the ones for triangular membrane elements.

The internal force and displacement vectors in the basic coordinate system without rigid body movements can be denoted by

$$\tilde{\boldsymbol{f}}_p = \left\{\tilde{m}_{x1} \;\; \tilde{m}_{y1} \;\; \tilde{m}_{x2} \;\; \tilde{m}_{y2} \;\; \tilde{m}_{x3} \;\; \tilde{m}_{y3}\right\}^T \tag{3.23a}$$

$$\tilde{\boldsymbol{d}}_p = \left\{\tilde{\theta}_{x1} \;\; \tilde{\theta}_{y1} \;\; \tilde{\theta}_{x2} \;\; \tilde{\theta}_{y2} \;\; \tilde{\theta}_{x3} \;\; \tilde{\theta}_{y3}\right\}^T \tag{3.23b}$$

$$\delta \tilde{\boldsymbol{f}}_p = \tilde{\boldsymbol{K}}_p \delta \tilde{\boldsymbol{d}}_p \tag{3.23c}$$

The internal force and displacement vectors in the local coordinate system with rigid body movements are

$$\boldsymbol{f}_p = \left\{ f_{z1} \;\; m_{x1} \;\; m_{y1} \;\; f_{z2} \;\; m_{x2} \;\; m_{y2} \;\; f_{z3} \;\; m_{x3} \;\; m_{y3} \right\}^T \tag{3.24a}$$

$$\boldsymbol{d}_p = \left\{ u_{z1} \;\; \theta_{x1} \;\; \theta_{y1} \;\; u_{z2} \;\; \theta_{x2} \;\; \theta_{y2} \;\; u_{z3} \;\; \theta_{x3} \;\; \theta_{y3} \right\}^T \tag{3.24b}$$

$$\delta \boldsymbol{f}_p = \boldsymbol{K}_p \delta \boldsymbol{d}_p \tag{3.24c}$$

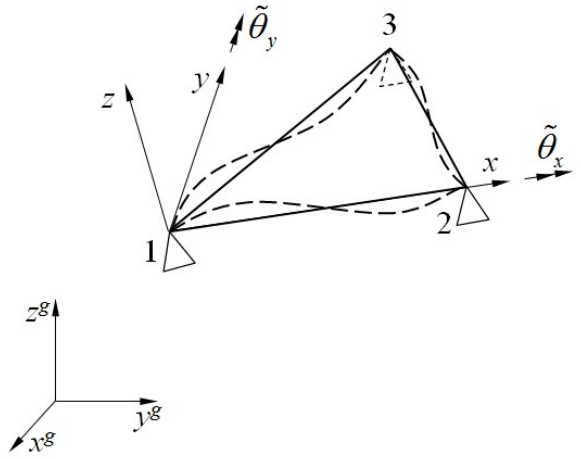

Figure 3.4 A triangular plate element with vertical displacements restrained

The variations of the rigid body rotations of a triangular plate element in the local coordinate system can be given by

$$\delta\omega_x = \frac{\delta u_{z3} - \delta u_{z1}}{y_3} - \frac{\delta u_{z2} - \delta u_{z1}}{y_3} \frac{x_3}{x_2} \tag{3.25a}$$

$$\delta\omega_y = \frac{\delta u_{z1} - \delta u_{z2}}{x_2} \tag{3.25b}$$

Then, the variations of the pure deformational rotations are

$$\delta\tilde{\theta}_{xi} = \delta\theta_{xi} - \delta\omega_x \quad (i=1,2,3) \tag{3.26a}$$

$$\delta\tilde{\theta}_{yi} = \delta\theta_{yi} - \delta\omega_y \quad (i=1,2,3) \tag{3.26b}$$

The basic-to-local transformation matrix can be rearranged from Eqs. (3.25) and (3.26) as

$$\delta\tilde{\boldsymbol{d}}_p = \boldsymbol{L}_p \delta\boldsymbol{d}_p \tag{3.27a}$$

where

$$\boldsymbol{L}_p = \begin{bmatrix} 1/y_3 - x_3/x_2y_3 & 1 & 0 & x_3/x_2y_3 & 0 & 0 & -1/y_3 & 0 & 0 \\ -1/x_2 & 0 & 1 & 1/\mathrm{x}_2 & 0 & 0 & 0 & 0 & 0 \\ 1/y_3 - x_3/x_2y_3 & 0 & 0 & x_3/x_2y_3 & 1 & 0 & -1/y_3 & 0 & 0 \\ -1/x_2 & 0 & 0 & 1/\mathrm{x}_2 & 0 & 1 & 0 & 0 & 0 \\ 1/y_3 - x_3/x_2y_3 & 0 & 0 & x_3/x_2y_3 & 0 & 0 & -1/y_3 & 1 & 0 \\ -1/x_2 & 0 & 0 & 1/\mathrm{x}_2 & 0 & 0 & 0 & 0 & 1 \end{bmatrix} \tag{3.27b}$$

By the principle of virtual work, the relationship of the internal force vectors between the two different systems can be given by

$$\boldsymbol{f}_p = \boldsymbol{L}_p{}^T \tilde{\boldsymbol{f}}_p \tag{3.28}$$

Eq. (3.28) can also be verified by the equilibrium equations of a triangular plate element. And the moments in these two systems are identical at the same degrees of freedom, such as $\tilde{m}_{xi} = m_{xi}$, $\tilde{m}_{yi} = m_{yi}$.

Then, the relationship of the stiffness matrices of a triangular plate element between these two systems can be given by

$$\boldsymbol{K}_p = \boldsymbol{L}_p^T \tilde{\boldsymbol{K}}_p \boldsymbol{L}_p \tag{3.29}$$

in which $\boldsymbol{K}_p$ is a 9×9 singular matrix in the local coordinate system, whereas $\tilde{\boldsymbol{K}}_p$ is a 6×6 non-singular matrix in the basic coordinate system.

3.3 A pure deformational method for quadrilateral shell elements

In this section, a pure deformational method for quadrilateral shell elements is presented, whose derivation process is similar to the one for triangular shell elements. However, it is more complicated, because the warping phenomenon exists in a quadrilateral shell element, in which the 4 corner nodes are not coplanar. Thus, different from the pure deformational method for flat triangular shell elements in which a membrane element and a plate element can be separately discussed, the coupling of a membrane element and a plate element due to warping effect makes the pure deformational method for quadrilateral shell elements should be discussed as a whole entity. The local coordinate system for a quadrilateral shell element, which is related to the variations of the rigid body rotations, should be determined at first.

3.3.1 Definition of the local coordinate system

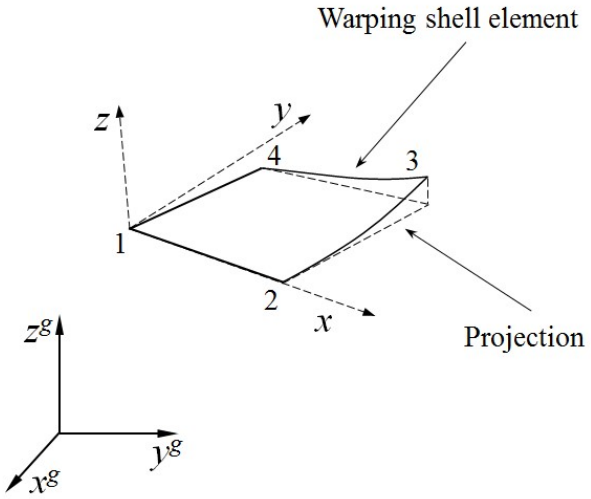

Figure 3.5 Local coordinate system of a quadrilateral shell element

As shown in the Figure 3.5, $x^g y^g z^g$ refers to the global coordinate system, while xyz the local coordinate system. In terms of the local coordinate system, the origin is located at the node 1 and the x-axis is aligned to the side 1-2 of the quadrilateral shell element, whereas the z-axis is normal to the side 1-2 and the side 1-4. Based on the local coordinate system, the nodes 1, 2, 4 are always coplanar and the warping occurs only in the node 3. Knowing the global coordinates of the 4 corner nodes of a warping quadrilateral shell element, $\boldsymbol{x}_i^g = \left\{ x_i^g \;\; y_i^g \;\; z_i^g \right\}^T$ (i=1,2,3,4), the axis vectors of the local coordinate system can be given by

$$\boldsymbol{e}_x = \frac{\boldsymbol{x}_2^g - \boldsymbol{x}_1^g}{\left\| \boldsymbol{x}_2^g - \boldsymbol{x}_1^g \right\|} \tag{3.30a}$$

$$\boldsymbol{e}_z = \frac{\boldsymbol{e}_x \times \left(\boldsymbol{x}_4^g - \boldsymbol{x}_1^g\right)}{\left\| \boldsymbol{e}_x \times \left(\boldsymbol{x}_4^g - \boldsymbol{x}_1^g\right) \right\|} \tag{3.30b}$$

$$\boldsymbol{e}_y = \boldsymbol{e}_z \times \boldsymbol{e}_x \tag{3.30c}$$

Then, the local-to-global transformation matrix for a quadrilateral shell element is

$$\boldsymbol{T}_e = \left[\boldsymbol{e}_x \;\; \boldsymbol{e}_y \;\; \boldsymbol{e}_z \right]^T \tag{3.31}$$

Then, the local node coordinates can be obtained as follows,

$$\boldsymbol{x}_i = \boldsymbol{T}_e \left(\boldsymbol{x}_i^g - \boldsymbol{x}_1^g \right) \;\; (i=1,2,3,4) \tag{3.32}$$

in which $\boldsymbol{x}_i = \{x_i \;\; y_i \;\; z_i\}^T$, and it can be noticed that $z_1 = z_2 = z_4 = 0$. A limitation for this definition of local coordinate system is that the analysis results obtained by the quadrilateral shell element may depend on the nodal ordering. However, it can be applied for many cases except for some certain stability problems with symmetry (Battini and Pacoste, 2004), while the effect of nodal ordering dependence is not obvious when meshes are refined. The most important reason for using this definition of local coordinate system is that the pure deformational method can be more easily applied for quadrilateral shell elements.

According to Eq. (3.32), the nodal coordinates in the local coordinate system can be given by

$$\boldsymbol{x}_1 = \{0 \;\; 0 \;\; 0\}^T, \;\; \boldsymbol{x}_2 = \{x_2 \;\; 0 \;\; 0\}^T, \;\; \boldsymbol{x}_3 = \{x_3 \;\; y_3 \;\; z_3\}^T, \;\; \boldsymbol{x}_4 = \{x_4 \;\; y_4 \;\; 0\}^T \tag{3.33}$$

It can be noted that there are six entries of the local node coordinates are zeros, which means that the corresponding degrees of freedom are restrained in the basic coordinate system. The symbols referring to the displacement and the internal force vectors of a quadrilateral shell element in the basic coordinate system are listed in the following. For a membrane element with drilling rotations, the displacement vector and the corresponding internal force vector are

$$\tilde{\boldsymbol{d}}_m = \left\{\tilde{u}_2 \;\; \tilde{u}_3 \;\; \tilde{v}_3 \;\; \tilde{u}_4 \;\; \tilde{v}_4 \;\; \tilde{\theta}_{z1} \;\; \tilde{\theta}_{z2} \;\; \tilde{\theta}_{z3} \;\; \tilde{\theta}_{z4}\right\}^T \tag{3.34a}$$

$$\tilde{\boldsymbol{f}}_m = \left\{\tilde{f}_{x2} \;\; \tilde{f}_{x3} \;\; \tilde{f}_{y3} \;\; \tilde{f}_{x4} \;\; \tilde{f}_{y4} \;\; \tilde{m}_{z1} \;\; \tilde{m}_{z2} \;\; \tilde{m}_{z3} \;\; \tilde{m}_{z4}\right\}^T \tag{3.34b}$$

For a plate element, the displacement vector and the corresponding internal force vector are

$$\tilde{\boldsymbol{d}}_p = \left\{\tilde{w}_3 \;\; \tilde{\theta}_{x1} \;\; \tilde{\theta}_{y1} \;\; \tilde{\theta}_{x2} \;\; \tilde{\theta}_{y2} \;\; \tilde{\theta}_{x3} \;\; \tilde{\theta}_{y3} \;\; \tilde{\theta}_{x4} \;\; \tilde{\theta}_{y4}\right\}^T \tag{3.35a}$$

$$\tilde{\boldsymbol{f}}_p = \left\{\tilde{f}_{z3} \;\; \tilde{m}_{x1} \;\; \tilde{m}_{y1} \;\; \tilde{m}_{x2} \;\; \tilde{m}_{y2} \;\; \tilde{m}_{x3} \;\; \tilde{m}_{y3} \;\; \tilde{m}_{x4} \;\; \tilde{m}_{y4}\right\}^T \tag{3.35b}$$

Every vector of a membrane element and a plate element only has 9 entries. Then, the displacement vector and the internal force vector of a quadrilateral shell element based on the basic coordinate system can be given by

$$\tilde{\boldsymbol{d}} = \left\{\tilde{\boldsymbol{d}}_m{}^T \;\; \tilde{\boldsymbol{d}}_p{}^T\right\}^T \tag{3.36a}$$

$$\tilde{\boldsymbol{f}} = \left\{\tilde{\boldsymbol{f}}_m{}^T \;\; \tilde{\boldsymbol{f}}_p{}^T\right\}^T \tag{3.36b}$$

In the local coordinate system, the displacement and the internal force vectors of a quadrilateral shell element are denoted by $\boldsymbol{d}$ and $\boldsymbol{f}$ as follows,

$$\boldsymbol{d} = \left\{ \boldsymbol{d}_1^T \;\; \boldsymbol{d}_2^T \;\; \boldsymbol{d}_3^T \;\; \boldsymbol{d}_4^T \right\}^T \tag{3.37a}$$

$$\boldsymbol{d}_i = \left\{ u_{xi} \;\; u_{yi} \;\; u_{zi} \;\; \theta_{xi} \;\; \theta_{yi} \;\; \theta_{zi} \right\}^T \tag{3.37b}$$

$$\boldsymbol{f} = \left\{ \boldsymbol{f}_1^T \;\; \boldsymbol{f}_2^T \;\; \boldsymbol{f}_3^T \;\; \boldsymbol{f}_4^T \right\}^T \tag{3.37c}$$

$$\boldsymbol{f}_i = \left\{ f_{xi} \;\; f_{yi} \;\; f_{zi} \;\; m_{xi} \;\; m_{yi} \;\; m_{zi} \right\}^T \tag{3.37d}$$

The relationship of the variables between the basic and local coordinate systems is detailed in the next section.

3.3.2 Relationship between local and basic coordinate systems

First, the variations of the rigid body rotations of a quadrilateral shell element in the local coordinate system can be expressed with the variations of the local translational displacements as

$$\delta\omega_x = \frac{\delta u_{z4} - \delta u_{z1}}{y_4} - \frac{\delta u_{z2} - \delta u_{z1}}{y_4}\frac{x_4}{x_2} \tag{3.38a}$$

$$\delta\omega_y = \frac{\delta u_{z1} - \delta u_{z2}}{x_2} \tag{3.38b}$$

$$\delta\omega_z = \frac{\delta u_{y2} - \delta u_{y1}}{x_2} \tag{3.38c}$$

As shown in Figure 3.6, for a quadrilateral membrane element, the variations of the pure deformations can be given by

$$\delta\tilde{u}_2 = \delta u_{x2} - \delta u_{x1} \tag{3.39a}$$

$$\delta\tilde{u}_3 = \delta u_{x3} - \delta u_{x1} + y_3\delta\omega_z - z_3\delta\omega_y \tag{3.39b}$$

$$\delta\tilde{v}_3 = \delta u_{y3} - \delta u_{y1} - x_3\delta\omega_z + z_3\delta\omega_x \tag{3.39c}$$

$$\delta\tilde{u}_4 = \delta u_{x4} - \delta u_{x1} + y_4\delta\omega_z \tag{3.39d}$$

$$\delta\tilde{v}_4 = \delta u_{y4} - \delta u_{y1} - x_4\delta\omega_z \tag{3.39e}$$

$$\delta\tilde{\theta}_{zi} = \delta\theta_{zi} - \delta\omega_z \quad (i=1,2,3,4) \tag{3.39f}$$

where the warping in the node 3 is considered in Eqs. (3.39b, c).

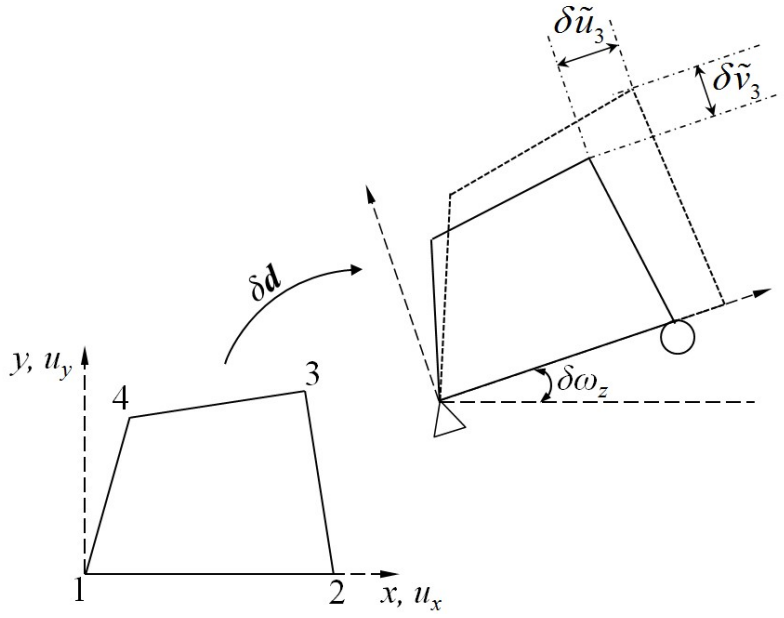

Figure 3.6 Deformation of a quadrilateral membrane element

Then, the transformation matrix from local to basic coordinate system can be derived as

$$\boldsymbol{L}_m = \frac{\partial \tilde{\boldsymbol{d}}_m^{\,T}}{\partial \boldsymbol{d}} \tag{3.40a}$$

$$\delta \tilde{\boldsymbol{d}}_m = \boldsymbol{L}_m \delta \boldsymbol{d} \tag{3.40b}$$

in which $\boldsymbol{L}_m$ is a 9×24 matrix.

By the principle of virtual work, the relationship of the internal force vectors between these two different systems can be given by

$$\boldsymbol{f} = \boldsymbol{L}_m^{\,T} \boldsymbol{p}_m \tag{3.41}$$

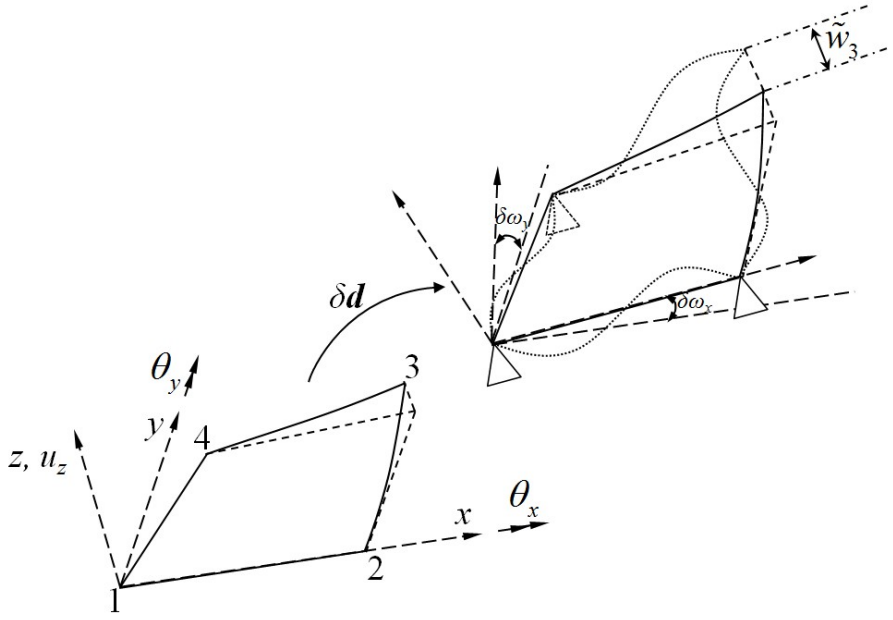

Figure 3.7 Deformation of a quadrilateral plate element

With the similar way used in a membrane element, the variations of the pure deformations of a plate element as shown in Figure 3.7 can be given in the following,

$$\delta\tilde{w}_3 = \delta u_{z3} - \delta u_{z1} - y_3\delta\omega_x + x_3\delta\omega_y \tag{3.42a}$$

$$\delta\tilde{\theta}_{xi} = \delta\theta_{xi} - \delta\omega_x \quad (i=1,2,3,4) \tag{3.42b}$$

$$\delta\tilde{\theta}_{xi} = \delta\theta_{xi} - \delta\omega_y \quad (i=1,2,3,4) \tag{3.42c}$$

Because there is no restraint on the node 3, so the vertical deflection of the node 3 occurs and is given in Eq. (3.42a). The basic-to-local transformation matrix can be given by

$$\boldsymbol{L}_p = \frac{\partial \tilde{\boldsymbol{d}}_p^{\,T}}{\partial \boldsymbol{d}} \tag{3.43a}$$

$$\delta\tilde{\boldsymbol{d}}_p = \boldsymbol{L}_p\delta\boldsymbol{d} \tag{3.43b}$$

in which the matrix $\boldsymbol{L}_p$ is also a 9×24 matrix as well as $\boldsymbol{L}_m$.

Like a membrane element, the internal force vectors of a plate element in these two coordinate systems have the relationship as

$$\boldsymbol{f} = \boldsymbol{L}_p^{\,T}\boldsymbol{p}_p \tag{3.44}$$

Combining the variables of a membrane element and a plate element together, we have

$$\delta\tilde{\boldsymbol{d}} = \boldsymbol{L}\delta\boldsymbol{d} \tag{3.45a}$$

$$\boldsymbol{f} = \boldsymbol{L}^T \tilde{\boldsymbol{f}} \tag{3.45b}$$

$$\boldsymbol{L} = \begin{bmatrix} \boldsymbol{L}_m \\ \boldsymbol{L}_p \end{bmatrix}_{18\times 24} \tag{3.45c}$$

3.3.3 Local stiffness matrix

In this thesis, the stiffness matrix of a quadrilateral shell element is derived based on the flat facet which is the projection of a warping shell element and the warping effect is regarded as eccentricities at nodes. Thus, different for flat triangular shell elements, quadrilateral shell elements have one more local system which the projection under the basic coordinate system. Thus, the relationship between the projection and the basic coordinate system should be established.

The warping only existing at the node 3 is regarded as an eccentricity, which means that there is a rigid beam between the real node and the projected node. With this assumption, the displacements of the projection of the membrane element can be given by

$$\delta\overline{w}_3 = \delta\tilde{w}_3 - z_3\,\delta\tilde{\theta}_{y3} \tag{3.46a}$$

$$\delta\overline{w}_3 = \delta\tilde{w}_3 + z_3\,\delta\tilde{\theta}_{y3} \tag{3.46b}$$

in which the horizontal line "-" above a variable means that it belongs to the projection.

Then, through Eqs. (3.45) and (3.46), we have

$$\delta \bar{\boldsymbol{d}} = \boldsymbol{E}\,\boldsymbol{L}\,\delta \boldsymbol{d} \tag{3.47a}$$

$$\boldsymbol{f} = \boldsymbol{L}^T \boldsymbol{E}^T \bar{\boldsymbol{f}} \tag{3.47b}$$

$$\boldsymbol{E}_{i,i} = 1 \quad (i=1\sim 18); \quad \boldsymbol{E}_{2,16} = -z_3 \; ; \quad \boldsymbol{E}_{3,15} = z_3 \tag{3.47c}$$

where the matrix $\boldsymbol{E}$ represents the transformation matrix from the projection to the warping shell element. It can be seen that a plate element is not affected by the warping, in which the local vertical deflections and the pure bending rotations at the node 3 are the same as those in the projection.

Getting rigid of the restrained degrees of freedom as shown in Figures 3.6 and 3.7, the pure deformational stiffness matrix for the projection, which is an 18×18 non-singular matrix, can be obtained and has the relationship in the following,

$$\delta \bar{\boldsymbol{f}} = \bar{\boldsymbol{K}} \delta \bar{\boldsymbol{d}} \tag{3.48}$$

Because the pure deformational method is element-independent, the stiffness matrix $\bar{\boldsymbol{K}}$ can be formulated by any 4-nodes flat quadrilateral membrane element and plate element. If needed, the stiffness matrix $\bar{\boldsymbol{K}}$ can also allow for material nonlinearity.

Through Eqs. (3.47) and (3.48), the tangent stiffness matrix of a warping quadrilateral shell element based on the local coordinate system can be derived as follows,

$$\begin{aligned} \delta \boldsymbol{f} &= \boldsymbol{L}^T \boldsymbol{E}^T \delta \bar{\boldsymbol{f}} \\ &= \boldsymbol{L}^T \boldsymbol{E}^T \bar{\boldsymbol{K}} \boldsymbol{E}\,\boldsymbol{L}\,\delta \boldsymbol{d} = \boldsymbol{K}\,\delta \boldsymbol{d} \end{aligned} \tag{3.49a}$$

$$\boldsymbol{K} = \boldsymbol{L}^T \boldsymbol{E}^T \bar{\boldsymbol{K}} \boldsymbol{E}\,\boldsymbol{L} \tag{3.49b}$$

in which $\boldsymbol{K}$ is the stiffness matrix of a warping quadrilateral shell element based on the local coordinate system and a 24×24 singular matrix used to assemble the global stiffness matrix of the whole structure after being transformed into the global coordinate system.

3.4 Summary

In this section, the pure deformational method often adopted in the derivation of beam-column elements is extended to triangular shell elements and quadrilateral shell elements. The pure deformational stiffness matrix should be transformed into the singular stiffness matrix in the local coordinate system for assembling the global stiffness matrix of the whole structures, so it seems that the pure deformational method is useless. However, there are several advantages can be obtained using this method.

Firstly, the proposed pure deformational method is element-independent, so any membrane element and plate element can be simplified using this method. Secondly, it decreases the number of degrees of freedom of an element, so makes the derivation and formulation simpler, especially for the elements having complicated displacement interpolations, while the pertaining application for the derivation of shell elements is shown in Chapter 5. Thirdly, for geometrically nonlinear analysis, the initial local linear stiffness matrix of an element may be stored for calling in the computational process, so the pure deformational stiffness matrix whose dimensions are decreased can save computer storage. Fourth, the pure deformation method is not only for the elements with linear strains, the second order effect of the local element can also be

considered. Because the formulations considering nonlinear strains, such as the Green-Lagrangian strains, are very complicated, the pure deformational method is helpful to simplify them through decreasing element variables. Finally, the pure deformational method is intimately related to the element-independent co-rotational (EICR) algorithm and can contribute to a novel EICR formulation which is simpler than the conventional one firstly introduced by Rankin and Brogan (1986), while the relevant derivation is presented in the next chapter.

CHAPTER 4

NOVEL EICR FORMULATIONS BASED ON PURE DEFORMATIONAL METHOD

In this chapter, the novel element-independent co-rotational (EICR) formulations for triangular and quadrilateral shell elements are proposed based on the proposed pure deformational method. They are consistent with the conventional EICR method firstly proposed by Rankin and Brogan (1986) but become much simpler. The proposed two EICR formulations for triangular and quadrilateral shell elements respectively introduced in Chapters 5 and 6 are novel general frameworks for geometrically nonlinear shell elements and inherit the property of element-independence from the conventional method.

Different from the conventional EICR method with the strictly physical and mathematical derivation, the proposed EICR method follows another kind of co-rotational method introduced by Levy and Gal (2001). Its derivation of the geometric stiffness matrix is on the basis of load perturbation of linear equilibrium equations of a shell element in the local coordinate system and the local geometric stiffness matrix is derived as the gradients of the nodal internal forces, which is similar to the approach proposed by Meek and Tan (1983) to derive the geometric stiffness matrix of a beam-column element. In the derivation, the local geometric stiffness is divided into three parts: the in-plane geometric stiffness matrix of the membrane element, the in-plane geometric stiffness matrix of the plate element and

the out-of-plane geometric stiffness matrix of the shell element. However, the formulation is only used for flat triangular shell elements and is not a completely element-independent co-rotational algorithm. Thus, this chapter not only follows the idea to derive the geometric stiffness matrix for triangular shell elements but also extends it into quadrilateral shell elements based on the pure deformational modes. Further, a simplified element-independent co-rotational formulation degenerated from the proposed method is introduced. The presented formulations are simpler than the existing co-rotational formulations and save computational cost.

4.1 Large rotations

In a 2D plane shown in Figure 4.1, an arbitrary position vector $\boldsymbol{x}$, pointing from the fixed origin to an arbitrary point, can be defined by a given parameter angle α in the global coordinate system as

$$\boldsymbol{x} = \|\boldsymbol{x}\| \begin{Bmatrix} \cos\alpha \\ \sin\alpha \end{Bmatrix} \tag{4.1}$$

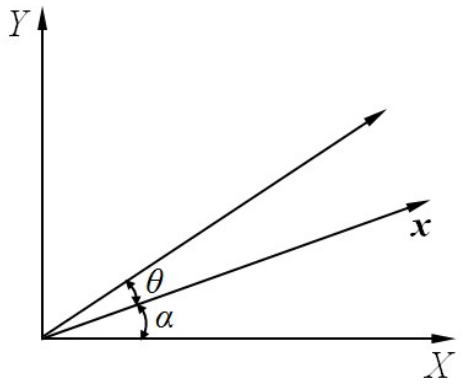

Figure 4.1 A unit vectors in a 2D plane

When the vector $\boldsymbol{x}$ rotates to a new position with an incremental rotation θ, it becomes

$$\boldsymbol{x}^n = \|\boldsymbol{x}\| \begin{Bmatrix} \cos(\alpha+\theta) \\ \sin(\alpha+\theta) \end{Bmatrix} \tag{4.2}$$

The incremental rotation can be directly added to the initial angle regardless of its size since there is only one parameter θ to define the new position. The situation is completely different when incremental rotations occur in a 3D space, due to the non-commutative nature of 3D large rotations.

As shown in Figure 4.2, if there is an arbitrary position vector $\boldsymbol{x}$ in a 3D space having angles α, β, γ between the vector and the X-axis, the Y-axis, and the Z-axis, respectively, then we have

$$\boldsymbol{x} = \|\boldsymbol{x}\| \begin{Bmatrix} \cos\alpha \\ \cos\beta \\ \cos\gamma \end{Bmatrix} \tag{4.3}$$

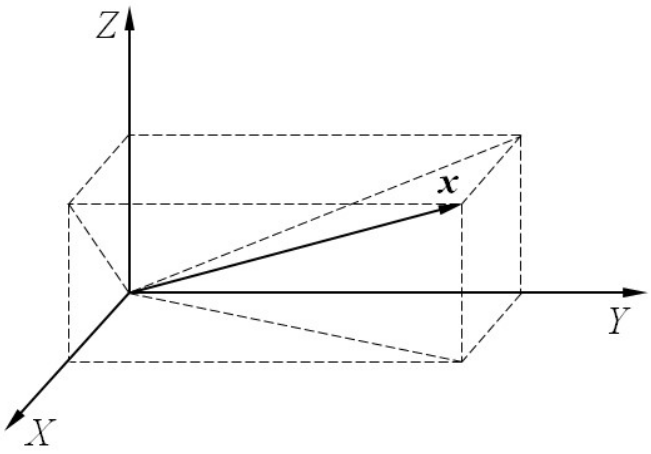

Figure 4.2 A unit vector in a 3D space

When the vector $\boldsymbol{x}$ moves to a new position with an incremental rotation vector $\boldsymbol{\theta} = \{\theta_x \ \theta_y \ \theta_z\}^T$ in the global coordinate system, the new angles between the vector $\boldsymbol{x}^n$ and the global axes could not be updated correctly by directly adding the incremental rotations to the initial angles. Thus, it is a problem to obtain the new vector $\boldsymbol{x}^n$ for an incremental rotation vector $\boldsymbol{\theta}$.

In fact, there is not only one path for an incremental rotation vector to determine the new position of the vector $\boldsymbol{x}$ in a 3D space. The new vector $\boldsymbol{x}^n$ cannot be uniquely defined by incremental rotations including three parameters, while the history of incremental rotations should also be considered. Generally speaking, there are two common methods to define the history of incremental rotations.

4.1.1 Rotations around global axes

This method assumes that the incremental rotations $\boldsymbol{\theta}$ are around the global *X*-axis, *Y*-axis and *Z*-axis, or other orders, sequentially. Similar applications by the approach for beam-column elements are discussed by Chan and Chui (2000) and Chan (1992), whereas for shell elements by Surana (1983).

For example, it is assumed that the vector $\boldsymbol{x}$ rotates around the *X*-axis by θ_x, around the *Y*-axis by θ_y, and around the *Z*-axis by θ_z to a new position and becomes the new vector $\boldsymbol{x}^n$. So, the vector $\boldsymbol{x}$ rotates three times to the final position, and the corresponding transformation matrix for each rotation around the global axes can be given by

$$\boldsymbol{R}(\theta_x)=\begin{bmatrix}1 & 0 & 0\\ 0 & \cos\theta_x & \sin\theta_x\\ 0 & -\sin\theta_x & \cos\theta_x\end{bmatrix} \tag{4.4a}$$

$$\boldsymbol{R}(\theta_y)=\begin{bmatrix}\cos\theta_y & 0 & \sin\theta_y\\ 0 & 1 & 0\\ -\sin\theta_y & 0 & \cos\theta_y\end{bmatrix} \tag{4.4b}$$

$$\boldsymbol{R}(\theta_z)=\begin{bmatrix}\cos\theta_z & \sin\theta_z & 0\\ -\sin\theta_z & \cos\theta_z & 0\\ 0 & 0 & 1\end{bmatrix} \tag{4.4c}$$

Then, the new vector can be determined by

$$\boldsymbol{x}^n=\boldsymbol{R}(\theta_z)\boldsymbol{R}(\theta_y)\boldsymbol{R}(\theta_x)\boldsymbol{x}=\boldsymbol{R}_{xyz}(\boldsymbol{\theta})\boldsymbol{x} \tag{4.5a}$$

with

$$\boldsymbol{R}_{xyz}(\boldsymbol{\theta})=\begin{bmatrix}\cos\theta_y\cos\theta_z & \cos\theta_z\sin\theta_x\sin\theta_y-\cos\theta_x\sin\theta_y & \cos\theta_x\cos\theta_z\sin\theta_y+\sin\theta_x\sin\theta_z\\ \cos\theta_y\sin\theta_z & \cos\theta_x\sin\theta_z+\sin\theta_x\sin\theta_y\cos\theta_z & \cos\theta_x\sin\theta_y\sin\theta_z-\cos\theta_z\sin\theta_x\\ -\sin\theta_y & \cos\theta_y\sin\theta_x & \cos\theta_x\cos\theta_y\end{bmatrix} \tag{4.5b}$$

When the rotation order is changed to be around the *Z*-axis firstly, then the *Y*-axis, then the *X*-axis, the transformation matrix becomes

$$\boldsymbol{R}_{zyx}(\boldsymbol{\theta})=\begin{bmatrix}\cos\theta_y\cos\theta_z & -\cos\theta_y\sin\theta_z & \sin\theta_y\\ \cos\theta_x\sin\theta_z+\sin\theta_x\sin\theta_y\cos\theta_z & \cos\theta_x\cos\theta_z-\sin\theta_x\sin\theta_y\sin\theta_z & -\sin\theta_x\cos\theta_y\\ \sin\theta_x\sin\theta_z-\cos\theta_x\sin\theta_y\cos\theta_z & \sin\theta_x\cos\theta_z+\cos\theta_x\sin\theta_y\sin\theta_z & \cos\theta_x\cos\theta_y\end{bmatrix} \tag{4.5c}$$

It can be seen that different rotation orders with identical rotations lead to different transformation matrices, due to the non-commutative nature of 3D large rotations. In a word, this method is simple and approximate and sometimes the order of the rotations should be discussed in the derivation of geometrically nonlinear analysis scheme.

4.1.2 Rotations around a unit axis

The other technique to derive the transformation matrix is based on assumption that the incremental rotations are around a unit vector by an angle of rotation, which is the Euler theorem (Brannon, 2002) and detailed by Argyris (1982) for its application in geometrically nonlinear finite element method. Figure 4.3 shows a vector $\boldsymbol{x}$ rotates about a unit axis $\boldsymbol{n}$ by a rotation angle θ and becomes the new vector $\boldsymbol{x}^n$. And the unit axis $\boldsymbol{n}$ and the rotation angle θ can be defined by the incremental rotations $\boldsymbol{\theta} = \{\theta_x \ \theta_y \ \theta_z\}^T$ as

$$\boldsymbol{n} = \begin{Bmatrix} n_1 \\ n_2 \\ n_3 \end{Bmatrix} = \begin{Bmatrix} \theta_x / \theta \\ \theta_y / \theta \\ \theta_z / \theta \end{Bmatrix} \tag{4.6a}$$

$$\theta = \sqrt{\theta_x^2 + \theta_y^2 + \theta_z^2} \tag{4.6b}$$

where the rotation angle θ obeys the right-hand screw rule about the unit axis $\boldsymbol{n}$.

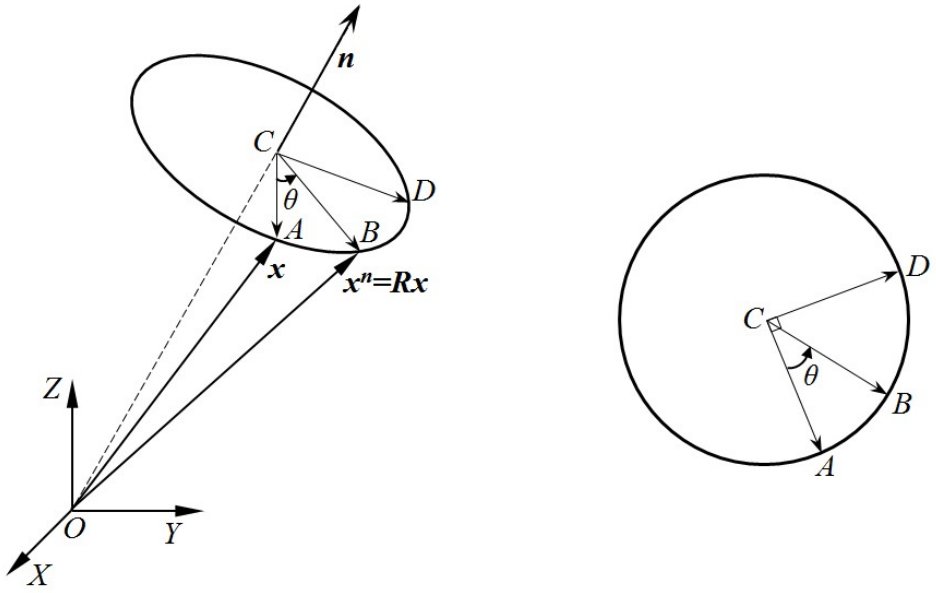

Figure 4.1 Rotation of a vector $\boldsymbol{x}$ around a unit axis $\boldsymbol{n}$ by a rotation angle θ

The projection of $\boldsymbol{x}$ on the unit axis $\boldsymbol{n}$, $\overrightarrow{OA}$, can be given by

$$\overrightarrow{OC} = (\boldsymbol{x} \cdot \boldsymbol{n})\boldsymbol{n} \tag{4.7a}$$

Then, the vector $\overrightarrow{CA}$ on the plane of rotation *CAB* is

$$\overrightarrow{CA} = \overrightarrow{OA} - \overrightarrow{OC} = \boldsymbol{x} - (\boldsymbol{x} \cdot \boldsymbol{n})\boldsymbol{n} \tag{4.7b}$$

The vector $\overrightarrow{CD}$, which is on the plane of rotation *CAB* and perpendicular the plane *OCA*, can be determined by

$$\overrightarrow{CD} = \boldsymbol{n} \times \boldsymbol{x} \tag{4.7c}$$

Then, the vector $\overrightarrow{CB}$ can be obtained by

$$\begin{aligned} \overrightarrow{CB} &= \cos\theta \overrightarrow{CA} + \sin\theta \overrightarrow{CD} \\ &= \cos\theta\left(\boldsymbol{x} - (\boldsymbol{x} \cdot \boldsymbol{n})\boldsymbol{n}\right) + \sin\theta\left(\boldsymbol{n} \times \boldsymbol{x}\right) \end{aligned} \tag{4.7d}$$

Finally, the new vector $\boldsymbol{x}^n$ after rotation is

$$\begin{aligned}\boldsymbol{x}^n &= \boldsymbol{R}\boldsymbol{x} = \overrightarrow{OC} + \overrightarrow{CB} \\ &= (\boldsymbol{x}\cdot\boldsymbol{n})\boldsymbol{n} + \cos\theta\big(\boldsymbol{x} - (\boldsymbol{x}\cdot\boldsymbol{n})\boldsymbol{n}\big) + \sin\theta\big(\boldsymbol{n}\times\boldsymbol{x}\big)\end{aligned} \tag{4.7e}$$

Rearrangement of Eq. (4.7e) gives the so-called Euler-Rodrigues formula as

$$\boldsymbol{R}\boldsymbol{x} = \boldsymbol{n}(\boldsymbol{n}\cdot\boldsymbol{x}) + \cos\theta\big(\boldsymbol{x} - \boldsymbol{n}(\boldsymbol{n}\cdot\boldsymbol{x})\big) + \sin\theta\big(\boldsymbol{n}\times\boldsymbol{x}\big) \tag{4.7f}$$

Substituting the vector identities given in Eqs. (4.8a to 4.8d) into Eq. (4.7f), the Euler-Rodrigues formula can be rewritten in Eq. (4.8e).

$$\boldsymbol{n}\times\boldsymbol{x} = \boldsymbol{N}\boldsymbol{x} \tag{4.8a}$$

$$\boldsymbol{N} = \mathbf{Spin}(\boldsymbol{n}) = \begin{bmatrix} 0 & -n_3 & n_2 \\ n_3 & 0 & -n_1 \\ -n_2 & n_1 & 0 \end{bmatrix} \tag{4.8b}$$

$$\boldsymbol{x} - \boldsymbol{n}(\boldsymbol{n}\cdot\boldsymbol{x}) = -\boldsymbol{n}\times(\boldsymbol{n}\times\boldsymbol{x}) \tag{4.8c}$$

$$\boldsymbol{N} = \mathbf{Spin}(\boldsymbol{n}) = \begin{bmatrix} 0 & -n_3 & n_2 \\ n_3 & 0 & -n_1 \\ -n_2 & n_1 & 0 \end{bmatrix} \tag{4.8d}$$

$$\begin{aligned}\boldsymbol{R}\boldsymbol{x} &= \boldsymbol{n}(\boldsymbol{n}\cdot\boldsymbol{x}) + \big(1-\cos\theta-1\big)\big(\boldsymbol{n}\times(\boldsymbol{n}\times\boldsymbol{x})\big) + \sin\theta\boldsymbol{N}\boldsymbol{x} \\ &= \boldsymbol{n}(\boldsymbol{n}\cdot\boldsymbol{x}) - \boldsymbol{n}\times(\boldsymbol{n}\times\boldsymbol{x}) + \big(1-\cos\theta\big)\big(\boldsymbol{n}\times(\boldsymbol{n}\times\boldsymbol{x})\big) + \sin\theta\boldsymbol{N}\boldsymbol{x} \\ &= \boldsymbol{x} + \big(1-\cos\theta\big)\boldsymbol{N}^2\boldsymbol{x} + \sin\theta\boldsymbol{N}\boldsymbol{x}\end{aligned} \tag{4.8e}$$

Finally, the transformation matrix $\boldsymbol{R}$ can be given by

$$\boldsymbol{R}(\boldsymbol{\theta}) = \boldsymbol{I} + \sin\theta\boldsymbol{N} + \big(1-\cos\theta\big)\boldsymbol{N}^2 \tag{4.8f}$$

The operational symbol **Spin(·)** in Eq. (4.8d) refers to a skew-symmetric spin tensor from a three-dimensional rotation vector, while the transformation matrix $\boldsymbol{R}$ is also regarded as the rotation matrix and called the Rodrigues-Cayley representation.

In turn, the rotation vector $\boldsymbol{\theta}$ can be obtained from the rotation matrix $\boldsymbol{R}$. It can be noted that

$$\boldsymbol{N} = \frac{\boldsymbol{R} - \boldsymbol{R}^T}{2\sin\theta} \tag{4.9a}$$

Thus, the corresponding rotation vector can be evaluated as follows,

$$\boldsymbol{\theta}(\boldsymbol{R}) = \begin{Bmatrix} \theta_x \\ \theta_y \\ \theta_z \end{Bmatrix} = \frac{\theta}{2\sin\theta} \begin{Bmatrix} R_{32} - R_{23} \\ R_{13} - R_{31} \\ R_{21} - R_{12} \end{Bmatrix} = \frac{\arcsin\tau}{2\tau} \begin{Bmatrix} R_{32} - R_{23} \\ R_{13} - R_{31} \\ R_{21} - R_{12} \end{Bmatrix} \tag{4.9b}$$

in which $\tau = \sqrt{(R_{23}-R_{32})^2 + (R_{13}-R_{31})^2 + (R_{21}-R_{12})^2}$ and R_{ij} (i,j=1,2,3) is the entry of rotation matrix $\boldsymbol{R}$. In the equation, the range of θ is [0, 90].

It should be noted that numerical instability would occur when θ is closed to zero, so the Taylor expansion of Equation (4.9b) is adopted. In program, when $\theta \le 0.05$, the coefficient in Equation (4.9b) becomes

$$\frac{\theta}{2\sin\theta} \approx \frac{1}{2} + \frac{1}{12}\theta^2 + \frac{7}{720}\theta^4 \tag{4.10}$$

This method is used more often in recent years by many researchers for geometrically nonlinear finite element method, such as the TL, UL and EICR formulations. The co-rotational methods with the 3D rotation description in beam, triangular and quadrilateral shell elements have been detailed by Nour-Omid and Rankin (1991) and

Felippa and Haugen (2005), whereas the 3D rotation description is also used in the present studies.

4.2 Conventional co-rotational formulations

Three common element-independent co-rotational (EICR) formulations are reviewed and introduced for comparison with the proposed methods in the thesis. Different from the classical total Lagrangian (TL) and updated Lagrangian (UL) formulations, the geometric stiffness of the EICR algorithm is formulated by the nodal internal forces rather than the stresses at element integration points. Thus, its geometric stiffness formulation is not directly related to stresses and displacement interpolations, and this is the basis for element-independence of these formulations. Also, due to the avoidance of numerical integration for the geometric stiffness, the EICR formulation can save computational cost when compared with the TL and UL formulations. Strictly speaking, not all of these three common EICR formulations are completely element-independent due to various problems. However, they have the identical property that their geometric stiffness matrices are all explicit and formed by nodal internal forces, and they all need to derive the variations of rigid body rotations for the local element frame.

4.2.1 General formulation

The concept of “element-independent co-rotational (EICR) formulation” was first introduced by Rankin and Brogan (1986) and improved by Nour-Omid and Rankin

(1991). A detailed discussion of the method was given by Felippa and Haugen (2005). The pertaining studies and applications of the general EICR formulation for different shell elements allowing for geometrical nonlinearity or material nonlinearity are numerous, including the references (Battini and Pacoste, 2006; Eriksson and Pacoste, 2002; Pacoste, 1998; Skallerud and Haugen, 1999). Recently, the approach was still used by Zhou *et al.* (2016) to test the performance of several existing linear shell elements in geometrically nonlinear analyses.

As mentioned previously, the basis of the method is to separate rigid body motions from pure deformations. So, the existing linear elements could be utilized to describe pure deformational part and extended to geometrically nonlinear analyses by the EICR formulation directly. The derivation of the EICR algorithm is strict and complete, involved with complicated operations. A brief introduction of the formulation is given in the following.

Considering a shell element with the initial configuration C_0, its global coordinates are $\boldsymbol{x}_i^g$ at each node i. Then, the element has a new configuration C_n after movements and deformations, while the node i has a total translation vector $\boldsymbol{u}_i^g$ and a total rotation matrix $\boldsymbol{R}_i^g$ in the global coordinate system. In addition to the global coordinate system, there are two additional local coordinate systems for the configuration C_0 and C_n attached to the shell element, whereas their local-to-global transformation matrices are $\boldsymbol{T}_0$ and $\boldsymbol{T}_n$ respectively. Thus, the local deformational translation vector at each node can be given by

$$\tilde{\boldsymbol{u}}_i^d = \boldsymbol{T}_n\left(\boldsymbol{u}_i^g + \boldsymbol{x}_i^g - \boldsymbol{x}_o^g - \boldsymbol{u}_o^g\right) - \boldsymbol{T}_0\left(\boldsymbol{x}_i^g - \boldsymbol{x}_o^g\right) \tag{4.11}$$

in which $\boldsymbol{x}_o^g$ and $\boldsymbol{u}_o^g$ are the global coordinates and the total translation vector of the origin of the local coordinate system respectively. Additionally, the tilde ˜ in the parameters means that they are based on the local coordinate system at configuration C_n, and the superscript "*d*" means the variables belong to local pure deformational part.

In terms of the local deformational rotation matrix attached to the node *i*, it can be derived by the theory of large rotation introduced in Section 4.1.2 as follows,

$$\tilde{\boldsymbol{R}}_i^d = \boldsymbol{T}_n \boldsymbol{R}_i^g \boldsymbol{T}_0^T \tag{4.12}$$

To obtain the tangent stiffness matrix of the shell element, the relationship between the variations of the global displacement vector and the local deformational displacement vector should to be established. Then, taking a variation of Eq. (4.11) gives

$$\begin{aligned} \delta\tilde{\boldsymbol{u}}_i^d &= \delta\boldsymbol{T}_n\left(\boldsymbol{u}_i^g + \boldsymbol{x}_i^g - \boldsymbol{x}_o^g - \boldsymbol{u}_o^g\right) + \boldsymbol{T}_n\left(\delta\boldsymbol{u}_i^g - \delta\boldsymbol{u}_o^g\right) \\ &= \delta\boldsymbol{T}_n\boldsymbol{T}_n^T\tilde{\boldsymbol{x}}_i + \left(\delta\tilde{\boldsymbol{u}}_i - \delta\tilde{\boldsymbol{u}}_o\right) \\ &= \mathbf{Spin}(\tilde{\boldsymbol{x}}_i)\delta\tilde{\boldsymbol{\omega}} + \left(\delta\tilde{\boldsymbol{u}}_i - \delta\tilde{\boldsymbol{u}}_o\right) \end{aligned} \tag{4.13}$$

in which $\tilde{\boldsymbol{x}}_i$ is the node coordinates based on the configuration C_n, and $\delta\tilde{\boldsymbol{\omega}}$ is the variation of rigid body rotation vector of the shell element based on the configuration C_n.

Taking a variation of Eq. (4.12), we have

$$\begin{aligned} \delta\tilde{\boldsymbol{R}}_i^d &= \delta\boldsymbol{T}_n \boldsymbol{R}_i \boldsymbol{T}_0^T + \boldsymbol{T}_n \delta\boldsymbol{R}_i \boldsymbol{T}_0^{\mathrm{T}} \\ &= \left[\mathbf{Spin}\left(\delta\tilde{\boldsymbol{\omega}}_i\right) - \mathbf{Spin}\left(\delta\tilde{\boldsymbol{\omega}}\right)\right]\tilde{\boldsymbol{R}}_i^d \end{aligned} \tag{4.14}$$

With the equation

$$\delta \tilde{\boldsymbol{R}}_i^d = \mathbf{Spin}\left(\delta \tilde{\boldsymbol{\omega}}_i^d\right) \tilde{\boldsymbol{R}}_i^d \tag{4.15}$$

we have

$$\delta \tilde{\boldsymbol{\omega}}_i^d = \delta \tilde{\boldsymbol{\omega}}_i - \delta \tilde{\boldsymbol{\omega}} \tag{4.16}$$

where $\delta \tilde{\boldsymbol{\omega}}_i^d$ and $\delta \tilde{\boldsymbol{\omega}}_i$ are the variations of the deformational and total rotation vectors at the node i based on the local coordinate system at the configuration C_{n} respectively.

Combining all the translations and rotations shown in Eq. (4.14) and Eq. (4.16) into the elemental displacement vectors, we can obtain the relationship as follows,

$$\delta \tilde{\boldsymbol{d}}^d = \tilde{\boldsymbol{P}} \delta \tilde{\boldsymbol{d}} \tag{4.17}$$

in which $\delta \tilde{\boldsymbol{d}}^d$ and $\delta \tilde{\boldsymbol{d}}$ are the deformational and total displacement vectors based on the configuration C_n respectively. The matrix $\tilde{\boldsymbol{P}}$ is the projector operator obtained by Eqs. (4.13) and (4.16) which reflects the changes of element dimensions between the configuration C_0 and C_n.

In addition, it should be noted that the local deformational rotations $\delta \tilde{\boldsymbol{\omega}}_i^d$ are non-additive, which means that they cannot be directly used to derive the internal forces by the stiffness matrix of the local shell element. Thus, they should be modified to be additive and corresponding to the local deformational internal forces in the following,

$$\delta \tilde{\boldsymbol{d}}^d = \tilde{\boldsymbol{H}} \tilde{\boldsymbol{P}} \delta \tilde{\boldsymbol{d}} \tag{4.18}$$

in which the matrix $\tilde{\boldsymbol{H}}$ is to transform non-additive rotations into the additive ones. The detailed derivation and expression of the matrix $\tilde{\boldsymbol{H}}$ can be found in the publications by Felippa and Haugen (2005) and Skallerud and Haugen (1999). However, it is not used in the proposed co-rotational formulation, since it has little influence on results.

Finally, the relationship between the variations of the local deformational displacement vector and global total displacement vector can be given by

$$\delta\tilde{\boldsymbol{d}}^{d} = \tilde{\boldsymbol{H}}\tilde{\boldsymbol{P}}\boldsymbol{T}\delta\boldsymbol{d} \tag{4.19}$$

in which the matrix $\boldsymbol{T}$ is composed of $\boldsymbol{T}_n$ along diagonal.

Through the principle of virtual work, the corresponding transformation of internal force vectors between these two coordinate systems can be obtained by

$$\boldsymbol{f} = \boldsymbol{T}^{T}\tilde{\boldsymbol{P}}^{T}\tilde{\boldsymbol{H}}^{T}\tilde{\boldsymbol{f}}^{d} \tag{4.20}$$

Then, the global tangent stiffness can be obtained by taking a variation of Eq. (4.20) as

$$\begin{aligned}\delta\boldsymbol{f} &= \delta\boldsymbol{T}^{T}\tilde{\boldsymbol{P}}^{T}\tilde{\boldsymbol{H}}^{T}\tilde{\boldsymbol{f}}^{d} + \boldsymbol{T}^{T}\delta\tilde{\boldsymbol{P}}^{T}\tilde{\boldsymbol{H}}^{T}\tilde{\boldsymbol{f}}^{d} + \boldsymbol{T}^{T}\tilde{\boldsymbol{P}}^{T}\delta\tilde{\boldsymbol{H}}^{T}\tilde{\boldsymbol{f}}^{d} + \boldsymbol{T}^{T}\tilde{\boldsymbol{P}}^{T}\tilde{\boldsymbol{H}}^{T}\delta\tilde{\boldsymbol{f}}^{d} \\ &= \left(\boldsymbol{K}_{GR} + \boldsymbol{K}_{GP} + \boldsymbol{K}_{GM} + \boldsymbol{K}_{M}\right)\delta\boldsymbol{d}\end{aligned} \tag{4.21}$$

where $\boldsymbol{K}_{GR}$ is the rotational geometric stiffness, $\boldsymbol{K}_{GP}$ the equilibrium projection geometric stiffness, $\boldsymbol{K}_{GM}$ the moment-correction geometric stiffness and $\boldsymbol{K}_{M}$ the material stiffness.

Some researchers omit the matrix $\tilde{\boldsymbol{H}}$ and the moment-correction geometric stiffness $\boldsymbol{K}_{GM}$ to simplify the general EICR formulation. The omission may have little impact on accuracy when a single load-step is not large. In addition, it is worth noting that the tangent stiffness matrix in Eq. (4.21) is non-symmetric, which is not suitable for the commonly used symmetric solver. However, Nour-Omid and Rankin (1991) proved that the symmetric part of the tangent stiffness allows Newton iteration to retain its quadratic rate of convergence.

4.2.2 Co-rotational method based on load perturbation

Another co-rotational method used in a flat triangular shell element was presented by Levy and Gal (2001), Levy and Spillers (2003) and Gal and Levy (2006). In their method, the derivation of the geometric stiffness matrix is somewhat different but consistent with the approach described in Section 4.2.1, in which the formulation is based on the load perturbation of the linear equilibrium equations for a flat triangular shell element in its local coordinate system. In addition, the local flat triangular shell element combines the constant stress triangular (CST) flat triangular membrane element introduced in the book wrote by Zienkiewicz (1977) and the discrete Kirchhoff flat triangular (DKT) plate element proposed by Batoz *et al.* (1980b).

The local geometric stiffness matrix of the flat triangular shell element is derived as the gradient of the nodal force vector and divided into three parts as follows,

$$\left[\mathbf{K}_G^e\right]_{TOTAL}^{shell} = \left[\mathbf{K}_G^e\right]_{IP}^{mem} + \left[\mathbf{K}_G^e\right]_{IP}^{plate} + \left[\mathbf{K}_G^e\right]_{OP}^{shell} \tag{4.22}$$

in which the three matrices on the right of Eq. (4.22) are the in-plane geometric stiffness matrix of the membrane element, the in-plane geometric stiffness matrix of the plate element and the out-of-plane geometric stiffness matrix of the shell element, respectively. Specifically, the first two parts are due to the changes of the dimensions of the flat triangular membrane and plate elements respectively, whereas the physical meanings of their sum are the same as the equilibrium projection geometric stiffness $\boldsymbol{K}_{GP}$ in Eq. (4.21), although their expressions are different. The matrix $\tilde{\boldsymbol{H}}$, which is used to transform non-additive rotations into additive ones, is omitted, so the moment-correction geometric stiffness does not exist in Eq. (4.22). Also, the out-of-plane geometric stiffness matrix of the shell element in Eq. (4.22) is equal to the rotational geometric stiffness $\boldsymbol{K}_{GR}$ in Eq. (4.21) when they are transformed in the same coordinate system and both are due to the rigid body rotations of the shell element on its nodal forces.

Compared with the first co-rotational formulation introduced in Section 4.2.1, this formulation has a drawback that the geometric stiffness matrices due to the changes of the dimensions of the membrane and plate elements are not element-independent since the in-plane geometric stiffness matrices are related to the formulations of the membrane and plate elements. But the method provides another thought to derive the geometric stiffness by taking the gradient nodal forces through load perturbation of the shell element, which is easier to visualize through physical interpretation than the first method. Further, the derivation contributes to the proposed co-rotational method.

4.2.3 Co-rotational method without removing rigid body motions completely

This is another EICR algorithm for shell element frame which was firstly introduced by Izzuddin (2005), whereas the pertaining applications for many different shell element studies can be found in the references (Izzuddin and Liang, 2016; Li et al., 2011b; Li and Vu-Quoc, 2007; Li et al., 2013; Liang and Izzuddin, 2015, 2016). Unlike the former two co-rotational formulations, it does not extract pure deformations from total deformations completely. Like the first co-rotational method, this algorithm starts from the establishment of the relationship between the local and global variables, but the local deformations in the formulation are not pure. For convenient comparison between these two different co-rotational methods, the formulation presented by Izzuddin and Liang (2016) is introduced with the notations used in the first co-rotational formulation.

Firstly, the relationships between the local and global nodal variables are given by

$$\tilde{\boldsymbol{u}}_i^d = \boldsymbol{T}_n\left(\boldsymbol{u}_i^g + \boldsymbol{x}_i^g - \boldsymbol{x}_o^g\right) - \boldsymbol{T}_0\left(\boldsymbol{x}_i^g - \boldsymbol{x}_o^g\right) \tag{4.23a}$$

$$\tilde{\boldsymbol{r}}_i = \overline{\boldsymbol{T}}_n \boldsymbol{n}_i\,,\quad \overline{\boldsymbol{T}}_n = [\boldsymbol{e}_x \;\; \boldsymbol{e}_y]^T \tag{4.23b, c}$$

where the subscript *i* means that the variables belong to the node *i*, the superpose tilde "~" in the variables means that they are local; $\tilde{\boldsymbol{r}}_i = \left\{\tilde{\theta}_{xi} \;\; \tilde{\theta}_{yi}\right\}^T$ represents the two rotations at the node *i* in the local *yz* and *xz* planes, respectively; $\boldsymbol{n}_i$ represents the normal vector at the node *i* and is related to global rotations; The local-to-global transformation matrix $\overline{\boldsymbol{T}}_n$ used in Eq. (4.23b) consists of the two triad vectors along

the local *x*-axis and *y*-axis, while the drilling rotations about the local *z*-axis are not taken into account.

The following derivation is identical to the first classical method and the relationship between the local and global internal forces is given by

$$\boldsymbol{f} = \boldsymbol{L}^T \tilde{\boldsymbol{f}} \tag{4.24a}$$

$$\boldsymbol{L} = \frac{\partial \tilde{\boldsymbol{d}}}{\partial \boldsymbol{d}^T} \tag{4.24b}$$

in which $\tilde{\boldsymbol{d}}$ and $\boldsymbol{d}$ are the displacement vectors in the local and global coordinate system respectively.

Thus, the element tangent stiffness matrix in the global coordinate system can be obtained as follows,

$$\boldsymbol{K}_t^g = \frac{\partial \boldsymbol{f}}{\partial \boldsymbol{d}^T} = \boldsymbol{L}^T \tilde{\boldsymbol{K}}_e \boldsymbol{L} + \frac{\partial \boldsymbol{L}^T}{\partial \boldsymbol{d}^T} \boldsymbol{f} \tag{4.25}$$

in which $\tilde{\boldsymbol{K}}_e$ is the local material stiffness matrix.

Compared with Eq. (4.11) used in the general method, Eq. (4.23) neglects the global translations of the origin of the local coordinate system. Also, the large rotation tensor is not used and the drilling rotations are not considered. Thus, it very clearly shows that the co-rotational algorithm is only suitable for shell elements without drilling rotations and the local deformations are not pure. Actually, using the local deformations shown in Eq. (4.23) to obtain the local internal forces is also correct in some situations since the local material stiffness matrix allows for small rigid body

rotations of the element. However, the co-rotational formulation may not have good performance in problems involved with large rotations in a single large load-step.

Additionally, the global tangent stiffness matrix in Eq. (4.25) is seemingly more concise than the first method, but this is not true because their derivation processes are similar. Except for the difference on the local deformations, this method simply uses one single transformation matrix to establish the relationship between the local and global coordinate systems, while the general method divides the transformation matrix into several parts with concise physical interpretation. In fact, in this formulation, the derivations of the transformation matrix and the geometric stiffness matrix are still very complicated as well as the general EICR formulation. Although this method has some limitations listed above, it produces a symmetric tangent stiffness matrix, which is a great advance in terms of storage requirement and computational efficiency.

4.3 A novel EICR formulation for triangular shell elements

Different from the existing co-rotational methods introduced in Section 4.2, the proposed EICR method takes advantage of the pure deformational method proposed in Chapter 3. In the pure deformational method, the stiffness matrices of the membrane and plate elements are constructed on the basis of the basic coordinate system without rigid body motions and further transformed into the local coordinate system allowing for rigid body motions. Thus, the definition of the local coordinate system is identical to the one used in Chapter 3, while the local frame attached to a flat triangular shell element is defined as shown in Figure 4.2. The triad vectors for

the local coordinate system (xyz) of a shell element are expressed with the nodal coordinates $\boldsymbol{x}_i^g = \left\{ x_i^g \quad y_i^g \quad z_i^g \right\}^T$ (i=1,2,3) in the global coordinate system ($x^g y^g z^g$) as

$$\boldsymbol{e}_x = \frac{\boldsymbol{x}_2^g - \boldsymbol{x}_1^g}{\left\| \boldsymbol{x}_2^g - \boldsymbol{x}_1^g \right\|} \tag{4.26a}$$

$$\boldsymbol{e}_z = \boldsymbol{e}_x \times \frac{\boldsymbol{x}_3^g - \boldsymbol{x}_1^g}{\left\| \boldsymbol{x}_3^g - \boldsymbol{x}_1^g \right\|} \tag{4.26b}$$

$$\boldsymbol{e}_y = \boldsymbol{e}_z \times \boldsymbol{e}_x \tag{4.26c}$$

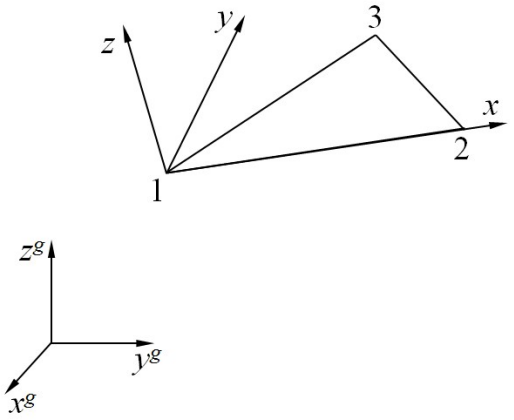

Figure 4.2 Definition of the local coordinate system of a triangular shell element

Then, the local-to-global transformation matrix of a flat triangular shell element can be given by

$$\boldsymbol{T}_e = \left[\boldsymbol{e}_x \quad \boldsymbol{e}_y \quad \boldsymbol{e}_z \right]^T \tag{4.27}$$

As the origin of the local coordinate system is set to the node 1, the corner node coordinates in the local coordinate system (*xyz*) can be given by

$$\boldsymbol{x}_i = \boldsymbol{T}_e \left(\boldsymbol{x}_i^g - \boldsymbol{x}_1^g \right) \quad (i=1,2,3) \tag{4.28}$$

in which $\boldsymbol{x}_i = \{x_i \;\; y_i \;\; z_i\}^T$. Also, it can be noted that $x_1 = y_1 = z_1 = z_2 = z_3 = 0$.

Before the derivation of the proposed EICR formulation, the relationship between the global and basic coordinate systems should be established. In Chapter 3, Eq. (3.42b) has introduced how to transform the internal forces from the basic coordinate system into the local coordinate system. Then, the internal forces in the global coordinate system can be given by

$$\boldsymbol{f}^g = \boldsymbol{T}^T \boldsymbol{L}^T \tilde{\boldsymbol{f}} \tag{4.29a}$$

$$\boldsymbol{f}^g = \left\{ \boldsymbol{f}_1^{gT} \;\; \boldsymbol{f}_2^{gT} \;\; \boldsymbol{f}_3^{gT} \right\}^T \tag{4.29b}$$

$$\boldsymbol{f}_i^g = \left\{ f_{xi}^g \;\; f_{yi}^g \;\; f_{zi}^g \;\; m_{xi}^g \;\; m_{yi}^g \;\; m_{zi}^g \right\}^T \tag{4.29c}$$

in which the transformation matrix $\boldsymbol{T}$ is composed of 6 matrices $\boldsymbol{T}_e$ in Eq. (4.27) along diagonal. The symbol $\boldsymbol{f}^g$ is the internal force vector in the global coordinate system and the corresponding displacement vector in the global coordinate system is detailed as follows,

$$\boldsymbol{d}^g = \left\{ \boldsymbol{d}_1^{gT} \;\; \boldsymbol{d}_2^{gT} \;\; \boldsymbol{d}_3^{gT} \right\}^T \tag{4.29d}$$

$$\boldsymbol{d}_i^g = \left\{ u_{xi}^g \;\; u_{yi}^g \;\; u_{zi}^g \;\; \theta_{xi}^g \;\; \theta_{yi}^g \;\; \theta_{zi}^g \right\}^T \tag{4.29e}$$

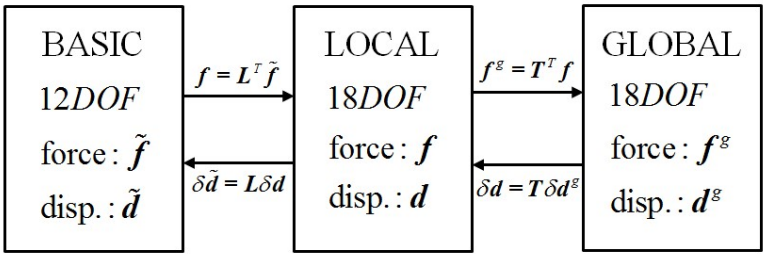

Figure 4.3 Relationships between three coordinate systems

Thus, the relationships between these different systems by making use of the previous equations are concluded in Figure 4.3.

Different from the general EICR formulation with strict derivation introduced in Section 4.2.1, the non-additive property of the pure deformational rotations is omitted herein since it has little influence on results. The omission is also adopted by many other kinds of co-rotational formulations.

4.3.1 Tangent stiffness

Following the derivation of the general EICR formulation introduced in Section 4.2.1, taking a variation of Eq. (4.29a) gives

$$\delta \boldsymbol{f}^g = \boldsymbol{T}^T \boldsymbol{L}^T \delta \tilde{\boldsymbol{f}} + \delta \boldsymbol{T}^T \boldsymbol{L}^T \tilde{\boldsymbol{f}} + \boldsymbol{T}^T \delta \boldsymbol{L}^T \tilde{\boldsymbol{f}} \tag{4.30}$$

where the first term leads to the material stiffness, and the last two terms refer to the changes of rigid body motions and the changes of element dimensions respectively.

Moreover, Eq. (4.30) can yield

$$\delta \boldsymbol{f}^g = \boldsymbol{T}^T \left(\boldsymbol{K}_e + \boldsymbol{K}_g^r + \boldsymbol{K}_g^m + \boldsymbol{K}_g^p \right) \boldsymbol{T} \delta \boldsymbol{d}^g \tag{4.31}$$

in which $\boldsymbol{K}_e$ is the material stiffness matrix of a triangular shell element based on the local coordinate system; $\boldsymbol{K}_g^r$ is due to the rigid body motions of the element, corresponding to the second term in Eq. (4.30); $\boldsymbol{K}_g^m$ and $\boldsymbol{K}_g^p$ are caused by the changes of dimensions of the membrane and plate elements respectively, while the sum of them similar to the third term in Eq. (4.30).

However, different from the general EICR formulation, the proposed co-rotational method adopts the derivation similar to the method introduced in Section 4.2.2, in which the local geometric stiffness is derived by taking the gradient of nodal forces through the load perturbation of a shell element. In addition, the pure deformational method is integrated to make the derivation and formulation simpler than the other co-rotational methods. In the next, every part of the tangent stiffness in the local coordinate system shown in Eq. (4.31) is presented.

4.3.1.1 Material stiffness

In terms of the material stiffness matrix of a triangular shell element in the local coordinate system, $\boldsymbol{K}_e$, the proposed pure deformational method in Chapter 3 is also used here. When the stiffness matrices of a membrane element and a plate element in the basic coordinate system, $\tilde{\boldsymbol{K}}_m$ and $\tilde{\boldsymbol{K}}_p$, are obtained, they can be transformed into the local coordinate system as follows,

$$\boldsymbol{K}_m = \boldsymbol{L}_m{}^T \tilde{\boldsymbol{K}}_m \boldsymbol{L}_m \tag{4.32a}$$

$$\boldsymbol{K}_p = \boldsymbol{L}_p{}^T \tilde{\boldsymbol{K}}_p \boldsymbol{L}_p \tag{4.32b}$$

in which the matrices $\boldsymbol{L}_m$ and $\boldsymbol{L}_p$ are the basic-to-local transformation matrices for a membrane element and a plate element respectively.

It should be noted that the stiffness matrices $\tilde{\boldsymbol{K}}_m$ and $\tilde{\boldsymbol{K}}_p$ are calculated based on the initial dimensions of the triangular element and fixed in the whole progress of the geometrically nonlinear analysis. However, the basic-to-local transformation matrices $\boldsymbol{L}_m$ and $\boldsymbol{L}_p$ should be updated in accordance with the local nodal coordinates at the current time, so that the local material stiffness can consider the changes of element dimensions. In addition, it should be noted that the transformation matrices $\boldsymbol{L}_m$ and $\boldsymbol{L}_p$ have the same function as the projector matrix used in the general EICR formulation introduced in Section 4.2.1. However, the general method uses the projector matrix to keep the element self-equilibrated and modify the variables which are affected by the changes of element dimensions, while the transformation matrices $\boldsymbol{L}_m$ and $\boldsymbol{L}_p$ in the proposed method are utilized to generate the variables which are not included in the basic coordinate system. Thus, the proposed method is more concise and simpler than the general method. In terms of each part of the geometric stiffness, they should also be updated with the changes of element dimensions.

4.3.1.2 Geometric stiffness due to rigid body rotations of the element

In the local coordinate system, the variations of the local forces and moments at the node *i* due to small rigid body rotations of the element are given by Goldstein (1950) as follows,

$$\delta \boldsymbol{n}_i = \delta\boldsymbol{\omega} \times \boldsymbol{n}_i = -\mathbf{Spin}(\boldsymbol{n}_i)\delta\boldsymbol{\omega} \tag{4.33a}$$

$$\delta \boldsymbol{m}_i = \delta\boldsymbol{\omega} \times \boldsymbol{m}_i = -\mathbf{Spin}(\boldsymbol{m}_i)\delta\boldsymbol{\omega} \tag{4.33b}$$

in which $\boldsymbol{n}_i = \left\{ f_{xi} \;\; f_{yi} \;\; f_{zi} \right\}^T$ and $\boldsymbol{m}_i = \left\{ m_{xi} \;\; m_{yi} \;\; m_{zi} \right\}^T$ (i=1,2,3) are the internal forces and moments at the node i respectively; $\delta\boldsymbol{\omega} = \left\{ \delta\omega_x \;\; \delta\omega_y \;\; \delta\omega_z \right\}^T$ is the variation of rigid body rotation vector based on the local coordinate system and its entries are shown in Eqs. (3.4) and (3.21).

Combining all the local nodal forces and moments into the local internal force vector of a triangular shell element and taking advantage of Eqs. (4.33) give

$$\delta \boldsymbol{f} = \text{-}\boldsymbol{A} \cdot \boldsymbol{G} \delta \boldsymbol{d} = \boldsymbol{K}_g^r \delta \boldsymbol{d} \tag{4.34a}$$

with

$$\boldsymbol{f} = \left\{ \boldsymbol{n}_1^T \;\; \boldsymbol{m}_1^T \;\; \boldsymbol{n}_2^T \;\; \boldsymbol{m}_2^T \;\; \boldsymbol{n}_3^T \;\; \boldsymbol{m}_3^T \right\}^T \tag{4.34b}$$

in which the local displacement vector of a triangular shell element, $\boldsymbol{d}$, can be detailed by

$$\boldsymbol{u}_i = \left\{ u_{xi} \;\; u_{yi} \;\; u_{zi} \right\}^T \tag{4.34c}$$

$$\boldsymbol{\theta}_i = \left\{ \theta_{xi} \;\; \theta_{yi} \;\; \theta_{zi} \right\}^T \tag{4.34d}$$

$$\boldsymbol{d} = \left\{ \boldsymbol{u}_1^T \;\; \boldsymbol{\theta}_1^T \;\; \boldsymbol{u}_2^T \;\; \boldsymbol{\theta}_2^T \;\; \boldsymbol{u}_3^T \;\; \boldsymbol{\theta}_3^T \right\}^T \tag{4.34e}$$

Also, the matrix $\boldsymbol{A}$ containing the internal forces at the current time is

$$\boldsymbol{A}=\begin{bmatrix}\mathbf{Spin}(\boldsymbol{n}_1)\\ \mathbf{Spin}(\boldsymbol{m}_1)\\ \mathbf{Spin}(\boldsymbol{n}_2)\\ \mathbf{Spin}(\boldsymbol{m}_2)\\ \mathbf{Spin}(\boldsymbol{n}_3)\\ \mathbf{Spin}(\boldsymbol{m}_3)\end{bmatrix} \tag{4.35a}$$

and the matrix $\boldsymbol{G}$ connecting the variations of rigid body rotations to the variations of local displacements can be given by

$$\boldsymbol{G}=\begin{bmatrix}\dfrac{\partial\boldsymbol{\omega}}{\partial\boldsymbol{u}_1^T} & \dfrac{\partial\boldsymbol{\omega}}{\partial\boldsymbol{\theta}_1^T} & \dfrac{\partial\boldsymbol{\omega}}{\partial\boldsymbol{u}_2^T} & \dfrac{\partial\boldsymbol{\omega}}{\partial\boldsymbol{\theta}_2^T} & \dfrac{\partial\boldsymbol{\omega}}{\partial\boldsymbol{u}_2^T} & \dfrac{\partial\boldsymbol{\omega}}{\partial\boldsymbol{\theta}_3^T}\end{bmatrix} \tag{4.35b}$$

Substituting Eqs. (3.4) and (3.21) into the matrix $\boldsymbol{G}$, we have

$$\frac{\partial\boldsymbol{\omega}}{\partial\boldsymbol{u}_1^T}=\begin{bmatrix}0 & 0 & \dfrac{x_3-x_2}{x_2y_3}\\ 0 & 0 & \dfrac{1}{x_2}\\ 0 & -\dfrac{1}{x_2} & 0\end{bmatrix} \tag{4.35c}$$

$$\frac{\partial\boldsymbol{\omega}}{\partial\boldsymbol{u}_2^T}=\begin{bmatrix}0 & 0 & -\dfrac{x_3}{x_2y_3}\\ 0 & 0 & -\dfrac{1}{x_2}\\ 0 & \dfrac{1}{x_2} & 0\end{bmatrix} \tag{4.35d}$$

$$\frac{\partial \boldsymbol{\omega}}{\partial \boldsymbol{u}_3^T} = \begin{bmatrix} 0 & 0 & \dfrac{1}{y_3} \\ 0 & 0 & 0 \\ 0 & 0 & 0 \end{bmatrix} \tag{4.35e}$$

$$\frac{\partial \boldsymbol{\omega}}{\partial \boldsymbol{\theta}_1^T} = \frac{\partial \boldsymbol{\omega}}{\partial \boldsymbol{\theta}_2^T} = \frac{\partial \boldsymbol{\omega}}{\partial \boldsymbol{\theta}_3^T} = \mathbf{0}_{3\times 3} \tag{4.35f}$$

Finally, the geometric stiffness matrix of a flat triangular shell element due to rigid body rotations of the element in the local coordinate system, $\boldsymbol{K}_g^r$, can be determined.

4.3.1.3 Geometric stiffness due to changes of dimensions of a membrane element

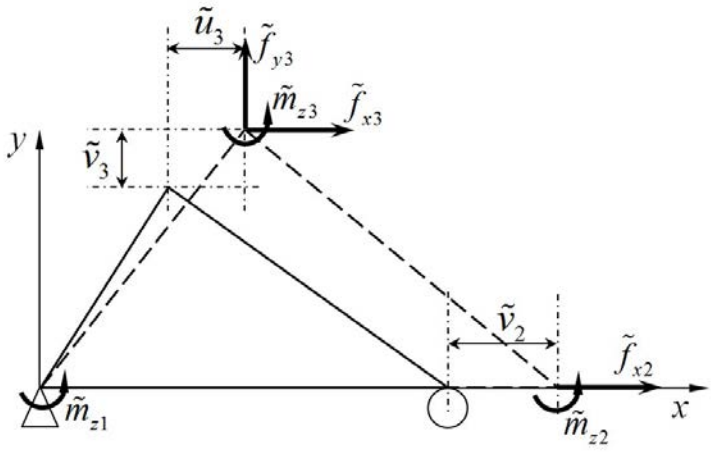

Figure 4.4 A pure deformational membrane element

Figure 4.4 depicts the pure deformations of a membrane element due to the applied forces and moments in the basic coordinate system. In the model, the basic internal forces $\tilde{\boldsymbol{f}}$ can be regarded as the constant action forces, while the reaction forces varied with the changes of element dimensions to keep the element-equilibrium.

Hence, the gradients of the reaction forces can be used to derive the geometric stiffness due to the changes of element dimensions.

For the current configuration of a membrane element, the equilibrium equations can be established by

$$\sum f_x = 0: \quad f_{x1} + \tilde{f}_{x2} + \tilde{f}_{x3} = 0 \tag{4.36a}$$

$$\sum f_y = 0: \quad f_{y1} + f_{y2} + \tilde{f}_{y3} = 0 \tag{4.36b}$$

$$\sum m_z = 0 \, at \, the \, node \, 1: \quad f_{y2}x_2 - \tilde{f}_{x3}y_3 + \tilde{f}_{y3}x_3 + \sum_{i=1}^{3} \tilde{m}_{zi} = 0 \tag{4.36c}$$

After deformation, the equilibrium equations become

$$\sum fx = 0: \quad f_{x1}^{n+1} + \tilde{f}_{x2} + \tilde{f}_{x3} = 0 \tag{4.37a}$$

$$\sum fy = 0: \quad f_{y1}^{n+1} + f_{y2}^{n+1} + \tilde{f}_{y3} = 0 \tag{4.37b}$$

$$\sum m_z = 0 \, at \, the \, node \, 1: \quad f_{y2}^{n+1}x_2^{n+1} - \tilde{f}_{x3}y_3^{n+1} + \tilde{f}_{y3}x_3^{n+1} + \sum_{i=1}^{3} \tilde{m}_{zi} = 0 \tag{4.37c}$$

in which the internal forces without tilde "~" are the reaction forces at the restrained degrees of freedom and they are equal to the internal forces at the same degrees of freedom in the local coordinate system.

It can also be noticed that the basic internal forces have the same values as the local internal forces at the same degrees of freedom. The superscript "n+1" refers to the variables based on the deformed configuration. Thus, the variables with superscript "n+1", including the reaction forces and the node coordinates, can be given by

$$\left(\text{var.}\right)^{n+1} = \left(\text{var.}\right) + \delta\left(\text{var.}\right) \tag{4.38}$$

Substituting Eqs. (4.36) and (4.38) into Eqs. (4.37) and neglecting the high order variations, then the variations of the reaction forces can be obtained as follows

$$\delta f_{x1} = 0 \tag{4.39a}$$

$$\delta f_{y1} = \frac{1}{x_2}(-\tilde{f}_{x3}\delta\tilde{v}_3 + \tilde{f}_{y3}\delta\tilde{u}_3 + f_{y2}\delta\tilde{u}_2) \tag{4.39b}$$

$$\delta f_{y2} = -\delta f_{y1} \tag{4.39c}$$

where the local internal force f_{y2} can be obtained by $\boldsymbol{f}_m = \boldsymbol{L}_m{}^T \tilde{\boldsymbol{f}}_m$ based on the current configuration. The local geometric stiffness due to the changes of element dimensions can be derived by Eqs. (4.39), $\delta\tilde{\boldsymbol{d}}_m = \boldsymbol{L}_m \delta\boldsymbol{d}_m$ and $\boldsymbol{K}_g^m = \dfrac{\partial \boldsymbol{f}}{\partial \boldsymbol{d}^T}$. It can be noticed that the 18×18 geometric stiffness matrix, $\boldsymbol{K}_g^m$, has only two non-zero rows involved with δf_{y1} and δf_{y2} respectively. Also, the internal forces and the nodal

coordinates in the stiffness matrix should be updated in the procedure of nonlinear analysis.

4.3.1.4 Geometric stiffness due to changes of dimensions of a plate element

A pure deformational plate element is shown in Figure 4.5, in which the vertical displacements are constrained. Similar to the derivation for a membrane element, the basic internal moments can be regarded as action moments and the reaction forces at the restrained degrees of freedom are the shear forces $\{f_{z1}\ f_{z2}\ f_{z3}\}^T$ as same as the corresponding local internal forces.

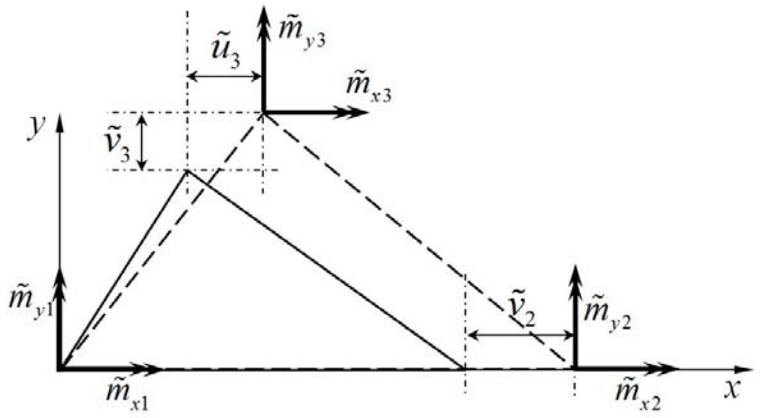

Figure 4.5 A pure deformational plate element

The equilibrium equations based on the current configuration of the plate element can be established as

$$\begin{aligned} &\sum f_z = 0: \\ &f_{z1} + f_{z2} + f_{z3} = 0 \end{aligned} \tag{4.40a}$$

$$\sum m_x = 0 \; about \; y \; axis:$$
$$\sum_{i=1}^{3} \tilde{m}_{xi} + f_{z3} y_3 = 0 \tag{4.40b}$$

$$\sum m_y = 0 \; about \; x \; axis:$$
$$\sum_{i=1}^{3} \tilde{m}_{yi} - f_{z2} x_2 - f_{z3} x_2 = 0 \tag{4.40c}$$

For the deformed configuration, the equilibrium equations are

$$\sum f_z = 0:$$
$$f_{z1}^{n+1} + f_{z2}^{n+1} + f_{z3}^{n+1} = 0 \tag{4.41a}$$

$$\sum m_x = 0 \; about \; y \; axis:$$
$$\sum_{i=1}^{3} \tilde{m}_{xi} + f_{z3}^{n+1} y_3^{n+1} = 0 \tag{4.41b}$$

$$\sum m_y = 0 \; about \; x \; axis:$$
$$\sum_{i=1}^{3} \tilde{m}_{yi} - f_{z2}^{n+1} x_2^{n+1} - f_{z3}^{n} x_2^{n+1} = 0 \tag{4.41c}$$

Substituting Eqs. (4.38) and (4.40) into Eqs. (4.41) and ignoring the high order variations, then the variations of the reaction shear forces can be given by

$$\delta f_{z1} = \frac{f_{z3}}{y_3}(1 - \frac{x_3}{x_2})\delta \tilde{v}_3 + \frac{f_{z3}}{x_2}\delta \tilde{u}_3 + \frac{f_{z2}}{x_2}\delta \tilde{u}_2 \tag{4.42a}$$

$$\delta f_{z2} = \frac{1}{x_2}(f_{z3}\frac{x_3}{y_3}\delta \tilde{v}_3 - f_{x3}\delta \tilde{u}_3 - f_{z2}\delta \tilde{u}_2) \tag{4.42b}$$

$$\delta f_{z3} = -\frac{f_{z3}}{y_3}\delta \tilde{v}_3 \tag{4.42c}$$

in which the local internal forces f_{zi} can be obtained by $\boldsymbol{f}_p = \boldsymbol{L}_p{}^T \tilde{\boldsymbol{f}}_p$ based on the current configuration. Then, the geometric stiffness matrix can be derived through Eqs. (4.42), $\delta\tilde{\boldsymbol{d}}_m = \boldsymbol{L}_m \delta\boldsymbol{d}_m$ and $\boldsymbol{K}_g^p = \dfrac{\partial \boldsymbol{f}}{\partial \boldsymbol{d}^T}$. It also can be seen that the number of the non-zero rows in the matrix $\boldsymbol{K}_g^p$ are only three. Also, the internal forces and nodal coordinates in the stiffness matrix should be updated in the procedure of nonlinear analysis.

4.3.2 Internal forces

The general EICR formulation should use the total pure deformations since the beginning of nonlinear analysis to get the internal forces, since the rotation corrector utilized to correct non-additive local rotations should be computed by the total local rotations. For the proposed co-rotational method, the rotation corrector is neglected and the incremental pure deformations can be used to calculate and update the internal forces, and the incremental deformations avoid recording rotation matrix for every node in the procedure of nonlinear analysis. Moreover, the total deformations can also be used for the proposed method. In the Section, three ways to obtain the internal forces are introduced and they have different accuracy and computational cost. Additionally, with the help of the pure deformational method, only 12 values of the basic internal forces rather than 18 values of the local internal forces are recorded for a shell element in analysis procedure, which significantly saves computer storage.

4.3.2.1 Total deformation

The general EICR method adopts the total pure deformations to get the internal forces, while the proposed method can also use them to obtain more accurate results. Due to the non-additive and non-commutative properties of 3D rotations, the rotation matrix rather than the rotation vector for every node is recorded during nonlinear analysis.

First, the initial data for a shell element should be computed and recorded, including the local-to-global transformation matrix $\boldsymbol{T}_e^{\,0}$, the rotation matrix for the node *i* in the global coordinate system, $\boldsymbol{R}_i^{g\,0}$, which is set to the identity matrix, and the global coordinates $\boldsymbol{x}_i^{g0}$. Also, for the last iteration, the known corresponding data are denoted as $\boldsymbol{T}_e^{\,n}$, $\boldsymbol{R}_i^{g\,n}$ $\boldsymbol{x}_i^{gn}$.

After one iterative process, the incremental displacement vector of a shell element in the global coordinate system can be obtained as follows,

$$\Delta \boldsymbol{d}^g = \left\{ \Delta \boldsymbol{d}_1^{gT} \;\; \Delta \boldsymbol{d}_2^{gT} \;\; \Delta \boldsymbol{d}_3^{gT} \right\}^T \tag{4.43a}$$

$$\Delta \boldsymbol{d}_i^g = \left\{ \Delta u_{xi}^g \;\; \Delta u_{yi}^g \;\; \Delta u_{zi}^g \;\; \Delta \theta_{xi}^g \;\; \Delta \theta_{yi}^g \;\; \Delta \theta_{zi}^g \right\}^T \tag{4.43b}$$

$$\Delta \boldsymbol{u}_i^g = \left\{ \Delta u_{xi}^g \;\; \Delta u_{yi}^g \;\; \Delta u_{zi}^g \right\}^T \tag{4. 43c}$$

$$\Delta \boldsymbol{\theta}_i^g = \left\{ \Delta \theta_{xi}^g \;\; \Delta \theta_{yi}^g \;\; \Delta \theta_{zi}^g \right\}^T \tag{4. 43d}$$

Then, the global nodal coordinates can be updated as

$$\boldsymbol{x}_i^{g\,n+1} = \boldsymbol{x}_i^{g\,n} + \Delta \boldsymbol{u}_i^g \tag{4.44}$$

and the local-to-global transformation matrix can be updated by the new global nodal coordinates as $\boldsymbol{T}_e^{\,n+1}$.

The local nodal coordinates can be always obtained by $\boldsymbol{x}_i = \boldsymbol{T}_e\left(\boldsymbol{x}_i^g - \boldsymbol{x}_1^g\right)$, so the non-zero local nodal coordinates at the initial and updated configurations are $\left\{x_2^0 \;\; x_3^0 \;\; y_3^0\right\}^T$, $\left\{x_2^{n+1} \;\; x_3^{n+1} \;\; y_3^{n+1}\right\}^T$ respectively. The total pure displacements can be given by

$$\begin{Bmatrix} \tilde{u}_2 \\ \tilde{u}_3 \\ \tilde{v}_3 \end{Bmatrix} = \begin{Bmatrix} x_2^{n+1} \\ x_3^{n+1} \\ y_3^{n+1} \end{Bmatrix} - \begin{Bmatrix} x_2^0 \\ x_3^0 \\ y_3^0 \end{Bmatrix} \tag{4.45}$$

In terms of the rotation matrix at the node *i*, the incremental global rotation vector should be transformed into the incremental rotation matrix by Eq. (4.8f) as

$$\Delta\boldsymbol{R}_i^g = \boldsymbol{R}\left(\Delta\boldsymbol{\theta}_i^g\right) \tag{4.46a}$$

and the global rotation matrix can be updated as

$$\boldsymbol{R}_i^{gn+1} = \Delta\boldsymbol{R}_i^g \boldsymbol{R}_i^{gn} \tag{4.46b}$$

Then, the total pure rotation matrix at the node *i* is given by

$$\boldsymbol{R}_i = \boldsymbol{T}_e^{\,n+1} \boldsymbol{R}_i^{gn+1} \boldsymbol{T}_e^{0\,T} \tag{4.47a}$$

and the corresponding rotations can be extract through the total pure rotation matrix by Eq. (4.9b) as follows

$$\tilde{\boldsymbol{\theta}}_i = \boldsymbol{\theta}\left(\boldsymbol{R}_i\right) \tag{4.47b}$$

After that, the total pure displacements and rotations can be integrated into the basic displacement vectors for a membrane element and a plate element, $\tilde{\boldsymbol{d}}_m$ and $\tilde{\boldsymbol{d}}_p$, respectively.

Next, the basic internal forces can be given by

$$\tilde{\boldsymbol{f}}_m^{n+1} = \tilde{\boldsymbol{K}}_m^0 \tilde{\boldsymbol{d}}_m \tag{4.48a}$$

$$\tilde{\boldsymbol{f}}_p^{n+1} = \tilde{\boldsymbol{K}}_p^0 \tilde{\boldsymbol{d}}_p \tag{4.48b}$$

in which the superscript "0" means that the stiffness matrix is formed by the initial dimensions of a shell element.

Transforming the basic internal forces into the local coordinate system gives

$$\boldsymbol{f}_m = \boldsymbol{L}_m^{n+1\,T} \tilde{\boldsymbol{f}}_m^{n+1} \tag{4.49a}$$

$$\boldsymbol{f}_p = \boldsymbol{L}_p^{n+1\,T} \tilde{\boldsymbol{f}}_p^{n+1} \tag{4.49b}$$

Finally, these local internal force vectors can be combined to the internal force vector of a shell element and then transformed into the global coordinate system to assemble the global internal force vector of the whole structures.

4.3.2.2 Directly Incremental deformation

Different from the former way, the incremental deformation method is used here to find the differences between the last and the updated configurations. For the incremental pure displacements, we have

$$\begin{Bmatrix} \Delta\tilde{u}_2 \\ \Delta\tilde{u}_3 \\ \Delta\tilde{v}_3 \end{Bmatrix} = \begin{Bmatrix} x_2^{n+1} \\ x_3^{n+1} \\ y_3^{n+1} \end{Bmatrix} - \begin{Bmatrix} x_2^{n} \\ x_3^{n} \\ y_3^{n} \end{Bmatrix} \tag{4.50}$$

There is no difference for the final internal forces between the total and incremental displacements as displacements are additive, while the difference is only on the rotations. Specifically, this method does not need to record the rotation matrix at the node *i*. Once the incremental rotation matrix $\Delta\boldsymbol{R}_i^g = \boldsymbol{R}\left(\Delta\boldsymbol{\theta}_i^g\right)$ is obtained, the incremental pure rotations can be given by

$$\Delta\boldsymbol{R}_i = \boldsymbol{T}_e^{n+1}\Delta\boldsymbol{R}_i^g\boldsymbol{T}_e^{n\,T} \tag{4.51a}$$

$$\Delta\tilde{\boldsymbol{\theta}}_i = \boldsymbol{\theta}\left(\Delta\boldsymbol{R}_i\right) \tag{4.51b}$$

Thus, the incremental pure deformation vector for a membrane element and a plate element, $\Delta\tilde{\boldsymbol{d}}_m$ and $\Delta\tilde{\boldsymbol{d}}_p$, can be acquired and the incremental basic internal forces are

$$\Delta\tilde{\boldsymbol{f}}_m = \tilde{\boldsymbol{K}}_m^0\Delta\tilde{\boldsymbol{d}}_m \tag{4.52a}$$

$$\Delta\tilde{\boldsymbol{f}}_p = \tilde{\boldsymbol{K}}_p^0\Delta\tilde{\boldsymbol{d}}_p \tag{4.52b}$$

Then, the total internal forces in the basic coordinate system can be updated by

$$\tilde{\boldsymbol{f}}_m^{n+1} = \tilde{\boldsymbol{f}}_m^n + \Delta\tilde{\boldsymbol{f}}_m \tag{4.53a}$$

$$\tilde{\boldsymbol{f}}_p^{n+1} = \tilde{\boldsymbol{f}}_p^n + \Delta\tilde{\boldsymbol{f}}_p \tag{4.53b}$$

in which the basic internal forces should be recorded during the iterative process in the method, different from the former method. However, recording the basic internal forces uses less computer storage than the rotation matrix at every node. And the flowing analysis procedure is identical to the former method.

The drawback of this method is that it involves the addition of pure rotations through the addition of basic internal forces, which violates the non-additive property of 3D rotations. However, pure rotations are small and should be small due to the plate theory. So, the treatment of this method to pure rotations is acceptable and has little impact on accuracy.

4.3.2.3 Indirectly Incremental deformation

The indirectly incremental deformation method is similar to the second one, except that there is a difference on the derivation of the incremental pure rotations. Through the local-to-global transformation matrices for the last and updated configurations of a shell element, $\boldsymbol{T}_e^{\,n}$ and $\boldsymbol{T}_e^{\,n+1}$, the incremental rigid body rotation matrix between these two configurations in the local coordinate system can be given by

$$\Delta\boldsymbol{R}_e = \boldsymbol{T}_e^{\,n}\boldsymbol{T}_e^{\,n+1\,T} \tag{4.54a}$$

Then, the incremental rigid body rotations of a shell element are

$$\Delta\boldsymbol{\omega} = \boldsymbol{\theta}\left(\Delta\boldsymbol{R}_e\right) \tag{4.54b}$$

and the incremental pure rotations at the node *i* can be given by

$$\Delta\tilde{\boldsymbol{\theta}}_i = \boldsymbol{T}_e^{n+1}\Delta\boldsymbol{\theta}_i^{g} - \Delta\boldsymbol{\omega} \quad (i=1,2,3) \tag{4.54c}$$

It can be seen that the indirectly incremental deformation method is the simplest among these three methods, in which the transformation between the rotation matrix and the vector is only performed once for the rigid body rotations of a shell element. However, its accuracy is worst. Considering both efficiency and accuracy, this thesis uses the second method, the directly incremental deformation method, to update internal forces in nonlinear analysis procedure.

4.4 A novel EICR formulation for quadrilateral shell elements

In this section, a novel co-rotational algorithm for quadrilateral shell elements is derived based on the pure deformational method, allowing for the warping phenomenon. The internal forces for the projection of a warping shell element, $\overline{\boldsymbol{f}}$, can be transformed into the warping shell in the global coordinate system as

$$\boldsymbol{f}^g = \boldsymbol{T}^T \boldsymbol{L}^T \boldsymbol{E}^T \overline{\boldsymbol{f}} \tag{4.55a}$$

$$\boldsymbol{f}^g = \left\{ \boldsymbol{f}_1^{gT} \;\; \boldsymbol{f}_2^{gT} \;\; \boldsymbol{f}_3^{gT} \;\; \boldsymbol{f}_4^{gT} \right\}^T \tag{4.55b}$$

$$\boldsymbol{f}_i^g = \left\{ f_{xi}^g \;\; f_{yi}^g \;\; f_{zi}^g \;\; m_{xi}^g \;\; m_{yi}^g \;\; m_{zi}^g \right\}^T \tag{4.55c}$$

in which $\boldsymbol{T}$ is composed of 8 matrices $\boldsymbol{T}_e$ in Eq. (3.28) along diagonal, $\boldsymbol{L}$ is the basic-to-local transformation matrix, $\boldsymbol{E}$ is the eccentricity matrix transforming the variables from the projection into the warping shell element.

The corresponding displacement vector in the global coordinate system is

$$\boldsymbol{d}^g = \left\{ \boldsymbol{d}_1^{gT} \;\; \boldsymbol{d}_2^{gT} \;\; \boldsymbol{d}_3^{gT} \;\; \boldsymbol{d}_4^{gT} \right\}^T \tag{4.55d}$$

$$\boldsymbol{d}_i^g = \left\{ u_{xi}^g \;\; u_{yi}^g \;\; u_{zi}^g \;\; \theta_{xi}^g \;\; \theta_{yi}^g \;\; \theta_{zi}^g \right\}^T \tag{4.55e}$$

Then, the relationships between these different systems by taking use of the previous equations can be concluded in Figure 4.6 as follows

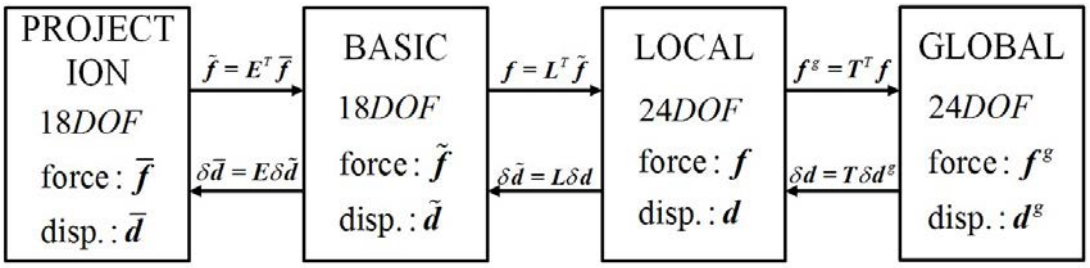

Figure 4.6 Relationships between different systems

4.4.1 Tangent stiffness

Taking a variation of Equation (4.55a), we have

$$\delta \boldsymbol{f}^g = \boldsymbol{T}^T \boldsymbol{L}^T \boldsymbol{E}^T \delta \bar{\boldsymbol{f}} + \delta \boldsymbol{T}^T \boldsymbol{L}^T \boldsymbol{E}^T \bar{\boldsymbol{f}} + \boldsymbol{T}^T \delta \boldsymbol{L}^T \boldsymbol{E}^T \bar{\boldsymbol{f}} + \boldsymbol{T}^T \boldsymbol{L}^T \delta \boldsymbol{E}^T \bar{\boldsymbol{f}} \tag{4.56a}$$

where the first term yields the material stiffness matrix and the remained three terms can deduce the geometric stiffness matrices which are formulated by the internal forces at the current time.

Then, we have

$$\delta \boldsymbol{f}^g = \boldsymbol{T}^T \left(\boldsymbol{K}_e + \boldsymbol{K}_g^r + \boldsymbol{K}_g^m + \boldsymbol{K}_g^p + \boldsymbol{K}_g^w \right) \boldsymbol{T} \delta \boldsymbol{d}^g \tag{4.56b}$$

in which the notions of matrices used in this equation is identical to the co-rotational formulation for triangular shell elements, in addition, $\boldsymbol{K}_g^w$ is the geometric stiffness due to warping effect. Also, it should be noted that this equation has one more system, the projection, than the equation for triangular shell elements in Eq. (4.31).

In the next, the derivation of every part of the local tangent stiffness is detailed with the novel co-rotational method based on pure deformational element model in the following.

4.4.1.1 Material stiffness

Different from triangular shell elements, quadrilateral shell elements have the warping effect. First, the material stiffness matrices of a membrane element and a plate element, $\bar{\boldsymbol{K}}_m$ and $\bar{\boldsymbol{K}}_p$, are formulated based on the projection which is also a pure deformational system with rigid body movements restrained. Due to the coupling of membrane and plate stiffness, they should be integrated together in the projection system as the 18×18 material stiffness $\bar{\boldsymbol{K}}_e$. Transforming it into the warping shell element based on the basic coordinate system gives

$$\tilde{\boldsymbol{K}}_e = \boldsymbol{E}^T \bar{\boldsymbol{K}}_e \boldsymbol{E} \tag{4.57a}$$

Then, it can be transformed into the local coordinate system by

$$\boldsymbol{K}_e = \boldsymbol{L}^T \tilde{\boldsymbol{K}}_e \boldsymbol{L} \tag{4.57b}$$

and becomes a 24×24 matrix. It should be noted that the material stiffness matrix $\overline{\boldsymbol{K}}_e$ is computed based on the projection of the shell element based on the initial configuration and constant for the whole nonlinear analysis procedure. Besides, the transformation matrices $\boldsymbol{E}$ and $\boldsymbol{L}$ should be updated according to the current configuration to reflect the changes of element dimensions and are detailed in Chapter 3.

4.3.1.2 Geometric stiffness due to rigid body rotations of the element

The derivation of this part of the geometric stiffness is the same as that for triangular shell elements and its expression can be obtained as follows,

$$\delta \boldsymbol{f} = -\boldsymbol{A} \cdot \boldsymbol{G}\, \delta \boldsymbol{d} = \boldsymbol{K}_g^r \delta \boldsymbol{d} \tag{4.58a}$$

$$\boldsymbol{A} = \begin{bmatrix} \mathbf{Spin}(\boldsymbol{n}_1) \\ \mathbf{Spin}(\boldsymbol{m}_1) \\ \vdots \\ \mathbf{Spin}(\boldsymbol{n}_4) \\ \mathbf{Spin}(\boldsymbol{m}_4) \end{bmatrix} \tag{4.58b}$$

in which the matrix $\boldsymbol{G}$ is used to connect the variations of the rigid body rotations of the element to the variations of the local nodal displacements and can be given by

$$\boldsymbol{G} = \frac{\partial \boldsymbol{\omega}}{\partial \boldsymbol{d}^T} = \left[\frac{\partial \boldsymbol{\omega}}{\partial \boldsymbol{u}_1^T} \; \frac{\partial \boldsymbol{\omega}}{\partial \boldsymbol{\theta}_1^T} \; \frac{\partial \boldsymbol{\omega}}{\partial \boldsymbol{u}_2^T} \; \frac{\partial \boldsymbol{\omega}}{\partial \boldsymbol{\theta}_2^T} \; \frac{\partial \boldsymbol{\omega}}{\partial \boldsymbol{u}_3^T} \; \frac{\partial \boldsymbol{\omega}}{\partial \boldsymbol{\theta}_3^T} \; \frac{\partial \boldsymbol{\omega}}{\partial \boldsymbol{u}_4^T} \; \frac{\partial \boldsymbol{\omega}}{\partial \boldsymbol{\theta}_4^T} \right] \tag{4.59a}$$

With the help of Eqs. (3.35), the submatrices of $\boldsymbol{G}$ can be detailed as follows,

$$\frac{\partial \boldsymbol{\omega}}{\partial \boldsymbol{u}_1^T} = \begin{bmatrix} 0 & 0 & (x_4 - x_2)/x_2 y_4 \\ 0 & 0 & 1/x_2 \\ 0 & -1/x_2 & 0 \end{bmatrix} \tag{4. 59b}$$

$$\frac{\partial \boldsymbol{\omega}}{\partial \boldsymbol{u}_2^T}=\begin{bmatrix}0 & 0 & -x_4/x_2y_4\\ 0 & 0 & -1/x_2\\ 0 & 1/x_2 & 0\end{bmatrix} \tag{4. 59c}$$

$$\frac{\partial \boldsymbol{\omega}}{\partial \boldsymbol{u}_4^T}=\begin{bmatrix}0 & 0 & 1/y_4\\ 0 & 0 & 0\\ 0 & 0 & 0\end{bmatrix} \tag{4. 59d}$$

$$\frac{\partial \boldsymbol{\omega}}{\partial \boldsymbol{u}_3^T}=\frac{\partial \boldsymbol{\omega}}{\partial \boldsymbol{\theta}_1^T}=\frac{\partial \boldsymbol{\omega}}{\partial \boldsymbol{\theta}_2^T}=\frac{\partial \boldsymbol{\omega}}{\partial \boldsymbol{\theta}_3^T}=\frac{\partial \boldsymbol{\omega}}{\partial \boldsymbol{\theta}_4^T}=\mathbf{0}_{3\times 3} \tag{4. 59e}$$

The internal forces and the local nodal coordinates used in this matrix should be updated according to the warping shell element at current configuration.

4.3.1.3 Geometric stiffness due to changes of element dimensions

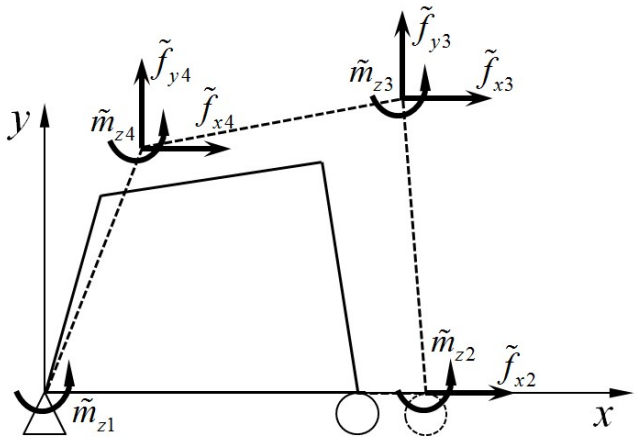

Figure 4.7 A pure deformational membrane element

As a quadrilateral shell element consists of a membrane element and a plate element, this part of the geometric stiffness is discussed separately. Based on a pure

deformational membrane element as shown in the Figure 4.7, three degrees of freedom are restrained, while the internal forces at the free degrees of freedom are regarded as action forces and invariant after deformation. Also, the internal forces at the constraints are the reaction forces which change after deformation to keep the element-equilibrium. Thus, the gradients of the reaction forces due to deformation can be used to deduce this part of geometric stiffness.

For the current configuration of a memb rane element, the equilibrium equations can be given by

$$\begin{aligned} &\sum f_x = 0: \\ &f_{x1} + \tilde{f}_{x2} + \tilde{f}_{x3} + \tilde{f}_{x4} = 0 \end{aligned} \tag{4.60a}$$

$$\begin{aligned} &\sum f_y = 0: \\ &f_{y1} + f_{y2} + \tilde{f}_{y3} + \tilde{f}_{y4} = 0 \end{aligned} \tag{4.60b}$$

$$\begin{aligned} &\sum m_z = 0 \, at \, the \, node \, 1: \\ &f_{y2}x_2 - \tilde{f}_{x3}y_3 + \tilde{f}_{y3}x_3 - \tilde{f}_{x4}y_4 + \tilde{f}_{y4}x_4 + \sum_{i=1}^{4} \tilde{m}_{zi} = 0 \end{aligned} \tag{4.60c}$$

After deformation, the action forces are invariant and the three reaction forces f_{x1}, f_{y1} and f_{y2} change into f_{x1}^{n+1}, f_{y1}^{n+1} and f_{y2}^{n+1}. Thus, the equili brium equations become

$$\begin{aligned} &\sum f_x = 0: \\ &f_{x1}^{n+1} + \tilde{f}_{x2} + \tilde{f}_{x3} + \tilde{f}_{x4} = 0 \end{aligned} \tag{4.61a}$$

$$\begin{aligned} &\sum f_y = 0: \\ &f_{y1}^{n+1} + f_{y2}^{n+1} + \tilde{f}_{y3} + \tilde{f}_{y4} = 0 \end{aligned} \tag{4.61b}$$

$$\begin{aligned}&\sum m_z = 0 \; at \; the \; node 1: \\ &f_{y2}^{n+1} x_2^{n+1} - \tilde{f}_{x3} y_3^{n+1} + \tilde{f}_{y3} x_3^{n+1} - \tilde{f}_{x4} y_4^{n+1} + \tilde{f}_{y4} x_4^{n+1} + \sum_{i=1}^{4} \tilde{m}_{zi} = 0\end{aligned} \tag{4.61c}$$

Following the co-rotational method for triangular elements and substituting Eqs. (4.60) into Eqs. (4.61), the variations of the reaction forces can be obtained as follows,

$$\delta f_{x1} = 0 \tag{4.62a}$$

$$\delta f_{y1} = \frac{1}{x_2}(-f_{y2}\delta\tilde{u}_2 - \tilde{f}_{y3}\delta\tilde{u}_3 + \tilde{f}_{x3}\delta\tilde{v}_3 - \tilde{f}_{y4}\delta\tilde{u}_4 + \tilde{f}_{x4}\delta\tilde{v}_4) \tag{4.62b}$$

$$\delta f_{y2} = -\delta f_{y1} \tag{4.62c}$$

Then, the geometric stiffness matrix due to the changes of dimensions of a membrane element in the local coordinate system, $\boldsymbol{K}_g^m$, can be obtained by Eqs. (4.62), $\boldsymbol{f} = \boldsymbol{L}^T \boldsymbol{E}^T \overline{\boldsymbol{f}}$, $\delta\tilde{\boldsymbol{d}} = \boldsymbol{L}\delta\boldsymbol{d}$ and $\boldsymbol{K}_g^m = \dfrac{\partial \boldsymbol{f}}{\partial \boldsymbol{d}^T}$.

In terms of the geometric stiffness due to changes of dimensions of a plate element, the warping phenomenon should be considered, since it affects the equilibrium of a plate element. The derivation is similar to the one for a membrane element, which is to find the variations of the reaction forces of a plate element. Figure 4.8 shows that the nodal vertical displacements are restrained except the node 3, whereas the reaction forces are the shear forces $\{f_{z1} \; f_{z2} \; f_{z4}\}^T$ at these three restrained nodes. For consideration of the warping effect at the node 3, the in-plane action forces, including $\tilde{f}_{x3}$ and $\tilde{f}_{y3}$, should be considered in the equilibrium equations.

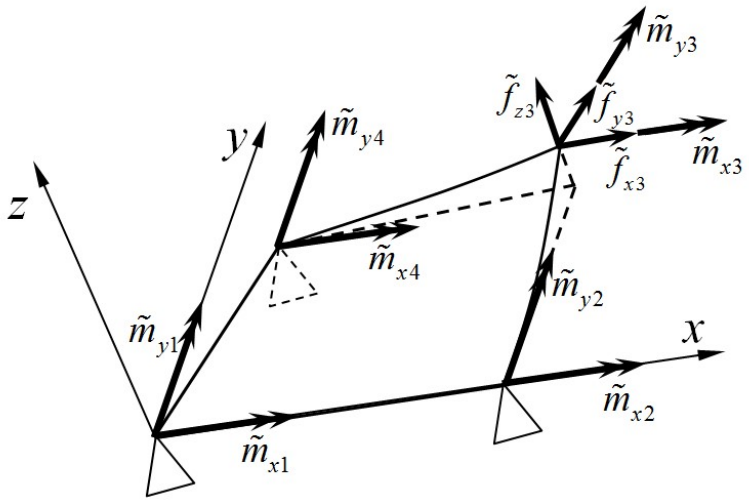

Figure 4.8 A pure deformational plate element

For the current configuration of a pure deformational plate element as shown in Figure 4.8, the equilibrium equations can be established as

$$\begin{aligned} &\sum f_z = 0: \\ &f_{z1} + f_{z2} + f_{z4} + \tilde{f}_{z3} = 0 \end{aligned} \tag{4.63a}$$

$$\begin{aligned} &\sum m_x = 0 \; about \; y \; axis: \\ &f_{z4} y_4 + \tilde{f}_{z3} y_3 - \tilde{f}_{y3} z_3 + \sum_{i=1}^{4} \tilde{m}_{xi} = 0 \end{aligned} \tag{4.63b}$$

$$\begin{aligned} &\sum m_y = 0 \; about \; x \; axis: \\ &- f_{z2} x_2 - f_{z4} x_4 - \tilde{f}_{z3} x_3 + \tilde{f}_{x3} z_3 + \sum_{i=1}^{4} \tilde{m}_{yi} = 0 \end{aligned} \tag{4.63c}$$

After deformation, the equilibrium equations change into

$$\begin{aligned} &\sum f_z = 0: \\ &f_{z1}^{n+1} + f_{z2}^{n+1} + f_{z4}^{n+1} + \tilde{f}_{z3} = 0 \end{aligned} \tag{4.64a}$$

$$\sum m_x = 0 \; about \; y \; axis:$$
$$f_{z4}^{n+1} y_4^{n+1} + \tilde{f}_{z3} y_3^{n+1} - \tilde{f}_{y3} z_3^{n+1} + \sum_{i=1}^{4} \tilde{m}_{xi} = 0 \tag{4.64b}$$

$$\sum m_y = 0 \; about \; x \; axis:$$
$$-f_{z2}^{n+1} x_2^{n+1} - f_{z4}^{n+1} x_4^{n+1} - \tilde{f}_{z3} x_3^{n+1} + \tilde{f}_{x3} z_3^{n+1} + \sum_{i=1}^{4} \tilde{m}_{yi} = 0 \tag{4.64c}$$

Through Eqs. (4.63) and (4.64) and omitting the high order variations, we have

$$\delta f_{z4} = \frac{1}{y_4}\left(-\tilde{f}_{z3}\delta\tilde{v}_3 - f_{z4}\delta\tilde{v}_4 + \tilde{f}_{y3}\delta\tilde{w}_3\right) \tag{4.65a}$$

$$\delta f_{z2} = \frac{1}{x_2}\left(-f_{z2}\delta\tilde{u}_2 - \tilde{f}_{z3}\delta\tilde{u}_3 + \tilde{f}_{z3}\frac{x_4}{y_4}\delta\tilde{v}_3 - f_{z4}\delta\tilde{u}_4 + f_{z4}\frac{x_4}{y_4}\delta\tilde{v}_4 + \left(\tilde{f}_{x3} - \tilde{f}_{y3}\frac{x_4}{y_4}\right)\delta\tilde{w}_3\right) \tag{4.65b}$$

$$\delta f_{z1} = -\delta f_{z2} - \delta f_{z4} \tag{4.65c}$$

Then, the geometric stiffness matrix due to the changes of dimensions of a plate element in the local coordinate system, $\boldsymbol{K}_g^p$, can be obtained by Eqs. (4.66), $\boldsymbol{f} = \boldsymbol{L}^T \boldsymbol{E}^T \overline{\boldsymbol{f}}$, $\delta\tilde{\boldsymbol{d}} = \boldsymbol{L}\delta\boldsymbol{d}$ and $\boldsymbol{K}_g^p = \frac{\partial \boldsymbol{f}}{\partial \boldsymbol{d}^T}$.

4.3.1.4 Geometric stiffness due to warping effect

The bending moments on the warping node 3 varies when the local coordinate z_3 changes. Thus, the load perturbation can deduce the geometric stiffness due to warping effect. The relationship of the virtual displacements and rotations at the node 3 between a warping shell element and its projection has been given in Eqs. (3.43),

then the corresponding forces and m oments in these two systems have the relationship as follows,

$$\tilde{m}_{x3}=z_3\,\tilde{f}_{y3}+\bar{m}_{x3} \tag{4.66a}$$

$$\tilde{m}_{y3}=-z_3\,\tilde{f}_{x3}+\bar{m}_{y3} \tag{4.66b}$$

Like the previous derivations, the forces and moments at the free DOF of the projection are active and do not change after deformation, while the moments at the node 3 vary and their variations are

$$\delta\tilde{m}_{x3}=\delta\tilde{w}_3\,\tilde{f}_{y3} \tag{4.67a}$$

$$\delta\tilde{m}_{y3}=-\delta\tilde{w}_3\,\tilde{f}_{x3} \tag{4.67b}$$

Then, the geometric stiffness matrix due to warping effect in the local coordinate system can be derived by Eqs. (4.67), $\boldsymbol{f}=\boldsymbol{L}^T\boldsymbol{E}^T\bar{\boldsymbol{f}}$, $\delta\tilde{\boldsymbol{d}}=\boldsymbol{L}\delta\boldsymbol{d}$ and $\boldsymbol{K}_g^w=\dfrac{\partial\boldsymbol{f}}{\partial\boldsymbol{d}^T}$.

4.4.2 Internal forces

To update the internal forces of a warping quadrilateral shell element in the global coordinate system, the key point is how to extract pure deformations of a shell element's projection from its global deformations. Then, through the known material stiffness matrix of a flat quadrilateral flat shell element, the internal forces of the projection $\bar{\boldsymbol{f}}$ can be acquired, then obtaining the global internal forces of the warping shell element. Similar to the co-rotational method for triangular shell

elements presented in Section 4.3, all the three methods to update internal forces can be used for quadrilateral shell elements. For the sake of simplification, the internal forces of quadrilateral shell element are presented here with the method of the directly incremental deformation introduced in Section 4.3.2.2.

After one iterative process, the incremental displacement vector of a warping quadrilateral shell element in the global coordinate system can be obtained as follows,

$$\Delta \boldsymbol{d}^g = \left\{ \Delta \boldsymbol{d}_1^{gT} \;\; \Delta \boldsymbol{d}_2^{gT} \;\; \Delta \boldsymbol{d}_3^{gT} \; \Delta \boldsymbol{d}_4^{gT} \right\}^T \tag{4.68a}$$

$$\Delta \boldsymbol{d}_i^g = \left\{ \Delta u_{xi}^g \;\; \Delta u_{yi}^g \;\; \Delta u_{zi}^g \;\; \Delta \theta_{xi}^g \;\; \Delta \theta_{yi}^g \;\; \Delta \theta_{zi}^g \right\}^T \tag{4.68b}$$

$$\Delta \boldsymbol{u}_i^g = \left\{ \Delta u_{xi}^g \;\; \Delta u_{yi}^g \;\; \Delta u_{zi}^g \right\}^T \tag{4.68c}$$

$$\Delta \boldsymbol{\theta}_i^g = \left\{ \Delta \theta_{xi}^g \;\; \Delta \theta_{yi}^g \;\; \Delta \theta_{zi}^g \right\}^T \tag{4.68d}$$

Then, the global nodal coordinates can be updated as

$$\boldsymbol{x}_i^{g\,n+1} = \boldsymbol{x}_i^{g\,n} + \Delta \boldsymbol{u}_i^g \tag{4.69}$$

The local-to-global transformation matrix can be updated by the new global nodal coordinates and Eqs. (3.30) as $\boldsymbol{T}_e^{n+1}$, then the new local coordinates $\boldsymbol{x}_i^{n+1}$ and the eccentricity matrix $\boldsymbol{E}^{n+1}$ can be obtained by Eqs. (3.47).

Following the same way presented in Section 4.3.2.2, the incremental pure deformation between the last and updated configurations can be obtained as $\Delta \tilde{\boldsymbol{d}}$, which can be transformed into the corresponding projection and used to compute the incremental internal forces of the projection as follows,

$$\Delta\bar{\boldsymbol{f}} = \bar{\boldsymbol{K}}_e^0 \Delta\bar{\boldsymbol{d}} = \bar{\boldsymbol{K}}_e^0 \boldsymbol{E}^{n+1} \Delta\tilde{\boldsymbol{d}} \tag{4.70}$$

in which the stiffness matrix of the warping quad rilateral shell element's projection, $\bar{\boldsymbol{K}}_e^0$, is calculated based on initial dimensions all the time, so it can be recorded during elastic analyses. Also, there is no doubt that the 18×18 stiffness matrix $\bar{\boldsymbol{K}}_e^0$ needs less computer storage than the 24×24 stiffness matrix in a conventional method.

Then, the internal forces for the projection can be updated and recorded for the next iteration as follows,

$$\bar{\boldsymbol{f}}^{n+1} = \bar{\boldsymbol{f}}^{n} + \Delta\bar{\boldsymbol{f}} \tag{4.71}$$

Finally, the internal force vector of a warping quadrilateral shell element in the global coordinate system for the updated configuration can be given by

$$\boldsymbol{f}^{gn+1} = \boldsymbol{T}^{n+1\,T} \boldsymbol{L}^{n+1\,T} \boldsymbol{E}^{n+1\,T} \bar{\boldsymbol{f}}^{n+1} \tag{4.72}$$

4.5 A novel simplified EICR formulation

In this section, the simplified element-independent co-rotational formulations for triangular and quadrilateral shell elements are proposed, based on the novel formulations presented in Sections 4.3 and 4.4. Both the conventional and the proposed co-rotational methods are derived based on the assumption of large displacements, but small strains. With the assumption of small strains, the proposed co-rotational algorithms can be simplified further.

4.5.1 Triangular shell elements

As mentioned previously, the local geometric stiffness matrix of a flat triangular shell element can be divided into three parts, including the geometric stiffness matrix due to changes of dimensions of a membrane element and a plate element respectively and the geometric stiffness matrix due to rigid body rotations of a shell element. In the case of quadrilateral shell elements, the local geometric stiffness matrix has one more part which is due to the warping effect. In fact, based on the assumption of small strains, the dimensions of a shell element can be fixed and then the geometric stiffness matrices due to changes of element dimensions can be neglected, while the local internal forces should be revised correspondingly.

Thus, for a triangular shell element at the current configuration, the tangent stiffness in the global coordinate system can be given by

$$\delta \boldsymbol{f}^{g} = \boldsymbol{T}^{n\,T}\left(\boldsymbol{K}_{e}^{0} + \boldsymbol{K}_{g}^{rn}\right)\boldsymbol{T}^{n}\delta \boldsymbol{d}^{g} \tag{4.73}$$

in which the local material stiffness matrix $\boldsymbol{K}_{e}^{0}$ is assembled by the stiffness matrices of a membrane element and a plate element as follows,

$$\boldsymbol{K}_{m}^{0} = \boldsymbol{L}_{m}^{0\,T}\tilde{\boldsymbol{K}}_{m}^{0}\boldsymbol{L}_{m}^{0} \tag{4.74a}$$

$$\boldsymbol{K}_{p}^{0} = \boldsymbol{L}_{p}^{0\,T}\tilde{\boldsymbol{K}}_{p}^{0}\boldsymbol{L}_{p}^{0} \tag{4.74b}$$

where the superscript “0” means that these matrices are always formed based on the initial configuration in the whole analysis, which is different from the co-rotational

methods introduced previously. The superscript "*n*" means that the matrices are calculated based on the current configuration.

After defamation, the local and global internal forces can be updated by

$$\boldsymbol{f}_m^{n+1} = \boldsymbol{L}_m^{0\,T} \tilde{\boldsymbol{f}}_m^{n+1} \tag{4.75a}$$

$$\boldsymbol{f}_p^{n+1} = \boldsymbol{L}_p^{0\,T} \tilde{\boldsymbol{f}}_p^{n+1} \tag{4.75b}$$

$$\boldsymbol{f}^{gn+1} = \boldsymbol{T}^{n+1\,T} \boldsymbol{f}^{n+1} \tag{4.75c}$$

in which the basic-to-local transformation matrices adopt the initial dimensions of a shell element. This is because the changes of element dimensions are neglected in the simplified co-rotational method.

4.5.2 Quadrilateral shell elements

In terms of the simplified co-rotational algorithm for quadrilateral shell elements, the tangent stiffness matrix in the current configuration can be given by

$$\delta \boldsymbol{f}^g = \boldsymbol{T}^{n\,T} \left(\boldsymbol{K}_e + \boldsymbol{K}_g^{rn} + \boldsymbol{K}_g^{wn} \right) \boldsymbol{T}^n \delta \boldsymbol{d}^g \tag{4.76a}$$

$$\boldsymbol{K}_e = \boldsymbol{L}^{0\,T} \boldsymbol{E}^{n\,T} \bar{\boldsymbol{K}}_e^0 \boldsymbol{E}^n \boldsymbol{L}^0 \tag{4.76b}$$

After deformation, the local internal forces can be updated by

$$\boldsymbol{f}^{gn+1} = \boldsymbol{T}^{n+1\,T} \boldsymbol{L}^{0\,T} \boldsymbol{E}^{n+1\,T} \bar{\boldsymbol{f}}^{n+1} \tag{4.77}$$

in which the local-to-global transformation matrix and the eccentricity matrix should be updated based on the current configuration, while the basic-to-local transformation matrix $\boldsymbol{L}$ reflecting the changes of element dimensions still adopt the initial dimensions and becomes the matrix only expanding degrees of freedom of a quadrilateral shell element.

4.6 Summary

A novel element-independent co-rotational formulation based on the pure deformational method is proposed in this chapter, in which the geometric stiffness is regarded as the gradients of nodal forces and derived through load perturbation of equilibrium equations for a shell element. The proposed co-rotational method has a clear physical meaning than the other conventional methods, and its derivation is simpler and does not need many complicated mathematical processes like the general co-rotational formulation. In addition, unlike the conventional methods, in which the projector is used to modify the internal forces and keep the self-equilibrium of a shell element, the proposed approach adopts the basic-to-local transformation matrix to compute the internal forces at the restrained degrees of freedom and transform the basic internal forces into the local internal forces. Although the projector and the basic-to-local transformation matrix have the same function, the latter one is simpler. Also, the proposed method only needs to record the internal forces at the free degrees of freedom in the basic coordinate system, which can save computer storage. Thus, the novel EICR method can improve the computational efficiency of geometrically nonlinear analysis.

Based on the physical interpretation of the novel EICR method and the assumption of small strains, the simplified EICR method is proposed, which is much simpler than the other co-rotational methods. Thus, the simplified co-rotational method is used for the computational procedure of nonlinear analysis in the next chapters and implemented in the program NIDA. Its good performance on accuracy and efficiency is validated in Chapter 7 by numerical examples.

CHAPTER 5

A NONLINEAR TRIANGULAR SHELL ELEMENT BASED ON SIMPLIFIED EICR METHOD

In this chapter, a novel geometrically nonlinear triangular shell element is proposed, which is based on the simplified element-independent co-rotational (EICR) formulation introduced in Section 4.5. The local linear flat triangular shell element consists of a membrane element and a plate bending element. Many studies have shown that the two elements are reliable with good performances. The membrane element is the Optimal Triangle (OPT) element with drilling degrees of freedom proposed by Felippa (2003), while the plate element is the refined discrete Kirchhoff triangular (RDKTM) element allowing for transverse shear deformation. The RDKTM element was developed on the basis of the discrete Kirchhoff triangular (DKT) element and proposed by Chen and Cheung (1998).

Thus, the flat triangular shell element proposed herein can consider drilling degrees of freedom and transverse shear deformation. The significant improvement is that the proposed element is locking-free without the use of reduced integration. Also, the pure deformational method is used to simplify the local element formulations and the novel simplified element-independent co-rotational (EICR) algorithm is adopted to consider geometrically nonlinearity of shell structures.

5.1 Optimal Triangle (OPT) membrane element with drilling rotations

The Optimal Triangle (OPT) element with drilling degrees of freedom is introduced in this section. The element is derived by the assumed natural deviatoric strain (ANDES) formulation and composed of a basic component and a higher order component. Besides, at least ten parameters are used in the stiffness matrix to make the element as a template and then the expression of the stiffness matrix is more complicated than the other triangular membrane elements. For this reason, the pure deformational method is adopted in the OPT element in order to significantly simplify its formulation and enhance the computational efficiency. To highlight the merits of the pure deformational method, the general formulation presented in literature is also introduced and further compared with the proposed simplified formulation based on the pure deformational method.

5.1.1 Formulation of the OPT membrane element

In the section, the ANDES (assumed natural deviatoric strain) membrane element template is introduced, in which the OPT membrane element is one of instances befitting the ANDES template. The ANDES template was derived by Felippa (2003) based on the membrane element with nine degrees of freedom including six nodal translations and three nodal rotations. Several parameters are contained in the template element and different membrane elements can be obtained according to the values of these parameters. Membrane elements based on the ANDES template were

incorporated into the general element-independent co-rotational (EICR) formulation to test their performance in geometrically nonlinear analysis by Zhou *et al.* (2016), in which the OPT and the ALL-3I membrane elements predict better results than the others. The ALL-3I refers to Allman element (Allman, 1988b) integrated by 3-point interior rule. The proposed simplified co-rotational formulation adopts the OPT membrane element to conduct geometrically nonlinear analysis of shell structures.

As shown in Figure 5.1, the OPT membrane element is a 3-node triangular element with drilling rotations and is described in a 2D plane. So, its nodal displacement vector can be given by

$$\boldsymbol{d}_m = \{u_1 \;\; v_1 \;\; \theta_{z1} \;\; u_2 \;\; v_2 \;\; \theta_{z2} \;\; u_3 \;\; v_3 \;\; \theta_{z3}\}^T \tag{5.1}$$

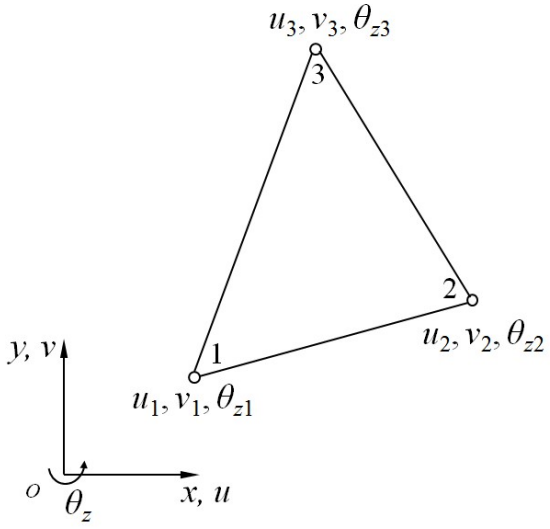

Figure 5.1 OPT membrane element in a 2D plane

The stiffness template consists of a basic and a higher order component as follows,

$$\boldsymbol{K}_m = \boldsymbol{K}_{mb} + \boldsymbol{K}_{mh} \tag{5.2}$$

in which $\boldsymbol{K}_{mb}$ is the basic stiffness matrix taking care of consistency and $\boldsymbol{K}_{mh}$ is the higher order stiffness matrix taking care of rank sufficiency and accuracy.

The basic stiffness is given by

$$\boldsymbol{K}_{mb} = \frac{1}{A}\boldsymbol{B}_{mb}\boldsymbol{D}_m\boldsymbol{B}_{mb}{}^T \tag{5.3}$$

in which A is the element area, $\boldsymbol{B}_{mb}$ and $\boldsymbol{D}_m$ are the strain-displacement matrix and the elastic constitutive matrix respectively and can be expressed as

$$\boldsymbol{B}_{mb} = \frac{1}{2}\begin{bmatrix} y_{23} & 0 & x_{32} \\ 0 & x_{32} & y_{23} \\ \frac{1}{6}\alpha_b y_{23}(y_{13}-y_{21}) & \frac{1}{6}\alpha_b x_{32}(x_{31}-x_{12}) & \frac{1}{3}\alpha_b(x_{31}y_{13}-x_{12}y_{21}) \\ y_{31} & 0 & x_{13} \\ 0 & x_{13} & y_{31} \\ \frac{1}{6}\alpha_b y_{31}(y_{21}-y_{32}) & \frac{1}{6}\alpha_b x_{13}(x_{12}-x_{23}) & \frac{1}{3}\alpha_b(x_{12}y_{21}-x_{23}y_{32}) \\ y_{12} & 0 & x_{21} \\ 0 & x_{21} & y_{12} \\ \frac{1}{6}\alpha_b y_{12}(y_{32}-y_{13}) & \frac{1}{6}\alpha_b x_{21}(x_{23}-x_{31}) & \frac{1}{3}\alpha_b(x_{23}y_{32}-x_{31}y_{13}) \end{bmatrix} \tag{5.4}$$

$$\boldsymbol{D}_m = \frac{Et}{1-v^2}\begin{bmatrix} 1 & v & 0 \\ v & 1 & 0 \\ 0 & 0 & 0.5(1-v) \end{bmatrix} \tag{5.5}$$

in which $x_{ij} = x_i - x_j$, $y_{ij} = y_i - y_j$ (i, j=1,2,3) and α_b is a free parameter for the template, whereas E and v are the Young's modulus and the Poisson's ratio respectively and t refers to the element thickness.

The higher order component of the ANDES template developed by Felippa and Militello (1992) is derived based on the natural strains along the three side directions of the element as shown in Figure 5.2. The relationship between the natural strain vector $\boldsymbol{\epsilon} = \{\epsilon_{12} \ \epsilon_{23} \ \epsilon_{31}\}^T$ and Cartesian strain vector $\boldsymbol{\varepsilon} = \{\varepsilon_{xx} \ \varepsilon_{yy} \ \varepsilon_{xy}\}^T$ in the local coordinate system can be given by

$$\boldsymbol{\varepsilon} = \boldsymbol{T}_e \boldsymbol{\epsilon} \tag{5.6a}$$

$$\boldsymbol{T}_e = \frac{1}{4A}\begin{bmatrix} y_{23}y_{13}l_{21}^2 & y_{31}y_{21}l_{32}^2 & y_{12}y_{32}l_{13}^2 \\ x_{23}x_{13}l_{21}^2 & x_{31}x_{21}l_{32}^2 & x_{12}x_{32}l_{13}^2 \\ (y_{23}x_{31}+x_{32}y_{13})l_{21}^2 & (y_{31}x_{12}+x_{13}y_{21})l_{32}^2 & (y_{12}x_{23}+x_{21}y_{32})l_{13}^2 \end{bmatrix} \tag{5.6b}$$

in which l_{ij} is the length of the element side between the node *i* and *j* and equals to $\sqrt{x_{ij}^2 + y_{ij}^2}$.

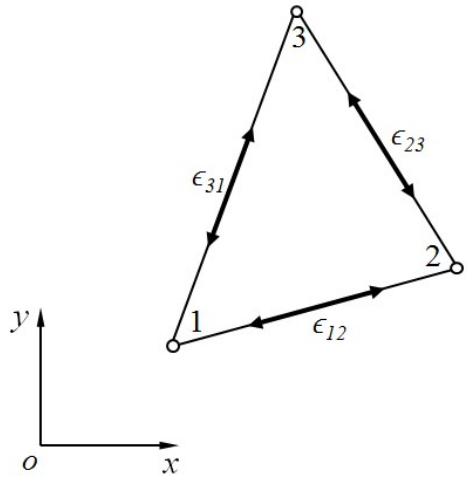

Figure 5.2 Directions of the natural strains

Thus, the elastic constitutive matrix $\boldsymbol{D}_{nat}$ used for the natural stresses and strains is given as

$$\boldsymbol{D}_{nat} = \boldsymbol{T}_e^T \boldsymbol{D}_m \boldsymbol{T}_e \tag{5.7}$$

The drilling rotations in the higher order component are hierarchical and the hierarchical nodal drilling rotations $\tilde{\theta}_{zi}$ can be extracted from the total nodal rotations θ_{zi} by subtracting the mean rotation θ_{z0} as follows

$$\tilde{\theta}_{zi} = \theta_{zi} - \theta_{z0} \tag{5.8}$$

where

$$\theta_{z0} = \frac{1}{4A}\left(x_{23}u_1 + x_{31}u_2 + x_{12}u_3 + y_{23}v_1 + y_{31}v_2 + y_{12}v_3\right) \tag{5.9}$$

Introducing Eq. (5.9) into Eq. (5.8) for the three nodes of the element gives

$$\begin{Bmatrix} \tilde{\theta}_{z1} \\ \tilde{\theta}_{z2} \\ \tilde{\theta}_{z3} \end{Bmatrix} = \frac{1}{4A}\begin{bmatrix} x_{32} & y_{32} & 4A & x_{13} & y_{13} & 0 & x_{21} & y_{21} & 0 \\ x_{32} & y_{32} & 0 & x_{13} & y_{13} & 4A & x_{21} & y_{21} & 0 \\ x_{32} & y_{32} & 0 & x_{13} & y_{13} & 0 & x_{21} & y_{21} & 4A \end{bmatrix} \boldsymbol{d}_m = \boldsymbol{T}_{\theta u}\boldsymbol{d}_m \tag{5.10}$$

Before the presentation of the higher order stiffness matrix, three matrices $\boldsymbol{Q}_1$, $\boldsymbol{Q}_2$ and $\boldsymbol{Q}_3$ depending on the nine free non-dimensional parameters β_1 through β_9 are introduced in the following,

$$\boldsymbol{Q}_1 = \frac{2A}{3}\begin{bmatrix} \frac{\beta_1}{l_{21}^2} & \frac{\beta_2}{l_{21}^2} & \frac{\beta_3}{l_{21}^2} \\ \frac{\beta_4}{l_{32}^2} & \frac{\beta_5}{l_{32}^2} & \frac{\beta_6}{l_{32}^2} \\ \frac{\beta_7}{l_{13}^2} & \frac{\beta_8}{l_{13}^2} & \frac{\beta_9}{l_{13}^2} \end{bmatrix} \tag{5.11a}$$

$$\boldsymbol{Q}_2 = \frac{2A}{3}\begin{bmatrix} \frac{\beta_9}{l_{21}^2} & \frac{\beta_7}{l_{21}^2} & \frac{\beta_8}{l_{21}^2} \\ \frac{\beta_3}{l_{32}^2} & \frac{\beta_1}{l_{32}^2} & \frac{\beta_2}{l_{32}^2} \\ \frac{\beta_6}{l_{13}^2} & \frac{\beta_4}{l_{13}^2} & \frac{\beta_5}{l_{13}^2} \end{bmatrix} \tag{5.11b}$$

$$\boldsymbol{Q}_3 = \frac{2A}{3}\begin{bmatrix} \frac{\beta_5}{l_{21}^2} & \frac{\beta_6}{l_{21}^2} & \frac{\beta_4}{l_{21}^2} \\ \frac{\beta_8}{l_{32}^2} & \frac{\beta_9}{l_{32}^2} & \frac{\beta_7}{l_{32}^2} \\ \frac{\beta_3}{l_{13}^2} & \frac{\beta_1}{l_{13}^2} & \frac{\beta_2}{l_{13}^2} \end{bmatrix} \tag{5.11c}$$

The matrix $\boldsymbol{Q}_i$ relates the natural strain vector $\boldsymbol{\epsilon}_i$ at the node *i* to the hierarchical nodal drilling rotation vector $\tilde{\boldsymbol{\psi}}$. Thus, the natural strain vector $\boldsymbol{\epsilon}$ at the point with area coordinates $\{\xi_1 \ \xi_2 \ \xi_3\}^T$ within the triangular membrane element can be expressed as follows

$$\boldsymbol{\epsilon} = \boldsymbol{Q}\tilde{\boldsymbol{\psi}} \tag{5.12}$$

where

$$\boldsymbol{Q} = \xi_1\boldsymbol{Q}_1 + \xi_2\boldsymbol{Q}_2 + \xi_3\boldsymbol{Q}_3 \tag{5.13}$$

The 3×3 higher order stiffness matrix $\boldsymbol{K}_\theta$, associated with the hierarchical drilling rotations, can be evaluated by the numerical integration using the midpoints of the three element sides in the following,

$$\boldsymbol{K}_\theta = A\left(\boldsymbol{Q}_4^T \boldsymbol{D}_{nat} \boldsymbol{Q}_4 + \boldsymbol{Q}_5^T \boldsymbol{D}_{nat} \boldsymbol{Q}_5 + \boldsymbol{Q}_6^T \boldsymbol{D}_{nat} \boldsymbol{Q}_6\right) \tag{5.14}$$

where

$$\boldsymbol{Q}_4 = \frac{1}{2}\left(\boldsymbol{Q}_1 + \boldsymbol{Q}_2\right) \tag{5.15a}$$

$$\boldsymbol{Q}_5 = \frac{1}{2}\left(\boldsymbol{Q}_2 + \boldsymbol{Q}_3\right) \tag{5.15b}$$

$$\boldsymbol{Q}_6 = \frac{1}{2}\left(\boldsymbol{Q}_3 + \boldsymbol{Q}_1\right) \tag{5.15c}$$

Transforming the higher order stiffness matrix $\boldsymbol{K}_\theta$ into the matrix $\boldsymbol{K}_{mh}$ corresponding to the displacement vector $\boldsymbol{u}_m$, we have

$$\boldsymbol{K}_{mh} = \frac{3}{4}\beta_0 \boldsymbol{T}_{\theta u}{}^T \boldsymbol{K}_\theta \boldsymbol{T}_{\theta u} \tag{5.16}$$

Finally, the stiffness template of ANDES membrane element containing 11 free parameters can be detailed as follows,

$$\boldsymbol{K}_m\left(\alpha_b, \beta_0, \beta_1, ..., \beta_9\right) = \frac{1}{A}\boldsymbol{B}_{mb}\boldsymbol{D}_m \boldsymbol{B}_{mb}{}^T + \frac{3}{4}\beta_0 \boldsymbol{T}_{\theta u}{}^T \boldsymbol{K}_\theta \boldsymbol{T}_{\theta u} \tag{5.17}$$

For the OPT membrane element adopted in this thesis, the 11 free parameters are defined in Table 5.1.

Table 5.1 Values of the 11 free parameters for the OPT membrane element

α_b	β_0	β_1	β_2	β_3	β_4	β_5	β_6	β_7	β_8	β_9
3/2	$\frac{1-4v^2}{2}$	1	2	1	0	1	-1	-1	-1	-2

5.1.2 Simplification of the OPT element based on the pure deformational method

It can be seen that the original OPT membrane element is complicated, since several matrices with large sizes are used in the expression of the stiffness matrix $\boldsymbol{K}_m$. Thus, in this section, the pure deformational method proposed in Chapter 3 will be used to simplify the expression of the stiffness matrix and further decrease its size.

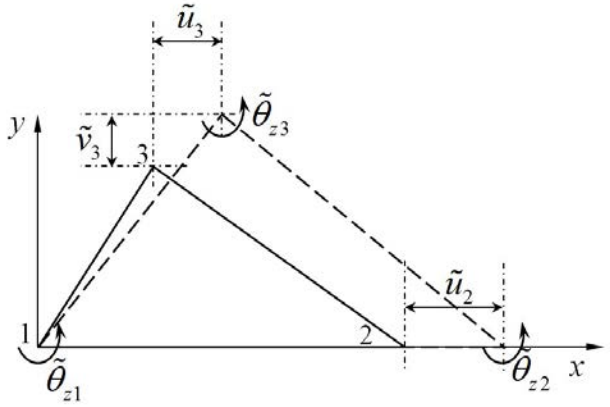

Figure 5.3 Basic coordinate system of the triangular membrane element

First, as the *x*-axis of the local coordinate system is aligned with the element side 1-2 and the origin is set to the node 1 as shown in Figure 5.3, three nodal coordinates are known and equal to zero as follows,

$$x_1 = y_1 = y_2 = 0 \tag{5.18}$$

Then, the basic displacement vector of the triangular shell element is defined by

$$\tilde{\boldsymbol{d}}_m = \left\{\tilde{u}_2 \;\; \tilde{u}_3 \;\; \tilde{v}_3 \;\; \tilde{\theta}_{z1} \;\; \tilde{\theta}_{z2} \;\; \tilde{\theta}_{z3}\right\}^T \tag{5.19}$$

Thus, the stiffness template of the ANDES element in the basic coordinate system can be simplified with the above conditions and becomes

$$\tilde{\boldsymbol{K}}_m\left(\alpha_b, \beta_0, \beta_1, ..., \beta_9\right) = \frac{1}{A}\tilde{\boldsymbol{B}}_{mb}\boldsymbol{D}_m\tilde{\boldsymbol{B}}_{mb}{}^T + \frac{3}{4}\beta_0\tilde{\boldsymbol{T}}_{\theta u}{}^T\boldsymbol{K}_\theta\tilde{\boldsymbol{T}}_{\theta u} \tag{5.20a}$$

$$\tilde{\boldsymbol{B}}_{mb} = \frac{1}{2}\begin{bmatrix} y_3 & 0 & -x_3 \\ 0 & 0 & x_2 \\ 0 & x_2 & 0 \\ \frac{1}{6}\alpha_b y_3{}^2 & \frac{1}{6}\alpha_b(x_3{}^2 - x_2{}^2) & -\frac{1}{3}\alpha_b x_3 y_3 \\ -\frac{1}{6}\alpha_b y_3{}^2 & \frac{1}{6}\alpha_b x_3(2x_2 - x_3) & -\frac{1}{3}\alpha_b y_3 x_{23} \\ 0 & \frac{1}{6}\alpha_b x_2(x_2 - 2x_3) & \frac{1}{3}\alpha_b x_2 y_3 \end{bmatrix} \tag{5.20b}$$

$$\tilde{\boldsymbol{T}}_{\theta u} = \frac{1}{4A}\begin{bmatrix} -x_3 & x_2 & 0 & 4A & 0 & 0 \\ -x_3 & x_2 & 0 & 0 & 4A & 0 \\ -x_3 & x_2 & 0 & 0 & 0 & 4A \end{bmatrix} \tag{5.20c}$$

in which the matrices $\tilde{\boldsymbol{B}}_{mb}$ and $\tilde{\boldsymbol{T}}_{\theta u}$ are degenerated from the matrices $\boldsymbol{B}_{mb}$ and $\boldsymbol{T}_{\theta u}$, respectively, while the other matrices in the right side of Eq. (5.17) do not need to change and can be used directly in the new expression.

Compared with the 12×12 matrix $\boldsymbol{K}_m$ in Eq. (5.17), the 9×9 matrix $\tilde{\boldsymbol{K}}_m$ in Eq. (5.20a) is much simpler. Also, according to Chapter 3, the two matrices have the relationship in the following,

$$\boldsymbol{K}_m = \boldsymbol{L}_m{}^T \tilde{\boldsymbol{K}}_m \boldsymbol{L}_m \tag{5.21a}$$

$$\boldsymbol{L}_m = \begin{bmatrix} -1 & 0 & 0 & 1 & 0 & 0 & 0 & 0 & 0 \\ -1 & -y_3/x_2 & 0 & 0 & y_3/x_2 & 0 & 1 & 0 & 0 \\ 0 & -1+x_3/x_2 & 0 & 0 & -x_3/x_2 & 0 & 0 & 1 & 0 \\ 0 & 1/x_2 & 1 & 0 & -1/x_2 & 0 & 0 & 0 & 0 \\ 0 & 1/x_2 & 0 & 0 & -1/x_2 & 1 & 0 & 0 & 0 \\ 0 & 1/x_2 & 0 & 0 & -1/x_2 & 0 & 0 & 0 & 1 \end{bmatrix} \tag{5.21b}$$

5.2 Refined triangular Mindlin plate element

In this section, the refined triangular Mindlin plate element, so-called RDKTM, is introduced. The element is proposed by Chen and Cheung (2001) based on the Mindlin-Reissner plate theory. As a three-node triangular element, it is accurate for both thin and thick plates and free of locking for very thin plates. Furthermore, different from the classical Mindlin plate elements which require C^0 continuity, it does not need reduced or selective integration to overcome transverse shear locking, and therefore the zero energy modes causing mechanisms of structures can be avoided.

The derivation of the element is similar to the DKT (discrete Kirchhoff triangular) element which is a well-known three-node triangular plate element proposed by Batoz et al. (1980a) based on the Kirchhoff hypothesis. In the derivation of the DKT

element, the six-node triangular element including three corner nodes and three mid-side nodes is adopted at first and the interpolation functions for the bending rotations are quadric. Then, the variables at the mid-side nodes can be eliminated using the cubic functions for the element sides referring to the classical Euler–Bernoulli beam element. Finally, the six-node element can degenerate into the three-node element, i.e. only corner nodes. As the RDKTM element is based on the Mindlin-Reissner plate hypothesis, its derivations are similar to conventional DKT element. The basic difference is that the functions for the element sides are based on the Timoshenko beam hypothesis and transverse shear strains should be considered and constituted.

After that, Batoz (1982) proposed a new version of DKT element with explicit expression to replace numerical integration for the stiffness matrix. The new formulation is simple with significantly reduction of computer time compared with the previous study using three numerical integration points. Thus, the method is also adopted in this thesis to present the explicit expression of the RDKTM element. The difference is that the proposed pure deformational method is applied here to further simplify the formulation of the RDKTM element.

5.2.1 Timoshenko beam function

As mentioned before, the DKT element which is based on the Kirchhoff hypothesis successfully employs the cubic function in Euler–Bernoulli beam element to establish its formulation. By contrast, the interpolation function for the Timoshenko beam element is adopted in the RDKTM element. However, like classical Mindlin plate

elements, the shear locking phenomenon also exists in the classical Timoshenko beam element which uses two independent linear interpolation functions to describe the deflections and rotations over the element respectively. Thus, the reduced numerical integration should be used in the classical Timoshenko beam element to remove the shear locking.

An alternative method to make the Timoshenko beam element locking-free and obtain accurate solutions for both thin and thick plates is via the consistent displacement function (Tang *et al.*, 2015) to derive the formulation. In this method, the deflection of the Timoshenko beam element is still assumed as a cubic function. However, different from the displacement-based method, except for the nodal displacement values, the governing equations are also used in the derivation. Thus, the derivation belongs to the mixed type element method and is detailed in the following.

First, for using the Timoshenko beam function in the derivation of the RDKTM plate element, a strip plate with Length L, width b and thickness t is considered, as shown in Figure 5.4.

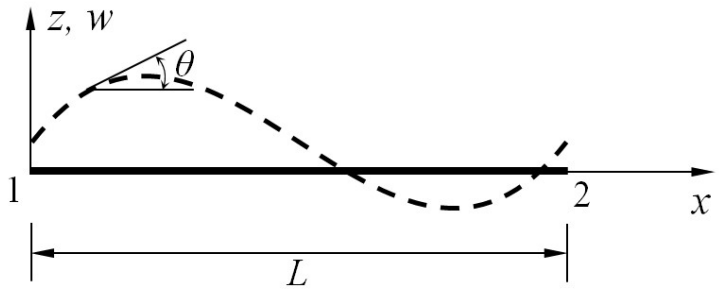

Figure 5.4 Timoshenko beam element

According to the Timoshenko beam hypothesis, when the pressure load is neglected, the governing differential equations can be given in the following,

$$\theta - \frac{dw}{dx} = \lambda_e L^2 \frac{d^2\theta}{dx^2} \tag{5.22a}$$

$$\frac{d\theta}{dx} - \frac{d^2w}{dx^2} = 0 \tag{5.22b}$$

where w and θ are the displacement and rotation at the point x along the neutral axis respectively and $\lambda_e = \frac{t^2}{5L^2(1-v)}$.

Assuming the displacement function is cubic and taking use of Eq. (5.22b), we have

$$w = c_3x^3 + c_2x^2 + c_1x + c_0 \tag{5.23a}$$

$$\theta = 3c_3x^2 + 2c_2x + c_4 \tag{5.23b}$$

It can be seen that there are five uncertain coefficients c_0 to c_4. Taking use of Eq. (5.22a) and the boundary conditions given in Eq. (5.24), we can solve these five coefficients and further obtain the displacement and rotation functions expressed in Eq.(5.25).

$$w|_{x=0} = w_1, \quad \theta|_{x=0} = \theta_1 \tag{5.24a}$$

$$w|_{x=L} = w_2, \quad \theta|_{x=L} = \theta_2 \tag{5.24b}$$

$$\begin{aligned} w = {} & \left(L_1 + \mu_e L_1 L_2 \left(L_1 - L_2\right)\right) w_1 + \left(L_2 + \mu_e L_1 L_2 \left(L_2 - L_1\right)\right) w_2 \\ & + 0.5L\left(L_1 L_2 + \mu_e L_1 L_2 \left(L_1 - L_2\right)\right)\theta_1 \\ & + 0.5L\left(-L_1 L_2 + \mu_e L_1 L_2 \left(L_1 - L_2\right)\right)\theta_2 \end{aligned} \tag{5.25a}$$

$$\begin{aligned}\theta = &-\left(6L_1L_2/L\right)\mu_e w_1 + \left(6L_1L_2/L\right)\mu_e w_2 \\ &+L_1\left(1-3\mu_e L_2\right)\theta_1 + L_2\left(1-3\mu_e L_1\right)\theta_2\end{aligned} \tag{5.25b}$$

in which $L_1 = 1 - x/L$, $L_2 = x/L$, $\mu_e = \dfrac{1}{1+12\lambda_e}$.

Then, the shear strain of the strip plate, which is constant without pressure load, is obtained as

$$\gamma = \frac{dw}{dx} - \theta = \left(1-\mu_e\right)\left(\frac{w_2 - w_1}{L} - \frac{\theta_1 + \theta_2}{2}\right) \tag{5.26}$$

5.2.2 Derivation of the RDKTM plate element

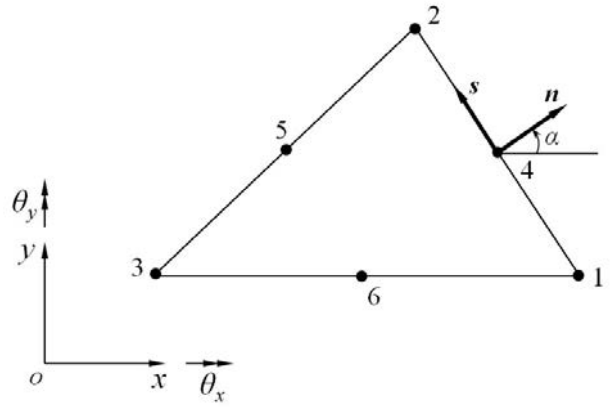

Figure 5.5 A six-node triangular plate element with mid-side nodes

Figure 5.5 shows a six-node triangular plate element and the displacement functions can be defined by

$$\theta_x = \sum_{i=1}^{3} N_i \theta_{xi} + \sum_{k=4}^{6} N_k \theta_{xk} \tag{5.27a}$$

$$\theta_y = \sum_{i=1}^{3} N_i \theta_{yi} + \sum_{k=4}^{6} N_k \theta_{yk} \tag{5.27b}$$

$$w = \sum_{i=1}^{3} N_i w_i + \sum_{k=4}^{6} N_k w_k \tag{5.27c}$$

in which N_i and N_k are the shape functions expressed with the area coordinate ξ_i and can be detailed as follows,

$$N_1 = (2\xi_1 - 1)\xi_1, \quad N_2 = (2\xi_2 - 1)\xi_2, \quad N_3 = (2\xi_3 - 1)\xi_3 \tag{5.28a, b, c}$$

$$N_4 = 4\xi_1\xi_2, \quad N_5 = 4\xi_2\xi_3, \quad N_6 = 4\xi_3\xi_1 \tag{5.28e, f, g}$$

Then, to eliminate the displacement and rotation values at the mid-side node *k* on the side *i-j*, the interpolation function given in Eq. (5.25b) should be used. According to Eq. (5.25b), the normal rotation of the side *i-j* at the mid-side node *k* can be given by

$$\theta_{nk} = \frac{1.5\mu_{ij}}{S_{ij}}\left(w_j - w_i\right) + \frac{1 - 1.5\mu_{ij}}{2}\left(\theta_{ni} + \theta_{nj}\right) \tag{5.29a}$$

where i=1,2,3; j=mod(i,3)+1; k=i+3; $S_{ij} = \sqrt{(x_j - x_i)^2 + (y_j - y_i)^2}$ is the length of the side *i-j*; the parameter $\mu_{ij} = \dfrac{1}{1 + 12\lambda_{ij}}$, $\lambda_{ij} = \dfrac{t^2}{5S_{ij}^{\,2}(1 - v)}$; and θ_{ni}, θ_{nj} are the normal rotations at the corner node *i* and *j* on the side *i-j* respectively.

Assuming the tangential rotation θ_s along a side of the element varies linearly, the tangential rotation θ_{sk} at the mid-side node *k* can be given by

$$\theta_{sk} = \frac{1}{2}\left(\theta_{si} + \theta_{sj}\right) \tag{5.29b}$$

in which θ_{si} and θ_{sj} are the tangential rotations at the corner node *i* and *j* on the side *i-j* respectively.

Consequently, as shown in Figure 5.5, the rotations θ_{ni} and θ_{si} at the corner node *i* on the side *i-j* can be expressed as

$$\begin{Bmatrix} \theta_{ni} \\ \theta_{si} \end{Bmatrix} = \begin{bmatrix} l_{ij} & m_{ij} \\ -m_{ij} & l_{ij} \end{bmatrix} \begin{Bmatrix} \theta_{xi} \\ \theta_{ji} \end{Bmatrix} \tag{5.30}$$

where $l_{ij} = \cos\alpha_{ij} = \dfrac{y_j - y_i}{S_{ij}}$ and $m_{ij} = \sin\alpha_{ij} = \dfrac{x_i - x_j}{S_{ij}}$ are the direction cosine and the direction sine of the side *i-j* respectively.

For the interpolation functions of the six-node triangular element shown in Eqs. (5.27a, b), the rotations θ_{xk} and θ_{yk} at the mid-side node *k* can be eliminated by the relationship as follows,

$$\begin{Bmatrix} \theta_{xk} \\ \theta_{yk} \end{Bmatrix} = \begin{bmatrix} l_{ij} & -m_{ij} \\ m_{ij} & l_{ij} \end{bmatrix} \begin{Bmatrix} \theta_{nk} \\ \theta_{sk} \end{Bmatrix} \tag{5.31}$$

Taking use of Eqs. (5.29) and (5.30), the rotation interpolation functions of the plate element can be modified as

$$\begin{Bmatrix} \theta_x \\ \theta_y \end{Bmatrix} = \begin{bmatrix} \hat{\boldsymbol{N}}_1 & \hat{\boldsymbol{N}}_2 & \hat{\boldsymbol{N}}_3 \end{bmatrix} \boldsymbol{d}_p \tag{5.32a}$$

$$\hat{\boldsymbol{N}}_i = \begin{bmatrix} P_{i1} & P_{i2} & P_{i3} \\ Q_{i1} & Q_{i2} & Q_{i3} \end{bmatrix} \tag{5.32b}$$

$$P_{i1} = -d_i N_{i+3} + d_j N_{j+3} \tag{5.32c}$$

$$P_{i2} = N_i - e_i N_{i+3} - e_j N_{j+3} \tag{5.32d}$$

$$P_{i3} = b_i N_{i+3} + b_j N_{j+3} \tag{5.32e}$$

$$Q_{i1} = a_i N_{i+3} - a_j N_{j+3} \tag{5.32f}$$

$$Q_{i2} = b_i N_{i+3} + b_j N_{j+3} \tag{5.32g}$$

$$Q_{i3} = N_i + c_i N_{i+3} + c_j N_{j+3} \tag{5.32h}$$

$$i = 1,2,3; \quad j = 3\,\mathrm{floor}(1/i) + i - 1. \tag{5.32i}$$

in which $\boldsymbol{d}_p = \left\{w_1 \;\; \theta_{x1} \;\; \theta_{y1} \;\; w_2 \;\; \theta_{x2} \;\; \theta_{y2} \;\; w_3 \;\; \theta_{x3} \;\; \theta_{y3}\right\}^T$ is the displacement vector of the three-node triangular plate element and the coefficients used in Eq. (5.32b) to (5.32h) are given by

$$a_i = -\frac{3}{2}\frac{m_{ij}\mu_{ij}}{S_{ij}}, \quad b_i = -\frac{3}{4} l_{ij} m_{ij} \mu_{ij}, \quad c_i = \frac{1}{2} - \frac{3}{4} m_{ij}^2 \mu_{ij} \tag{5.33a, b, c}$$

$$d_i = \frac{3}{2}\frac{l_{ij}\mu_{ij}}{S_{ij}}, \quad e_i = -\frac{1}{2} + \frac{3}{4} m_{ij}^2 \mu_{ij} \tag{5.33d, e}$$

Thus, the six-node triangular plate element shown in Figure 5.5 has degenerated into the three-node element. Then, the bending strains which are the curvatures of the triangular plate element can be given by

$$\boldsymbol{\kappa}=\begin{Bmatrix}\kappa_x\\ \kappa_y\\ \kappa_{xy}\end{Bmatrix}=\begin{Bmatrix}\dfrac{\partial\theta_y}{\partial x}\\ -\dfrac{\partial\theta_x}{\partial y}\\ \dfrac{\partial\theta_y}{\partial y}-\dfrac{\partial\theta_x}{\partial x}\end{Bmatrix}=\boldsymbol{B}_b\boldsymbol{d}_p=\begin{bmatrix}\boldsymbol{B}_{b1} & \boldsymbol{B}_{b2} & \boldsymbol{B}_{b3}\end{bmatrix}\boldsymbol{d}_p \tag{5.34a}$$

$$\boldsymbol{B}_{bi}=\begin{bmatrix}\dfrac{\partial Q_{i1}}{\partial x} & \dfrac{\partial Q_{i2}}{\partial x} & \dfrac{\partial Q_{i3}}{\partial x}\\ -\dfrac{\partial P_{i1}}{\partial y} & -\dfrac{\partial P_{i2}}{\partial y} & -\dfrac{\partial P_{i3}}{\partial y}\\ \dfrac{\partial Q_{i1}}{\partial y}-\dfrac{\partial P_{i1}}{\partial x} & \dfrac{\partial Q_{i2}}{\partial y}-\dfrac{\partial P_{i2}}{\partial x} & \dfrac{\partial Q_{i3}}{\partial y}-\dfrac{\partial P_{i3}}{\partial x}\end{bmatrix},\ i=1,2,3 \tag{5.34b}$$

where the matrix $\boldsymbol{B}_b$ is the bending strain-displacement matrix.

Regarding the shear strains of the triangular plate element, its derivation is also started from the shear strains of the element sides. Through the shear strain of a strip plate shown in Eq. (5.26), the constant shear strain along the side *i*-*j* can be given by

$$\gamma_{ij}=\left(1-\mu_{ij}\right)\left(\frac{w_j-w_i}{S_{ij}}-\frac{\theta_{ni}+\theta_{nj}}{2}\right) \tag{5.35a}$$

Also, the shear strain along the side *j*-*k* is also constant and equals to

$$\gamma_{jk}=\left(1-\mu_{jk}\right)\left(\frac{w_k-w_j}{S_{jk}}-\frac{\theta_{nj}+\theta_{nk}}{2}\right) \tag{5.35b}$$

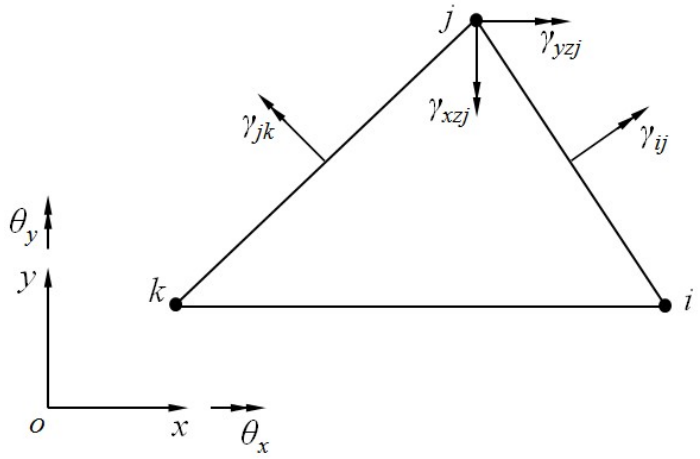

Figure 5.6 Shear strains of triangular plate element

Assuming that the projections of the shear strains at the node *j* on the side *i*-*j* and *j*-*k* are equal to the constant shear strains of these two sides respectively according to Figure 5.6, we have

$$\gamma_{ij} = l_{ij}\gamma_{yzj} - m_{ij}\gamma_{xzj} \tag{5.36a}$$

$$\gamma_{jk} = l_{jk}\gamma_{yzj} - m_{jk}\gamma_{xzj} \tag{5.36b}$$

Thus, the shear strains at the node *j* can be solved by Eqs. (5.36) and given by

$$\begin{Bmatrix} \gamma_{xzj} \\ \gamma_{yzj} \end{Bmatrix} = \frac{1}{l_{ij}m_{jk} - l_{jk}m_{ij}} \begin{bmatrix} l_{jk} & -l_{ij} \\ m_{jk} & -m_{ij} \end{bmatrix} \begin{Bmatrix} \gamma_{ij} \\ \gamma_{jk} \end{Bmatrix} \tag{5.37}$$

in which i=1,2,3; j=mod(i,3)+1; k=mod(j,3)+1.

Then, the shear strains of the triangular plate element can be linearly interpolated by the nodal shear strains as follows,

$$\boldsymbol{\gamma} = \begin{Bmatrix} \gamma_{xz} \\ \gamma_{yz} \end{Bmatrix} = \sum_{i=1}^{3} \xi_i \begin{Bmatrix} \gamma_{xzi} \\ \gamma_{yzi} \end{Bmatrix} = \bar{\boldsymbol{N}} \begin{Bmatrix} \gamma_{12} \\ \gamma_{23} \\ \gamma_{31} \end{Bmatrix} \tag{5.38a}$$

$$\bar{\boldsymbol{N}} = \begin{bmatrix} \frac{l_{31}}{C_1}\xi_1 - \frac{l_{23}}{C_2}\xi_2 & \frac{l_{12}}{C_2}\xi_2 - \frac{l_{31}}{C_3}\xi_3 & \frac{l_{23}}{C_3}\xi_3 - \frac{l_{12}}{C_1}\xi_1 \\ \frac{m_{31}}{C_1}\xi_1 - \frac{m_{23}}{C_2}\xi_2 & \frac{m_{12}}{C_2}\xi_2 - \frac{m_{31}}{C_3}\xi_3 & \frac{m_{23}}{C_3}\xi_3 - \frac{m_{12}}{C_1}\xi_1 \end{bmatrix} \tag{5.38b}$$

$$C_1 = l_{12}m_{31} - l_{31}m_{12} \tag{5.38c}$$

$$C_2 = l_{23}m_{12} - l_{12}m_{23} \tag{5.38d}$$

$$C_3 = l_{31}m_{23} - l_{23}m_{31} \tag{5.38e}$$

Through Eqs. (5.30) and (5.35), the constant shear strains along each side of the plate element can be given by

$$\begin{Bmatrix} \gamma_{12} \\ \gamma_{23} \\ \gamma_{31} \end{Bmatrix} = \bar{\boldsymbol{B}}_s \boldsymbol{u}_p = \begin{bmatrix} \bar{\boldsymbol{B}}_{s1} & \bar{\boldsymbol{B}}_{s2} & \bar{\boldsymbol{B}}_{s3} \end{bmatrix} \boldsymbol{d}_p \tag{5.39a}$$

$$\bar{\boldsymbol{B}}_{s1} = \begin{bmatrix} \frac{-1+\mu_{12}}{l_{12}} & \frac{1}{2}l_{12}\left(-1+\mu_{12}\right) & \frac{1}{2}m_{12}\left(-1+\mu_{12}\right) \\ 0 & 0 & 0 \\ \frac{1-\mu_{31}}{l_{31}} & \frac{1}{2}l_{31}\left(-1+\mu_{31}\right) & \frac{1}{2}m_{31}\left(-1+\mu_{31}\right) \end{bmatrix} \tag{5.39b}$$

$$\bar{\boldsymbol{B}}_{s2} = \begin{bmatrix} \frac{1-\mu_{12}}{l_{12}} & \frac{1}{2}l_{12}\left(-1+\mu_{12}\right) & \frac{1}{2}m_{12}\left(-1+\mu_{12}\right) \\ \frac{-1+\mu_{23}}{l_{23}} & \frac{1}{2}l_{23}\left(-1+\mu_{23}\right) & \frac{1}{2}m_{23}\left(-1+\mu_{23}\right) \\ 0 & 0 & 0 \end{bmatrix} \tag{5.39c}$$

$$\bar{\boldsymbol{B}}_{s3}=\begin{bmatrix} 0 & 0 & 0 \\ \dfrac{1-\mu_{23}}{l_{23}} & \dfrac{1}{2}l_{23}\left(-1+\mu_{23}\right) & \dfrac{1}{2}m_{23}\left(-1+\mu_{23}\right) \\ \dfrac{-1+\mu_{31}}{l_{31}} & \dfrac{1}{2}l_{31}\left(-1+\mu_{31}\right) & \dfrac{1}{2}m_{31}\left(-1+\mu_{31}\right) \end{bmatrix} \tag{5.39d}$$

Finally, the shear strain-displacement matrix can be given by

$$\boldsymbol{\gamma}=\boldsymbol{B}_s\boldsymbol{d}_p \tag{5.40a}$$

$$\boldsymbol{B}_s=\bar{\boldsymbol{N}}\bar{\boldsymbol{B}}_s \tag{5.40b}$$

To derive the stiffness matrix of the three-node triangular plate element, the variational formulation including the bending and shear modes over the plate element area A is given by

$$\Pi_p=\int_A\boldsymbol{\kappa}^T\boldsymbol{D}_b\boldsymbol{\kappa}dA+\int_A\boldsymbol{\gamma}^T\boldsymbol{D}_s\boldsymbol{\gamma}dA-\int_A\boldsymbol{d}_p{}^T\boldsymbol{f}_pdA \tag{5.41}$$

where $\boldsymbol{D}_b$ and $\boldsymbol{D}_s$ are the constitutive matrices as follows,

$$\boldsymbol{D}_b=\frac{Et^3}{12(1-v^2)}\begin{bmatrix} 1 & v & 0 \\ v & 1 & 0 \\ 0 & 0 & 0.5(1-v) \end{bmatrix} \tag{5.42a}$$

$$\boldsymbol{D}_s=\frac{5Et}{12(1+v)}\begin{bmatrix} 1 & 0 \\ 0 & 1 \end{bmatrix} \tag{5.42b}$$

Taking variation of Eq. (5.41) gives

$$\boldsymbol{K}_p\boldsymbol{d}_p=\boldsymbol{f}_p \tag{5.43a}$$

$$\boldsymbol{K}_p = \boldsymbol{K}_b + \boldsymbol{K}_s \tag{5.43b}$$

in which $\boldsymbol{K}_p$ is the stiffness matrix of the plate element including two parts, i.e. the bending stiffness matrix $\boldsymbol{K}_b$ and shear stiffness matrix $\boldsymbol{K}_s$. The matrices $\boldsymbol{K}_b$ and $\boldsymbol{K}_s$. are given by

$$\boldsymbol{K}_b = \int_A \boldsymbol{B}_b^T \boldsymbol{D}_b \boldsymbol{B}_b dA \tag{5.44a}$$

$$\boldsymbol{K}_s = \int_A \boldsymbol{B}_s^T \boldsymbol{D}_s \boldsymbol{B}_s dA \tag{5.44b}$$

The two matrices can be computed by the numerical integration and alternatively, their explicit expressions can be derived and directly inputted in the program for elastic analyses. It is clear that the explicit expressions are more efficient than the numerical integration. However, the formulations of the strain-displacement matrices $\boldsymbol{B}_b$ and $\boldsymbol{B}_s$ are very complicated and therefore it is difficult to obtain their explicit expressions. Thus, in the thesis several effective measures are used to derive and simplify the explicit expressions of the stiffness matrices of the RDKTM plate element based on the proposed pure deformational method.

5.2.3 Simplification of the RDKTM plate element based on the pure deformational method

In this section, the proposed pure deformational method is used to decrease the dimensions of the strain-displacement matrices $\boldsymbol{B}_b$ and $\boldsymbol{B}_s$. Their expressions are based on the basic coordinate system which is same as the OPT membrane element as

shown in Section 5.1. Further, the method proposed by Batoz (1982) is adopted here to derive the explicit formulations of the stiffness matrices $\boldsymbol{K}_b$ and $\boldsymbol{K}_s$ of the RDKTM plate element.

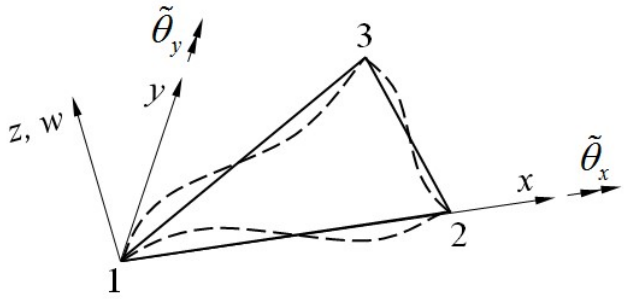

Figure 5.7 Basic coordinate system of the triangular plate element

Figure 5.7 depicts the basic coordinate system of the triangular plate element which is identical to the triangular membrane element and has the same coordinate values, including $x_1 = y_1 = y_2 = 0$. Also, the vertical translations are restrained and only bending rotations are remained in the pure deformational model. The displacement vector in the basis coordinate system can be given by

$$\tilde{\boldsymbol{d}}_p = \{\tilde{\theta}_{x1}\ \tilde{\theta}_{y1}\ \tilde{\theta}_{x2}\ \tilde{\theta}_{y2}\ \tilde{\theta}_{x3}\ \tilde{\theta}_{y3}\}^T \tag{5.45}$$

in which these rotations in $\tilde{\boldsymbol{d}}_p$ are identical to those in $\boldsymbol{d}_p$ in the local coordinate system.

Thus, the strain-displacement matrices in the basic coordinate system can be directly obtained through $\boldsymbol{B}_b$ and $\boldsymbol{B}_s$, without the columns associated with the translational

degrees of freedom. Then, the bending strain-displacement matrix in the basic coordinate system can be given by

$$\tilde{\boldsymbol{B}}_b = \begin{bmatrix} \tilde{\boldsymbol{B}}_{b1} & \tilde{\boldsymbol{B}}_{b2} & \tilde{\boldsymbol{B}}_{b3} \end{bmatrix} \tag{5.46a}$$

$$\tilde{\boldsymbol{B}}_{bi} = \begin{bmatrix} \dfrac{\partial Q_{i2}}{\partial x} & \dfrac{\partial Q_{i3}}{\partial x} \\ -\dfrac{\partial P_{i2}}{\partial y} & -\dfrac{\partial P_{i3}}{\partial y} \\ \dfrac{\partial Q_{i2}}{\partial y} - \dfrac{\partial P_{i2}}{\partial x} & \dfrac{\partial Q_{i3}}{\partial y} - \dfrac{\partial P_{i3}}{\partial x} \end{bmatrix}, \; i=1,2,3 \tag{5.46b}$$

The shear strain-displacement matrix in the basic coordinate system is

$$\tilde{\boldsymbol{B}}_s = \bar{\boldsymbol{N}}\tilde{\tilde{\boldsymbol{B}}}_s \tag{5.47a, b}$$

$$\tilde{\tilde{\boldsymbol{B}}}_s = \begin{bmatrix} \tilde{\tilde{\boldsymbol{B}}}_{s1} & \tilde{\tilde{\boldsymbol{B}}}_{s2} & \tilde{\tilde{\boldsymbol{B}}}_{s3} \end{bmatrix} \tag{5.47a, b}$$

$$\tilde{\tilde{\boldsymbol{B}}}_{s1} = \frac{1}{2}\begin{bmatrix} l_{12}\left(-1+\mu_{12}\right) & m_{12}\left(-1+\mu_{12}\right) \\ 0 & 0 \\ l_{31}\left(-1+\mu_{31}\right) & m_{31}\left(-1+\mu_{31}\right) \end{bmatrix} \tag{5.47c}$$

$$\tilde{\tilde{\boldsymbol{B}}}_{s2} = \frac{1}{2}\begin{bmatrix} l_{12}\left(-1+\mu_{12}\right) & m_{12}\left(-1+\mu_{12}\right) \\ l_{23}\left(-1+\mu_{23}\right) & m_{23}\left(-1+\mu_{23}\right) \\ 0 & 0 \end{bmatrix} \tag{5.47d}$$

$$\tilde{\tilde{\boldsymbol{B}}}_{s3} = \frac{1}{2}\begin{bmatrix} 0 & 0 \\ l_{23}\left(-1+\mu_{23}\right) & m_{23}\left(-1+\mu_{23}\right) \\ l_{31}\left(-1+\mu_{31}\right) & m_{31}\left(-1+\mu_{31}\right) \end{bmatrix} \tag{5.47e}$$

It can be seen that the 3×9 matrices $\boldsymbol{B}_b$ and $\boldsymbol{B}_s$ have been degenerated into the 3×6 matrices $\tilde{\boldsymbol{B}}_b$ and $\tilde{\boldsymbol{B}}_s$. The operation can simplify the derivation of the explicit formulation for the triangular plate element.

According to the method proposed by Batoz (1982), the matrix $\tilde{\boldsymbol{B}}_b$ can be decomposed into the product of the 3×9 matrix $\boldsymbol{h}_b$ and the 9×6 matrix $\boldsymbol{\alpha}_b$, in which the matrix $\boldsymbol{\alpha}_b$ is independent of the area coordinate ξ_i. The decomposition can be given by

$$\tilde{\boldsymbol{B}}_b = \frac{1}{2A}\boldsymbol{h}_b\boldsymbol{\alpha}_b \tag{5.48a}$$

$$\boldsymbol{h}_b = \begin{bmatrix} \xi_1 & \xi_1 & \xi_3 & 0 & 0 & 0 & 0 & 0 & 0 \\ 0 & 0 & 0 & \xi_1 & \xi_2 & \xi_3 & 0 & 0 & 0 \\ 0 & 0 & 0 & 0 & 0 & 0 & \xi_1 & \xi_2 & \xi_3 \end{bmatrix} \tag{5.48b}$$

in which the components of the matrix $\boldsymbol{\alpha}_b$ only are dependent on the geometry and the Poisson's ratio of the plate element. Because the matrix $\boldsymbol{\alpha}_b$ is large, it is divided into two parts for easy presentation in the following,

$$\boldsymbol{\alpha}_b = \begin{bmatrix} \boldsymbol{\alpha}_{b1} & \boldsymbol{\alpha}_{b2} \end{bmatrix} \tag{5.49a}$$

$$\boldsymbol{\alpha}_{b1} = \begin{bmatrix} 0 & 4(c_1-1)y_3 & 0 \\ 0 & -4c_1y_3 & 0 \\ -b_3y_3 & -4c_3y_3 & 4b_2y_3 \\ 4(1+e_3)x_2-2x_3 & -4b_3x_2 & 2x_3 \\ -2x_{32} & 0 & 2\left((1+2e_2)x_2+x_3\right) \\ 4e_3x_{32} & -4b_3x_{32} & -4e_2x_3 \\ 2(2b_3x_2+y_3) & 4(c_3-1)x_2-4(c_1-1)x_3 & -2y_3 \\ 2y_3 & 4c_1x_{32} & 4b_2x_2-2y_3 \\ 4b_3x_{32}-4e_3y_3 & 4(c_3x_{32}+b_3y_3) & -4b_2x_3+4e_2y_3 \end{bmatrix} \tag{5.49b}$$

$$\boldsymbol{\alpha}_{b2}=4\begin{bmatrix} 0 & 0 \\ c_1y_3 & 0 \\ (1-c_1)y_3 & b_{23}y_3 \\ c_2y_3 & e_3x_2 \\ 0 & e_2x_2 \\ -b_2x_2 & -(1+e_3)x_2+e_{32}x_3 \\ b_2x_3 & b_3x_2 \\ -c_1x_3 & b_2x_2 \\ c_{21}x_2+(c_1-1)x_3 & -b_2x_3+b_3x_{32} \\ -c_2x_3-b_2y_3 & +e_{23}y_3 \end{bmatrix}\begin{bmatrix} 0 \\ 0 \\ c_{23}y_3 \\ -b_3x_2 \\ -b_2x_2 \\ b_3x_{23}+b_2x_3 \\ c_3x_2 \\ c_2x_2 \\ (1-c_3)x_2 \\ +c_{32}x_3+b_{32}y_3 \end{bmatrix} \tag{5.49c}$$

in which $(.)_{ij}=(.)_i-(.)_j$.

Through the decomposition of the matrix $\tilde{\boldsymbol{B}}_b$, the integration of the stiffness matrix becomes more easily. In the basic coordinate system, the stiffness matrix can be integrated as follows,

$$\tilde{\boldsymbol{K}}_b=\int_A \tilde{\boldsymbol{B}}_b{}^T\boldsymbol{D}_b\tilde{\boldsymbol{B}}_b dA=\frac{1}{2A}\boldsymbol{\alpha}_b{}^T\boldsymbol{H}_b\boldsymbol{\alpha}_b{}^T \tag{5.50a}$$

$$\boldsymbol{H}_b=\frac{1}{2A}\int_A \boldsymbol{h}_b{}^T\boldsymbol{D}_b\boldsymbol{h}_b dA \tag{5.50b}$$

Also, we have the equations as

$$\xi_3=1-\xi_1-\xi_2 \tag{5.51a}$$

$$dA=2A d\xi_1 d\xi_2 \tag{5.51b}$$

Introducing Eqs. (5.51) into Eqs. (5.50), it gives

$$\boldsymbol{H}_b=\int_0^1\int_0^{1-\xi_1}\boldsymbol{h}_b{}^T\boldsymbol{D}_b\boldsymbol{h}_b d\xi_2 d\xi_1 \tag{5.52a}$$

$$\boldsymbol{H}_b = \frac{1}{24}\frac{Et^3}{12(1-v^2)}\begin{bmatrix} \boldsymbol{R} & v\boldsymbol{R} & \boldsymbol{0} \\ v\boldsymbol{R} & \boldsymbol{R} & \boldsymbol{0} \\ \boldsymbol{0} & \boldsymbol{0} & 0.5(1-\mathrm{v})\boldsymbol{R} \end{bmatrix} \tag{5.52b}$$

$$\boldsymbol{R}=\begin{bmatrix} 2 & 1 & 1 \\ 1 & 2 & 1 \\ 1 & 1 & 2 \end{bmatrix} \tag{5.52c}$$

in which $\boldsymbol{H}_b$ is a 9×9 matrix.

Finally, the bending stiffness matrix in the basic coordinate system can be explicitly given. In fact, the derivation introduced in the last section can be directly conducted based on the pure deformational model instead of the element model with rigid body movements, which can simplify the derivation process further.

For the shear stiffness matrix, the 2×3 matrix $\bar{\boldsymbol{N}}$ can be decomposed into the product of the 2×6 matrix $\boldsymbol{h}_s$ and the 6×3 matrix $\boldsymbol{\alpha}_s$ using the same method, in which the matrix $\boldsymbol{\alpha}_s$ is independent of the area coordinate ξ_i. Then, we have

$$\bar{\boldsymbol{N}} = \frac{1}{2A}\boldsymbol{h}_s\boldsymbol{\alpha}_s \tag{5.53a}$$

$$\boldsymbol{h}_s = \begin{bmatrix} \xi_1 & \xi_2 & \xi_3 & 0 & 0 & 0 \\ 0 & 0 & 0 & \xi_1 & \xi_2 & \xi_3 \end{bmatrix} \tag{5.53b}$$

in which the matrix $\boldsymbol{\alpha}_s$ can be simplified with the known coordinate values, $x_1 = y_1 = y_2 = 0$, as follows,

$$\boldsymbol{\alpha}_s = \begin{bmatrix} x_2 y_3 & 0 & 0 \\ x_2 y_3 & 0 & 0 \\ 0 & -l_{23} y_3 & -l_{31} y_3 \\ -x_2 x_3 & 0 & -l_{31} x_2 \\ -x_2 x_{32} & l_{23} x_2 & 0 \\ 0 & l_{23} x_3 & l_{31} x_{32} \end{bmatrix} \tag{5.53c}$$

Then, the shear stiffness matrix in the basic coordinate system can be given by

$$\tilde{\boldsymbol{K}}_s = \int_A \tilde{\boldsymbol{B}}_s{}^T \boldsymbol{D}_s \tilde{\boldsymbol{B}}_s dA = \frac{1}{2A} \tilde{\tilde{\boldsymbol{B}}}_s{}^T \boldsymbol{\alpha}_s{}^T \boldsymbol{H}_s \boldsymbol{\alpha}_s \tilde{\tilde{\boldsymbol{B}}}_s \tag{5.54a}$$

$$\begin{aligned} \boldsymbol{H}_s &= \frac{1}{2A} \int_A \boldsymbol{h}_s{}^T \boldsymbol{D}_s \boldsymbol{h}_s dA \\ &= \frac{1}{24} \frac{5Et}{12(1+v)} \begin{bmatrix} \boldsymbol{R} & \boldsymbol{0} \\ \boldsymbol{0} & \boldsymbol{R} \end{bmatrix} \end{aligned} \tag{5.54b}$$

in which $\boldsymbol{H}_s$ is a 6×6 matrix.

Thus, based on the basic coordinate system, the 6×6 stiffness matrix of the triangular Mindlin plate element with bending and shear parts can be given by

$$\tilde{\boldsymbol{K}}_p = \tilde{\boldsymbol{K}}_b + \tilde{\boldsymbol{K}}_s \tag{5.55}$$

The matrix $\tilde{\boldsymbol{K}}_p$ should be further transformed to the local coordinate system by

$$\boldsymbol{K}_p = \boldsymbol{L}_p{}^T \tilde{\boldsymbol{K}}_p \boldsymbol{L}_p \tag{5.56a}$$

$$\boldsymbol{L}_p = \begin{bmatrix} 1/y_3 - x_3/x_2 y_3 & 1 & 0 & x_3/x_2 y_3 & 0 & 0 & -1/y_3 & 0 & 0 \\ -1/x_2 & 0 & 1 & 1/\mathrm{x}_2 & 0 & 0 & 0 & 0 & 0 \\ 1/y_3 - x_3/x_2 y_3 & 0 & 0 & x_3/x_2 y_3 & 1 & 0 & -1/y_3 & 0 & 0 \\ -1/x_2 & 0 & 0 & 1/\mathrm{x}_2 & 0 & 1 & 0 & 0 & 0 \\ 1/y_3 - x_3/x_2 y_3 & 0 & 0 & x_3/x_2 y_3 & 0 & 0 & -1/y_3 & 1 & 0 \\ -1/x_2 & 0 & 0 & 1/\mathrm{x}_2 & 0 & 0 & 0 & 0 & 1 \end{bmatrix} \tag{5.56b}$$

The proposed triangular plate element can provide accurate solutions for both thin and thick plates. Moreover, when the shear deformation could be neglected, it can automatically degenerate into the DKT element if the parameter μ_{ij} for each side is set to 0, which can further simplify the formulation and enhance the computational efficiency.

In addition, the pure deformational method is very different from the general method. For the former approach, the complicated and redundant derivation process can be conducted based on the pure deformational model with less degree of freedom than the general method. Thus, there is no doubt that the pure deformational method can make the derivation of elements easier and produces simpler formulations.

5.3 Geometrically nonlinear analysis

In this section, the procedure of geometrically nonlinear analysis for the triangular shell element is detailed, which has been coded in the nonlinear finite element program NIDA (2015). The whole procedure is based on the simplified co-rotational formulation introduced in Chapter 4, which is a simplified version of the co-rotational method and inherits the property of element-independence. Thus, the triangular shell element which consists of the OPT membrane element and the RDKTM plate element can be easily embedded into the simplified co-rotational algorithm to conduct the geometrically nonlinear analysis of shell structures. Two key factors for geometrically nonlinear analysis scheme, the tangent stiffness matrix and the internal forces, are respectively introduced in the following.

5.3.1 Tangent stiffness

Compared to the general EICR formulation, the simplified EICR formulation neglects the projector matrix which reflects the changes of element dimensions and the operation greatly decreases the computation of the tangent stiffness matrix. In the process of nonlinear analysis, the tangent stiffness matrix of the shell element is continually updated based on the current configuration C_n, in which the global coordinates are $\boldsymbol{x}_i^g = \left\{x_i^g \;\; y_i^g \;\; z_i^g\right\}^T$ and the local internal force vector is

$$\boldsymbol{f} = \left\{\boldsymbol{n}_1^T \;\; \boldsymbol{m}_1^T \;\; \boldsymbol{n}_2^T \;\; \boldsymbol{m}_2^T \;\; \boldsymbol{n}_3^T \;\; \boldsymbol{m}_3^T\right\}^T \tag{5.57}$$

in which $\boldsymbol{n}_i = \left\{f_{xi} \;\; f_{yi} \;\; f_{zi}\right\}^T$ and $\boldsymbol{m}_i = \left\{m_{xi} \;\; m_{yi} \;\; m_{zi}\right\}^T$ represent the local internal forces and moments at the node i (i=1,2,3) respectively.

The definition of the local coordinate system should be identical to that of the OPT membrane element and the RDKTM plate element introduced before, in which the local x-axis is aligned to the side 1-2 and the plane xy coincides with the triangular facet. Then, the triad vectors for the local coordinate system of the triangular shell element at current configuration can be given by

$$\boldsymbol{e}_x = \frac{\boldsymbol{x}_2^g - \boldsymbol{x}_1^g}{\left\|\boldsymbol{x}_2^g - \boldsymbol{x}_1^g\right\|} \tag{5.58a}$$

$$\boldsymbol{e}_z = \boldsymbol{e}_x \times \frac{\boldsymbol{x}_3^g - \boldsymbol{x}_1^g}{\left\|\boldsymbol{x}_3^g - \boldsymbol{x}_1^g\right\|} \tag{5.58b}$$

$$\boldsymbol{e}_y = \boldsymbol{e}_z \times \boldsymbol{e}_x \tag{5.58c}$$

Then, the corresponding local-to-global transformation matrix can be written as

$$\boldsymbol{T}_e = \begin{bmatrix} \boldsymbol{e}_x & \boldsymbol{e}_y & \boldsymbol{e}_z \end{bmatrix}^T \tag{5.59}$$

The local tangent stiffness matrix of the triangular shell element based on the simplified co-rotational algorithm as introduced in Chapter 4 has two parts. One is the local material stiffness matrix of shell element $\boldsymbol{K}_e$, which is assembled by the stiffness matrices of the OPT membrane element and the RDKTM plate element shown in Eqs. (5.21) and (5.56) respectively. The local material stiffness matrix is always computed using the initial local coordinates and does not need to be modified by the projector matrix used in the general EICR formulation. Thus, for elastic problems, the local material stiffness matrix could be stored in the process of nonlinear analysis to save computational cost. Moreover, the material stiffness matrix based on the pure deformational model can be stored to save computer storage, although it needs the transformation from the basic to the local coordinate system and re-assembles the local material stiffness matrix.

The other part of the local tangent stiffness matrix in the simplified EICR formulation is the local geometric stiffness matrix introduced in Chapter 4 and can be given by

$$\boldsymbol{K}_g = \text{-}\boldsymbol{A}\boldsymbol{G} \tag{5.60a}$$

$$\boldsymbol{A}=\begin{bmatrix}\mathbf{Spin}(\boldsymbol{n}_1)\\ \mathbf{Spin}(\boldsymbol{m}_1)\\ \mathbf{Spin}(\boldsymbol{n}_2)\\ \mathbf{Spin}(\boldsymbol{m}_2)\\ \mathbf{Spin}(\boldsymbol{n}_3)\\ \mathbf{Spin}(\boldsymbol{m}_3)\end{bmatrix} \tag{5.60b}$$

$$\boldsymbol{G}=\begin{bmatrix}\boldsymbol{G}_1 & \mathbf{0}_{3\times3} & \boldsymbol{G}_2 & \mathbf{0}_{3\times3} & \boldsymbol{G}_3 & \mathbf{0}_{3\times3}\end{bmatrix} \tag{5.60c}$$

$$\boldsymbol{G}_1=\begin{bmatrix}0 & 0 & \dfrac{x_3-x_2}{x_2y_3}\\ 0 & 0 & \dfrac{1}{x_2}\\ 0 & -\dfrac{1}{x_2} & 0\end{bmatrix} \tag{5.60d}$$

$$\boldsymbol{G}_2=\begin{bmatrix}0 & 0 & -\dfrac{x_3}{x_2y_3}\\ 0 & 0 & -\dfrac{1}{x_2}\\ 0 & \dfrac{1}{x_2} & 0\end{bmatrix} \tag{5.60e}$$

$$\boldsymbol{G}_3=\begin{bmatrix}0 & 0 & \dfrac{1}{y_3}\\ 0 & 0 & 0\\ 0 & 0 & 0\end{bmatrix} \tag{5.60f}$$

in which $\mathbf{0}_{3\times3}$ is the 3×3 matrix whose components are all zero. Also, it should be noted that the matrix $\boldsymbol{G}$ is calculated by the initial local coordinates during the whole nonlinear analysis as same as the local material stiffness matrix of the shell element.

As mentioned before, the co-rotational algorithm has the drawback that its tangent stiffness matrix is unsymmetrical and it can be noticed that the local geometric stiffness matrix $\boldsymbol{K}_g$ is either unsymmetrical herein. However, most commercial finite element packages, including the program NIDA, use solvers requiring a symmetric matrix to save computer storage. Thus, the local geometric stiffness matrix $\boldsymbol{K}_g$ can be symmetrized as follows,

$$\boldsymbol{K}_g^{sym} = \frac{1}{2}(\boldsymbol{K}_g + \boldsymbol{K}_g{}^T) \tag{5.61}$$

Finally, the tangent stiffness matrix of the shell element in the global coordinate system is

$$\boldsymbol{K}_t = \boldsymbol{T}^T(\boldsymbol{K}_e + \boldsymbol{K}_g^{sym})\boldsymbol{T} \tag{5.62}$$

where the matrix $\boldsymbol{T}$ is composed of the local-to-global transformation matrix $\boldsymbol{T}_e$ along diagonal.

The symmetrized stiffness can keep the convergence rate and obtain accurate solutions as same as the original unsymmetrical one, which was proved by Nour-Omid and Rankin (1991). However, in my experience, the symmetrized stiffness in the simplified EICR formulation is hard to get convergence for some very extreme cases which may never happen in practical engineering structures. The problem is discussed with numerical examples in Chapter 7.

5.3.2 Internal forces

The internal forces in the simplified EICR formulation are different from that in the general EICR formulation and neglect the changes of element dimensions. For the process of extracting local pure deformations from the global total deformations, the simplified method is identical to the general one, which is detailed in Chapter 4. Thus, the process to get the internal forces of the triangular shell element in the simplified EICR formulation is briefly introduced in the following.

In the nonlinear analysis, the incremental displacements and rotations of the triangular shell element in the global coordinate system can be expressed as

$$\Delta \boldsymbol{d}^{g} = \left\{ \Delta \boldsymbol{d}_1^{gT} \;\; \Delta \boldsymbol{d}_2^{gT} \;\; \Delta \boldsymbol{d}_3^{gT} \right\}^{T} \tag{5.63a}$$

$$\Delta \boldsymbol{d}_i^{g} = \left\{ \Delta u_{xi}^{g} \;\; \Delta u_{yi}^{g} \;\; \Delta u_{zi}^{g} \;\; \Delta \theta_{xi}^{g} \;\; \Delta \theta_{yi}^{g} \;\; \Delta \theta_{zi}^{g} \right\}^{T} \tag{5.63b}$$

$$\Delta \boldsymbol{u}_i^{g} = \left\{ \Delta u_{xi}^{g} \;\; \Delta u_{yi}^{g} \;\; \Delta u_{zi}^{g} \right\}^{T} \tag{5.63c}$$

$$\Delta \boldsymbol{\theta}_i^{g} = \left\{ \Delta \theta_{xi}^{g} \;\; \Delta \theta_{yi}^{g} \;\; \Delta \theta_{zi}^{g} \right\}^{T} \tag{5.63d}$$

Then, the global coordinates of the node *i* can be updated as

$$\boldsymbol{x}_i^{g\,n+1} = \boldsymbol{x}_i^{g\,n} + \Delta \boldsymbol{u}_i^{g} \tag{5.64}$$

After that, the local-to-global transformation matrix $\boldsymbol{T}_e$ and local coordinates $\boldsymbol{x}_i$ can be updated with the new global coordinates.

With the procedure proposed in Chapter 4, the increments of the pure deformation vectors corresponding to the membrane element and the plate element denoted as $\Delta \tilde{\boldsymbol{d}}_m$ and $\Delta \tilde{\boldsymbol{d}}_p$ respectively can be extracted from the incremental displacements

and rotations in the global coordinate system. Then, the associated incremental internal forces of the OPT membrane element and the RDKTM plate element in the basic coordinate system can be given by

$$\Delta\tilde{\boldsymbol{f}}_m = \tilde{\boldsymbol{K}}_m^0 \Delta\tilde{\boldsymbol{d}}_m \tag{5.65a}$$

$$\Delta\tilde{\boldsymbol{f}}_p = \tilde{\boldsymbol{K}}_p^0 \Delta\tilde{\boldsymbol{d}}_p \tag{5.65b}$$

where the matrices $\tilde{\boldsymbol{K}}_m^0$ and $\tilde{\boldsymbol{K}}_p^0$ refer to the material stiffness matrix of the OPT membrane element and the RDKTM plate element computed based on the initial local nodal coordinates, respectively.

Transforming these incremental internal forces into the local coordinate system, there follows

$$\Delta\boldsymbol{f}_m = \boldsymbol{L}_m^{0\,T} \Delta\tilde{\boldsymbol{f}}_m \tag{5.66a}$$

$$\Delta\boldsymbol{f}_p = \boldsymbol{L}_p^{0\,T} \Delta\tilde{\boldsymbol{f}}_p \tag{5.66b}$$

in which the basic-to-local transformation matrices $\boldsymbol{L}_m^0$ and $\boldsymbol{L}_p^0$ are computed by the initial local nodal coordinates. After using them to assemble the incremental internal forces of the shell element, $\Delta\boldsymbol{f}$, the internal force vector in the local coordinate system can be updated as follows,

$$\boldsymbol{f}^{n+1} = \boldsymbol{f}^n + \Delta\boldsymbol{f} \tag{5.67}$$

Finally, transforming the local internal force vector into the global coordinate system gives

$$\boldsymbol{F}^{n+1} = \boldsymbol{T}^{n+1T} \boldsymbol{f}^{n+1} \tag{5.68}$$

5.3.3 Computational procedure

The iterative-incremental procedure of geometrically nonlinear analysis based on the simplified co-rotational triangular shell is used for elastic problems and has been implemented in the program NIDA. Under the New-Raphson solution, the procedure is summarized in the following.

1. Define and initialize the global variables and parameters.

   - *Ninc* = the total number of load increments
   - *Nite* = the maximum iteration number
   - n = the n^{th} load step
   - i = the i^{th} iteration
   - $\mathbf{K}^i$ = the assembled global tangent stiffness matrix at the i^{th} iteration
   - $\mathbf{P}^n$ = the externally applied global nodal force vector at the n^{th} load step
   - $\mathbf{F}^i$ = the global internal forces for the whole structure at the i^{th} iteration
   - $\mathbf{U}$ = the global nodal displacements for the whole structure

2. Define and compute the local variables and parameters for each shell element.

   (a) Compute the local-to-global transformation matrix $\boldsymbol{T}_e$.

(b) Compute the initial local coordinates $\boldsymbol{x}=\{x_2\ x_3\ y_3\}^T$.

(c) Compute the basic-to-local transformation matrices $\boldsymbol{L}_m^0$ and $\boldsymbol{L}_p^0$ for the membrane element and the plate element respectively with the initial local coordinates. They can be stored and called for the following procedure.

(d) Compute and store the stiffness matrices of the membrane element and plate element in the basic coordinate system, $\tilde{\boldsymbol{K}}_m^0$ and $\tilde{\boldsymbol{K}}_p^0$, respectively, with the initial local coordinates.

(e) Initialize the local internal forces $\boldsymbol{f}$.

3. Start loop over load increments (for *n*=1 to *Ninc*).

(a) Update external load $\mathbf{P}^n=\mathbf{P}^{n-1}+\Delta\mathbf{P}$.

(b) Set residual forces $\mathbf{g}^i=\mathbf{P}^n$.

(c) Start iterations begin with *i*=1 (while divergence and *i*≤*Nite*)

i. For each shell element, get the tangent stiffness through $\boldsymbol{K}_t=\boldsymbol{T}^T(\boldsymbol{K}_e+\boldsymbol{K}_g^{sym})\boldsymbol{T}$.

ii. Assemble the global tangent stiffness matrix $\mathbf{K}^i$.

iii. Solve for the incremental global nodal displacements $\Delta\mathbf{U}=(\mathbf{K}^i)^{-1}\mathbf{g}^i$ and update $\mathbf{U}:=\mathbf{U}+\Delta\mathbf{U}$.

iv. For each shell element, extract incremental pure deformations $\Delta\tilde{\boldsymbol{d}}_m$ and $\Delta\tilde{\boldsymbol{d}}_p$ from $\Delta\mathbf{U}$, get the incremental local internal forces $\Delta\boldsymbol{f}$ and update $\boldsymbol{f} := \boldsymbol{f} + \Delta\boldsymbol{f}$.

v. Assemble the global internal forces $\mathbf{F}^i$.

vi. Update geometry.

vii. Computer residual forces $\mathbf{g}^i = \mathbf{P}^n - \mathbf{F}^i$.

viii. Terminate iterative process if converged, otherwise go to next iteration.

4. Terminate whole analysis process.

It is worth to point out that several details could be changed in the computational procedure according to the needs of programmers. For example, in the previous procedure, the local material stiffness matrices of the membrane and plate elements, $\tilde{\boldsymbol{K}}_m^0$ and $\tilde{\boldsymbol{K}}_p^0$, are computed and stored in the beginning, so that the local material stiffness matrix of the shell element, $\boldsymbol{K}_e$, should be re-assembled for every iteration, although it does not change during the whole analysis. The operation can save computer storage, since the storage of $\boldsymbol{K}_e$ is larger than the sum of $\tilde{\boldsymbol{K}}_m^0$ and $\tilde{\boldsymbol{K}}_p^0$, but needs more computations. Alternatively, we could record the initial local coordinates, repeatedly compute the matrices $\tilde{\boldsymbol{K}}_m^0$ and $\tilde{\boldsymbol{K}}_p^0$, and then assemble $\boldsymbol{K}_e$ for every iteration to save more storage, but need more computational cost. Thus, this is a trade-off between computer storage and computational cost.

It should be also pointed out that the variables need to be updated carefully. The global displacements **U** and local internal forces $\boldsymbol{f}$ are constantly updated during iterations in the computational procedure. Alternatively, these variables could be updated until a load increment iterates successfully. The latter way is very useful when material nonlinearity is considered, which is discussed in the next section. However, for the elastic problems, these two methods are the same for the accuracy and convergence rate. Further, the former does not need to define more variables and then can save computer storage.

It can be found that the computational procedure is very concise. Compared with the general EICR formulation whose tangent stiffness matrix contains four parts with complicated expressions, the proposed formulation just needs two parts including the material stiffness and the geometric stiffness. Both two stiffness matrices are explicit and do not need numerical integration, meanwhile, the pure deformational method is used to make the local material stiffness simpler. In addition, the numerical examples introduced in Chapter 7 show that the procedure has good performances on accuracy and efficiency for geometrically nonlinear analysis of shell structures.

5.4 Geometrically nonlinear elastoplastic analysis

In this section, the geometrically nonlinear formulation of the triangular shell element based on the simplified co-rotational algorithm is extended to consider material elastoplasticity. In the co-rotational algorithm, the large rigid body motions and the pure deformations producing strains are separated. Thus, it is very convenient to derive the formulation of the local shell element allowing for elastoplasticity in the

basic coordinate system, taking advantage of the existing simplified EICR formulation to implement geometrically nonlinear elastoplastic analysis of shell structures.

There are two widely used approaches to consider material nonlinearity in shell elements, i.e., the layered approach and the non-layered approach. The layered approach, as its name implies, means that the shell thickness is divided into some layers, using actual plane stress description at each layer and each integration point of shell elements. The method can depict the plastic zone spreading along the shell thickness, obtaining approximately exact results. On the other hand, the non-layered approach does not need the division of shell thickness and are directly formulated with stress resultants, but the yield surface expressed with stress resultants is very complicated, which may lead to numerical problems. This thesis uses the layered approach, in which the elastoplastic constitutive model is on the basis of the von Mises yield criterion, the associated flow rule and the linear isotropic hardening. Further, a backward Euler return-mapping integration algorithm (Crisfield and Ciampi, 1997) is used to trace the yield surface.

As shown in Section 5.3, the whole computational procedure of geometrically nonlinear analysis based on the simplified co-rotational algorithm can proceed with using the explicit elastic material stiffness matrix. However, when the elastoplasticity is considered, the numerical integration over the shell element thickness and area should be used. In this chapter, the Allman membrane element (Allman, 1988b) is used instead of the OPT membrane element in the proposed procedure for geometrically nonlinear elastoplastic analysis. Although the performance of Allman membrane element is slightly worse than the OPT membrane element in terms of

drilling rotations, it is acceptable for practical applications of civil engineering structures.

In the next, the elastoplastic material model is introduced first. Then, the tangent stiffness matrix and the internal force vector of the triangular shell element for the geometrically nonlinear elastoplastic analysis scheme are presented. Finally, the pertaining computational procedure coded in the program NIDA is detailed.

5.4.1 Elastoplastic material behaviour

5.4.1.1 Elastoplastic theory for plane stress

In this study, the stresses located in the middle of a layer at an integration point of the local shell element are described with the plane stress state. Although transverse shear strains are considered in the RDKTM plate element, the plasticity due to the transverse shear stresses is neglected, which is feasible for most practical engineering structures. Because the maximum plane stresses due to membrane forces and bending moments always occur at the outermost surface, while the transverse shear stresses reach the maximum at the middle surface and the minimum at the outermost surface. Thus, neglecting transverse shear stresses in the elastoplastic analysis may not cause large errors but can simplify computations.

The plane stresses located in the middle of a layer at an integration point of the shell element in the local coordinate system at the current time can be denoted by

$$\boldsymbol{\sigma} = \begin{Bmatrix} \sigma_{xx} \\ \sigma_{yy} \\ \tau_{xy} \end{Bmatrix} \tag{5.69}$$

The von Mises yield function for the plane stress state can be given by

$$f = \sigma_e - \sigma_y \tag{5.70a}$$

in which σ_e and σ_y are the equivalent stress and the yield stress at the current time respectively.

Because the kinematic hardening is not considered, the current equivalent stress can be expressed by

$$\sigma_e = \left(\sigma_{xx}^2 + \sigma_{yy}^2 - \sigma_{xx}\sigma_{yy} + 3\tau_{xy}^2\right)^{1/2} \tag{5.70b}$$

Based on the linear isotropic strain hardening, the yield stress can be given by

$$\sigma_y = \sigma_0 + H\varepsilon_{ep} \tag{5.70c}$$

in which σ_0 is the initial yield stress, H is the constant hardening parameter and ε_{ep} is the equivalent plastic strain.

The one-dimensional stress-strain relationship is depicted in Figure 5.8 as follows,

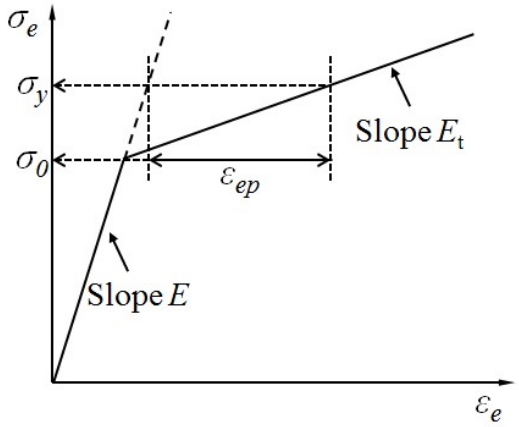

Figure 5.8 One-dimensional stress-strain relationship with linear isotropic hardening

From Figure 5.8, the constant isotropic hardening parameter can be expressed by

$$H = \frac{\partial \sigma_y}{\partial \varepsilon_{ep}} = \frac{E_t}{1 - E_t / E} \tag{5.71}$$

in which ε_{ep} is the equivalent plastic strain, E is the elastic modulus and E_t is the elastoplastic tangent modulus.

Adopting the Prandtl-Reuss flow rule which is an associated flow rule, the plastic material strain rate can be expressed as

$$\dot{\boldsymbol{\varepsilon}}_p = \begin{Bmatrix} \dot{\varepsilon}_{px} \\ \dot{\varepsilon}_{py} \\ \dot{\varepsilon}_{pxy} \end{Bmatrix} = \dot{\lambda} \frac{\partial f}{\partial \boldsymbol{\sigma}} = \dot{\lambda} \mathbf{a} \tag{5.72}$$

where a superpose dot indicates the 'rate' form, so $\dot{\lambda}$ is the plastic strain rate multiplier, while $\mathbf{a}$ is a vector normal to the yield surface f=0 which can be detailed by

$$\mathbf{a}=\frac{\partial f}{\partial \boldsymbol{\sigma}}=\frac{1}{\sigma_e}\begin{Bmatrix}\sigma_{xx}-0.5\sigma_{yy}\\ \sigma_{yy}-0.5\sigma_{xx}\\ 3\tau_{xy}\end{Bmatrix} \tag{5.73}$$

The equivalent plastic strain rate due to the von Mises criterion is calculated from

$$\dot{\varepsilon}_{ep}=\frac{2}{\sqrt{3}}\left(\dot{\varepsilon}_{px}^2+\dot{\varepsilon}_{py}^2+\dot{\varepsilon}_{px}\dot{\varepsilon}_{py}+\frac{1}{4}\dot{\varepsilon}_{px}\right)^{1/2} \tag{5.74}$$

Through Eqs. (5.72) and (5.74), we can get

$$\dot{\varepsilon}_{ep}=\dot{\lambda},\quad \varepsilon_{ep}=\lambda \tag{5.75a, b}$$

The stress changes are related to the strain changes via

$$\dot{\boldsymbol{\sigma}}=\mathbf{C}(\dot{\boldsymbol{\varepsilon}}-\dot{\boldsymbol{\varepsilon}}_p)=\mathbf{C}(\dot{\boldsymbol{\varepsilon}}-\dot{\lambda}\mathbf{a}) \tag{5.76}$$

in which $\dot{\boldsymbol{\varepsilon}}$ is the total strain changes and has two parts including the elastic strain changes $\dot{\boldsymbol{\varepsilon}}_e$ and plastic strain changes $\dot{\boldsymbol{\varepsilon}}_p$, whereas $\mathbf{C}$ is the isotropic elastic modular matrix expressed by

$$\mathbf{C}=\frac{E}{1-v^2}\begin{bmatrix}1 & v & 0\\ v & 1 & 0\\ 0 & 0 & 0.5(1-v)\end{bmatrix} \tag{5.77}$$

When plastic flow occurs, the stresses should stay on the yield surface, which means that the change of the yield function should be zero, thus

$$\dot{f}=\left(\frac{\partial f}{\partial \boldsymbol{\sigma}}\right)^T\dot{\boldsymbol{\sigma}}+\frac{\partial f}{\partial \lambda}\dot{\lambda}=\mathbf{a}^T\dot{\boldsymbol{\sigma}}-H\dot{\lambda}=0 \tag{5.78}$$

Pre-multiplying Eq. (5.76) by the row vector $\mathbf{a}^T$ and taking advantages of Eq. (5.78), we have

$$\dot{\lambda} = \frac{\mathbf{a}^T \mathbf{C}\dot{\boldsymbol{\varepsilon}}}{\mathbf{a}^T \mathbf{C}\mathbf{a}+H} \tag{5.79}$$

Accordingly, substitution into Eq. (5.76) gives

$$\dot{\boldsymbol{\sigma}} = \mathbf{C}(\mathbf{I} - \frac{\mathbf{a}^T \mathbf{C}\mathbf{a}}{\mathbf{a}^T \mathbf{C}\mathbf{a}+H})\dot{\boldsymbol{\varepsilon}}=\mathbf{C}_t\dot{\boldsymbol{\varepsilon}} \tag{5.80}$$

in which the symbol $\mathbf{C}_t$ is the tangential modular matrix.

5.4.1.2 Integration algorithm

The implicit backward Euler numerical integration algorithm is adopted for the integration of the rate equations.

For a layer at an integration point of the shell element, it is assumed that its state at the last time step t_n is known, which means that the quantities including the stresses $\boldsymbol{\sigma}^n$, the plastic strain multiplier λ^n are given. When the incremental strains $\Delta\boldsymbol{\varepsilon}$ occur at the current time step t_{n+1}, the problem to determine the state can be solved by the integration of Eq. (5.76) as follows

$$\boldsymbol{\sigma} - \boldsymbol{\sigma}^n = \mathbf{C}\Delta\boldsymbol{\varepsilon} - \mathbf{C}\int_{t_n}^{t_{n+1}} \dot{\lambda}\mathbf{a}dt \tag{5.81}$$

Through the backward Euler integration theory, the equation can be rewritten as

$$\boldsymbol{\sigma} = \boldsymbol{\sigma}^n + \mathbf{C}\Delta\boldsymbol{\varepsilon} - \Delta\lambda\mathbf{C}\mathbf{a} = \boldsymbol{\sigma}^{tr} - \Delta\lambda\mathbf{C}\mathbf{a} \tag{5.82}$$

in which $\boldsymbol{\sigma}^{tr}$ is the trial elastic stresses, $\Delta\lambda = \int_{t_n}^{t_{n+1}} \dot{\lambda} dt$ and the normal vector $\mathbf{a}$ is determined by the stresses $\boldsymbol{\sigma}$ at the current time step t_{n+1}.

Thus, Eq. (5.82) is an implicit function. To solve this equation and update the state at the current time step t_{n+1}, the two-step predictor-corrector return mapping algorithm is used and introduced in the following.

5.4.1.3 Return mapping algorithm

First, in the predictor step, the trial elastic stresses $\boldsymbol{\sigma}^{tr}$ can be used to judge whether the plastic strains are produced at the current time. If the trial stresses are found to lie within the yield surface, the trial state represents the solution at the current time step t_{n+1}. Otherwise, the real stresses are corrected in the iterations with the trial stresses as initial conditions.

To establish an iterative loop to get the final real state at the current time step t_{n+1}, the residual stresses can be set up to represent the difference between the real stresses and the backward Euler stresses as follows

$$\mathbf{r} = \boldsymbol{\sigma} - (\boldsymbol{\sigma}^{tr} - \Delta\lambda \mathbf{C}\mathbf{a}) \tag{5.83}$$

in which $\mathbf{r}$ should be reduced to zero through iterations and the final stresses should stay on the yield surface.

A first-order Taylor expansion of Eq. (5.83) can be given by

$$\mathbf{r} = \mathbf{r}_0 + \dot{\boldsymbol{\sigma}} + \dot{\lambda}\mathbf{C}\mathbf{a} + \Delta\lambda \mathbf{C}\frac{\partial \mathbf{a}}{\partial \boldsymbol{\sigma}}\dot{\boldsymbol{\sigma}} \tag{5.84}$$

in which $\mathbf{r}_0$ is the updated value of $\mathbf{r}$.

Setting $\mathbf{r} = \mathbf{0}$ gives

$$\dot{\boldsymbol{\sigma}} = -\left(\mathbf{I} + \Delta\lambda \mathbf{C} \frac{\partial \mathbf{a}}{\partial \boldsymbol{\sigma}} \right)^{-1} = -\mathbf{Q}^{-1} \left(\mathbf{r}_0 + \dot{\lambda} \mathbf{C} \mathbf{a} \right) \tag{5.85a}$$

$$\mathbf{Q} = \mathbf{I} + \Delta\lambda \mathbf{C} \frac{\partial \mathbf{a}}{\partial \boldsymbol{\sigma}} \tag{5.85b}$$

Also, a first order Taylor series on the yield function (5.70a) gives

$$f = f_0 + \frac{\partial f}{\partial \boldsymbol{\sigma}} \dot{\boldsymbol{\sigma}} + \frac{\partial f}{\partial \varepsilon_{ep}} \dot{\varepsilon}_{ep} = f_0 + \mathbf{a}^T \dot{\boldsymbol{\sigma}} - H \dot{\lambda} = 0 \tag{5.86}$$

in which f_0 is the updated value of f.

Through Eqs. (5.84) and (5.85), we have

$$\dot{\lambda} = \frac{f_0 - \mathbf{a}^T \mathbf{Q}^{-1} \mathbf{r}_0}{\mathbf{a}^T \mathbf{Q}^{-1} \mathbf{C} \mathbf{a} + H} \tag{5.87}$$

Then, the current state can be updated with these incremental quantities. The detailed state updated procedure used in the program NIDA is introduced in the following.

1. Predictor step:

   (a) Compute the trial elastic stresses $\boldsymbol{\sigma}^{tr} = \boldsymbol{\sigma}^{n} + \mathbf{C}\Delta\boldsymbol{\varepsilon}$.

   (b) Compute and check the yield function $f(\boldsymbol{\sigma}^{tr})$:

i. If $f(\boldsymbol{\sigma}^{tr}) \le 0$, update the stresses as $\boldsymbol{\sigma}^{n+1} = \boldsymbol{\sigma}^{tr}$, while the other plastic quantities remain the same as the last time step t_n. Meanwhile, the elastic modular matrix is stored for the next load step.

ii. If $f(\boldsymbol{\sigma}^{tr}) > 0$, yielding occurs and go to the corrector step.

2. Corrector step:

(a) In the initial step, use $\boldsymbol{\sigma}^{tr}$ to get $f(\boldsymbol{\sigma}^{tr})$ and $\mathbf{a}(\boldsymbol{\sigma}^{tr})$, and the incremental plastic strain multiplier can be obtained by $\Delta\lambda = \dfrac{f}{\mathbf{a}^T\mathbf{C}\mathbf{a} + H}$.

(b) Compute the updated stresses $\boldsymbol{\sigma} = \boldsymbol{\sigma}^{tr} - \Delta\lambda\mathbf{C}\mathbf{a}$, the updated yield stress $\sigma_y = \sigma_0 + H(\lambda^n + \Delta\lambda)$ and the updated yield function $f_0 = f(\boldsymbol{\sigma})$.

(c) Set $\boldsymbol{\sigma}^i = \boldsymbol{\sigma}^{tr}$, $\boldsymbol{\sigma}^{i+1} = \boldsymbol{\sigma}$.

(d) Start iterations with i=1 (while $f_0 < 10^{-4}\sigma_y$).

i. Compute $\mathbf{r}_0 = \boldsymbol{\sigma}^{i+1} - (\boldsymbol{\sigma}^i - \Delta\lambda\mathbf{C}\mathbf{a}^{i+1})$ and $\mathbf{Q} = \mathbf{I} + \Delta\lambda\mathbf{C}\left(\dfrac{\partial\mathbf{a}}{\partial\boldsymbol{\sigma}}\right)^{i+1}$.

ii. Compute $\dot{\lambda} = \dfrac{f_0 - \mathbf{a}^T\mathbf{Q}^{-1}\mathbf{r}_0}{\mathbf{a}^T\mathbf{Q}^{-1}\mathbf{C}\mathbf{a} + H}$ and $\dot{\boldsymbol{\sigma}} = -\mathbf{Q}^{-1}\left(\mathbf{r}_0 + \dot{\lambda}\mathbf{C}\mathbf{a}^{i+1}\right)$.

iii. Update $\boldsymbol{\sigma}^{i+1} = \boldsymbol{\sigma}^{i+1} + \dot{\boldsymbol{\sigma}}$, $\Delta\lambda = \Delta\lambda + \dot{\lambda}$.

iv. Compute $\sigma_y = \sigma_0 + H(\lambda^n + \Delta\lambda)$ and $f_0 = f\left(\boldsymbol{\sigma}^{i+1}\right)$.

v. Terminate iterative process if converged, otherwise go to next iteration.

(e) Updated the current state as $\boldsymbol{\sigma}^{n+1} = \boldsymbol{\sigma}^{i+1}$, $\lambda^{n+1} = \lambda^n + \Delta\lambda$.

(f) Compute and store the tangent modular matrix in Eq. (5.80) for the next load step.

5.4.2 Tangent stiffness

5.4.2.1 Membrane element with drilling rotations

Different from the elastic analysis scheme introduced in Section 5.3, the membrane element with drilling rotations proposed by Allman (1988b) is used to replace the OPT membrane element, and the stresses and strains at integration points are needed to consider material nonlinearity. To simplify the formulation, the pure deformational method can also be used here. Unlike the original formulation, the membrane element is formulated in the basic coordinate system as shown in Figure 5.3, with 6 rather than 9 degrees of freedom. The displacement interpolations defined with area coordinates $\{\xi_1 \ \xi_2 \ \xi_3\}$ can be given by

$$\begin{aligned}\tilde{u} = {} & \tilde{u}_2\xi_2 + \tilde{u}_3\xi_3 + b_{23}y_3\xi_2\xi_3 - b_{31}y_3\xi_1\xi_3 \\ & a_{23}y_3\xi_2\xi_3\left(\xi_3 - \xi_2\right) - a_{31}y_3\xi_1\xi_3\left(\xi_1 - \xi_3\right)\end{aligned} \tag{5.88a}$$

$$\begin{aligned}\tilde{v} = {} & \tilde{v}_3\xi_3 - b_{12}x_2\xi_1\xi_2 + b_{23}x_{23}\xi_2\xi_3 + b_{31}x_3\xi_1\xi_3 \\ & -a_{12}x_2\xi_1\xi_2\left(\xi_2 - \xi_1\right) + a_{23}x_{23}\xi_2\xi_3\left(\xi_3 - \xi_2\right) + a_{31}x_3\xi_1\xi_3\left(\xi_1 - \xi_3\right)\end{aligned} \tag{5.88b}$$

in which the coefficients a_{ij} and b_{ij} are

$$a_{ij} = \frac{1}{2}\left(\tilde{\theta}_{zi} + \tilde{\theta}_{zj}\right) - \Omega_0 \tag{5.89a}$$

$$b_{ij} = \frac{1}{2}\left(\tilde{\theta}_{zj} - \tilde{\theta}_{zi}\right) \tag{5.89b}$$

where i=1,2,3, j=mod(i,3)+1 and Ω_0 is the rotation of the constant strain triangular membrane element with area A as

$$\Omega_0 = \frac{1}{4A}\left(\tilde{u}_2 x_3 - \tilde{u}_3 x_2\right) \tag{5.90}$$

These formulations have used the displacement boundary conditions $x_1 = y_1 = y_2 = 0$. It is clear that the proposed formulations are much simpler than the original method.

After that, the strain-displacement matrix of the membrane element based on the basic coordinate system can be given by

$$\boldsymbol{\varepsilon} = \begin{Bmatrix} \varepsilon_x \\ \varepsilon_y \\ \varepsilon_{xy} \end{Bmatrix} = \begin{Bmatrix} \dfrac{\partial \tilde{u}}{\partial x} \\ \dfrac{\partial \tilde{v}}{\partial y} \\ \dfrac{\partial \tilde{v}}{\partial x} - \dfrac{\partial \tilde{u}}{\partial y} \end{Bmatrix} = \tilde{\boldsymbol{B}}_m \tilde{\boldsymbol{u}}_m \tag{5.91}$$

with

$$\begin{bmatrix} \dfrac{\partial \tilde{u}}{\partial x} & \dfrac{\partial \tilde{u}}{\partial y} \\ \dfrac{\partial \tilde{v}}{\partial x} & \dfrac{\partial \tilde{v}}{\partial y} \end{bmatrix} = \begin{bmatrix} \dfrac{\partial \tilde{u}}{\partial \xi_1} & \dfrac{\partial \tilde{u}}{\partial \xi_2} & \dfrac{\partial \tilde{u}}{\partial \xi_3} \\ \dfrac{\partial \tilde{v}}{\partial \xi_1} & \dfrac{\partial \tilde{v}}{\partial \xi_2} & \dfrac{\partial \tilde{v}}{\partial \xi_3} \end{bmatrix} \begin{bmatrix} \dfrac{\partial \xi_1}{\partial x} & \dfrac{\partial \xi_1}{\partial y} \\ \dfrac{\partial \xi_2}{\partial x} & \dfrac{\partial \xi_2}{\partial y} \\ \dfrac{\partial \xi_3}{\partial x} & \dfrac{\partial \xi_3}{\partial y} \end{bmatrix} \tag{5.92a}$$

$$\begin{Bmatrix} \xi_1 \\ \xi_2 \\ \xi_3 \end{Bmatrix} = \frac{1}{x_2 y_3} \begin{Bmatrix} x_2 y_3 - y x_{23} - x y_3 \\ x y_3 - y x_3 \\ x_2 y \end{Bmatrix} \tag{5.92b}$$

5.4.2.2 Layered shell element

To reflect the spreading plasticity through the thickness, the shell element is divided into *m* layers with equal thickness, as shown in Figure 5.9.

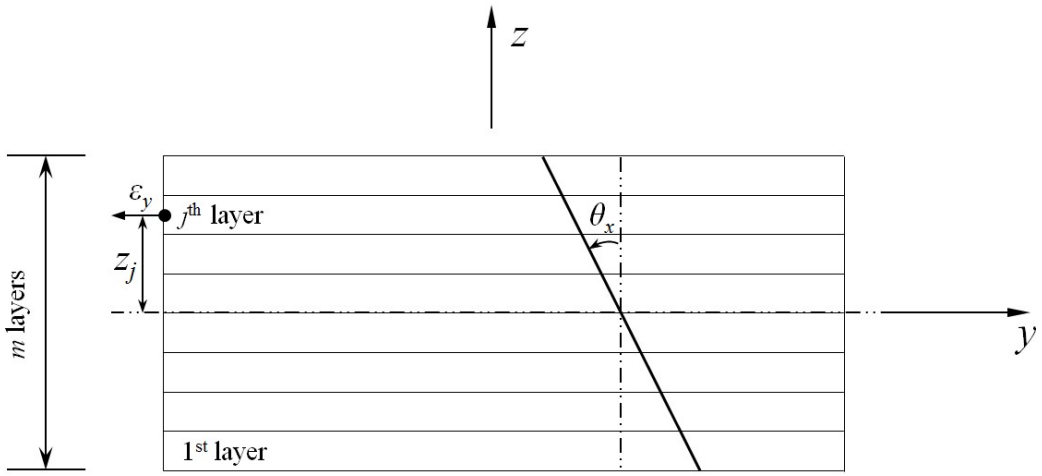

Figure 5.9 Layered shell element

The strains of the j^{th} layer using the values at the mid-point of the layer can be given by

$$\boldsymbol{\varepsilon}_j = \begin{Bmatrix} \varepsilon_x \\ \varepsilon_y \\ \varepsilon_{xy} \end{Bmatrix} + z_j \begin{Bmatrix} \kappa_x \\ \kappa_y \\ \kappa_{xy} \end{Bmatrix} = \tilde{\boldsymbol{B}}_m \tilde{\boldsymbol{d}}_m + z_j \tilde{\boldsymbol{B}}_b \tilde{\boldsymbol{d}}_p \tag{5.93}$$

Then, the stresses of the j^{th} layer are

$$\boldsymbol{\sigma}_j = \mathbf{C}_j \tilde{\boldsymbol{B}}_m \tilde{\boldsymbol{d}}_m + z_j \mathbf{C}_j \tilde{\boldsymbol{B}}_b \tilde{\boldsymbol{d}}_p \tag{5.94a}$$

$$z_j = \frac{t}{2m}(2j-1) - \frac{t}{2}, j=1 \text{ to } m \tag{5.94b}$$

in which $\mathbf{C}_j$ is the tangential modular matrix for the j^{th} layer given in Eq. (5.80) under plasticity and the elastic modular matrix shown in Eq. (5.77) under elasticity, and t is the thickness of the shell element.

The virtual work due to membrane and bending strains over the shell element area can be expressed as

$$\begin{aligned}\delta W &= \int_A \sum_{j=1}^{m} \boldsymbol{\sigma}_j^T \delta \boldsymbol{\varepsilon}_j \Delta t dA - \boldsymbol{f}_{ext}^T \delta \tilde{\boldsymbol{d}} \\ &= \int_A \sum_{j=1}^{m} (\mathbf{C}_j \tilde{\boldsymbol{B}}_m \tilde{\boldsymbol{d}}_m + z_j \mathbf{C}_j \tilde{\boldsymbol{B}}_b \tilde{\boldsymbol{d}}_p)^T (\tilde{\boldsymbol{B}}_m \delta \tilde{\boldsymbol{d}}_m + z_j \tilde{\boldsymbol{B}}_b \delta \tilde{\boldsymbol{d}}_p) \Delta t dA \\ &= \int_A \sum_{j=1}^{m} \begin{pmatrix} \tilde{\boldsymbol{d}}_m^T \tilde{\boldsymbol{B}}_m^T \mathbf{C}_j \tilde{\boldsymbol{B}}_m \delta \tilde{\boldsymbol{d}}_m + z_j \tilde{\boldsymbol{d}}_p^T \tilde{\boldsymbol{B}}_b^T \mathbf{C}_j \tilde{\boldsymbol{B}}_m \delta \tilde{\boldsymbol{d}}_m \\ + z_j \tilde{\boldsymbol{d}}_m^T \tilde{\boldsymbol{B}}_m^T \mathbf{C}_j \tilde{\boldsymbol{B}}_b \delta \tilde{\boldsymbol{d}}_p + z_j^2 \tilde{\boldsymbol{d}}_b^T \tilde{\boldsymbol{B}}_b^T \mathbf{C}_j \tilde{\boldsymbol{B}}_b \delta \tilde{\boldsymbol{d}}_p \end{pmatrix} \Delta t dA - \boldsymbol{f}_{ext}^T \delta \tilde{\boldsymbol{d}}\end{aligned} \tag{5.95}$$

where $\boldsymbol{f}_{ext}$ is the external forces and $\Delta t = \dfrac{t}{m}$ is the layer thickness.

Through Eq. (5.95), the material stiffness matrix due to membrane and bending effects in the basic coordinate system can be given by

$$\tilde{\boldsymbol{K}}_e = \begin{bmatrix} \tilde{\boldsymbol{K}}_1 & \tilde{\boldsymbol{K}}_2 \\ \tilde{\boldsymbol{K}}_3 & \tilde{\boldsymbol{K}}_4 \end{bmatrix} \tag{5.96a}$$

$$\tilde{\boldsymbol{K}}_1 = \int_A \tilde{\boldsymbol{B}}_m^T \left(\sum_{j=1}^{m} \mathbf{C}_j \Delta t \right) \tilde{\boldsymbol{B}}_m dA \tag{5.96b}$$

$$\tilde{\boldsymbol{K}}_2 = \int_A \tilde{\boldsymbol{B}}_m^T \left(\sum_{j=1}^{m} z_j \Delta t \mathbf{C}_j \right) \tilde{\boldsymbol{B}}_b dA \tag{5.96c}$$

$$\tilde{\boldsymbol{K}}_3 = \int_A \tilde{\boldsymbol{B}}_b^T \left(\sum_{j=1}^{m} z_j \Delta t \mathbf{C}_j \right) \tilde{\boldsymbol{B}}_m dA \tag{5.96d}$$

$$\tilde{\boldsymbol{K}}_4 = \int_A \tilde{\boldsymbol{B}}_b^T \left(\sum_{j=1}^{m} z_j^2 \Delta t \mathbf{C}_j \right) \tilde{\boldsymbol{B}}_b dA \tag{5.96e}$$

in which the material stiffness matrix $\tilde{\boldsymbol{K}}_e$ is 12×12 in the basic coordinate system, corresponding to the basic displacement vector $\left\{ \tilde{\boldsymbol{d}}_m^T \ \tilde{\boldsymbol{d}}_p^T \right\}^T$. To solve these integrations over the shell element area, the numerical integration with 3 interior points are used, including the points expressed with area coordinates: $\left\{ \frac{1}{6}, \frac{1}{6}, \frac{2}{3} \right\}$, $\left\{ \frac{1}{6}, \frac{2}{3}, \frac{1}{6} \right\}$, $\left\{ \frac{2}{3}, \frac{1}{6}, \frac{1}{6} \right\}$. In addition, the shear stiffness matrix $\tilde{\boldsymbol{K}}_s$ shown in Eq. (5.54a) can be add to $\tilde{\boldsymbol{K}}_4$ when transverse shear deformation is considered, while $\tilde{\boldsymbol{K}}_s$ is still elastic here, since the plasticity due to transverse shear stresses is neglected.

After integration, the material stiffness matrix in the basic coordinate system should be transformed into the local coordinate system as follows,

$$\boldsymbol{K}_e = \boldsymbol{L}^T \tilde{\boldsymbol{K}}_e \boldsymbol{L} \tag{5.97}$$

where $\boldsymbol{L}$ is the basic-to-local transformation matrix with 12×18 sizes and is derived in line with the matrix $\boldsymbol{L}_m$ and $\boldsymbol{L}_p$ with

$$\boldsymbol{L} = \frac{\partial \boldsymbol{d}}{\partial \tilde{\boldsymbol{d}}^T} \tag{5.98}$$

Finally, the tangent stiffness matrix in the global coordinate system can be given by

$$\boldsymbol{K}_t = \boldsymbol{T}^T (\boldsymbol{K}_e + \boldsymbol{K}_g^{sym}) \boldsymbol{T} \tag{5.99}$$

Compared with the elastic analysis scheme introduced in Section 5.3, the material stiffness matrix allowing for plasticity is computed based on the layered shell element rather than the local elastic shell element, but the geometric stiffness matrix is identical.

5.4.3 Internal forces

In the procedure of geometrically nonlinear elastic analysis introduced in Section 5.3, the iterative displacements which are the incremental displacements between two iteration steps are used to compute the internal forces based on the results of the last iteration. For the elastoplastic analysis, the iterative displacements cannot be used, since they may lead to "spurious unloading" during iterations. Specifically, in a geometrically nonlinear elastic problem, a solution with larger displacements than the real ones may be obtained in the first iteration. Then, opposite unloading displacements will be got in the next iteration to correct the solution. There is no problem for elastic analysis. However, when the plasticity is considered, this situation may cause numerical problems. It is well known that the plastic problems are related to the loading history. Using the iterative displacements, each iteration step is recorded in the loading history, including spurious unloading to revise results. The process may be far from reality, which will increase the computational cost and lead to a wrong solution. Thus, the incremental displacements rather than the iterative displacements should be used for elastoplastic problems to update the internal forces. Different from the iterative displacements, the incremental displacements are accumulated from the first iteration to the current iteration at the current load step,

thus the starting point of the incremental displacements is fixed at the beginning of the current load step and therefore avoids the influence of spurious unloading to the loading history.

In the computational procedure, the iterative pure deformations in the basic coordinate system can be extracted from the iterative global displacements. Then, adding the iterative pure deformations to the incremental pure deformations of the last iteration, so the incremental pure deformations of the membrane element $\Delta\tilde{\boldsymbol{d}}_m$ and the plate element $\Delta\tilde{\boldsymbol{d}}_p$ since the beginning of the current load step can be obtained.

The incremental strains of the j^{th} layer at the integration point k at the current time can be given by

$$\Delta\boldsymbol{\varepsilon}_{j,k} = \tilde{\boldsymbol{B}}_m\Delta\tilde{\boldsymbol{d}}_m + z_j\tilde{\boldsymbol{B}}_b\Delta\tilde{\boldsymbol{d}}_p \text{ , } j\text{=1 to } m\text{, } k\text{=1 to 3} \tag{5.100}$$

Then, the trial stresses of the j^{th} layer at the integration point k at the current time can be obtained as follows,

$$\boldsymbol{\sigma}_{j,k}^{tr} = \boldsymbol{\sigma}_{j,k}^{n} + \mathrm{C}\Delta\boldsymbol{\varepsilon}_{j,k} \tag{5.101}$$

in which $\boldsymbol{\sigma}_{j,k}^{n}$ is the stresses determined at the last load step.

After that, the two-step predictor-corrector return mapping algorithm introduced in Section 5.4.1 is used to determine the real stresses $\boldsymbol{\sigma}_{j,k}$. The internal forces of the membrane and plate elements based on the basic coordinate system can be obtained by

$$\tilde{\boldsymbol{f}}_m^{\,n+1} = \sum_{k=1}^{3} \tilde{\boldsymbol{B}}_m^{\,T} \left(\sum_{j=1}^{m} \boldsymbol{\sigma}_{j,k} \Delta t \right) w_k A \tag{5.102a}$$

$$\tilde{\boldsymbol{f}}_p^{\,n+1} = \sum_{k=1}^{3} \tilde{\boldsymbol{B}}_b^{\,T} \left(\sum_{j=1}^{m} z_j \boldsymbol{\sigma}_{j,k} \Delta t \right) w_k A \tag{5.102b}$$

in which w_k is the weight factor and equal to $\frac{1}{3}$.

When transverse shear deformation is considered, the internal forces due to the transverse shear effect can be updated as $\tilde{\boldsymbol{f}}_s^{\,n+1} = \tilde{\boldsymbol{f}}_s^{\,n} + \tilde{\boldsymbol{K}}_s \Delta \tilde{\boldsymbol{d}}_p$, and accordingly the internal force vector of the plate element should be modified as

$$\tilde{\boldsymbol{f}}_p^{\,n+1} = \sum_{k=1}^{3} \tilde{\boldsymbol{B}}_b^{\,T} \left(\sum_{j=1}^{m} z_j \boldsymbol{\sigma}_{j,k} \Delta t \right) w_k A + \tilde{\boldsymbol{f}}_s^{\,n+1} \tag{5.102c}$$

where the internal force vector due to the transverse shear effect $\tilde{\boldsymbol{f}}_s^{\,n}$ is determined at the last load step.

Transforming the basic internal force vectors into the local coordinate system gives

$$\boldsymbol{f}_m^{\,n+1} = \boldsymbol{L}_m^{0\,T} \tilde{\boldsymbol{f}}_m^{\,n+1} \tag{5.103a}$$

$$\boldsymbol{f}_p^{\,n+1} = \boldsymbol{L}_p^{0\,T} \tilde{\boldsymbol{f}}_p^{\,n+1} \tag{5.103b}$$

Combining them to get the internal force vector of the shell element, $\boldsymbol{f}^{n+1}$, and then the global internal force vector at current time can be given by

$$\boldsymbol{F}^{n+1} = \boldsymbol{T}^{n+1T} \boldsymbol{f}^{n+1} \tag{5.104}$$

5.4.4 Computational procedure

The computational procedure of geometrically nonlinear elastoplastic analysis with the simplified EICR formulation and the incremental displacements has been implemented in the program NIDA. The procedure based on the New-Raphson solution is detailed in the following.

1. Define and initialize the global variables and parameters.

   - *Ninc* = the total number of load increments
   - *Nite* = the maximum iteration number
   - m = the number of layers for a shell element
   - n = the n^{th} load step
   - i = the i^{th} iteration
   - j = the j^{th} layer of a shell element
   - k = the k^{th} integration point
   - $\mathbf{K}^i$ = the assembled global tangent stiffness matrix at the i^{th} iteration
   - $\mathbf{P}^n$ = the externally applied global nodal force vector at the n^{th} load step
   - $\mathbf{F}^i$ = the global internal forces at for the whole structure at the i^{th} iteration
   - $\mathbf{U}$ = the global nodal displacements for the whole structure

2. Define and compute the local variables and parameters for each layered shell element.

(a) Compute the local-to-global transformation matrix $\boldsymbol{T}_e$.

(b) Compute the initial local coordinates $\boldsymbol{x}=\{x_2 \;\; x_3 \;\; y_3\}^T$.

(c) Compute the basic-to-local transformation matrices $\boldsymbol{L}_m^0$ and $\boldsymbol{L}_p^0$ for the membrane element and the plate element respectively with the initial local coordinates. They can be stored and called for the following procedure.

(d) Initialize the stresses $\boldsymbol{\sigma}_{j,k}$ of the j^{th} layer at the integration point k.

(e) Initialize the elastic modular matrix $\mathbf{C}_{j,k}$ of the j^{th} layer at the integration point k.

3. Start loop over load increments (for n=1 to *Ninc*).

(a) Update external load $\mathbf{P}^n=\mathbf{P}^{n-1}+\Delta\mathbf{P}$.

(b) Set residual forces $\mathbf{g}^i=\mathbf{P}^n$.

(c) Start iterations begin with i=1 (while divergence and $i\le$*Nite*).

i. For each layered shell element, get the tangent stiffness through $\boldsymbol{K}_t=\boldsymbol{T}^T(\boldsymbol{K}_e+\boldsymbol{K}_g^{sym})\boldsymbol{T}$.

ii. Assemble the global tangent stiffness matrix $\mathbf{K}^i$.

iii. Solve for the incremental global nodal displacements $\Delta\mathbf{U}=(\mathbf{K}^i)^{-1}\mathbf{g}^i$ and update $\mathbf{U}:=\mathbf{U}+\Delta\mathbf{U}$.

iv. For each shell element, extract iterative pure deformation $\Delta\tilde{\boldsymbol{d}}_m^i$ and $\Delta\tilde{\boldsymbol{d}}_p^i$ from $\Delta\mathbf{U}$ and add them to the incremental pure deformations

accumulated from the first iteration as $\Delta\tilde{\boldsymbol{d}}_m = \Delta\tilde{\boldsymbol{d}}_m^{i-1} + \Delta\tilde{\boldsymbol{d}}_m^{i}$, $\Delta\tilde{\boldsymbol{d}}_p = \Delta\tilde{\boldsymbol{d}}_p^{i-1} + \Delta\tilde{\boldsymbol{d}}_p^{i}$.

v. For the j^{th} layer at the integration point k, compute the incremental strains $\Delta\boldsymbol{\varepsilon}_{j,k} = \tilde{\boldsymbol{B}}_m\Delta\tilde{\boldsymbol{d}}_m + z_j\tilde{\boldsymbol{B}}_b\Delta\tilde{\boldsymbol{d}}_p$ and the trial stresses $\boldsymbol{\sigma}_{j,k}^{tr} = \boldsymbol{\sigma}_{j,k}^{n} + \mathrm{C}\Delta\boldsymbol{\varepsilon}_{j,k}$.

vi. Determine the real stresses $\boldsymbol{\sigma}_{j,k}$ with the two-step predictor-corrector return mapping algorithm. If the point yields, $\mathbf{C}_{j,k}$ is the tangential modular matrix, otherwise, is the elastic modular matrix for the next iteration.

vii. Compute the internal forces through $\tilde{\boldsymbol{f}}_m = \sum_{k=1}^{3}\tilde{\boldsymbol{B}}_m{}^T\left(\sum_{j=1}^{m}\boldsymbol{\sigma}_{j,k}\Delta t\right)w_k A$, $\tilde{\boldsymbol{f}}_p = \sum_{k=1}^{3}\tilde{\boldsymbol{B}}_b{}^T\left(\sum_{j=1}^{m}z_j\boldsymbol{\sigma}_{j,k}\Delta t\right)w_k A$ and then the internal force vector in the global coordinate system $\boldsymbol{F}$.

viii. Assemble the global internal forces $\mathbf{F}^i$.

ix. Update geometry.

x. Compute residual forces $\mathbf{g}^i = \mathbf{P}^n - \mathbf{F}^i$.

xi. Terminate iterative process if converged, otherwise go to next iteration.

4. Terminate whole analysis process.

5.5 Summary

In this chapter, the simplified EICR formulation for triangular shell elements is used to realize geometrically nonlinear elastic and elastoplastic analysis of shell structures, with a simple and explicit geometric stiffness matrix. Besides, the pure deformational method is adopted to simplify the formulations of local triangular shell element and decrease the size of the material matrix accordingly. Thus, the presented formulations and computational procedures are simpler than the traditional nonlinear analysis schemes, such as the conventional (EICR) formulation, the total Lagrangian (TL) formulation and the updated Lagrangian (UL) formulation based on the Green-Lagrangian strains. In addition, the performances of the proposed formulations on accuracy and efficiency are validated in Chapter 7 through numerical examples. Thus, these proposed techniques are robust and significant for nonlinear analysis of civil engineering structures.

CHAPTER 6

A NONLINEAR QUADRILATERAL SHELL ELEMENT BASED ON SIMPLIFIED EICR METHOD

In this chapter, a novel nonlinear analysis scheme for quadrilateral shell elements with drilling rotations is proposed based on the simplified EICR formulation, which is similar to the nonlinear triangular shell element introduced in Chapter 5. However, the pure deformational method is not used here, because a quadrilateral shell element is sensitive to nodal ordering due to the warping effect when using an element side as one axis of the local coordinate system. Thus, to overcome the nodal ordering dependency, the bisector definition of the local coordinate system is used here, although it makes the derivation of the local geometric stiffness matrix more complicated. Note that the proposed simplified co-rotational formulation for quadrilateral shell elements is also element-independent, since its geometric stiffness matrix is formed by the nodal internal forces rather than the stresses at integration points. Thus, different from the total Lagrangian (TL) and updated Lagrangian (UL) formulations, the proposed geometrically nonlinear formulation has an explicit geometric stiffness matrix and does not need numerical integration, with saving computational cost.

In this study, the membrane element with drilling rotations proposed by Ibrahimbegovic et al. (1990) and the plate element allowing for transverse shear deformation presented by Chen and Cheung (2000) are used to generate a new flat quadrilateral shell element. The two local elements will be introduced in Section 6.1 and 6.2 respectively. Note that they are derived based on a facet which is the projection of shell element. Thus, the warping effect of the quadrilateral shell element should be taken into account, and its contribution to the local geometric stiffness is derived in the simplified co-rotational formulation for quadrilateral shell elements.

To fully interpret the advances of the proposed simplified co-rotational formulation for quadrilateral shell elements, the updated Lagrangian (UL) formulation for a quadrilateral shell element with transverse shear, warping and drilling rotations in geometrically nonlinear analysis, proposed by author of the thesis (Tang *et al.*, 2016), is introduced in Section 6.3. The UL formulation also adopts the co-rotational concept, in which the geometric stiffness is formulated by the UL formulation in the local coordinate system and needs numerical integration, unlike the EICR formulation. Through comparison of the derivations between these two different geometrically nonlinear analysis schemes, it is easy to find the advances of the simplified EICR formulation for quadrilateral shell elements. Further, the novel simplified EICR formulation is used to implement geometrically nonlinear analysis in Section 6.4 and geometrically nonlinear elastoplastic analysis in Section 6.5. The elastoplastic analysis procedure for the quadrilateral shell element is identical to that for the triangular shell element shown in Chapter 5 and briefly introduced in Section 6.5.

6.1 A four-node quadrilateral membrane element with drilling rotations

An accurate 4-node quadrilateral membrane element containing drilling degrees of freedom by Ibrahimbegovic *et al.* (1990) is adopted here and shown in Figure 6.1. The classical displacement interpretations including drilling rotations proposed by Allman (1988a) expressed with the isoparametric coordinates (r, s) can be given by

$$u_x = \sum_{i=1}^{4} N_i(r,s)\, u_{xi} + \sum_{i=1}^{4} N_{i+4}(r,s) \cos\alpha_{ij} \frac{S_{ij}}{8}\left(\theta_{zj} - \theta_{zi}\right) \tag{6.1a}$$

$$u_y = \sum_{i=1}^{4} N_i(r,s)\, u_{yi} + \sum_{i=1}^{4} N_{i+4}(r,s) \sin\alpha_{ij} \frac{S_{ij}}{8}\left(\theta_{zi} - \theta_{zj}\right) \tag{6.1b}$$

$$\theta_z = \sum_{i=1}^{4} N_i(r,s)\, \theta_{zi} \tag{6.1c}$$

$$i = 1,2,3,4;\ \ j = \mathrm{mod}(i,4) + 1 \tag{6.1d}$$

in which S_{ij} is the length of the element side associated with the nodes i and j, α_{ij} represents the angle between the outward unit normal vector on the element side i-j and the x-axis, so $\cos\alpha_{ij} = \dfrac{y_j - y_i}{S_{ij}}$ and $\sin\alpha_{ij} = \dfrac{x_i - x_j}{S_{ij}}$.

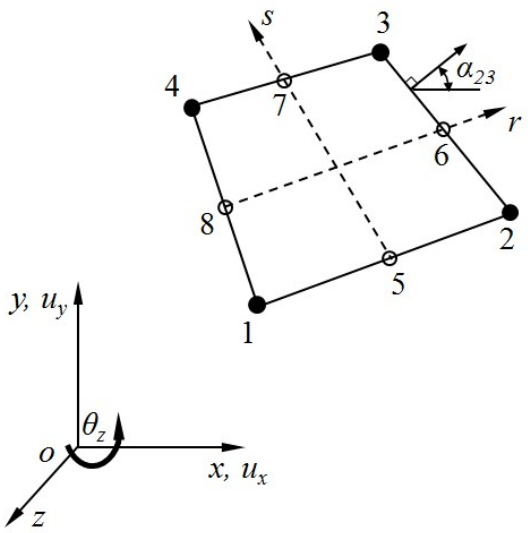

Figure 6.1 A quadrilateral membrane element

The shape functions are given as follows,

$$N_i(r,s)=\frac{1}{4}(1+r_i r)(1+s_i s);\ \ i=1,2,3,4 \tag{6.2a}$$

$$N_i(r,s)=\frac{1}{2}(1-r^2)(1+s_i s);\ \ i=5,7 \tag{6.2b}$$

$$N_i(r,s)=\frac{1}{2}(1+r_i r)(1-s^2);\ \ i=6,8 \tag{6.2c}$$

in which r_i and s_i are the isoparametric coordinates at the node *i*.

The relationship between strains and displacements are

$$\boldsymbol{\varepsilon} = \begin{Bmatrix} \varepsilon_x \\ \varepsilon_y \\ \gamma_{xy} \end{Bmatrix} = \begin{Bmatrix} \dfrac{\partial u_x}{\partial x} \\ \dfrac{\partial u_y}{\partial y} \\ \dfrac{\partial u_x}{\partial y} + \dfrac{\partial u_y}{\partial x} \end{Bmatrix} \tag{6.3}$$

Substituting Eqs. (6.1) into (6.3), the strain-displacement matrix can be given by

$$\boldsymbol{\varepsilon} = \boldsymbol{B}_m \boldsymbol{d}_m \tag{6.4a}$$

$$\boldsymbol{B}_m = \begin{bmatrix} \boldsymbol{B}_{m1} & \boldsymbol{B}_{m2} & \boldsymbol{B}_{m3} & \boldsymbol{B}_{m4} \end{bmatrix} \tag{6.4b}$$

$$\boldsymbol{B}_{mi} = \begin{bmatrix} \dfrac{\partial N_i}{\partial x} & 0 & \dfrac{1}{8}\left(\dfrac{\partial N_{k+4}}{\partial x} y_{ik} - \dfrac{\partial N_{i+4}}{\partial x} y_{ji} \right) \\ 0 & \dfrac{\partial N_i}{\partial y} & \dfrac{1}{8}\left(\dfrac{\partial N_{k+4}}{\partial y} x_{ki} - \dfrac{\partial N_{i+4}}{\partial y} x_{ij} \right) \\ \dfrac{\partial N_i}{\partial y} & \dfrac{\partial N_i}{\partial x} & \dfrac{1}{8}\left(\dfrac{\partial N_{k+4}}{\partial y} y_{ik} - \dfrac{\partial N_{i+4}}{\partial y} y_{ji} \right) + \dfrac{1}{8}\left(\dfrac{\partial N_{k+4}}{\partial x} x_{ki} - \dfrac{\partial N_{i+4}}{\partial x} x_{ij} \right) \end{bmatrix} \tag{6.4c}$$

$$i = 1,2,3,4;\ \ j = \mathrm{mod}(i,4) + 1;\ \ k = 4\,\mathrm{floor}(i,4) + i + 1 \tag{6.4d}$$

$$\boldsymbol{d}_m = \begin{Bmatrix} u_{x1} & u_{y1} & \theta_{z1} & u_{x2} & u_{y2} & \theta_{z2} & u_{x3} & u_{y3} & \theta_{z3} & u_{x4} & u_{y4} & \theta_{z4} \end{Bmatrix}^T \tag{6.4e}$$

in which $\boldsymbol{d}_m$ is the displacement vector of a 4-node quadrilateral membrane element, while the local nodal coordinates having two subscripts refer to the subtraction of two coordinates, e.g., $x_{ij} = x_i - x_j$, $y_{ij} = y_i - y_j$.

Also, the relationship of partial derivatives between the local and isoparametric coordinate systems is

$$\begin{Bmatrix} \dfrac{\partial N_i}{\partial x} \\ \dfrac{\partial N_i}{\partial y} \end{Bmatrix} = \boldsymbol{J}^{-1} \begin{Bmatrix} \dfrac{\partial N_i}{\partial r} \\ \dfrac{\partial N_i}{\partial s} \end{Bmatrix}, \; i=1\sim 8 \tag{6.5a}$$

$$\boldsymbol{J} = \frac{\partial(x,y)}{\partial(r,s)} = \begin{bmatrix} \displaystyle\sum_{i=1}^{4} \frac{\partial N_i}{\partial r} x_i & \displaystyle\sum_{i=1}^{4} \frac{\partial N_i}{\partial r} y_i \\ \displaystyle\sum_{i=1}^{4} \frac{\partial N_i}{\partial s} x_i & \displaystyle\sum_{i=1}^{4} \frac{\partial N_i}{\partial s} y_i \end{bmatrix} \tag{6.5b}$$

in which the interpolations for the local coordinates (x, y) are still bilinear, since the sides of the quadrilateral membrane element are assumed as straight.

The elastic stress-strain law for a membrane element can be written as

$$\boldsymbol{\sigma} = \begin{Bmatrix} \sigma_x \\ \sigma_y \\ \tau_{xy} \end{Bmatrix} = \boldsymbol{D_m} \boldsymbol{\varepsilon} \tag{6.6a}$$

$$\boldsymbol{D_m} = \frac{E}{1-v^2} \begin{bmatrix} 1 & v & 0 \\ v & 1 & 0 \\ 0 & 0 & 0.5(1-v) \end{bmatrix} \tag{6.6b}$$

where E and v are Young's modulus and Poisson's ratio respectively.

For the 4-node quadrilateral membrane element, a mixed variational formulation of linear elastic behaviour with independent rotation fields proposed by Hughes and Brezzi (1989) is used, which also combines the displacement field with an independent rotation interpolation to get accurate results. With the index-free notion in references (Hughes and Brezzi, 1989; Ibrahimbegovic et al., 1990), the mixed variational formulation can be given by

$$\begin{aligned}\Pi_\gamma(\mathbf{v},\boldsymbol{\omega},\text{skew}\,\boldsymbol{\tau}) = &\frac{1}{2}\int_\Omega(\text{symm}\,\nabla\mathbf{v})\cdot\mathbf{C}\cdot(\text{symm}\,\nabla\mathbf{v})\,d\Omega\\ &+\int_\Omega \text{skew}\,\boldsymbol{\tau}^T\cdot(\text{skew}\,\nabla\mathbf{v}-\boldsymbol{\omega})d\Omega\\ &-\frac{1}{2}\gamma^{-1}\int_\Omega|\text{skew}\,\boldsymbol{\tau}|^2 d\Omega-\int_\Omega\mathbf{v}\cdot\mathbf{f}d\Omega\end{aligned} \tag{6.7a}$$

in which $\boldsymbol{v}$, $\boldsymbol{\omega}$ and $\boldsymbol{\tau}$ are trial displacements, rotations and stresses respectively in the region Ω; γ is a problem-dependent parameter and $\mathbf{C}$ is the constitutive modulus tensor. ∇ refers to the vector differential operator, while the symbol "symm" and "skew" mean the symmetric and skew-symmetric part of a second-rank tensor respectively, e.g.,

$$\text{symm}\,\nabla\mathbf{v}=\frac{1}{2}(\nabla\mathbf{v}+\nabla\mathbf{v}^T) \tag{6.7b}$$

$$\text{skew}\,\boldsymbol{\tau}=\frac{1}{2}(\boldsymbol{\tau}-\boldsymbol{\tau}^T) \tag{6.7c}$$

Then, the mixed variational formulation is modified to a simplified form for easy visualization and adopts the unified notions used in the thesis. The tensor $\text{skew}\,\boldsymbol{\tau}$ in Eq. (6.7a) is an independent field for an element, whereas every entry of the tensor $(\boldsymbol{\tau}-\boldsymbol{\tau}^{\mathrm{T}})$ is assumed as a constant parameter τ_0^e over the element. Then, the membrane element with thickness *t* and area *A* can be given as follows,

$$\begin{aligned}\Pi = &\frac{t}{2}\int_A\boldsymbol{\varepsilon}^T\boldsymbol{D}_m\boldsymbol{\varepsilon}dA+t\int_A\tau_0^e\left(\frac{1}{2}\frac{\partial u_y}{\partial x}-\frac{1}{2}\frac{\partial u_x}{\partial y}-\theta_z\right)dA\\ &-\frac{t}{2\gamma}\int_A\tau_0^{e2}dA-\boldsymbol{d}_m{}^T\boldsymbol{f}_m\end{aligned} \tag{6.8}$$

where γ shown in the third integral term is a problem-dependent parameter which was advised by Hughes and Brezzi (1989) to be replaced by shear modulus *G* for

isotropic elasticity and Dirichlet boundary value problems. The last term is the external work, in which $\boldsymbol{d}_m$ and $\boldsymbol{f}_m$ are the nodal displacement and internal force vectors for the membrane element, respectively.

Taking a variation of Eq. (6.8) gives

$$\begin{aligned} 0 = \delta\Pi = t\int_A \boldsymbol{\varepsilon}^T \boldsymbol{D}_m \delta\boldsymbol{\varepsilon} dA + t\delta\tau_0^e \int_A \left(\frac{1}{2}\frac{\partial u_y}{\partial x} - \frac{1}{2}\frac{\partial u_x}{\partial y} - \theta_z \right) dA \\ + t\tau_0^e \int_A \left(\frac{1}{2}\frac{\partial \delta u_y}{\partial x} - \frac{1}{2}\frac{\partial \delta u_x}{\partial y} - \delta\theta_z \right) dA \\ - \frac{At}{\gamma}\tau_0^e \delta\tau_0^e - \delta\boldsymbol{d}_m{}^T \boldsymbol{f}_m \end{aligned} \tag{6.9}$$

After simplification and rearrangement of Eq. (6.9), we have

$$\begin{bmatrix} \boldsymbol{K}_{mm} & \boldsymbol{k}_{mh} \\ \boldsymbol{k}_{mh}{}^T & -\gamma^{-1}At \end{bmatrix} \begin{Bmatrix} \boldsymbol{d}_m \\ \tau_0^e \end{Bmatrix} = \begin{Bmatrix} \boldsymbol{f}_m \\ 0 \end{Bmatrix} \tag{6.10a}$$

$$\boldsymbol{K}_{mm} = t\int_A \boldsymbol{B}_m{}^T \boldsymbol{D}_m \boldsymbol{B}_m dA \tag{6.10b}$$

$$\boldsymbol{k}_{mh} = t\int_A \boldsymbol{b}_h dA \tag{6.10c}$$

in which $\boldsymbol{K}_{mm}$, $\boldsymbol{k}_{mh}$, $\boldsymbol{k}_{mh}{}^T$ and $-\gamma^{-1}At$ are obtained by the first to fourth terms in Eq. (6.9), respectively, the vector $\boldsymbol{b}_h$ can be detailed as follows,

$$\boldsymbol{b}_h = \left\{ \boldsymbol{b}_{h1}{}^T \quad \boldsymbol{b}_{h2}{}^T \quad \boldsymbol{b}_{h3}{}^T \quad \boldsymbol{b}_{h4}{}^T \right\}^T \tag{6.11a}$$

$$\boldsymbol{b}_{hi}=\begin{Bmatrix} -\frac{1}{2}\frac{\partial N_i}{\partial y} \\ \frac{1}{2}\frac{\partial N_i}{\partial x} \\ -\frac{1}{16}\left(\frac{\partial N_{k+4}}{\partial y}y_{ik}-\frac{\partial N_{i+4}}{\partial y}y_{ji}\right)+\frac{1}{16}\left(\frac{\partial N_{k+4}}{\partial x}x_{ki}-\frac{\partial N_{i+4}}{\partial x}x_{ij}\right)-N_i \end{Bmatrix} \tag{6.11b}$$

$$i=1,2,3,4;\ \ j=\mathrm{mod}(i,4)+1;\ \ k=4\mathrm{floor}(i,4)+i+1 \tag{6.11c}$$

Through the static condensation to eliminate the skew-symmetric part of the stress τ_0^e for Eq. (6.10a), we have

$$\boldsymbol{K}_m\boldsymbol{d}_m=\boldsymbol{f}_m \tag{6.12a}$$

$$\boldsymbol{K}_m=\boldsymbol{K}_{mm}+\boldsymbol{K}_{mh} \tag{6.12b}$$

$$\boldsymbol{K}_{mh}=\frac{\gamma}{At}\boldsymbol{k}_{mh}\boldsymbol{k}_{mh}^{\ T} \tag{6.12c}$$

To solve the matrix $\boldsymbol{K}_{mm}$ and the vector $\boldsymbol{k}_{mh}$, the two-dimensional 8-point integration rule having the same accuracy as the 3×3 Gauss rule is adopted. The 8-point integration rule in the isoparametric coordinate system is shown in Figure 6.2, in which the weight factors w_α and w_β are used for the solid and hollow points, respectively.

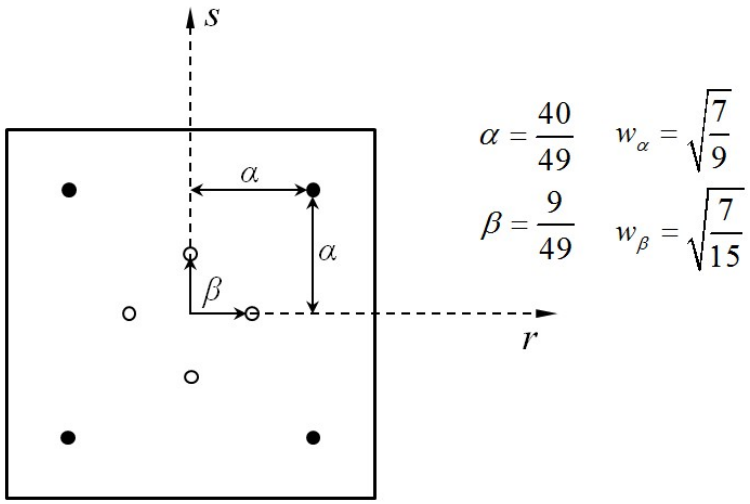

Figure 6.2 The two-dimensional 8-point integration rule

6.2 A four-node quadrilateral plate element with shear deformation

The plate element used in the thesis is derived based on the Mindlin-Reissner plate theory with consideration of transverse shear deformation. Similar to the derivation of the triangular plate element introduced in Section 5.2, the exact displacement function of the Timoshenko's beam is used to derive the displacement interpolations of the plate element, in which the plate element sides have the same deformation as the Timoshenko's beam element using a cubic interpolation.

As shown in Figure 6.3, the quadrilateral plate element has 4 corner nodes and 4 mid-side nodes, and its rotation interpolations in the isoparameter coordinate system (r, s) can be given by

$$\theta_x = \sum_{i=1}^{4} N_i(r,s)\theta_{xi} + \sum_{k=4}^{8} N_k(r,s)\theta_{xk} \tag{6.13a}$$

$$\theta_y = \sum_{i=1}^{4} N_i(r,s)\theta_{yi} + \sum_{k=4}^{8} N_k(r,s)\theta_{xk} \tag{6.13b}$$

The shape functions are

$$N_i(r,s) = \frac{1}{4}(1+r_i r)(1+s_i s)(r_i r + s_i s - 1);\ \ i = 1,2,3,4 \tag{6.14a}$$

$$N_k(r,s) = \frac{1}{2}(1-r^2)(1+s_k s);\ \ k = 5,7 \tag{6.14b}$$

$$N_k(r,s) = \frac{1}{2}(1+r_k r)(1-s^2);\ \ k = 6,8 \tag{6.14c}$$

in which r_i and s_i are the isoparametric coordinates at the corners node *i*, r_k and s_k the isoparametric coordinates at the mid-side node *k*.

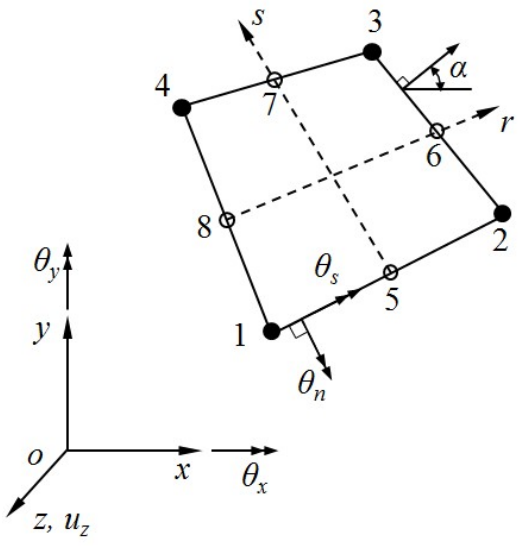

Figure 6.3 A quadrilateral plate element

To eliminate the rotations at the mid-side nodes, we should use the expressions of normal and tangential rotations at the mid-side nodes as follows,

$$\theta_{nk} = \frac{1.5\mu_{ij}}{S_{ij}}\left(u_{zj} - u_{zi}\right) + \frac{1-1.5\mu_{ij}}{2}\left(\theta_{ni} + \theta_{nj}\right) \tag{6.15a}$$

$$\theta_{sk} = \frac{\theta_{si} + \theta_{sj}}{2} \tag{6.15b}$$

$$i = 1,2,3,4; \quad j = \mathrm{mod}\left(i,4\right)+1; \quad k = i+4\,. \tag{6.15c}$$

in which Eq. (6.15a) is derived from the Timoshenko's beam element, Eq. (6.15b) assumes the tangential rotations vary linearly along the element sides, S_{ij} is the side length between the node *i* and *j*, μ_{ij} is the parameter determined by the element side as

$$\mu_{ij} = \frac{1}{1+12\lambda_{ij}} \tag{6.16a}$$

$$\lambda_{ij} = \frac{t^2}{5S_{ij}{}^2(1-v)} \tag{6.16b}$$

where *t* is the plate thickness and *v* is the Poisson ratio.

Besides, along the element side between the node *i* and *j*, the tangential and normal rotations at the corner nodes in Eqs. (6.15) can be transformed into the local coordinate system by

$$\begin{Bmatrix} \theta_{ni} \\ \theta_{si} \end{Bmatrix} = \begin{bmatrix} l_{ij} & m_{ij} \\ -m_{ij} & l_{ij} \end{bmatrix} \begin{Bmatrix} \theta_{xi} \\ \theta_{yi} \end{Bmatrix} \tag{6.17a}$$

while at the mid-side nodes, we have

$$\begin{Bmatrix} \theta_{xk} \\ \theta_{yk} \end{Bmatrix} = \begin{bmatrix} l_{ij} & -m_{ij} \\ m_{ij} & l_{ij} \end{bmatrix} \begin{Bmatrix} \theta_{nk} \\ \theta_{sk} \end{Bmatrix} \tag{6.17b}$$

in which $l_{ij} = \cos\alpha_{ij} = \dfrac{y_j - y_i}{S_{ij}}$ and $m_{ij} = \sin\alpha_{ij} = \dfrac{x_i - x_j}{S_{ij}}$ are the direction cosine and direction sine of the element side *i*-*j*, respectively.

Then, substituting Eqs. (6.17) and (6.15) into the rotation interpolations shown in Eqs. (6.13) gives

$$\begin{Bmatrix} \theta_x \\ \theta_y \end{Bmatrix} = \begin{bmatrix} \boldsymbol{N}_1 & \boldsymbol{N}_2 & \boldsymbol{N}_3 & \boldsymbol{N}_4 \end{bmatrix} \boldsymbol{d}_p \tag{6.18a}$$

$$\boldsymbol{N}_i = \begin{bmatrix} P_{i1} & P_{i2} & P_{i3} \\ Q_{i1} & Q_{i2} & Q_{i3} \end{bmatrix} \tag{6.18b}$$

$$P_{i1} = -d_i N_{i+4} + d_j N_{j+4} \tag{6.18c}$$

$$P_{i2} = N_i - e_i N_{i+4} - e_j N_{j+4} \tag{6.18d}$$

$$P_{i3} = b_i N_{i+4} + b_j N_{j+4} \tag{6.18e}$$

$$Q_{i1} = a_i N_{i+4} - a_j N_{j+4} \tag{6.18f}$$

$$Q_{i2} = b_i N_{i+4} + b_j N_{j+4} \tag{6.18g}$$

$$Q_{i3} = N_i + c_i N_{i+4} + c_j N_{j+4} \tag{6.18h}$$

$$i = 1,2,3,4; \quad j = 4\,\mathrm{floor}(1/i) + i - 1. \tag{6.18i}$$

in which $\boldsymbol{u}_p = \left\{u_{z1}\ \theta_{x1}\ \theta_{y1}\ u_{z2}\ \theta_{x2}\ \theta_{y2}\ u_{z3}\ \theta_{x3}\ \theta_{y3}\ u_{z4}\ \theta_{x4}\ \theta_{y4}\right\}^T$ is the displacement vector of the four-node quadrilateral plate element in the local coordinate system, while the coefficients are given by

$$a_i = -\frac{3}{2}\frac{m_{ij}\mu_{ij}}{S_{ij}} \tag{6.19a}$$

$$b_i = -\frac{3}{4}l_{ij}m_{ij}\mu_{ij} \tag{6.19b}$$

$$c_i = \frac{1}{2} - \frac{3}{4}m_{ij}^2\mu_{ij} \tag{6.19c}$$

$$d_i = \frac{3}{2}\frac{l_{ij}\mu_{ij}}{S_{ij}} \tag{6.19d}$$

$$e_i = -\frac{1}{2} + \frac{3}{4}m_{ij}^2\mu_{ij} \tag{6.19e}$$

The bending curvatures of the plate element can be given by

$$\boldsymbol{\kappa} = \begin{Bmatrix}\kappa_x\\ \kappa_y\\ \kappa_{xy}\end{Bmatrix} = \begin{Bmatrix}\dfrac{\partial\theta_y}{\partial x}\\ -\dfrac{\partial\theta_x}{\partial y}\\ \dfrac{\partial\theta_y}{\partial y} - \dfrac{\partial\theta_x}{\partial x}\end{Bmatrix} = \boldsymbol{B}_b\boldsymbol{d}_p = \left[\boldsymbol{B}_{b1}\ \ \boldsymbol{B}_{b2}\ \ \boldsymbol{B}_{b3}\ \ \boldsymbol{B}_{b4}\right]\boldsymbol{d}_p \tag{6.20a}$$

$$\boldsymbol{B}_{bi} = \begin{bmatrix}\dfrac{\partial Q_{i1}}{\partial x} & \dfrac{\partial Q_{i2}}{\partial x} & \dfrac{\partial Q_{i3}}{\partial x}\\ -\dfrac{\partial P_{i1}}{\partial y} & -\dfrac{\partial P_{i2}}{\partial y} & -\dfrac{\partial P_{i3}}{\partial y}\\ \dfrac{\partial Q_{i1}}{\partial y} - \dfrac{\partial P_{i1}}{\partial x} & \dfrac{\partial Q_{i2}}{\partial y} - \dfrac{\partial P_{i2}}{\partial x} & \dfrac{\partial Q_{i3}}{\partial y} - \dfrac{\partial P_{i3}}{\partial x}\end{bmatrix} \tag{6.20b}$$

where the matrix $\boldsymbol{B}_b$ is the bending strain-displacement matrix and the transformation of partial derivatives between the isoparameter and local coordinate systems can be referred to Eqs. (6.5).

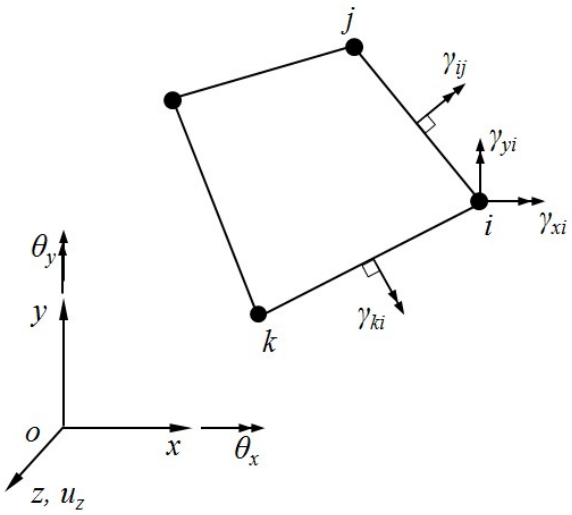

Figure 6.4 Shear strains of a quadrilateral plate element

Figure 6.4 interprets how to determine the shear strains at corner nodes. Referring to the Timoshenko's beam element, the constant shear strains along the sides *i*-*j* and *k*-*i* can be respectively given by

$$\gamma_{ij} = \left(1-\mu_{ij}\right)\left(\frac{u_{zj}-u_{zi}}{S_{ij}} - \frac{\theta_{ni}+\theta_{nj}}{2}\right) \tag{6.21a}$$

$$\gamma_{ki} = \left(1-\mu_{ki}\right)\left(\frac{u_{zi}-u_{zk}}{S_{ki}} - \frac{\theta_{nk}+\theta_{ni}}{2}\right) \tag{6.21b}$$

At the node *i*, these two shear strains in Eqs. (6.21) can be transformed into the local coordinate system by

$$\begin{Bmatrix} \gamma_{ki} \\ \gamma_{ij} \end{Bmatrix} = \begin{bmatrix} l_{ki} & m_{ki} \\ l_{ij} & m_{ij} \end{bmatrix} \begin{Bmatrix} \gamma_{xi} \\ \gamma_{yi} \end{Bmatrix} \tag{6.22a}$$

$$i=1,2,3,4;\ j=\mathrm{mod}(i,4)+1;\ k=4\mathrm{floor}(1/i)+i-1 \tag{6.22b}$$

After rearrangement of Eq. (6.22a) , we have

$$\begin{Bmatrix} \gamma_{xi} \\ \gamma_{yi} \end{Bmatrix} = \frac{1}{l_{ki}m_{ij} - l_{ij}m_{ki}} \begin{bmatrix} m_{ij} & -m_{ki} \\ -l_{ij} & l_{ki} \end{bmatrix} \begin{Bmatrix} \gamma_{ki} \\ \gamma_{ij} \end{Bmatrix} \tag{6.22c}$$

Note that the direction of shear strains at the node *i*, corresponding to the shear stresses in the local coordinate system, should be

$$\begin{Bmatrix} \gamma_{xzi} \\ \gamma_{yzi} \end{Bmatrix} = \begin{Bmatrix} -\gamma_{yi} \\ \gamma_{xi} \end{Bmatrix} = \frac{1}{l_{ki}m_{ij} - l_{ij}m_{ki}} \begin{bmatrix} l_{ij} & -l_{ki} \\ m_{ij} & -m_{ki} \end{bmatrix} \begin{Bmatrix} \gamma_{ij} \\ \gamma_{ki} \end{Bmatrix} \tag{6.22d}$$

The shear strain interpolations over the 4-node quadrilateral element is assumed to be bilinear, so we have

$$\boldsymbol{\gamma} = \begin{Bmatrix} \gamma_{xz} \\ \gamma_{yz} \end{Bmatrix} = \sum_{i=1}^{4} \tilde{N}_i(r,s) \begin{Bmatrix} \gamma_{xzi} \\ \gamma_{yzi} \end{Bmatrix} \tag{6.23}$$

where the shape functions are the same as Eq. (6.2a).

Substituting Eq. (6.22d) into (6.23) gives

$$\boldsymbol{\gamma} = \begin{Bmatrix} \gamma_{xz} \\ \gamma_{yz} \end{Bmatrix} = \tilde{\boldsymbol{N}} \begin{Bmatrix} \gamma_{12} \\ \gamma_{23} \\ \gamma_{34} \\ \gamma_{41} \end{Bmatrix} \tag{6.24a}$$

$$\tilde{\boldsymbol{N}}=\begin{bmatrix} \frac{\tilde{N}_1 l_{12}}{C_1}-\frac{\tilde{N}_2 l_{12}}{C_2} & \frac{\tilde{N}_2 l_{23}}{C_2}-\frac{\tilde{N}_3 l_{23}}{C_3} & \frac{\tilde{N}_3 l_{34}}{C_3}-\frac{\tilde{N}_4 l_{34}}{C_4} & \frac{\tilde{N}_4 l_{41}}{C_4}-\frac{\tilde{N}_1 l_{41}}{C_1} \\ \frac{\tilde{N}_1 m_{12}}{C_1}-\frac{\tilde{N}_2 m_{12}}{C_2} & \frac{\tilde{N}_2 m_{23}}{C_2}-\frac{\tilde{N}_3 m_{23}}{C_3} & \frac{\tilde{N}_3 m_{34}}{C_3}-\frac{\tilde{N}_4 m_{34}}{C_4} & \frac{\tilde{N}_4 m_{41}}{C_4}-\frac{\tilde{N}_1 m_{41}}{C_4} \end{bmatrix}$$

(6.24b)

$$C_i = l_{ki}m_{ij} - l_{ij}m_{ki} \tag{6.24c}$$

$$i=1,2,3,4;\ j=\mathrm{mod}(i,4)+1;\ k=4\mathrm{floor}(1/i)+i-1 \tag{6.24d}$$

Substituting Eq. (6.17a) into (6.21a), the constant shear strains along each side of the plate element can be expressed with the displacement vector as

$$\begin{Bmatrix} \gamma_{12} \\ \gamma_{23} \\ \gamma_{34} \\ \gamma_{41} \end{Bmatrix} = \tilde{\boldsymbol{B}}_s \boldsymbol{d}_p = \begin{bmatrix} \tilde{\boldsymbol{B}}_{s1} \\ \tilde{\boldsymbol{B}}_{s2} \\ \tilde{\boldsymbol{B}}_{s3} \\ \tilde{\boldsymbol{B}}_{s4} \end{bmatrix} \boldsymbol{d}_p \tag{6.25a}$$

$$\tilde{\boldsymbol{B}}_{s1} = (1-\mu_{12}) \begin{bmatrix} \frac{-1}{S_{12}} & \frac{-l_{12}}{2} & \frac{-m_{12}}{2} & \frac{1}{S_{12}} & \frac{-l_{23}}{2} & \frac{-m_{23}}{2} & 0 & 0 & 0 & 0 & 0 & 0 \end{bmatrix} \tag{6.25b}$$

$$\tilde{\boldsymbol{B}}_{s2} = (1-\mu_{23}) \begin{bmatrix} 0 & 0 & 0 & \frac{-1}{S_{23}} & \frac{-l_{23}}{2} & \frac{-m_{23}}{2} & \frac{1}{S_{23}} & \frac{-l_{34}}{2} & \frac{-m_{34}}{2} & 0 & 0 & 0 \end{bmatrix} \tag{6.25c}$$

$$\tilde{\boldsymbol{B}}_{s3} = (1-\mu_{34}) \begin{bmatrix} 0 & 0 & 0 & 0 & 0 & 0 & \frac{-1}{S_{34}} & \frac{-l_{34}}{2} & \frac{-m_{34}}{2} & \frac{1}{S_{34}} & \frac{-l_{41}}{2} & \frac{-m_{41}}{2} \end{bmatrix} \tag{6.25d}$$

$$\tilde{\boldsymbol{B}}_{s4} = (1-\mu_{41}) \begin{bmatrix} \frac{1}{S_{41}} & \frac{-l_{12}}{2} & \frac{-m_{12}}{2} & 0 & 0 & 0 & 0 & 0 & 0 & \frac{-1}{S_{41}} & \frac{-l_{41}}{2} & \frac{-l_{41}}{2} \end{bmatrix} \tag{6.25e}$$

Finally, the shear strain-displacement matrix can be given by

$$\boldsymbol{\gamma} = \boldsymbol{B}_s \boldsymbol{d}_p \tag{6.26a}$$

$$\boldsymbol{B}_s = \tilde{\boldsymbol{N}}\tilde{\boldsymbol{B}}_s \tag{6.26b}$$

The variational formulation considering bending and shear strains over the plate element is

$$\Pi_p = \int_A \boldsymbol{\kappa}^T \boldsymbol{D}_b \boldsymbol{\kappa} dA + \int_A \boldsymbol{\gamma}^T \boldsymbol{D}_s \boldsymbol{\gamma} dA - \int_A \boldsymbol{d}_p{}^T \boldsymbol{f}_p dA \tag{6.27}$$

where $\boldsymbol{D}_b$ and $\boldsymbol{D}_s$ are the constitutive matrices as follows

$$\boldsymbol{D}_b = \frac{Et^3}{12(1-v^2)}\begin{bmatrix} 1 & v & 0 \\ v & 1 & 0 \\ 0 & 0 & 0.5(1-v) \end{bmatrix} \tag{6.28a}$$

$$\boldsymbol{D}_s = \frac{5Et}{12(1+v)}\begin{bmatrix} 1 & 0 \\ 0 & 1 \end{bmatrix} \tag{6.28b}$$

Taking a variation of Eq. (6.27), the stiffness matrix of the linear elastic plate element allowing for transverse shear deformation can be given by

$$\boldsymbol{K}_p \boldsymbol{d}_p = \boldsymbol{f}_p \tag{6.29a}$$

$$\boldsymbol{K}_p = \boldsymbol{K}_b + \boldsymbol{K}_s \tag{6.29b}$$

$$\boldsymbol{K}_b = \int_A \boldsymbol{B}_b{}^T \boldsymbol{D}_b \boldsymbol{B}_b dA \tag{6.29c}$$

$$\boldsymbol{K}_s = \int_A \boldsymbol{B}_s{}^T \boldsymbol{D}_s \boldsymbol{B}_s dA \tag{6.29d}$$

in which the bending stiffness matrix $\boldsymbol{K}_b$ and the shear stiffness matrix $\boldsymbol{K}_s$ can be derived from the first and second terms in Eq. (6.27), respectively. Also, the

two-dimensional 8-point integration rule is used to calculate these two stiffness matrices similar to the quadrilateral membrane element introduced in Section 6.1

6.3 Updated Lagrangian formulation

In this section, the quadrilateral shell element consisting of the membrane element and the plate element introduced previously is extended to geometrically nonlinear analysis with the updated Lagrangian (UL) formulation based on the degenerated Green-Lagrangian strains. Different from the traditional UL method, the co-rotational concept used here allows for large rotations, while the tangent stiffness matrix is derived from the degenerated Green-Lagrangian strains based on the local coordinate system. The difference between the UL formulation and the EICR formulation lies in the latter does not use nonlinear strains to derive the tangent stiffness. In the calculation of the internal forces, the UL formulation uses pure deformations extracted from total deformations, which is identical to the EICR formulation.

6.3.1 Definition of local coordinate system

Different from the pure deformational method introduced in Chapter 3, a new definition of the local coordinate system, called bisector definition, is introduced here to eliminate the nodal ordering dependency, as shown in Figure 6.5.

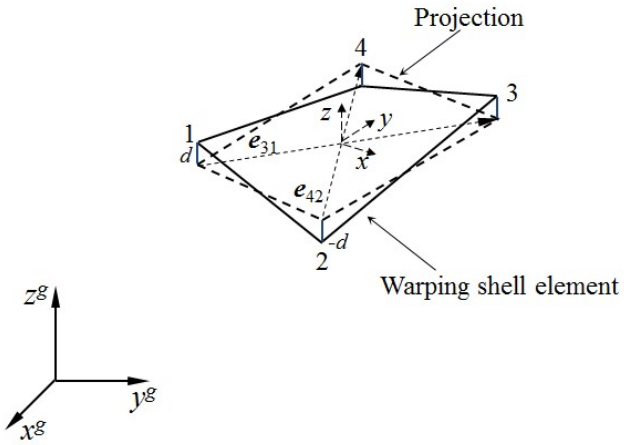

Figure 6.5 Definition of local coordinate system

The coordinates of the 4 corner nodes of the quadrilateral shell element in the global coordinate system ($x^g y^g z^g$) are $\boldsymbol{x}_i^g = \left\{ x_i^g \;\; y_i^g \;\; z_i^g \right\}^T$, i=1,2,3,4. Firstly, we define two normalized unit vectors in the followings,

$$\boldsymbol{e}_{13} = \frac{\boldsymbol{x}_3^g - \boldsymbol{x}_1^g}{\left\| \boldsymbol{x}_3^g - \boldsymbol{x}_1^g \right\|} \tag{6.30a}$$

$$\boldsymbol{e}_{24} = \frac{\boldsymbol{x}_4^g - \boldsymbol{x}_2^g}{\left\| \boldsymbol{x}_4^g - \boldsymbol{x}_2^g \right\|} \tag{6.30b}$$

Then, the triad vectors of local coordinate system (xyz) are given by

$$\boldsymbol{e}_x = \frac{\boldsymbol{e}_{13} - \boldsymbol{e}_{24}}{\left\| \boldsymbol{e}_{13} - \boldsymbol{e}_{24} \right\|} \tag{6.31a}$$

$$\boldsymbol{e}_y = \frac{\boldsymbol{e}_{13} + \boldsymbol{e}_{24}}{\left\| \boldsymbol{e}_{13} + \boldsymbol{e}_{24} \right\|} \tag{6.31b}$$

$$\boldsymbol{e}_z = \boldsymbol{e}_x \times \boldsymbol{e}_y \tag{6.31c}$$

Thus, the local-to-global transformation matrix for the quadrilateral shell element can be expressed as

$$\boldsymbol{T}_e = \begin{bmatrix} \boldsymbol{e}_x & \boldsymbol{e}_y & \boldsymbol{e}_z \end{bmatrix}^T \tag{6.32}$$

The origin of the local coordinate system is set to the centre of the quadrilateral shell element, so the local coordinates of the corner nodes can be given by

$$\boldsymbol{x}_i = \boldsymbol{T}_e(\boldsymbol{x}_i^g - \boldsymbol{x}_c^g)\text{, } i\text{=1,2,3,4} \tag{6.33a}$$

$$\boldsymbol{x}_c^g = \frac{1}{4}(\boldsymbol{x}_1^g + \boldsymbol{x}_2^g + \boldsymbol{x}_3^g + \boldsymbol{x}_4^g) \tag{6.33b}$$

where the local coordinates at the node i, $\boldsymbol{x}_i = \begin{Bmatrix} x_i & y_i & z_i \end{Bmatrix}^T$.

The projection of the warping shell element can be determined by the plane coordinates $\boldsymbol{x}_i = \begin{Bmatrix} x_i & y_i \end{Bmatrix}^T$, which can be used to compute the stiffness matrices of the membrane and the plate elements. In addition, the warping at corner nodes may occur, while it can be noticed that the local z-coordinates at every corner node having identical absolutely value, so we use the parameter d to denote the local z-coordinates with z_1=-z_2=z_3=-z_4=d.

6.3.2 Tangent stiffness based on the updated Lagrangian formulation

For a plate with large deflection, its vertical displacement component produces additional in-plane deformations. Thus, in the local coordinate system, the

strain-displacement relationship of the membrane element could be modified to account for the additional deflections via the degenerated Green-Lagrangian strains as follows,

$$\varepsilon_x = \frac{\partial u_x}{\partial x} + \frac{1}{2}\left(\frac{\partial u_z}{\partial x}\right)^2 \tag{6.34a}$$

$$\varepsilon_y = \frac{\partial u_y}{\partial y} + \frac{1}{2}\left(\frac{\partial u_z}{\partial y}\right)^2 \tag{6.34b}$$

$$\gamma_{xy} = \frac{\partial u_x}{\partial y} + \frac{\partial u_y}{\partial x} + \frac{\partial u_z}{\partial x}\frac{\partial u_z}{\partial y} \tag{6.34c}$$

In the traditional UL formulation, the full expression of Green-Lagrangian strains should be used in large rotation problems, since the strains have the ability to remove rigid body movements from total deformations. However, the degenerated strains cannot completely meet this requirement. With the co-rotational technique, the degenerated Green-Lagrangian strains can be used to describe the small local displacements. Moreover, the complicated expression of 3D large rotations is avoided in the displacement interpolations, so the tangent stiffness matrix becomes simpler. For the plate element, the relationship between the bending curvatures and the displacements does not change.

Referring to the classical updated Lagrangian formulation expressed in tensor form, which is presented by Bathe *et al.* (Bathe, 2006; Bathe and Bolourchi, 1979), the equilibrium equation of the deformed configuration is established with the geometry and variables at the current time as

$$\int_V C_{ijrs} e_{rs} \delta e_{ij} \, dV + \int_V \tau_{ij} \delta \eta_{ij} \, dV = \boldsymbol{R}^{n+1} - \int_V \tau_{ij} \delta e_{ij} \, dV \tag{6.35}$$

in which τ_{ij} denotes the Cauchy stress tensor at the current time, e_{ij} and η_{ij} are the linear and nonlinear components of the Green-Lagrange strain increments, respectively; C_{ijrs} is the components of the constitutive tensor and $\boldsymbol{R}^{n+1}$ is the externally applied load vector.

For the projection of a warping shell element in the local coordinate system, the first term of Eq. (6.35) leads to the linear strain incremental stiffness matrix $\boldsymbol{K}_e$ assembled by the material stiffness matrices of the membrane and plate elements introduced previously. The second term can be used to derive the geometric stiffness matrix $\boldsymbol{K}_g$ as follows,

$$\begin{aligned}
&\int_V \tau_{ij} \delta \eta_{ij} \, dV \\
&= \frac{t}{2} \int_A \left\{ N_x \;\; N_y \;\; N_{xy} \right\} . \left\{ \delta \left(\frac{\partial u_z}{\partial x} \right)^2 \;\; \delta \left(\frac{\partial u_z}{\partial y} \right)^2 \;\; \delta \frac{\partial u_z}{\partial x} \frac{\partial u_z}{\partial y} \right\}^T dA \\
&= t \int_A \left\{ N_x \;\; N_y \;\; N_{xy} \right\} [\mathbf{C}] \, \delta \{\boldsymbol{\theta}\} \, dA \\
&= t \int_A \{\boldsymbol{\theta}\}^T \begin{bmatrix} N_x & N_{xy} \\ N_{xy} & N_y \end{bmatrix} \delta \{\boldsymbol{\theta}\} \, dA
\end{aligned} \tag{6.36a}$$

$$[\mathbf{C}] = \begin{bmatrix} \dfrac{\partial u_z}{\partial x} & 0 \\ 0 & \dfrac{\partial u_z}{\partial y} \\ \dfrac{\partial u_z}{\partial y} & \dfrac{\partial u_z}{\partial x} \end{bmatrix} \tag{6.36b}$$

$$\{\boldsymbol{\theta}\} = \begin{Bmatrix} \dfrac{\partial u_z}{\partial x} \\ \dfrac{\partial u_z}{\partial y} \end{Bmatrix} = \begin{Bmatrix} -\theta_y \\ \theta_x \end{Bmatrix} \tag{6.36c}$$

in which N_x, N_y, and N_{xy} are the membrane forces of the shell element at the current time, respectively.

The vector $\{\boldsymbol{\theta}\}$ contains the local rotations and can be expressed with the rotation interpolations given in Eqs. (6.18). With regard to a plate element without considering transverse shear deformation, it yields

$$\{\boldsymbol{\theta}\} = \begin{Bmatrix} -\theta_y^l \\ \theta_x^l \end{Bmatrix} = [\mathbf{G}]\boldsymbol{d} \tag{6.37}$$

in which $\boldsymbol{d}$ is the displacement vector of the shell element in the local coordinate system, and the matrix $[\mathbf{G}]$ can be easily obtained by Eqs. (6.18).

For the plate element allowing for transverse shear deformation, we have

$$\{\boldsymbol{\theta}\} = \begin{bmatrix} -\theta_y + \gamma_{xz} \\ \theta_x + \gamma_{yz} \end{bmatrix} = [\mathbf{G}]_{shear}\boldsymbol{d} \tag{6.38}$$

in which the matrix $[\mathbf{G}]_{shear}$ can be derived with Eqs. (6.18) and (6.26).

To obtain the geometric stiffness matrix, taking a variation of Eq. (6.36a) gives

$$\begin{aligned} & t\int_A \delta\{\boldsymbol{\theta}\}^T \begin{bmatrix} N_x & N_{xy} \\ N_{xy} & N_y \end{bmatrix} \delta\{\boldsymbol{\theta}\} dA \\ & = \delta\boldsymbol{d}^T t\int_A [\mathbf{G}]^T \begin{bmatrix} {}^tN_x & {}^tN_{xy} \\ {}^tN_{xy} & {}^tN_y \end{bmatrix} [\mathbf{G}] dA\delta\boldsymbol{d} \end{aligned} \tag{6.39a}$$

$$\boldsymbol{K}_g = t\int_A [\mathbf{G}]^T \begin{bmatrix} {}^tN_x & {}^tN_{xy} \\ {}^tN_{xy} & {}^tN_y \end{bmatrix} [\mathbf{G}]\, dA \tag{6.39b}$$

in which the membrane forces are averaged over the projection of a warping shell element at the current time, while how to update them is introduced in the next section. The geometric stiffness matrix is also calculated by the two dimensional 8-point integration rule as same as the material stiffness matrices of the membrane and plate elements.

Then, the tangent stiffness matrix for the projection of the warping quadrilateral shell element in the local coordinate system can be given by

$$\boldsymbol{K}_t = \boldsymbol{K}_e + \boldsymbol{K}_g \tag{6.40}$$

In this chapter, the warping effect of the quadrilateral shell element is assumed to be small and regarded as eccentricities at nodes, so the relationship of displacement vectors between the projection and the warping shell element at the node *i* can be given by

$$\delta\overline{\boldsymbol{d}}_i = \boldsymbol{E}_i \delta\boldsymbol{d}_i \quad i=1,2,3,4 \tag{6.41a}$$

$$\boldsymbol{E}_i = \begin{bmatrix} 1 & 0 & 0 & 0 & -z_i & 0 \\ 0 & 1 & 0 & z_i & 0 & 0 \\ 0 & 0 & 1 & 0 & 0 & 0 \\ 0 & 0 & 0 & 1 & 0 & 0 \\ 0 & 0 & 0 & 0 & 1 & 0 \\ 0 & 0 & 0 & 0 & 0 & 1 \end{bmatrix} \tag{6.41b}$$

$$\delta\overline{\boldsymbol{d}}_i = \left\{\overline{u}_{xi}\ \ \overline{u}_{yi}\ \ \overline{u}_{zi}\ \ \overline{\theta}_{xi}\ \ \overline{\theta}_{yi}\ \ \overline{\theta}_{zi}\right\}^T \tag{6.41c}$$

$$\delta\boldsymbol{d}_i = \left\{u_{xi}\ \ u_{yi}\ \ u_{zi}\ \ \theta_{xi}\ \ \theta_{yi}\ \ \theta_{zi}\right\}^T \tag{6.41d}$$

where the parameter having a superposed horizontal line "-" means that it belongs to the projection.

Then, the tangent stiffness matrix of the warping shell element in the local coordinate system can be modified as follows,

$$\boldsymbol{K}_t = \boldsymbol{E}^T \left(\boldsymbol{K}_e + \boldsymbol{K}_g \right) \boldsymbol{E} \tag{6.42a}$$

$$\boldsymbol{E} = \begin{bmatrix} \boldsymbol{E}_1 & \boldsymbol{0} & \boldsymbol{0} & \boldsymbol{0} \\ \boldsymbol{0} & \boldsymbol{E}_2 & \boldsymbol{0} & \boldsymbol{0} \\ \boldsymbol{0} & \boldsymbol{0} & \boldsymbol{E}_3 & \boldsymbol{0} \\ \boldsymbol{0} & \boldsymbol{0} & \boldsymbol{0} & \boldsymbol{E}_4 \end{bmatrix} \tag{6.42b}$$

Finally, transforming the local tangent stiffness matrix into the global coordinate system gives

$$\boldsymbol{K}_t^g = \boldsymbol{T}^T \boldsymbol{E}^T \left(\boldsymbol{K}_e + \boldsymbol{K}_g \right) \boldsymbol{E} \boldsymbol{T} \tag{6.43}$$

in which the transformation matrix $\boldsymbol{T}$ is composed of $\boldsymbol{T}_e$ along diagonal and calculated based on the current configuration. In the incremental-iterative analysis procedure, the global tangent stiffness matrix is used to assemble the global stiffness matrix of the whole structure in every iteration step of the nonlinear analysis. Further, with the assumption of small strains, the local tangent stiffness matrix should be computed based on the initial dimensions of the shell element during the whole analysis process, while the transformation matrix and the eccentricity matrix are formed based on the current geometry.

6.3.3 Internal forces and element stresses

In the iterative procedure of nonlinear analysis, the resistant force vector of a structure model is assembled by the internal force vector of shell elements and used to check the convergence of calculations. After an iteration step, the incremental pure deformations are extracted from the incremental global displacements to compute the internal forces of the quadrilateral shell element based on the co-rotational concept.

6.3.3.1 Extraction of incremental pure deformations

The method of directly incremental deformation, introduced in Section 4.3.2.2, is used here to extract the incremental pure deformations and update the internal forces and stresses.

For the quadrilateral shell element in the last iteration, the local-to-global transformation matrix $\boldsymbol{T}_e^n$, the rotation matrix at the node *i* in the global coordinate system $\boldsymbol{R}_i^{gn}$, the global nodal coordinates $\boldsymbol{x}_i^{gn}$ and the local nodal coordinates $\boldsymbol{x}_i^n$ are known. After one iterative process, the incremental displacements of the quadrilateral shell element in the global coordinate system can be expressed as follows,

$$\Delta\boldsymbol{d}^g = \left\{\Delta\boldsymbol{d}_1^{gT} \;\; \Delta\boldsymbol{d}_2^{gT} \;\; \Delta\boldsymbol{d}_3^{gT} \;\; \Delta\boldsymbol{d}_4^{gT}\right\}^T \tag{6.44a}$$

$$\Delta\boldsymbol{d}_i^g = \left\{\Delta u_{xi}^g \;\; \Delta u_{yi}^g \;\; \Delta u_{zi}^g \;\; \Delta\theta_{xi}^g \;\; \Delta\theta_{yi}^g \;\; \Delta\theta_{zi}^g\right\}^T \tag{6.44b}$$

$$\Delta\boldsymbol{u}_i^g = \left\{\Delta u_{xi}^g \;\; \Delta u_{yi}^g \;\; \Delta u_{zi}^g\right\}^T \tag{6.44c}$$

$$\Delta\boldsymbol{\theta}_i^g = \left\{\Delta\theta_{xi}^g \;\; \Delta\theta_{yi}^g \;\; \Delta\theta_{zi}^g\right\}^T \tag{6.44d}$$

Then, the global nodal coordinates can be updated as below.

$$\boldsymbol{x}_i^{g\,n+1} = \boldsymbol{x}_i^{g\,n} + \Delta\boldsymbol{u}_i^g \tag{6.45}$$

The local-to-global transformation matrix $\boldsymbol{T}_e^{n+1}$ and the local nodal coordinates $\boldsymbol{x}_i^{n+1}$ of the quadrilateral shell element can be updated by the new global nodal coordinates accordingly.

Thus, the incremental pure displacements at the node *i* are

$$\Delta\boldsymbol{u}_i = \boldsymbol{x}_i^{n+1} - \boldsymbol{x}_i^n \tag{6.46a}$$

$$\Delta\boldsymbol{u}_i = \left\{\Delta u_{xi} \;\; \Delta u_{yi} \;\; \Delta u_{zi}\right\}^T \tag{6.46b}$$

In terms of the incremental pure rotations at the node *i*, they can be computed by the process in the following,

$$\Delta\boldsymbol{R}_i^g = \boldsymbol{R}\left(\Delta\boldsymbol{\theta}_i^g\right) \tag{6.47a}$$

$$\Delta\boldsymbol{R}_i = \boldsymbol{T}_e^{n+1}\Delta\boldsymbol{R}_i^g\boldsymbol{T}_e^{n\,T} \tag{6.47b}$$

$$\Delta\boldsymbol{\theta}_i = \boldsymbol{\theta}\left(\Delta\boldsymbol{R}_i\right) \tag{6.47c}$$

$$\Delta\boldsymbol{\theta}_i = \left\{\Delta\theta_{xi} \;\; \Delta\theta_{yi} \;\; \Delta\theta_{zi}\right\}^T \tag{6.47d}$$

in which the mutual transformation between a rotation vector and a rotation matrix is introduced in Chapter 4.

Note that the pure deformations in Eqs. (6.46) and (6.47) belong to the warping shell element and should be transformed into the projection as follows,

$$\Delta\bar{\boldsymbol{d}} = \boldsymbol{E}^{n+1}\Delta\boldsymbol{d} \tag{6.48}$$

6.3.3.2 Stresses updating

Different from the EICR formulation, the membrane stresses should be computed and recorded in the process of geometrically nonlinear analysis to formulate the geometric stiffness matrix. Based on the projection of the warping shell element, the increments of membrane stresses, bending moments and shear stresses can be respectively given by

$$\begin{Bmatrix} \Delta N_x \\ \Delta N_y \\ \Delta N_{xy} \end{Bmatrix} = \boldsymbol{D}_m \boldsymbol{B}_m^0 (r,s)\, \Delta\bar{\boldsymbol{d}}_m \tag{6.49a}$$

$$\begin{Bmatrix} \Delta M_x \\ \Delta M_y \\ \Delta M_{xy} \end{Bmatrix} = \boldsymbol{D}_b \boldsymbol{B}_b^0 (r,s)\, \Delta\bar{\boldsymbol{d}}_p \tag{6.49b}$$

$$\begin{Bmatrix} \Delta Q_{xy} \\ \Delta Q_{xz} \end{Bmatrix} = \boldsymbol{D}_s \boldsymbol{B}_s (r,s)\, \Delta\bar{\boldsymbol{d}}_p \tag{6.49c}$$

in which $\boldsymbol{B}_m^0(r,s)$, $\boldsymbol{B}_b^0(r,s)$ and $\boldsymbol{B}_s^0(r,s)$ are the generalized strain-displacement matrices of the membrane and the plate elements introduced previously and computed based on the initial dimensions of the shell element due to the small strains assumption, while r and s are the isoparametric coordinates. Then, the stresses can be updated by adding the incremental stresses to those from last iteration.

Besides, to achieve fast convergence in practical analyses, the averaged membrane stresses are used in the computation of the geometric stiffness matrix as follows,

$$\begin{Bmatrix} \Delta N_x \\ \Delta N_y \\ \Delta N_{xy} \end{Bmatrix} = \frac{1}{A}\int_A \begin{Bmatrix} \Delta N_x(r,s) \\ \Delta N_y(r,s) \\ \Delta N_{xy}(r,s) \end{Bmatrix} dA \tag{6.50a}$$

$$\begin{Bmatrix} N_x^{n+1} \\ N_y^{n+1} \\ N_{xy}^{n+1} \end{Bmatrix} = \begin{Bmatrix} N_x^{n} \\ N_y^{n} \\ N_{xy}^{n} \end{Bmatrix} + \begin{Bmatrix} \Delta N_x \\ \Delta N_y \\ \Delta N_{xy} \end{Bmatrix} \tag{6.50b}$$

6.3.3.3 Internal forces updating

The internal forces for both the UL and the EICR formulations should be calculated in the process of nonlinear analysis. Although the internal forces are not needed in the UL formulation to get the geometric stiffness, they are required in the computation of the residual forces to check the system equilibrium and continue iterations.

The incremental internal forces of the projection of the shell element are

$$\Delta\overline{\boldsymbol{f}}_m = \boldsymbol{K}_m^0 \Delta\overline{\boldsymbol{d}}_m \tag{6.51a}$$

$$\Delta\overline{\boldsymbol{f}}_p = \boldsymbol{K}_p^0 \Delta\overline{\boldsymbol{d}}_p \tag{6.51b}$$

Due to the assumption of small strains, the incremental internal forces are achieved based on the linear elastic stiffness of the shell element with initial geometry. The internal force vector of the projection of the shell element is recorded and accumulated after every iteration as

$$\overline{\boldsymbol{f}}^{n+1} = \overline{\boldsymbol{f}}^{n} + \Delta\overline{\boldsymbol{f}} \tag{6.52}$$

Then, the internal force vector of the warping shell element in the local coordinate system is

$$\boldsymbol{f}^{n+1} = \boldsymbol{E}^{n+1T}\,\overline{\boldsymbol{f}}^{n+1} \tag{6.53}$$

in which the eccentricity matrix is formed by the updated local *z*-coordinates.

Finally, to assemble the global internal force vector of the whole structure, the local internal force vector should be transformed into the global coordinate system as

$$\boldsymbol{f}^{g\,n+1} = \boldsymbol{T}^{n+1}\,\boldsymbol{f}^{n+1} \tag{6.54}$$

in which the transformation matrix $\boldsymbol{T}^{n+1}$ is composed of $\boldsymbol{T}_e^{n+1}$ along diagonal.

6.4 Simplified co-rotational formulation

The simplified EICR formulation is different from the UL formulation introduced in the last section, in which the geometric stiffness is derived from the load perturbation of equilibrium equations for the shell element. However, the two formulations have the identical procedure to get the internal forces of the shell element. Thus, this section only details the derivation for the tangent stiffness based on the simplified EICR method.

6.4.1 Tangent stiffness

As previously in Chapter 4, the simplified co-rotational method neglects the change of element dimensions due to the small strain assumption, different from the general EICR formulation. Thus, the tangent stiffness of the warping quadrilateral shell element has three parts, including the material stiffness, the geometric stiffness due to

rigid body rotations and the geometric stiffness due to warping. In the global coordinate system, the tangent stiffness matrix can be given by

$$\boldsymbol{K}_t^g = \boldsymbol{T}^T\left(\boldsymbol{K}_e + \boldsymbol{K}_{gr} + \boldsymbol{K}_{gw}\right)\boldsymbol{T} \tag{6.55}$$

in which $\boldsymbol{T}$ is the transformation matrix transforming the local tangent stiffness into the global coordinate system; $\boldsymbol{K}_e$ the local material stiffness matrix; $\boldsymbol{K}_{gr}$ and $\boldsymbol{K}_{gw}$ the local geometric stiffness matrices due to rigid body motions and warping, respectively.

Also, the definition of the local coordinate system used in the UL formulation rather than the one introduced in Chapter 4 is used here. This is because the bisector definition can overcome the nodal ordering dependency, although it makes the derivation of the geometric stiffness more complicated.

6.4.4.1 Local material stiffness matrix

The local material stiffness matrix is identical to the one used in the UL formulation, which is assembled by the stiffness matrices of the membrane and plate elements. Although it is always computed using the initial dimensions of the projection of the quadrilateral shell element, the eccentricity matrix should be updated according to the current local z-coordinates. Thus, the local material stiffness matrix can be given by

$$\boldsymbol{K}_e = \boldsymbol{E}^T\bar{\boldsymbol{K}}_e^0\boldsymbol{E} \tag{6.56}$$

in which the material stiffness matrix $\bar{\boldsymbol{K}}_e^0$ is calculated based on the initial dimensions of the projection. Thus, $\bar{\boldsymbol{K}}_e^0$ can be computed in the beginning of nonlinear analysis, stored and called in the following analysis procedure.

6.4.4.2 Geometric stiffness matrix due to rigid body rotations

Following the derivation introduced in Chapter 4, the geometric stiffness matrix due to rigid body rotations of the shell element can be given by

$$\boldsymbol{K}_{gr} = -\boldsymbol{A}\boldsymbol{G} \tag{6.57a}$$

$$\boldsymbol{A} = \begin{bmatrix} \mathbf{Spin}(\boldsymbol{n}_1) \\ \mathbf{Spin}(\boldsymbol{m}_1) \\ \vdots \\ \mathbf{Spin}(\boldsymbol{n}_4) \\ \mathbf{Spin}(\boldsymbol{m}_4) \end{bmatrix} \tag{6.57b}$$

$$\boldsymbol{G} = \begin{bmatrix} \dfrac{\partial \boldsymbol{\omega}}{\partial \boldsymbol{u}_1^T} & \dfrac{\partial \boldsymbol{\omega}}{\partial \boldsymbol{\theta}_1^T} & \dfrac{\partial \boldsymbol{\omega}}{\partial \boldsymbol{u}_2^T} & \dfrac{\partial \boldsymbol{\omega}}{\partial \boldsymbol{\theta}_2^T} & \cdots & \dfrac{\partial \boldsymbol{\omega}}{\partial \boldsymbol{u}_4^T} & \dfrac{\partial \boldsymbol{\omega}}{\partial \boldsymbol{\theta}_4^T} \end{bmatrix} \tag{6.57c}$$

in which the matrix $\boldsymbol{A}$ is formulated by the internal forces at the current time, and the matrix $\boldsymbol{G}$ connects the variations of rigid body rotations to the variations of nodal displacements based on the local coordinate system.

Thus, the variations of rigid body rotations are crucial in obtaining the geometric stiffness matrix. To derive the matrix, Figure 6.6 shows that a quadrilateral shell element moves from the initial configuration C_0 to the current configuration C_n. The variations of rigid body rotations are derived based on the local coordinate system.

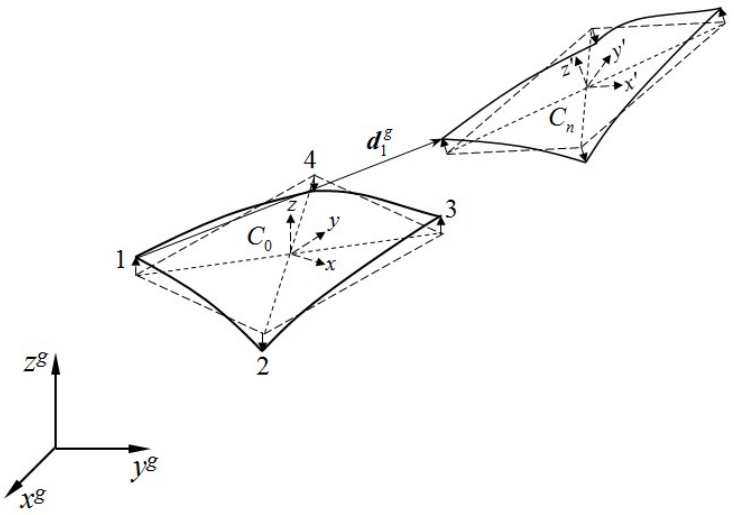

Figure 6.6 Deformation of a quadrilateral shell element

The local translational displacement vector at the node i is expressed as $\boldsymbol{u}_i = \{u_i \;\; v_i \;\; w_i\}^T$. Thus, the initial and current local nodal coordinates are $\boldsymbol{x}_i^0$ and $\boldsymbol{x}_i = \boldsymbol{x}_i^0 + \boldsymbol{u}_i$, respectively. In the procedure of derivation, the current local coordinate system is regarded as the global coordinate system, so the local-to-global transformation matrix is an identity matrix as follows,

$$\boldsymbol{T}_e = \left[\boldsymbol{e}_x \quad \boldsymbol{e}_y \quad \boldsymbol{e}_z\right]^T = \boldsymbol{I}_3 \tag{6.58}$$

The current local nodal coordinates are

$$\boldsymbol{x}_1 = \{x_1 \;\; y_1 \;\; d\}^T, \;\; \boldsymbol{x}_2 = \{x_2 \;\; y_2 \;\; -d\}^T \tag{6.59a}$$

$$\boldsymbol{x}_3 = \{x_3 \;\; y_3 \;\; d\}^T, \;\; \boldsymbol{x}_4 = \{x_4 \;\; y_4 \;\; -d\}^T \tag{6.59b}$$

The origin of the local coordinate system is set to the element centre, so the centre coordinates can be given by

$$\boldsymbol{x}_c = \frac{1}{4}(\boldsymbol{x}_1 + \boldsymbol{x}_2 + \boldsymbol{x}_3 + \boldsymbol{x}_4) = \{0\ \ 0\ \ 0\}^T \tag{6.60}$$

Through Eqs. (6.59) and (6.60), we can obtain the equations as follows,

$$\frac{-x_{31}}{a} = \frac{x_{42}}{b} \tag{6.61a}$$

$$\frac{y_{31}}{a} = \frac{y_{42}}{b} \tag{6.61b}$$

in which $a = \sqrt{{x_{31}}^2 + {y_{31}}^2}$, $b = \sqrt{{x_{42}}^2 + {y_{42}}^2}$, $x_{ij} = x_i - x_j$, $y_{ij} = y_i - y_j$.

Then, taking variations of the triad vectors, we have

$$\delta\boldsymbol{e}_x = \left(\frac{\boldsymbol{I}_3}{\left\|\boldsymbol{e}_{31} - \boldsymbol{e}_{42}\right\|} - \frac{\left(\boldsymbol{e}_{31} - \boldsymbol{e}_{42}\right) \otimes \left(\boldsymbol{e}_{31} - \boldsymbol{e}_{42}\right)^T}{\left\|\boldsymbol{e}_{31} - \boldsymbol{e}_{42}\right\|^3} \right) \left(\delta\boldsymbol{e}_{31} - \delta\boldsymbol{e}_{42}\right) \tag{6.62a}$$

$$\delta\boldsymbol{e}_y = \left(\frac{\boldsymbol{I}_3}{\left\|\boldsymbol{e}_{31} + \boldsymbol{e}_{42}\right\|} - \frac{\left(\boldsymbol{e}_{31} + \boldsymbol{e}_{42}\right) \otimes \left(\boldsymbol{e}_{31} + \boldsymbol{e}_{42}\right)^T}{\left\|\boldsymbol{e}_{31} + \boldsymbol{e}_{42}\right\|^3} \right) \left(\delta\boldsymbol{e}_{31} + \delta\boldsymbol{e}_{42}\right) \tag{6.62b}$$

$$\delta\boldsymbol{e}_z = \delta\boldsymbol{e}_x \times \boldsymbol{e}_y + \boldsymbol{e}_x \times \delta\boldsymbol{e}_y \tag{6.62c}$$

in which $\otimes$ denotes Kronecker product, $\boldsymbol{e}_{31} = \dfrac{\boldsymbol{x}_3 - \boldsymbol{x}_1}{\left\|\boldsymbol{x}_3 - \boldsymbol{x}_1\right\|}$ and $\boldsymbol{e}_{42} = \dfrac{\boldsymbol{x}_4 - \boldsymbol{x}_2}{\left\|\boldsymbol{x}_4 - \boldsymbol{x}_2\right\|}$.

Besides, we have

$$\delta \boldsymbol{e}_{31} = \left(\frac{\boldsymbol{I}_3}{\|\boldsymbol{x}_3 - \boldsymbol{x}_1\|} - \frac{(\boldsymbol{x}_3 - \boldsymbol{x}_1) \otimes (\boldsymbol{x}_3 - \boldsymbol{x}_1)^T}{\|\boldsymbol{x}_3 - \boldsymbol{x}_1\|^3} \right) (\delta \boldsymbol{x}_3 - \delta \boldsymbol{x}_1) \tag{6.63a}$$

$$\delta \boldsymbol{e}_{42} = \left(\frac{\boldsymbol{I}_3}{\|\boldsymbol{x}_4 - \boldsymbol{x}_2\|} - \frac{(\boldsymbol{x}_4 - \boldsymbol{x}_2) \otimes (\boldsymbol{x}_4 - \boldsymbol{x}_2)^T}{\|\boldsymbol{x}_4 - \boldsymbol{x}_2\|^3} \right) (\delta \boldsymbol{x}_4 - \delta \boldsymbol{x}_2) \tag{6.63b}$$

$$\delta \boldsymbol{x}_3 - \delta \boldsymbol{x}_1 = \delta \boldsymbol{u}_3 - \delta \boldsymbol{u}_1 \tag{6.63c}$$

$$\delta \boldsymbol{x}_4 - \delta \boldsymbol{x}_2 = \delta \boldsymbol{u}_4 - \delta \boldsymbol{u}_2 \tag{6.63d}$$

Finally, the variations of triad vectors can be given by

$$\delta \boldsymbol{e}_x = \left\{ 0 \;\; \frac{x_{42}(a\delta\tilde{v}_{42} - b\delta\tilde{v}_{31}) - y_{42}(b\delta\tilde{u}_{31} + a\delta\tilde{u}_{42})}{2ab^2} \;\; \frac{a\delta\tilde{w}_{42} - b\delta\tilde{w}_{31}}{2ax_{42}} \right\} \tag{6.64a}$$

$$\delta \tilde{\boldsymbol{e}}_y = \left\{ \frac{y_{42}(b\delta\tilde{u}_{31} + a\delta\tilde{u}_{42}) - x_{42}(a\delta\tilde{v}_{42} - b\delta\tilde{v}_{31})}{2ab^2} \;\; 0 \;\; \frac{b\delta\tilde{w}_{31} + a\delta\tilde{w}_{42}}{2ay_{42}} \right\} \tag{6.64b}$$

$$\delta \tilde{\boldsymbol{e}}_z = \left\{ \frac{b\delta\tilde{w}_{31} - a\delta\tilde{w}_{42}}{2ax_{42}} \;\; -\frac{b\delta\tilde{w}_{31} + a\delta\tilde{w}_{42}}{2ay_{42}} \;\; 0 \right\} \tag{6.64c}$$

With the help of the following relationship

$$\begin{bmatrix} \delta \boldsymbol{e}_x \\ \delta \boldsymbol{e}_y \\ \delta \boldsymbol{e}_z \end{bmatrix} = \begin{bmatrix} 0 & \delta\omega_z & -\delta\omega_y \\ -\delta\omega_z & 0 & \delta\omega_x \\ \delta\omega_y & -\delta\omega_x & 0 \end{bmatrix} \tag{6.65}$$

the variations of local rigid body rotations are

$$\delta\boldsymbol{\omega}=\begin{Bmatrix}\delta\omega_x\\ \delta\omega_y\\ \delta\omega_z\end{Bmatrix}=\begin{Bmatrix}\dfrac{b\delta w_{31}+a\delta w_{42}}{2ay_{42}}\\ \dfrac{b\delta w_{31}-a\delta w_{42}}{2ax_{42}}\\ \dfrac{-y_{42}\left(b\delta u_{31}+a\delta u_{42}\right)+x_{42}\left(a\delta v_{42}-b\delta v_{31}\right)}{2ab^2}\end{Bmatrix} \tag{6.66}$$

Substituting Eq. (6.66) into Eq. (6.57c), the detailed expression of the matrix $\boldsymbol{G}$ can be given as follows,

$$\boldsymbol{G}=\begin{bmatrix}\boldsymbol{G}_1 & \mathbf{0}_3 & \boldsymbol{G}_2 & \mathbf{0}_3 & \boldsymbol{G}_3 & \mathbf{0}_3 & \boldsymbol{G}_4 & \mathbf{0}_3\end{bmatrix} \tag{6.67a}$$

$$\boldsymbol{G}_1=\begin{bmatrix}0 & 0 & -\dfrac{b}{2ay_{42}}\\ 0 & 0 & -\dfrac{b}{2ax_{42}}\\ \dfrac{y_{42}}{2ab} & \dfrac{x_{42}}{2ab} & 0\end{bmatrix} \tag{6.67b}$$

$$\boldsymbol{G}_2=\begin{bmatrix}0 & 0 & -\dfrac{1}{2y_{42}}\\ 0 & 0 & \dfrac{1}{2x_{42}}\\ \dfrac{y_{42}}{2b^2} & -\dfrac{x_{42}}{2b^2} & 0\end{bmatrix} \tag{6.67c}$$

$$\boldsymbol{G}_3=-\boldsymbol{G}_1 \tag{6.67d}$$

$$\boldsymbol{G}_4=-\boldsymbol{G}_2 \tag{6.67e}$$

6.4.4.3 Geometric stiffness matrix due to warping

As introduced in Chapter 4, the variations of plate moments at the node *i* due to warping can be given by

$$\delta m_{xi}=\delta u_{zi}\, f_{yi} \quad (i=1,2,3,4) \tag{6.68a}$$

$$\delta m_{yi}=-\delta u_{zi}\, f_{xi} \quad (i=1,2,3,4) \tag{6.68b}$$

in which δu_{zi} is the variation of pure displacement along the local *z*-axis at the node *i*.

Based on the local coordinate system, the local *z*-coordinate at the node *i* can be given by

$$z_i = \boldsymbol{e}_z^{\,T}\left(\boldsymbol{x}_i - \boldsymbol{x}_c\right) \quad (i=1,2,3,4) \tag{6.69}$$

in which $\boldsymbol{e}_z = \{0\ 0\ 1\}^T$ and $\boldsymbol{x}_c = \{0\ 0\ 0\}^T$, following the assumption that the local-to-global transformation matrix is the Identity matrix.

Taking a variation of Eq. (6.69) gives

$$\begin{aligned}\delta u_{zi} &= \delta\boldsymbol{e}_z^{\,T}\left(\boldsymbol{x}_i - \boldsymbol{x}_c\right) + \boldsymbol{e}_z^{\,T}\left(\delta\boldsymbol{u}_i - \delta\boldsymbol{u}_c\right) \\ &= \delta\omega_y x_i - \delta\omega_x y_i + \delta u_{zi} - \frac{1}{4}\left(\delta u_{z1} + \delta u_{z2} + \delta u_{z3} + \delta u_{z4}\right)\end{aligned} \tag{6.70}$$

Substituting Eqs. (6.66) and (6.70) into (6.68), the local geometric stiffness matrix due to warping effect, $\boldsymbol{K}_{gw}$, can be given by

$$\boldsymbol{K}_{gw} = \frac{\partial \boldsymbol{f}}{\partial \boldsymbol{d}^T} \tag{6.71}$$

in which the non-zero entries of $\boldsymbol{K}_{gw}$ can be detailed as follows,

$$\boldsymbol{K}_{gw}\left(4;3,9,15,21\right) = f_{y1}\left\{-\frac{bp_1}{2a}+\frac{3}{4}, \frac{q_1}{2}-\frac{1}{4}, \frac{bp_1}{2a}-\frac{1}{4}, -\frac{q_1}{2}-\frac{1}{4}\right\} \tag{6.72a}$$

$$\boldsymbol{K}_{gw}(5;3,9,15,21) = -f_{x1}\left\{-\frac{bp_1}{2a}+\frac{3}{4},\frac{q_1}{2}-\frac{1}{4},\frac{bp_1}{2a}-\frac{1}{4},-\frac{q_1}{2}-\frac{1}{4}\right\} \tag{6.72b}$$

$$\boldsymbol{K}_{gw}(10;3,9,15,21) = f_{y2}\left\{-\frac{bp_2}{2a}-\frac{1}{4},\frac{q_2}{2}+\frac{3}{4},\frac{bp_2}{2a}-\frac{1}{4},-\frac{q_2}{2}-\frac{1}{4}\right\} \tag{6.72c}$$

$$\boldsymbol{K}_{gw}(11;3,9,15,21) = -f_{x2}\left\{-\frac{bp_2}{2a}-\frac{1}{4},\frac{q_2}{2}+\frac{3}{4},\frac{bp_2}{2a}-\frac{1}{4},-\frac{q_2}{2}-\frac{1}{4}\right\} \tag{6.72d}$$

$$\boldsymbol{K}_{gw}(16;3,9,15,21) = f_{y3}\left\{-\frac{bp_3}{2a}-\frac{1}{4},\frac{q_3}{2}-\frac{1}{4},\frac{bp_3}{2a}+\frac{3}{4},-\frac{q_3}{2}-\frac{1}{4}\right\} \tag{6.72e}$$

$$\boldsymbol{K}_{gw}(17;3,9,15,21) = -f_{x3}\left\{-\frac{bp_3}{2a}-\frac{1}{4},\frac{q_3}{2}-\frac{1}{4},\frac{bp_3}{2a}+\frac{3}{4},-\frac{q_3}{2}-\frac{1}{4}\right\} \tag{6.72f}$$

$$\boldsymbol{K}_{gw}(22;3,9,15,21) = f_{y4}\left\{-\frac{bp_4}{2a}-\frac{1}{4},\frac{q_4}{2}-\frac{1}{4},\frac{bp_4}{2a}-\frac{1}{4},-\frac{q_4}{2}+\frac{3}{4}\right\} \tag{6.72g}$$

$$\boldsymbol{K}_{gw}(23;3,9,15,21) = -f_{x4}\left\{-\frac{bp_4}{2a}-\frac{1}{4},\frac{q_4}{2}-\frac{1}{4},\frac{bp_4}{2a}-\frac{1}{4},-\frac{q_4}{2}+\frac{3}{4}\right\} \tag{6.72h}$$

$$p_i = \frac{x_i}{x_{42}} - \frac{y_i}{y_{42}},\quad q_i = \frac{x_i}{x_{42}} + \frac{y_i}{y_{42}} \tag{6.72i}$$

6.4.4.4 Symmetrized geometric stiffness

Like the simplified co-rotational formulation for triangular shell elements, the local geometric stiffness matrix for quadrilateral shell elements is also unsymmetrical and cannot be calculated in conventional solver. Thus, the local tangent stiffness should be modified as

$$\boldsymbol{K}_g = \boldsymbol{K}_{gr} + \boldsymbol{K}_{gw} \tag{6.73a}$$

$$\boldsymbol{K}_g^{sym} = \frac{1}{2}\left(\boldsymbol{K}_g + \boldsymbol{K}_g{}^T\right) \tag{6.73b}$$

$$\boldsymbol{K}_t = \boldsymbol{K}_e + \boldsymbol{K}_g^{sym} \tag{6.73c}$$

Then, the global stiffness matrix is

$$\boldsymbol{K}_t^g = \boldsymbol{T}^T \boldsymbol{K}_t \boldsymbol{T} \tag{6.74}$$

Nour-Omid and Rankin (1991) proved that the unsymmetrical term becomes zero when computations are converged, which is a sufficient condition for a quadratic rate of convergence in a Newton-Raphson type iteration.

6.4.2 Computational procedure

The simplified EICR formulation is coded into the program NIDA, and the procedure is similar to the nonlinear triangular shell element introduced in Chapter 5. However, the warping effect for the quadrilateral shell element should be noted and the pure deformational method is not used here, since the bisector definition of the local coordinate system is adopted to overcome the nodal ordering dependency. Also, the quadrilateral shell does not have the basic coordinate system, but the system is replaced by the projection of the shell element. Taking the New-Raphson solution for example, the procedure is summarized in the following.

1. Define and initialize the global variables and parameters.

   - *Ninc* = the total number of load increments

- *Nite* = the maximum iteration number
- n = the n^{th} load step
- i = the i^{th} iteration
- $\mathbf{K}^i$ = the assembled global tangent stiffness matrix at the i^{th} iteration
- $\mathbf{P}^n$ = the externally applied global nodal force vector at the n^{th} load step
- $\mathbf{F}^i$ = the global internal forces for the whole structure at the i^{th} iteration
- $\mathbf{U}$ = the global nodal displacements for the whole structure

2. Define and compute the local variables and parameters for each shell element.

   (a) Compute the local-to-global transformation matrix $\boldsymbol{T}_e$.

   (b) Compute the initial local node coordinates.

   (c) Compute the stiffness matrices of the membrane and plate elements in the projection with the initial local node coordinates, assemble them into the stiffness matrix for the projection of the shell element, $\bar{\boldsymbol{K}}_e^0$, and store it.

   (d) Initialize the local internal forces $\bar{\boldsymbol{f}}$ for the projection of the shell element.

3. Start loop over load increments (for n=1 to *Ninc*).

   (a) Update external load $\mathbf{P}^n = \mathbf{P}^{n-1} + \Delta\mathbf{P}$.

   (b) Set residual forces $\mathbf{g}^i = \mathbf{P}^n$.

   (c) Start iterations beginning with i=1 (while divergence and $i \le$ *Nite*).

i. For each shell element, get the global tangent stiffness matrix by $\boldsymbol{K}_t^g = \boldsymbol{T}^T(\boldsymbol{E}^T\overline{\boldsymbol{K}}_e^0\boldsymbol{E} + \boldsymbol{K}_g^{sym})\boldsymbol{T}$.

ii. Assemble the global tangent stiffness matrix for the whole structure $\mathbf{K}^i$.

iii. Solve for the incremental global nodal displacements $\Delta\mathbf{U} = (\mathbf{K}^i)^{-1}\mathbf{g}^i$.

iv. Update geometry.

v. For each warping shell element, extract incremental local deformations $\Delta\boldsymbol{d}$ from $\Delta\mathbf{U}$, transform it into the projection and get $\Delta\overline{\boldsymbol{d}}$, compute the incremental local internal forces for the projection by $\Delta\overline{\boldsymbol{f}} = \overline{\boldsymbol{K}}_e^0\Delta\overline{\boldsymbol{d}}$, update and store $\overline{\boldsymbol{f}}^i = \overline{\boldsymbol{f}}^{i-1} + \Delta\boldsymbol{f}$.

vi. For each shell element, compute the global internal force vector by $\boldsymbol{f}^{gi} = \boldsymbol{T}^{iT}\boldsymbol{E}^{iT}\overline{\boldsymbol{f}}^i$, and assemble it into $\mathbf{F}^i$.

vii. Compute residual forces $\mathbf{g}^i = \mathbf{P}^n - \mathbf{F}^i$.

viii. Terminate iterative process if converged, otherwise go to next iteration.

4. Terminate whole analysis process.

For the other technologies to solve finite element equations, such as the displacement-control and arch length methods, the processes to formulate the tangent stiffness matrix and the internal force vector are identical.

6.5 Geometrically nonlinear elastoplastic analysis

In this section, the proposed simplified co-rotational method for quadrilateral shell elements is extended into the geometrically nonlinear elastoplastic analysis. The procedure is similar to the nonlinear triangular shell element introduced in Chapter 5. Specifically, they both adopt the simplified co-rotational method to conduct geometrically nonlinear analysis, while the material nonlinearity is taken into account in the local material stiffness matrix. Following Chapter 5, the material nonlinear analysis adopts the layered approach, elastoplastic constitutive model based on the von Mises yield criterion, the associated flow rule and linear isotropic hardening, while a backward-Euler return-mapping integration algorithm is used to trace the yield surface. Also, to avoid the "spurious unloading" during analysis, the incremental displacements accumulated from the beginning of a load step is used, which is different from the analysis scheme with only geometrical nonlinearity introduced in Section 6.4. In addition, transverse shear deformation of the plate element is considered and assumed to be elastic.

However, several issues different from the nonlinear triangular shell element should be noted. First, the nonlinear quadrilateral shell element does not use the pure deformational method, since the bisector definition of the local coordinate system is used to overcome the nodal ordering dependency. Second, the quadrilateral membrane element adopts the mixed variational formulation, in which the linear stiffness has two parts, one is due to the strains and the other one is due to the skew-symmetric stresses, as introduced in Section 6.1. In the elastoplastic analysis, it is assumed that the stiffness due to the skew-symmetric stresses keeps elastic during the whole nonlinear analysis procedure. Third, the warping phenomenon exists in the

quadrilateral shell element. In the elastic analysis, the linear stiffness of the quadrilateral shell element is computed based on the projection and transformed into the warping shell element, so the strains and stresses at the projection rather than the warping shell element are obtainable and the elastoplasticity is considered in the projection. Although the operation is different from realistic situation, the numerical examples in Chapter 7 show that the results obtained by the quadrilateral shell element are very close to the proposed triangular shell element.

6.5.1 Tangent stiffness

Identical to the geometrically nonlinear elastoplastic analysis scheme for the triangular shell element in Chapter 5, the projection of the warping quadrilateral shell element is divided into *m* layers with equal thickness, as shown in Figure 5.9.

The strains at the midpoint of the j^{th} layer in the projection represent the whole layer as

$$\boldsymbol{\varepsilon}_j = \begin{Bmatrix} \varepsilon_x \\ \varepsilon_y \\ \varepsilon_{xy} \end{Bmatrix} + z_j \begin{Bmatrix} \kappa_x \\ \kappa_y \\ \kappa_{xy} \end{Bmatrix} = \boldsymbol{B}_m \bar{\boldsymbol{d}}_m + z_j \boldsymbol{B}_b \bar{\boldsymbol{d}}_p \tag{6.75a}$$

$$z_j = \frac{t}{2m}(2j-1) - \frac{t}{2}, j=1 \text{ to } m \tag{6.75b}$$

in which $\boldsymbol{B}_m$ and $\boldsymbol{B}_b$ have been introduced previously and are the strain-displacement matrix for the membrane element and the plate element corresponding to the projection, respectively. They are both computed by the initial

dimensions of the shell element during the whole nonlinear analysis procedure. Also, the displacement vectors $\bar{\boldsymbol{d}}_m$ and $\bar{\boldsymbol{d}}_p$ belong to the membrane and plate elements corresponding to the projection, respectively.

Then, the stresses at the j^{th} layer are

$$\boldsymbol{\sigma}_j = \mathbf{C}_j \boldsymbol{\varepsilon}_j = \mathbf{C}_j \boldsymbol{B}_m \bar{\boldsymbol{d}}_m + z_j \mathbf{C}_j \boldsymbol{B}_b \bar{\boldsymbol{d}}_p \tag{6.76}$$

in which $\mathbf{C}_j$ is the tangential modular matrix for the j^{th} layer shown in Eq. (5.80) under plasticity and the elastic modular matrix shown in Eq. (5.77) under elasticity.

The virtual work due to membrane and bending strains for the projection of the shell element can be expressed as

$$\begin{aligned}
\delta W &= \int_A \sum_{j=1}^{m} \boldsymbol{\sigma}_j^T \delta \boldsymbol{\varepsilon}_j \Delta t dA - \boldsymbol{f}_{ext}^T \delta \bar{\boldsymbol{d}} \\
&= \int_A \sum_{j=1}^{m} (\mathbf{C}_j \boldsymbol{B}_m \bar{\boldsymbol{d}}_m + z_j \mathbf{C}_j \boldsymbol{B}_b \bar{\boldsymbol{d}}_p)^T (\boldsymbol{B}_m \delta \bar{\boldsymbol{d}}_m + z_j \boldsymbol{B}_b \delta \bar{\boldsymbol{d}}_p) \Delta t dA \\
&= \int_A \sum_{j=1}^{m} \begin{pmatrix} \bar{\boldsymbol{d}}_m^T \boldsymbol{B}_m^T \mathbf{C}_j \boldsymbol{B}_m \delta \bar{\boldsymbol{d}}_m + z_j \bar{\boldsymbol{d}}_p^T \boldsymbol{B}_b^T \mathbf{C}_j \boldsymbol{B}_m \delta \bar{\boldsymbol{d}}_m \\ + z_j \bar{\boldsymbol{d}}_m^T \boldsymbol{B}_m^T \mathbf{C}_j \boldsymbol{B}_b \delta \bar{\boldsymbol{d}}_p + z_j^2 \bar{\boldsymbol{d}}_p^T \boldsymbol{B}_b^T \mathbf{C}_j \boldsymbol{B}_b \delta \bar{\boldsymbol{d}}_p \end{pmatrix} \Delta t dA - \boldsymbol{f}_{ext}^T \delta \bar{\boldsymbol{d}}
\end{aligned} \tag{6.77}$$

where $\boldsymbol{f}_{ext}$ is the external forces and $\Delta t = \dfrac{t}{m}$ is the layer thickness.

Then, the local material stiffness matrix due to membrane and bending strains can be given by

$$\bar{\boldsymbol{K}}_e = \begin{bmatrix} \bar{\boldsymbol{K}}_1 & \bar{\boldsymbol{K}}_2 \\ \bar{\boldsymbol{K}}_3 & \bar{\boldsymbol{K}}_4 \end{bmatrix} \tag{6.78a}$$

$$\bar{\boldsymbol{K}}_1 = \int_A \boldsymbol{B}_m^T \left(\sum_{j=1}^{m} \mathbf{C}_j \Delta t \right) \boldsymbol{B}_m dA \tag{6.78b}$$

$$\bar{\boldsymbol{K}}_2 = \int_A \boldsymbol{B}_m^T \left(\sum_{j=1}^{m} z_j \Delta t \mathbf{C}_j \right) \boldsymbol{B}_b dA \tag{6.78c}$$

$$\bar{\boldsymbol{K}}_3 = \int_A \boldsymbol{B}_b^T \left(\sum_{j=1}^{m} z_j \Delta t \mathbf{C}_j \right) \boldsymbol{B}_m dA \tag{6.78d}$$

$$\bar{\boldsymbol{K}}_4 = \int_A \boldsymbol{B}_b^T \left(\sum_{j=1}^{m} z_j^2 \Delta t \mathbf{C}_j \right) \boldsymbol{B}_b dA \tag{6.78e}$$

in which the matrix $\bar{\boldsymbol{K}}_e$ is the material stiffness based on the projection of the shell element. Note that it is corresponding to the displacement vector of the projection $\left\{ \bar{\boldsymbol{d}}_m{}^T \ \ \bar{\boldsymbol{d}}_p{}^T \right\}^T$. In the program, these four submatrices should be assembled into the matrix responding to the displacement vector $\bar{\boldsymbol{d}}$.

In addition, due to the mixed variational formulation for the membrane element, $\bar{\boldsymbol{K}}_1$ should be modified as

$$\bar{\boldsymbol{K}}_1 = \int_A \boldsymbol{B}_m^T \left(\sum_{j=1}^{m} \mathbf{C}_j \Delta t \right) \boldsymbol{B}_m dA + \bar{\boldsymbol{K}}_{mh} \tag{6.79}$$

in which the matrix $\bar{\boldsymbol{K}}_{mh}$ can be found in Eqs. (6.12).

When the shear deformation is considered, $\bar{\boldsymbol{K}}_4$ should be modified as

$$\bar{\boldsymbol{K}}_4 = \int_A \boldsymbol{B}_b^T \left(\sum_{j=1}^{m} z_j^2 \Delta t \mathbf{C}_j \right) \boldsymbol{B}_b dA + \bar{\boldsymbol{K}}_s \tag{6.80a}$$

$$\bar{\boldsymbol{K}}_s = \int_A \boldsymbol{B}_s^T \boldsymbol{D}_s \boldsymbol{B}_s dA \tag{6.80b}$$

in which $\bar{\boldsymbol{K}}_s$ is the shear stiffness matrix introduced in Section 6.2.

All of these stiffness matrices adopt the two dimensional 8-point integration rule. After integration, the material stiffness matrix for the projection should be transformed into the warping shell element as

$$\boldsymbol{K}_m = \boldsymbol{E}^T \bar{\boldsymbol{K}}_m \boldsymbol{E} \tag{6.81}$$

where the matrix $\boldsymbol{E}$ is the eccentricity matrix introduced in the last section and should be formulated by the current local *z*-coordinates.

Finally, the tangent stiffness matrix in the global coordinate system can be given by

$$\boldsymbol{K}_t^g = \boldsymbol{T}^T (\boldsymbol{K}_m + \boldsymbol{K}_g^{sym}) \boldsymbol{T} \tag{6.82}$$

in which the symmetrized local geometric stiffness matrix $\boldsymbol{K}_g^{sym}$ has been given in the last section.

6.5.2 Internal forces

To avoiding the “spurious unloading”, the incremental displacements, accumulated from the first iteration to the current iteration in a load step, is used to update the internal forces.

Assuming the incremental local displacements of the membrane and plate elements (the projection of the shell element) are $\Delta\bar{\boldsymbol{d}}_m$ and $\Delta\bar{\boldsymbol{d}}_p$, the incremental strains of the j^{th} layer at the integration point k can be given by

$$\Delta\boldsymbol{\varepsilon}_{j,k} = \boldsymbol{B}_m\Delta\bar{\boldsymbol{d}}_m + z_j\boldsymbol{B}_b\Delta\bar{\boldsymbol{d}}_p \text{ , } j\text{=1 to } m, \; k\text{=1 to 8} \tag{6.83}$$

Then, the trial stresses are

$$\boldsymbol{\sigma}^{tr}_{j,k} = \boldsymbol{\sigma}^{n}_{j,k} + \mathbf{C}\Delta\boldsymbol{\varepsilon}_{j,k} \tag{6.84}$$

in which $\boldsymbol{\sigma}^{n}_{j,k}$ is the stresses determined at the last load step, $\mathbf{C}$ is the elastic modular matrix.

The two-step predictor-corrector return mapping algorithm introduced in Section 5.4.1 is used to determine the real stresses $\boldsymbol{\sigma}_{j,k}$. Then, the internal forces of the projection can be obtained by

$$\bar{\boldsymbol{f}}_m^{\,n+1} = \sum_{k=1}^{8}\boldsymbol{B}_m^{\,T}\left(\sum_{j=1}^{m}\boldsymbol{\sigma}_{j,k}\Delta t\right)w_k A + \bar{\boldsymbol{K}}_{mh}\bar{\boldsymbol{d}}_m \tag{6.85a}$$

$$\bar{\boldsymbol{f}}_p^{\,n+1} = \sum_{k=1}^{3}\boldsymbol{B}_b^{\,T}\left(\sum_{j=1}^{m}z_j\boldsymbol{\sigma}_{j,k}\Delta t\right)w_k A \quad \text{(without shear deformation)} \tag{6.85b}$$

$$\bar{\boldsymbol{f}}_p^{\,n+1} = \sum_{k=1}^{3}\boldsymbol{B}_b^{\,T}\left(\sum_{j=1}^{m}z_j\boldsymbol{\sigma}_{j,k}\Delta t\right)w_k A + \bar{\boldsymbol{K}}_s\bar{\boldsymbol{d}}_p \quad \text{(with shear deformation)} \tag{6.85c}$$

where the displacement vectors $\bar{\boldsymbol{d}}_m$ and $\bar{\boldsymbol{d}}_p$ are accumulated from the beginning of the nonlinear analysis procedure.

After assembling $\bar{\boldsymbol{f}}_m^{n+1}$ and $\bar{\boldsymbol{f}}_p^{n+1}$ into $\bar{\boldsymbol{f}}^{n+1}$, the global internal force vector can be given by

$$\boldsymbol{f}^{gn+1} = \boldsymbol{T}^{n+1T} \boldsymbol{E}^{n+1T} \bar{\boldsymbol{f}}^{n+1} \tag{6.86}$$

in which the transformation matrix $\boldsymbol{T}^{n+1}$ and the eccentricity matrix $\boldsymbol{E}^{n+1}$ should be updated based on the current geometry.

6.5.3 Computational procedure

The computational procedure for the quadrilateral shell element in geometrically nonlinear elastoplastic analysis has been implemented in the program NIDA. The procedure based on the New-Raphson solution is detailed in the following.

1. Define and initialize the global variables and parameters.

   - *Ninc* = the total number of load increments
   - *Nite* = the maximum iteration number
   - *m* = the number of layers for a shell element
   - *n* = the n^{th} load step
   - *i* = the i^{th} iteration
   - *j* = the j^{th} layer of a shell element
   - *k* = the k^{th} integration point
   - $\mathbf{K}^i$ = the assembled global tangent stiffness matrix at the i^{th} iteration

- $\mathbf{P}^n$ = the externally applied global nodal force vector at the n^{th} load step
- $\mathbf{F}^i$ = the global internal forces at for the whole structure at the i^{th} iteration
- $\mathbf{U}$ = the global nodal displacements for the whole structure

2. Define and compute the local variables and parameters for each layered shell element.

   (a) Compute the local-to-global transformation matrix $\boldsymbol{T}_e$.

   (b) Compute the initial local node coordinates.

   (c) Initialize the stresses $\boldsymbol{\sigma}_{j,k}$ and the elastic modular matrix $\mathbf{C}_{j,k}$ at the j^{th} layer and the integration point k.

3. Start loop over load increments (for n=1 to *Ninc*).

   (a) Update external load $\mathbf{P}^n = \mathbf{P}^{n-1} + \Delta\mathbf{P}$.

   (b) Set residual forces $\mathbf{g}^j = \mathbf{P}^n$.

   (c) Start iterations beginning with i=1 (while divergence and $i \leq Nite$).

      i. For each shell element, get the tangent stiffness through $\boldsymbol{K}_t^g = \boldsymbol{T}^T(\boldsymbol{K}_m + \boldsymbol{K}_g^{sym})\boldsymbol{T}$.

      ii. Assemble the global tangent stiffness matrix for the whole structure $\mathbf{K}^i$.

      iii. Solve for the incremental global nodal displacements $\Delta\mathbf{U} = (\mathbf{K}^i)^{-1}\mathbf{g}^i$.

      iv. Update geometry.

v. For each shell element, compute the iterative deformation of projection $\Delta\bar{\boldsymbol{d}}_m^i$ and $\Delta\bar{\boldsymbol{d}}_p^i$ from $\Delta\mathbf{U}$, and add them to the incremental deformation accumulated from the first iteration as $\Delta\bar{\boldsymbol{d}}_m^n = \Delta\bar{\boldsymbol{d}}_m^{i-1} + \Delta\bar{\boldsymbol{d}}_m^i$, $\Delta\bar{\boldsymbol{d}}_p^n = \Delta\bar{\boldsymbol{d}}_p^{i-1} + \Delta\bar{\boldsymbol{d}}_p^i$.

vi. For the j^{th} layer at the integration point k, compute the incremental strains $\Delta\boldsymbol{\varepsilon}_{j,k} = \boldsymbol{B}_m\Delta\bar{\boldsymbol{d}}_m^n + z_j\boldsymbol{B}_b\Delta\bar{\boldsymbol{d}}_p^n$ and then the trial stresses $\boldsymbol{\sigma}_{j,k}^{tr} = \boldsymbol{\sigma}_{j,k}^n + \mathrm{C}\Delta\boldsymbol{\varepsilon}_{j,k}$.

vii. Determine the real stresses $\boldsymbol{\sigma}_{j,k}$ with the two-step predictor-corrector return mapping algorithm. If the point yields, $\mathbf{C}_{j,k}$ uses the tangential modular matrix; otherwise, uses the elastic modular matrix for the next iteration.

viii. For each shell element, compute the internal forces of projection $\bar{\boldsymbol{f}}_m$ and $\bar{\boldsymbol{f}}_p$, and then assemble them into $\bar{\boldsymbol{f}}^i$.

ix. For each shell element, compute the global internal force vector by $\boldsymbol{f}^{gi} = \boldsymbol{T}^{i\,T}\boldsymbol{E}^{i\,T}\bar{\boldsymbol{f}}^i$, and assemble it into $\mathbf{F}^i$.

x. Compute residual forces $\mathbf{g}^i = \mathbf{P}^n - \mathbf{F}^i$.

xi. Terminate iterative process if converged, otherwise go to next iteration.

4. Terminate whole analysis process.

6.6 Summary

In this chapter, the nonlinear quadrilateral shell element based on the simplified EICR formulation is proposed and coded into the program NIDA. Its performance will be verified in the numerical examples presented in Chapter 7.

From the previous chapters, it can be seen that the proposed simplified co-rotational formulation is simpler than the traditional co-rotational formulations. In this chapter, the co-rotational UL formulation is detailed and compared with the proposed simplified EICR formulation. Thus, the comparisons between the co-rotational UL and the proposed simplified EICR regarding their derivations and expressions are discussed in the following.

The proposed UL formulation is not like the traditional one but adopts the co-rotational concept, which is also proposed by author (Tang et al., 2016). However, its core is not changed. The Green-Lagrangian strains are used to describe the kinematics of a shell element and consider the geometrical nonlinearity. Then, it produces the geometric stiffness matrix formulated by the Cathy stresses with the adoption of numerical integration. Thus, the geometric stiffness matrix is related to the displacement interpolations. Even using same displacement interpolations, the geometric stiffness matrices with and without transverse shear deformation are different.

For the simplified EICR formulation for quadrilateral shell element, it focuses on the element frame. The geometric stiffness matrix is derived by the load perturbation of the equilibrium equations of a shell element, so it is formed by the nodal internal forces rather than stresses at the integration points, with explicit expression. Therefore,

the formulation is element-independent and any existing linear element can be extended into the geometrically nonlinear analysis. In addition, the geometric stiffness and the local material stiffness can be treated separately, no matter whether the local shell element considers transverse shear deformation or material nonlinearity.

In summary, the simplified EICR formulation is simpler and more efficient than the UL formulation, since the former has an explicit geometric stiffness matrix which does not need the numerical integration. However, the simplified EICR formulation has a drawback that the geometric stiffness matrix is not symmetric, like the general co-rotational method. In the program, the symmetric part of the stiffness is used to replace the unsymmetrical one, since finite element program usually uses a symmetric solver to save computer storage. Fortunately, the unsymmetrical part becomes zero when the system is in equilibrium and the symmetrized stiffness still can keep a quadratic rate of convergence. The differences regarding the accuracy and convergence between the unsymmetrical and symmetrized geometric stiffness are discussed in Chapter 7.

CHAPTER 7

VERIFICATION EXAMPLES

In this chapter, a batch of benchmark problems are solved with the proposed nonlinear triangular and quadrilateral shell elements coded in the program NIDA to verify their accuracy and efficiency. Sections 7.1 and 7.2 present the examples of geometrically nonlinear analysis and geometrically nonlinear elastoplastic analysis, respectively. To distinguish from the other shell elements in the existing literature and the commercial finite element packages, the proposed nonlinear shell elements in the program NIDA are named as SCRT3 and SCRQ4 for short, respectively, which means that they are the 3-node triangular and the 4-node quadrilateral shell elements respectively and consider geometrical nonlinearity based on the simplified EICR formulation.

In these examples, the convergence in iterations can be measured using the following criteria,

$$\mathrm{Norm}\left(\Delta\mathbf{U}\right) < TOLER \cdot \mathrm{Norm}\left(\mathbf{U}\right) \tag{7.1a}$$

$$\mathrm{Norm}\left(\Delta\mathbf{F}\right) < TOLER \cdot \mathrm{Norm}\left(\mathbf{F}\right) \tag{7.1b}$$

in which $\Delta\mathbf{U}$ and $\mathbf{U}$ are the incremental and total displacement vectors of the whole structure, respectively. Similarly, $\Delta\mathbf{F}$ is the residual force vector and $\mathbf{F}$ is the external load vector. For all the examples presented in the following, an iteration progress

terminates when the conditions in Eqs. (7.1) are met, and *TOLER* is taken as 0.001 in this thesis.

7.1 Geometrically nonlinear analysis of shell structures

The presented numerical examples of geometrically nonlinear analysis cover the problems of large displacements, large rotations, snap-through buckling, lateral torsional buckling, etc. The results obtained by the proposed shell elements are compared with those available in the existing literature and with those obtained using the SHELL181 element of the commercial finite element package ANSYS based on the same solution procedure and convergence criterion. SHELL181 is a four-node element with six degrees of freedom at each node and can degenerate into a triangular form, but the use of the triangular form is not recommended. Thus, only the quadrilateral form of the SHELL181 element is adopted in the following numerical examples, and the full integration method is used. Also, the SHELL181 element is suitable for analysing thin to moderately-thick shell structures and can be applied to linear, large rotation, and/or large strain nonlinear applications (ANSYS, 2017).

For the first three examples, the results obtained by the unsymmetrical geometric stiffness matrix and the symmetrized one are compared, and then the effects of the symmetrized geometric stiffness matrix on the accuracy and efficiency are discussed and evaluated. After that, the proposed shell elements only adopt the symmetrized geometric stiffness matrix for the following numerical examples unless otherwise stated.

7.1.1 Cantilever beam under an end moment

Figure 7.1 shows a cantilever beam subjected to a concentrated end moment *M*. This is a classical problem to examine the performance of an element undergoing large rotations. The geometric and material properties are given below.

Length L=10, width b=1, thickness t=0.1.

Young's modulus of elasticity E=1.2×10^6, Poisson's ratio v=0.

Based on the theoretical solution, the cantilever plate becomes a circular arc with radius *R* due to the applied moment *M*, and the analytical solution can be given in the following,

$$\frac{1}{R}=\frac{M}{EI} \tag{7.2}$$

When the cantilever plate rolls up into a complete circle, the applied end moment is

$$M_{\max}=2\pi\frac{EI}{L} \tag{7.3}$$

The analytical tip displacements along the horizontal and vertical directions can be expressed with the load factor $\lambda = M / M_{\max}$ as

$$u=L\left(\frac{\sin(2\pi\lambda)}{2\pi\lambda}-1\right) \quad (0<\lambda\le 1) \tag{7.4a}$$

$$w=L\left(\frac{1-\cos(2\pi\lambda)}{2\pi\lambda}\right) \quad (0<\lambda\le 1) \tag{7.4b}$$

$$u=w=0 \quad (\lambda=0) \tag{7.4c}$$

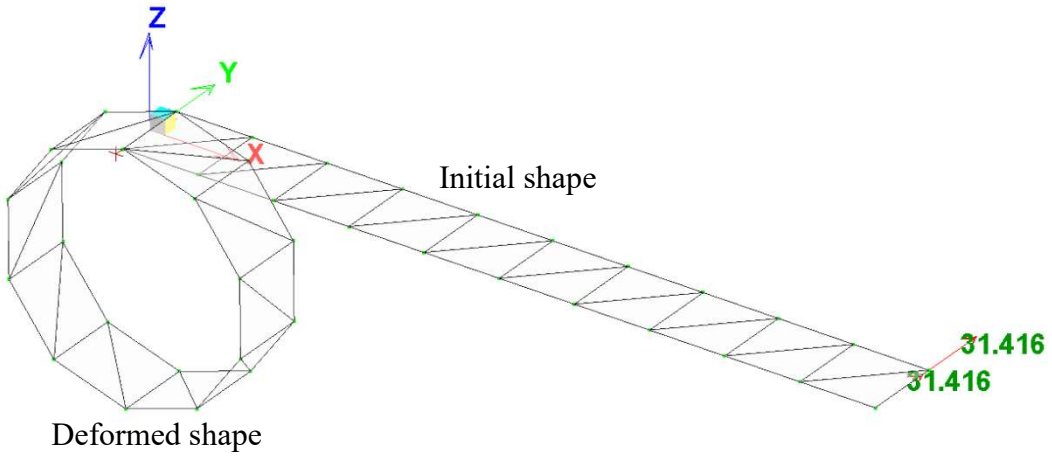

(a) SCRT3

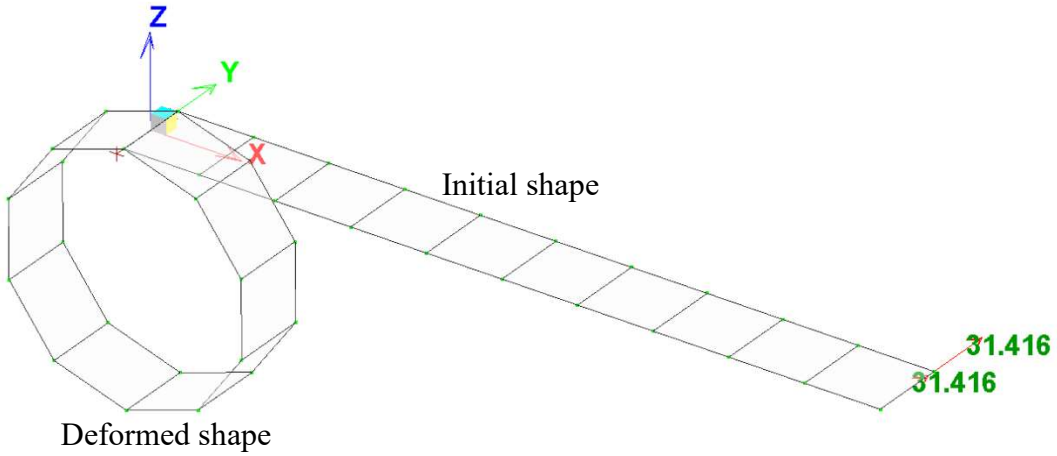

(b) SCRQ4

Figure 7.1 Cantilever beam subjected to an end moment

In this study, the cantilever plate is modelled with the SCRT3 and SCRQ4 elements respectively, using a 10×1 mesh as shown in Figure 7.1. The maximum end moment is divided into 5 equal load steps in the analysis. Figure 7.2 indicates that the load-displacement curves of this model meshed with the proposed shell elements using the unsymmetrical geometric stiffness matrices are very close to the exact solutions, even with such coarse meshes and only 5 load steps required.

Next, to study the influence of the symmetrized geometric stiffness on the accuracy and convergence rate, the detailed results and the numbers of iteration obtained by the proposed shell elements using the unsymmetrical and symmetrized geometric stiffness matrices are listed in Table 7.1 and Table 7.2, respectively.

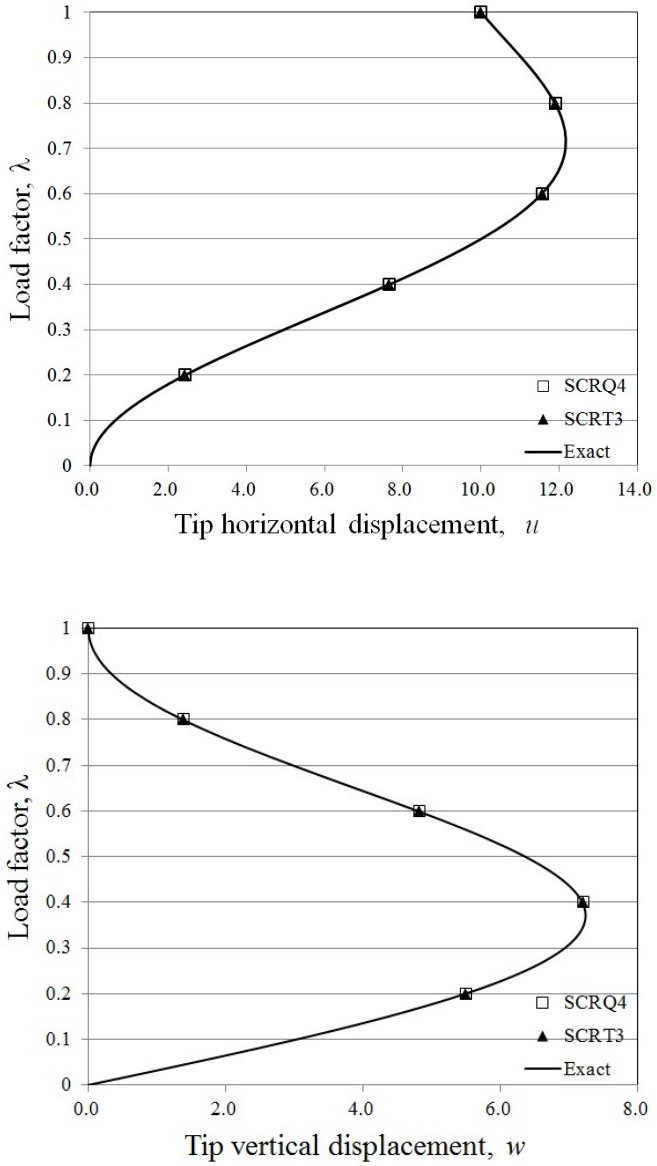

Figure 7.2 Load-displacement curves for cantilever beam subjected to an end moment

Table 7.1 Tip vertical displacements (w) obtained by different methods

λ	Exact	SCRT3 (uns.)	SCRT3 (sym.)	SCRQ4 (uns.)	SCRQ4 (sym.)
0.2	5.4987	5.5023	5.5067	5.5023	5.5024
0.4	7.1979	7.2168	7.2184	7.2168	7.2234
0.6	4.7986	4.8272	4.8158	4.8271	4.8360
0.8	1.3747	1.3894	-	1.3893	1.3978
1.0	0.0000	0.0001	-	0.0000	0.0023

Table 7.2 Numbers of iteration needed by different methods

λ	SCRT3 (uns.)	SCRT3 (sym.)	SCRQ4 (uns.)	SCRQ4 (sym.)
0.2	8	14	6	6
0.4	6	16	6	13
0.6	6	17	6	6
0.8	6	-	6	6
1.0	6	-	6	6
Total	32	-	30	37

Table 7.1 shows that the results from different methods are close to the exact solutions, so the symmetrized geometric stiffness has insignificant effects on the accuracy. In terms of the convergence rates as shown in Table 7.2, the proposed SCRQ4 elements using the unsymmetrical and the symmetrized geometric stiffness

matrices are close. However, the SCRT3 element using the symmetrized geometric stiffness matrix decreases the convergence rate in this example and cannot get convergence in the fourth and fifth steps. The whole analysis process can be completed when more load steps are used, although the convergence rate is always lower than the SCRT3 element using the unsymmetrical geometric stiffness matrix.

Thus, it is interesting to find that the symmetrized geometric stiffness has different performances for the triangular and quadrilateral shell elements. This may be because the triangular meshes for this example are not symmetrical and the proposed triangular shell element adopts the element side 1-2 as the local x-axis, which is not invariant to nodal ordering. In addition, it can be noted that this example is only subjected to a pure moment, so the symmetrized geometric stiffness matrix may produce unbalanced forces. Although the SCRT3 element using the symmetrized geometric stiffness matrix performs not well here, it is impossible to find a practical engineering structure like this example having so large rotations.

7.1.2 Cantilever beam subjected to a shear force

This model is the same as the one in Section 7.1.1, and the cantilever has the identical material properties, geometrical dimensions and meshes, except that Poisson's ratio is set to 0.3. In addition, a concentrated shear force is applied to the free end as shown in Figure 7.3. This is another classical benchmark example for checking the capability of an element undergoing large displacements and large rotations.

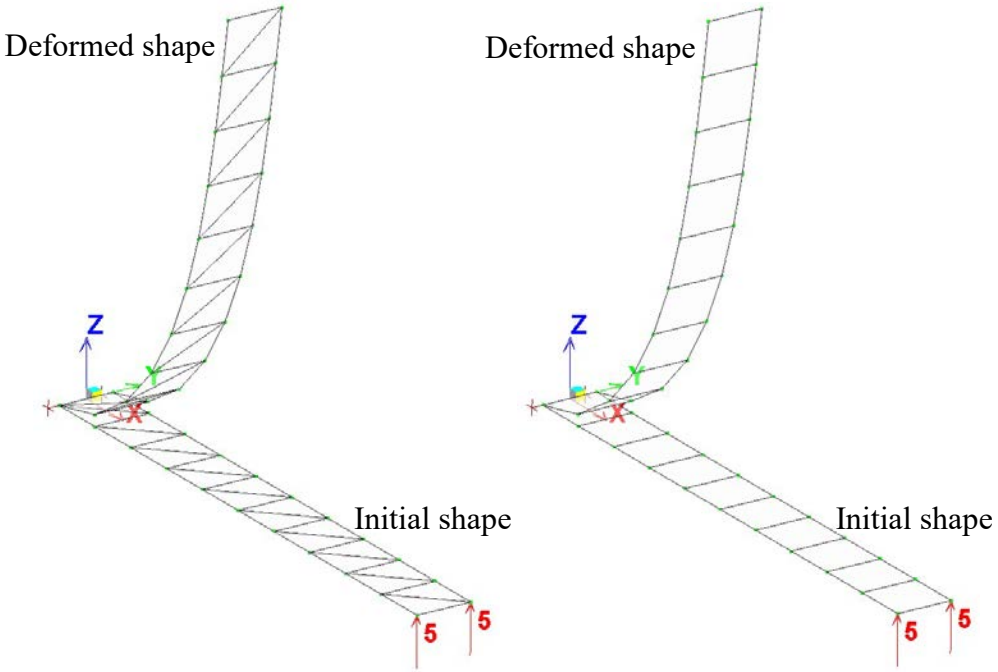

(a) SCRT3 (b) SCRQ4

Figure 7.3 Cantilever beam subjected to a shear force

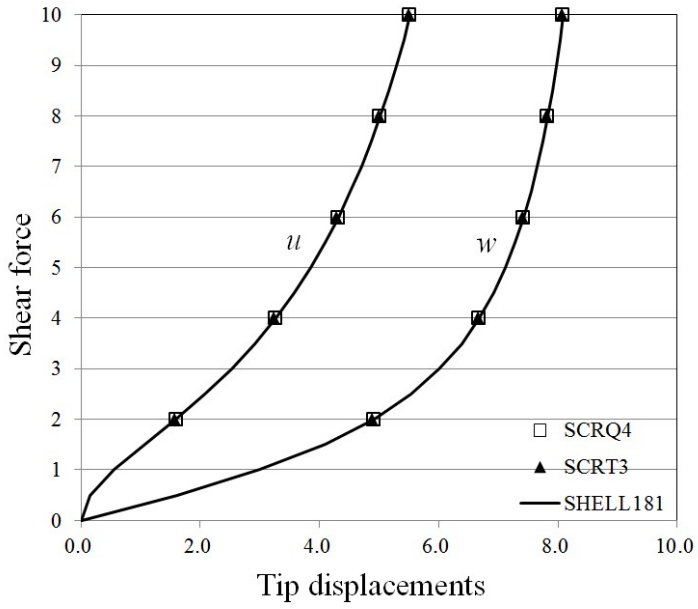

Figure 7.4 Load-displacement curves of cantilever beam under a shear force

In the simulation, the maximum shear force is set to 10 and divided into 5 equal load steps. Then, the load-displacement curves at the tip obtained by the proposed shell elements using the unsymmetrical geometric stiffness are depicted in Figure 7.4, compared with the SHELL181 element in ANSYS. Note that the SHELL181 element uses 20 equal load steps in the simulation, since it cannot get convergence with only 5 equal load steps.

It can be seen that the results obtained by the proposed shell elements and the SHELL181 element are in close agreement with each other. The detailed results and the convergence rates obtained by the proposed shell elements using the unsymmetrical and symmetrized geometric stiffness matrices are listed in Table 7.3 and 7.4, respectively.

Table 7.3 Tip vertical displacements (w) obtained by different methods

Shear force	SHELL181	SCRT3 (uns.)	SCRT3 (sym.)	SCRQ4 (uns.)	SCRQ4 (sym.)
2	4.9107	4.8862	4.8867	4.8995	4.8995
4	6.6777	6.6561	6.6561	6.6624	6.6625
6	7.4253	7.4094	7.4082	7.4120	7.4120
8	7.8299	7.8169	7.8168	7.8173	7.8174
10	8.0863	8.0764	8.0764	8.0755	8.0755

Table 7.4 Numbers of iterations used by different methods

Shear force	SCRT3 (uns.)	SCRT3 (sym.)	SCRQ4 (uns.)	SCRQ4 (sym.)
2	7	8	6	6
4	6	6	6	6
6	4	6	4	4
8	4	4	4	4
10	4	4	4	4
Total	25	28	24	24

In this example, the symmetrized geometric stiffness for the proposed shell elements has little influence on both the results and the convergence rates. In terms of the SHELL181 element in ANSYS, 20 equal load steps and 100 total iterations are needed to complete the whole analysis. Further, use of the automatic time stepping decreases the number of load step for the SHELL181 element, because the displacements of the first load step are very large and harder to get convergence than the following load steps. The SHELL181 element cannot get convergence for a large load step, while the proposed shell elements can handle this situation, using only 5 equal load steps and no more 30 total iterations. Thus, the advantages of the proposed shell elements in this example are obvious.

Further, to increase the effect of transverse shear deformation to the results and demonstrate the accuracy of the proposed shell elements considering shear deformation, the thickness of the cantilever beam is set to 1.0, which makes the beam cross section become square, meanwhile, the applied shear force **F** is changed to 400

and 2000 respectively. The final results obtained by the proposed shell elements using symmetrized geometric stiffness and the beam-column (BC) element proposed by Tang *et al.* (2015) are listed in Table 7.5.

Table 7.5 Tip vertical displacements (*w*) solved by different elements

Element Type	F=400			F=2000		
	w/ shear	w/o shear	relative error	w/ shear	w/o shear	relative error
SCRT3	1.3017	1.2913	0.81%	4.9252	4.8952	0.61%
SCRQ4	1.3084	1.2987	0.75%	4.9397	4.9115	0.57%
BC	1.3199	1.3100	0.76%	4.9739	4.9451	0.58%

It cannot be expected that the results obtained by these different types of elements completely agree well with each other. However, the relative errors show that the transverse shear deformation has similar influences on these different elements in these two load cases. Thus, the proposed shell elements can consider shear deformation correctly. Also, it can be noted that the effect of transverse shear deformation is smaller when the shear force is 2000, since the membrane contribution to the overall deflection becomes larger as the shear force increases.

7.1.3 Pinched hemispherical shell with a hole

A pinched hemispherical shell with a hole is a well-known and demanding benchmark example used to test shell elements. The hemispherical shell has an 18˚ hole at its top and is subjected to two inward and two outward radially applied forces F=400 along the X-axis and Y-axis respectively. The geometric and material properties are listed below.

Radius R=10, thickness t=0.04.

Elastic modulus E=6.825×10^7, Poisson's ratio v=0.3.

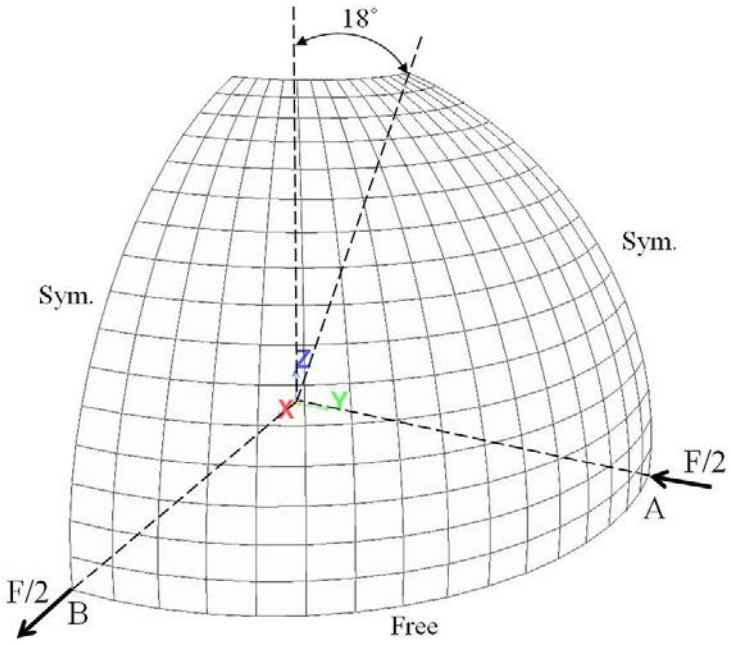

Figure 7.5 Pinched hemispherical shell with a hole

Due to the symmetry of this example, only one quarter is modelled with a 16×16 mesh of the SCRT3 and SCRQ4 elements respectively, as shown in Figure 7.5. Unlike the first two examples, warping phenomenon occurs in the quadrilateral shell

element. Thus, this example can verify the method dealing with warping effect used in the SCRQ4 element.

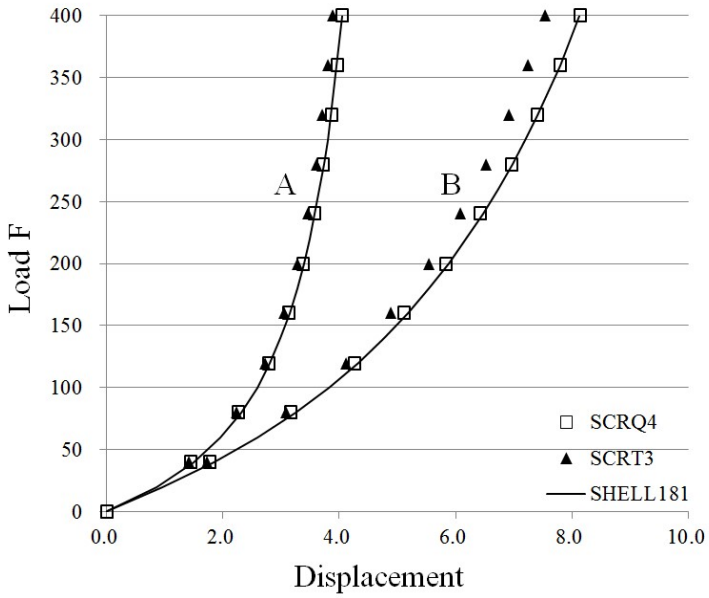

Figure 7.6 Load-displacement curves of pinched hemispherical shell with a hole

This example is analysed by the proposed shell elements using the symmetrized geometrically stiffness and only 10 equal load steps in NIDA, compared with the SHELL181 element using 20 equal load steps in ANSYS. It is found that the SHELL181 element cannot get convergence with 10 equal load steps. The radial displacements of the points A and B are monitored. The load-displacement curves at the points A and B for different shell elements are plotted in Figure 7.6, while the deformed shapes of the proposed shell elements are shown in Figure 7.7.

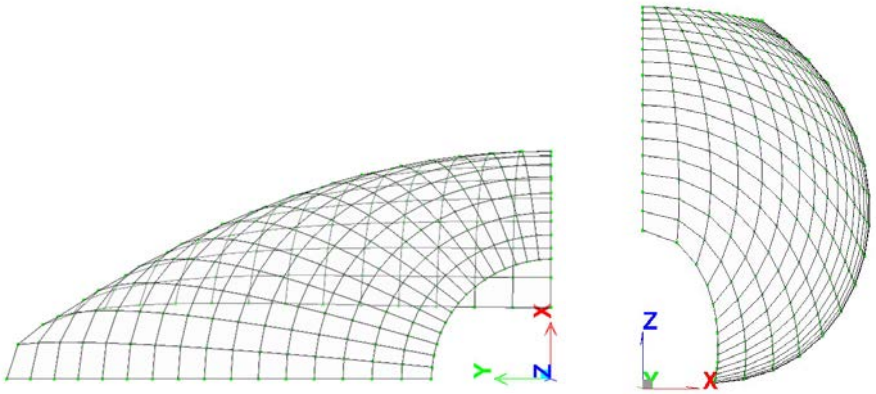

(a) SCRQ4

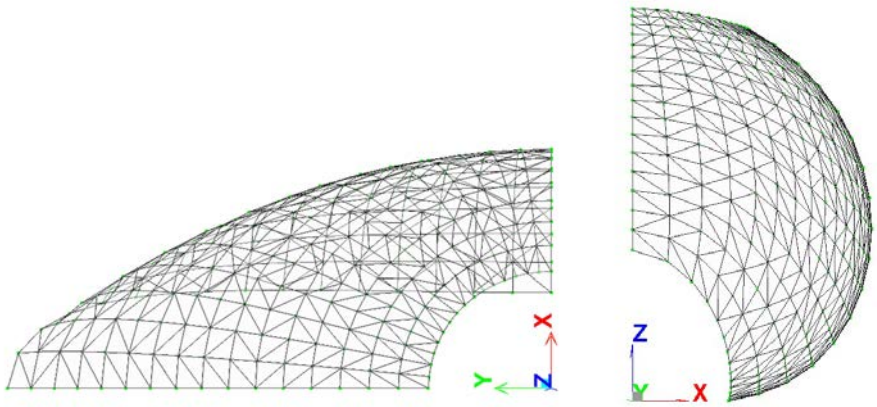

(b) SCRQ3

Figure 7.7 Deformed shapes of pinched hemispherical shell

Figure 7.6 shows that results obtained by the SCRQ4 element are very close to the SHELL181 element, while the SCRT3 is slightly stiffer. This may be due to the local triangular shell element formulation and its definition of the local coordinate system. In the following, to study the effect of the symmetrized geometric stiffness, the detailed results and the numbers of iterations for every load step obtained by the proposed shell elements using the unsymmetrical and symmetrized geometric stiffness matrices are listed in Table 7.6 and 7.7, respectively.

Table 7.6 Displacements at the point B obtained by different methods

F	SHELL181	SCRT3 (uns.)	SCRT3 (sym.)	SCRQ4 (uns.)	SCRQ4 (sym.)
40	1.8309	1.7305	1.7308	1.7842	1.7951
80	3.2468	3.0903	3.0912	3.1862	3.2065
120	4.3208	4.1120	4.1131	4.2621	4.2843
160	5.1751	4.9090	4.9101	5.1241	5.1455
200	5.8779	5.5517	5.5529	5.8370	5.8567
240	6.4691	6.0833	6.0845	6.4395	6.4573
280	6.9748	6.5316	6.5328	6.9568	6.9729
320	7.4128	6.9158	6.9169	7.4065	7.4210
360	7.7963	7.2492	7.2503	7.8014	7.8145
400	8.1349	7.5419	7.5429	8.1511	8.1630

Table 7.7 Numbers of iterations used by different methods

F	SCRT3 (uns.)	SCRT3 (sym.)	SCRQ4 (uns.)	SCRQ4 (sym.)
40	12	12	10	16
80	8	9	11	11
120	8	9	9	9
160	7	8	8	9
200	7	7	7	8
240	6	6	6	7

280	6	5	6	6
320	6	6	6	7
360	5	5	5	7
400	5	5	5	7
total	70	72	73	87

It can be seen that the symmetrized geometric stiffness has insignificant influence on the accuracy and efficiency of the SCRT3 element, although its solutions are not as good as the SCRQ4 element. The SCRQ4 element using the symmetrized geometric stiffness boosts the numbers of iterations in this example, probably due to the warping phenomenon. However, when the applied forces are divided into 20 equal load steps, both the unsymmetrical and symmetrized geometric stiffness matrices use 105 iterations in total. This illustrates that the warping effect on the convergence rate can be decreased by using more load steps. Also, the SHELL181 element requires 20 equal steps and 130 iterations in this example, performing worse than the proposed shell elements.

Although the symmetrized geometric stiffness has some influences on the accuracy, it is hard to come across displacements and rotations in practical civil engineering structures as large as those in the first three examples. Moreover, the convergence rate can be decreased or removed by using more load steps in the analysis. Thus, it is acceptable that the proposed shell elements using the symmetrized geometric stiffness matrices, and they are used in the following numerical examples by default.

7.1.4 Clamped semi-cylindrical shell under a point load

A semi-cylindrical shell is fully clamped at one end and subjected to a point load at the other free end, whereas its bottom is under a symmetrical condition, as shown in Figure 7.8. The geometric and material properties are shown below.

Radius R=1.016, thickness t=0.03, length of cylinder L=3.048.

Elastic modulus E=2.0685×10^7, Poisson's ratio v=0.3.

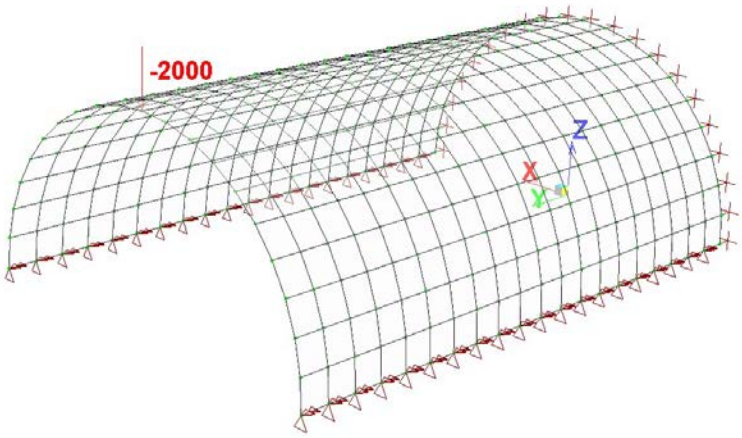

(a) SCRQ4

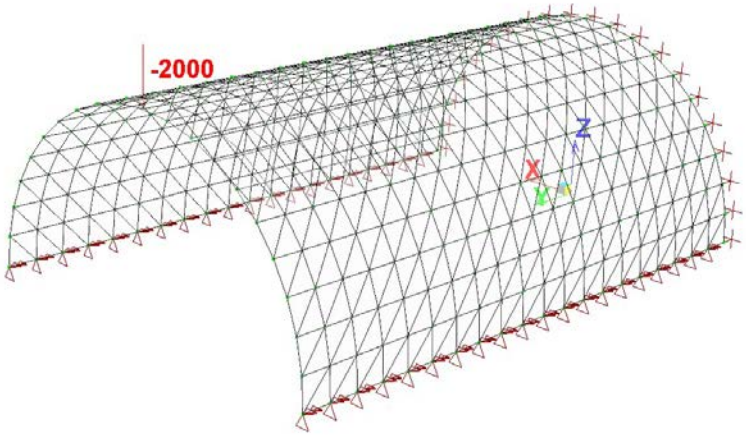

(b) SCRT3

Figure 7.8 Clamped semi-cylindrical shell under a point load

The maximum applied point load is F=2000. In the program NIDA, the shell structure is modelled with a 20×20 mesh of the proposed elements, while the maximum applied load is equally divided into 20 load steps.

The results obtained by the proposed shell elements are plotted in Figure 7.9, compared with the SHELL181 element in ANSYS. It can be seen that all of these elements are in good agreement. In addition, the SCRT3 and SCRQ4 elements need 115 and 142 iterations in total to finish the whole analysis respectively, in which the SCRQ4 element may be disturbed by the warping effect. It is found that the SHELL181 element cannot finish the analysis with a 20×20 mesh, so a 32×32 mesh is used, with 23 program-chosen load steps and 150 iterations.

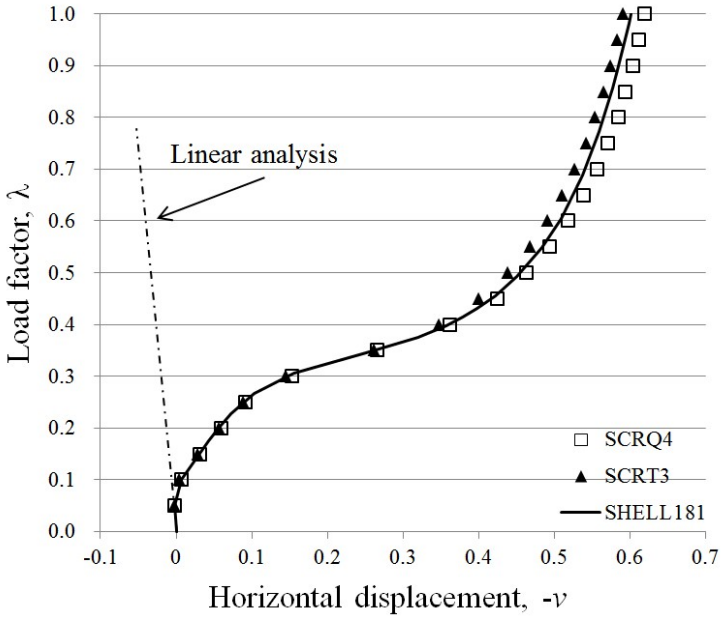

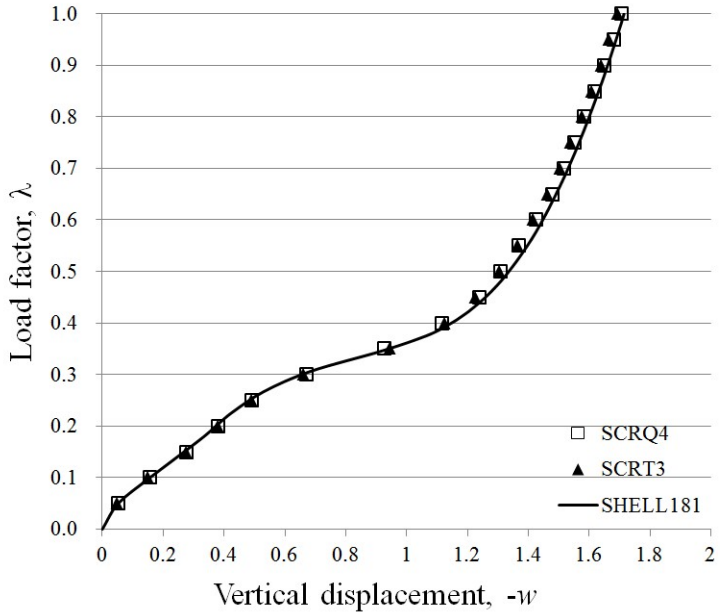

Figure 7.9 Load-displacement curves of clamped semi-cylindrical shell

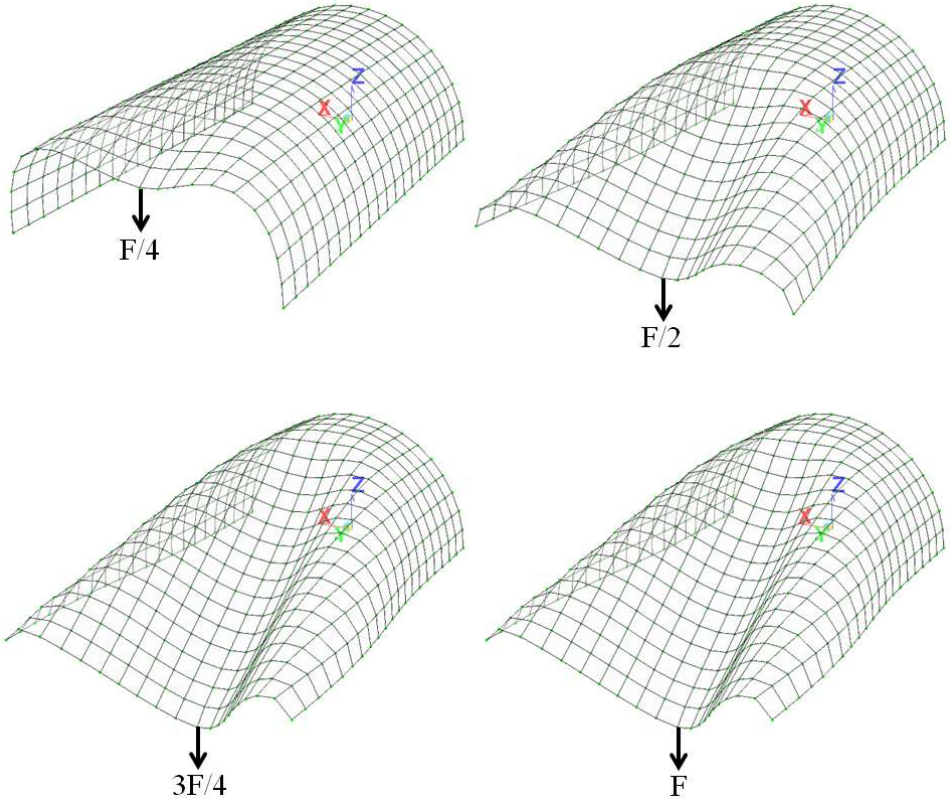

Figure 7.10 Deformed shapes of clamped semi-cylindrical shell

In this example, the proposed shell elements in NIDA are easier to get convergence with coarse meshes in a larger load step, compared with the SHELL181 element in ANSYS. In addition, the deformed shapes obtained by the SCRQ4 element in NIDA are shown in Figure 7.10, when the point load is $F/4$, $F/2$, $3F/4$ and F.

7.1.5 Annular plate under a line load at the free edge

Figure 7.11 shows annular plates modelled with SCRQ4 and SCRT3 elements in the program NIDA, respectively. This example suggested by Başar and Ding (1992) was widely used to test shell elements. One end of this structure is subjected a transverse line load and the other end is fully clamped. The annular plate undergoes large displacements and large rotations. The geometric and material properties are given below.

External diameter R_e=10, internal diameter R_i=6, thickness t=0.03.

Elastic modulus E=2.1×10^8, Poisson's ratio=0.

In the analysis, the maximum transverse line load is set to 6, while the annular plate is modelled with a 4×30 mesh of the proposed shell elements, as shown in Figure 7.11.

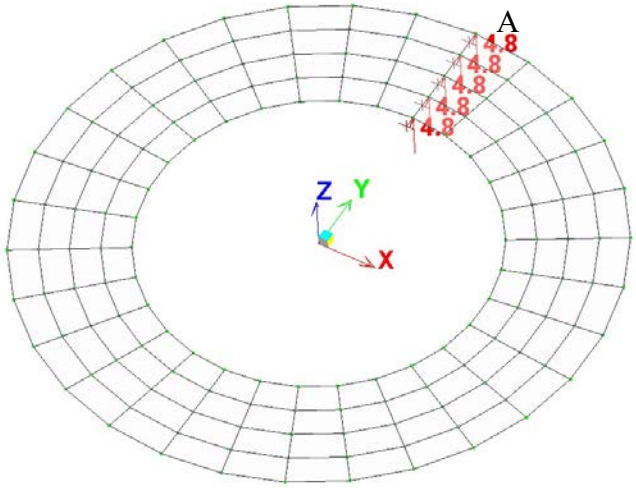

(a) SCRQ4

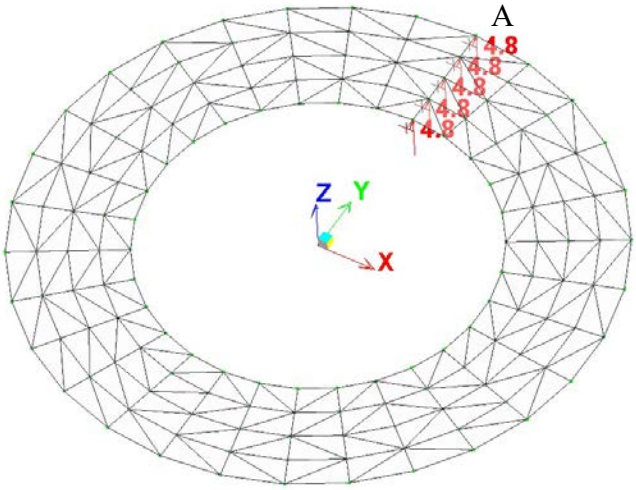

(b) SCRT3

Figure 7.11 Annular plate under a line load

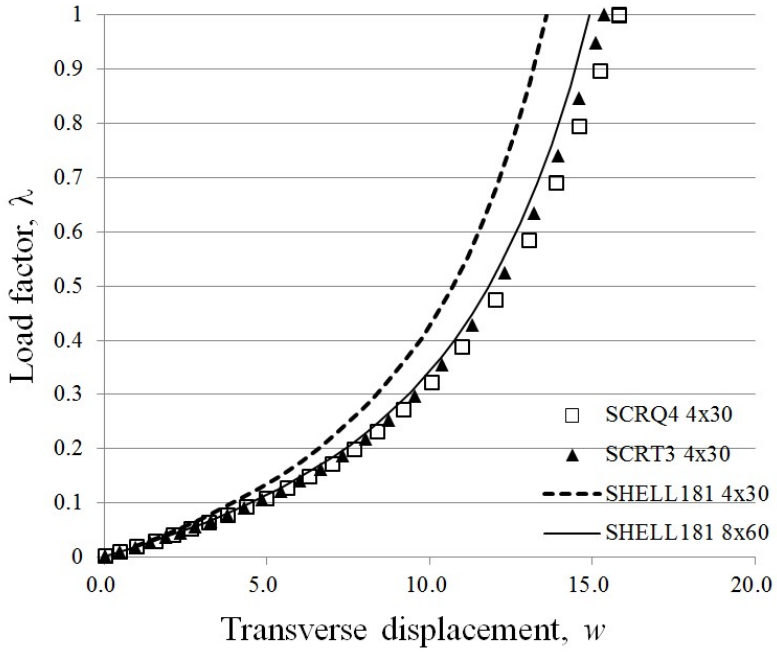

Figure 7.12 Load-displacement curves of annular plate under a line load

The load-displacement curves at the point A obtained by the proposed shell elements in NIDA are depicted in Figure 7.12, compared with the SHELL181 element. The results obtained by an 8×60 mesh of the SHELL181 element are also taken as reference. It can be seen that the results obtained by the proposed shell elements are close to the reference solutions, whereas the annular plate modelled with the SHELL181 element using a 4×30 mesh is slightly stiffer than the other elements. In addition, based on the combined arc-length with minimum residual displacement method in the program NIDA, the SCRT3 element totally needs 26 load steps and 215 iterations, while the SCRQ4 element needs 25 load steps and 203 iterations. For the SHELL181 elements using the program-chosen load stepping in ANSYS, the model using a 4×30 needs 31 load steps and 190 iterations, while an 8×60 mesh needs 25 load steps and 209 iterations.

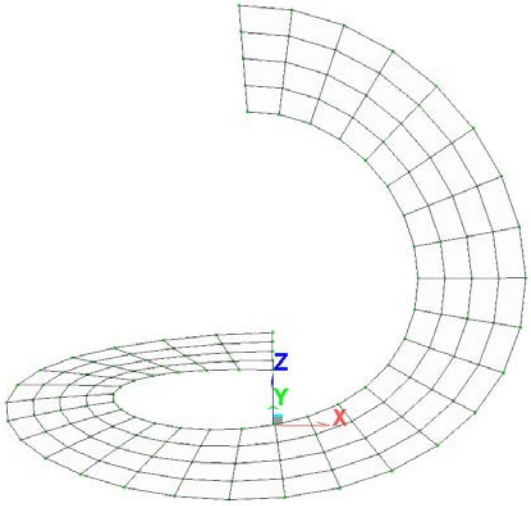

(a) SCRQ4

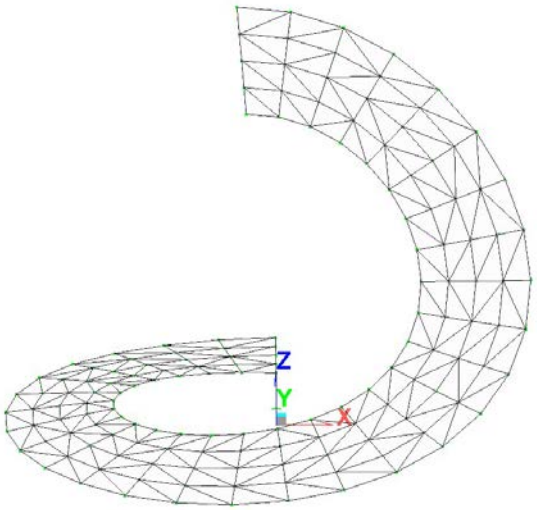

(b) SCRT3

Figure 7.13 Deformed shapes of annular plate

Thus, these different elements have similar iterations and computational efficiency, while the proposed shell elements perform better than the SHELL181 element in terms of accuracy in this example. Besides, the deformed shapes obtained by the proposed shell elements under the maximum load in the program NIDA are shown in Figure 7.13. It can be seen that these two deformed shapes are close to each other.

7.1.6 Clamped square plate under a concentrated force

Figure 7.14 depicts a square plate clamped along two opposite sides and subjected to a concentrated force at a point on the centreline. This example was used by Izzuddin (2005) to test his proposed co-rotational approach introduced in Section 4.2.3 under an irregular mesh. The geometric and material properties are shown below.

Side length L=400mm, thickness t=1.98.

Young's modulus E=2.15×10^{4}N/mm^2, Poisson's ratio v=0.3.

As shown in Figure 7.15, only half of the plate is modelled due to symmetry, in which a regular mesh and an irregular mesh of 10×5 elements are used. Also, the maximum concentrated force **F** is set to 250N and divided into 5 equal steps.

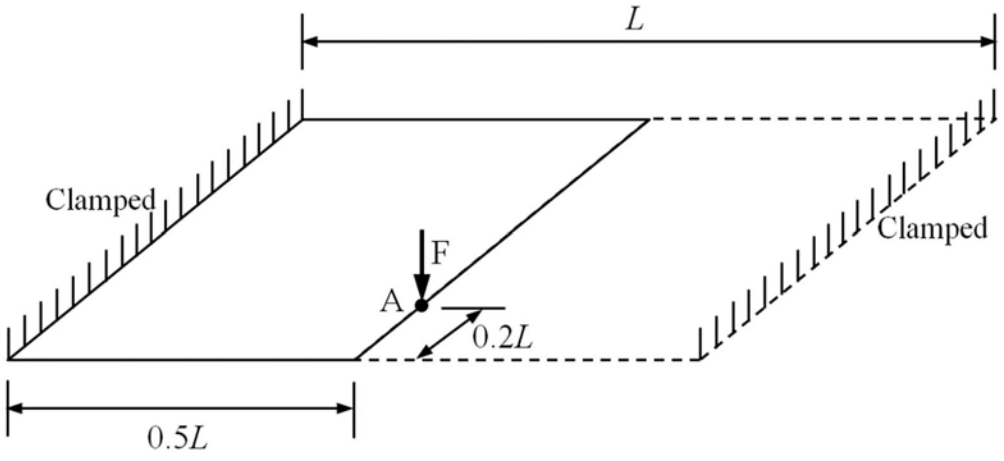

Figure 7.14 Clamped square plate subjected to a concentrated force

The results at the point A obtained by different methods are plotted in Figure 7.16, in which the solutions given by Izzuddin (2005) using a co-rotational approach with the quadratic (QD) Mindlin-Reissner local formulation for the regular mesh of 20×10 elements (20e) and increments of 5 equal load steps (5i) are captured from the figure in his paper.

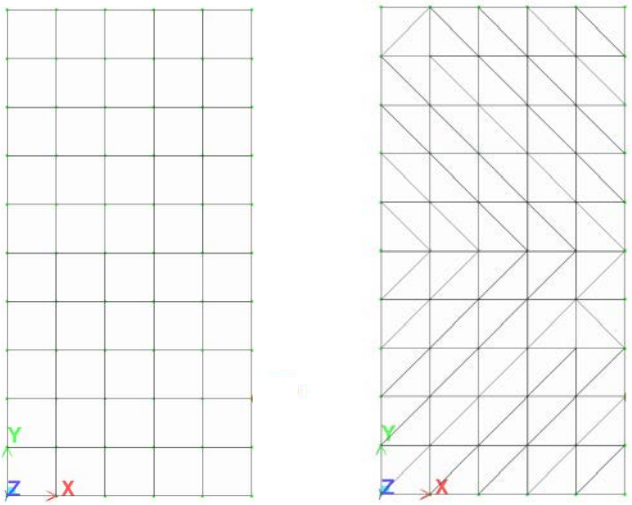

(a) Regular meshes

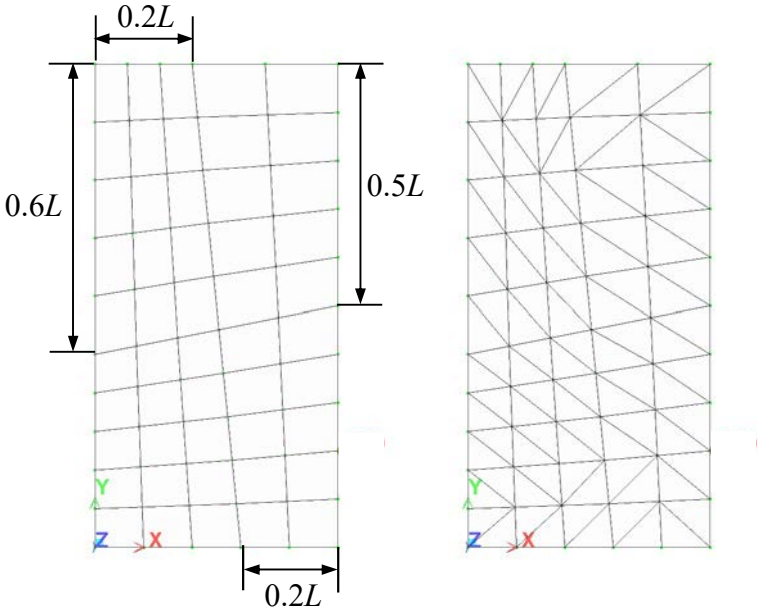

(b) Irregular meshes

Figure 7.15 Different meshing schemes of clamped square plate

Figure 7.16 shows that the vertical displacements at the point A obtained by the models using the regular mesh of different elements are close, except that the SHELL181 element is slightly stiffer. Further, the detailed results obtained by the regular and the irregular meshes of the proposed shell elements are listed in Table 7.8

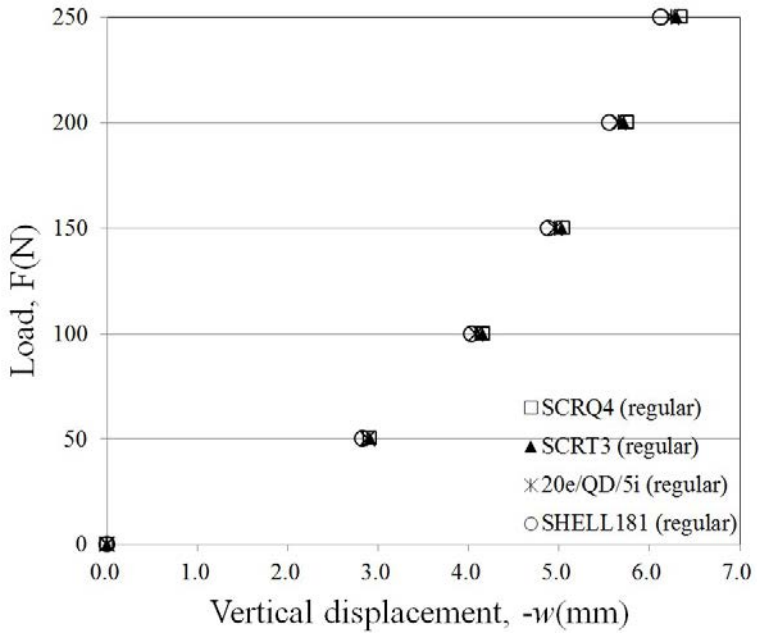

Figure 7.16 Load-displacement curves of clamped square plate

Table 7.8 Vertical displacements (-*w*) at the point A obtained by different models

F	SCRT3 (regular)	SCRT3 (irregular)	SCRQ4 (regular)	SCRQ4 (irregular)	SHELL181 (regular)
50	2.9137	2.9115	2.9095	2.9187	2.8252
100	4.1598	4.1567	4.1692	4.1802	4.0379
150	5.0309	5.0261	5.0530	5.0647	4.8830

200	5.7224	5.7156	5.7565	5.7684	5.5619
250	6.3048	6.2960	6.3506	6.3625	6.1267

Table 7.8 shows that the results obtained by the irregular mesh of the proposed shell elements are close to the regular mesh, so the proposed shell elements are insensitive to irregular meshes. In addition, using 5 equal load steps, both regular and irregular meshes of the proposed shell elements need 19 iterations in total, while the SHELL181 element needs 11 iterations. In summary, the proposed shell elements are more accurate than the SHELL181 element, but the latter is more efficient in this example undergoing relatively small displacements and rotations compared with the previous examples. This is maybe the stiffer element is helpful to get convergence quickly in this problem.

7.1.7 Clamped strip under torsion

Figure 7.17 shows a clamped flat strip subjected to a force couple at the free end. This example was used by Izzuddin and Liang (2016) to test the validity of shell elements against the invariance of nodal ordering, which showed that a shell element using one element side to define the local x-axis has different solutions after re-ordering of nodal numbering. Similarly, the validation is repeated here to test the proposed quadrilateral shell element, SCRQ4. The geometric and material properties are listed below.

Length L=12, width b=1, thickness t=0.1.

Young's modulus E=1.2×10^6, Poisson's ratio v=0.

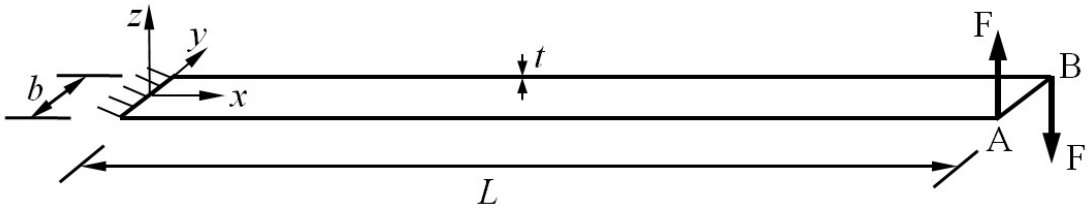

Figure 7.17 Clamped flat strip under torsion

In this example, the flat strip is modelled by a 12×1 mesh of the SCRQ4 element, while the maximum force couple is set to 100 and divided into 10 equal load steps in the program NIDA. Two different nodal ordering schemes are used to test the SCRQ4 element, as seen in Figure 7.18.

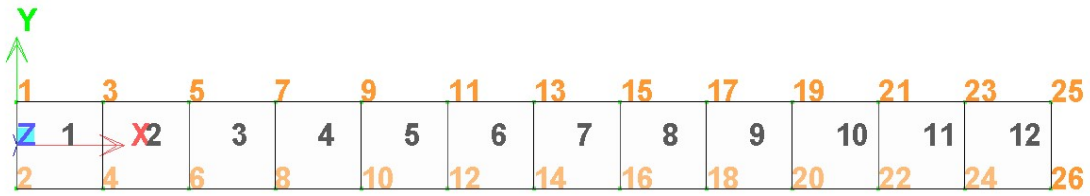

Nodal ordering

1st ordering:	2nd ordering:
1: 2, 4, 3, 1	***1***: 4, 3, 1, 2
2: 4, 6, 5, 3	***2***: 6, 5, 3, 4
…	…
12: 24, 26, 25, 23	***12***: 26, 25, 23, 24

Figure 7.18 Nodal ordering

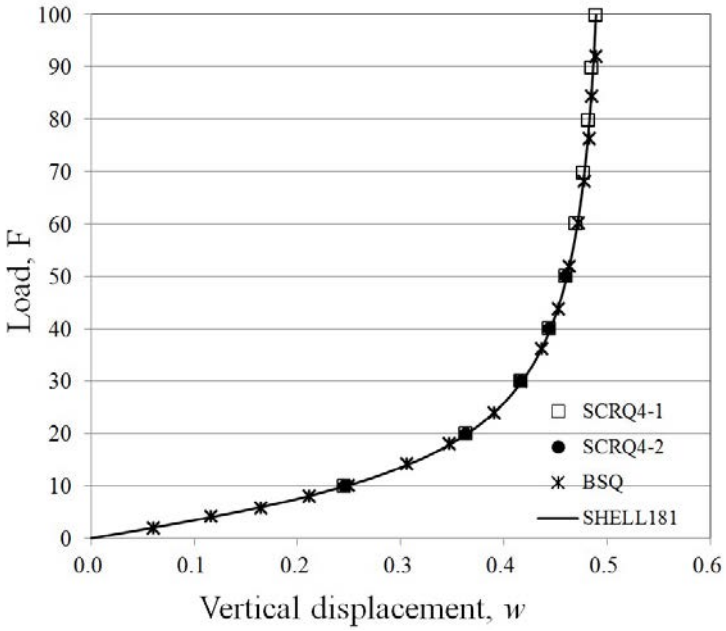

Figure 7.19 Load-displacement curves of clamped flat strip under torsion

The vertical displacements at the point A obtained by the SCRQ4 element using different nodal orderings in the program NIDA are plotted in Figure 7.19, compared with the solutions of the bisector quadrilateral (BSQ) shell element by Izzuddin and Liang (2016) and the SHELL181 element in ANSYS, in which the model in ANSYS uses a 24×2 mesh of the SHELL181 element. In Figure 7.19, SCRQ4-1 and SCRQ4-2 refer to the models adopting the 1st and the 2nd nodal ordering, respectively. These elements are in good agreement with each other. Further, to illustrate the good performance of the SCRQ4 element, the detailed results of the points A and B at every two load steps are listed in Table 7.9. Note that the load values of the SHELL181 element in this table are approximate except 100, since the program-chosen time stepping is used in ANSYS.

Table 7.9 Vertical displacements (*w*) at the points A and B

F	SCRQ4-1 A	SCRQ4-1 B	SCRQ4-2 A	SCRQ4-2 B	SHELL181 A	SHELL181 B
20	0.3632	-0.3632	0.3632	-0.3632	0.3632	-0.3632
40	0.4440	-0.4440	0.4440	-0.4440	0.4471	-0.4471
60	0.4705	-0.4705	0.4705	-0.4705	0.4725	-0.4725
80	0.4826	-0.4826	0.4826	-0.4826	0.4838	-0.4838
100	0.4892	-0.4892	0.4892	-0.4892	0.4894	-0.4894

Table 7.9 shows that the SCRQ4 element is invariant to nodal ordering as same as the SHELL181 element and their results are very close to each other. In terms of the convergence rate, the SCRQ4 element uses 10 equal load steps and 73 iterations to complete the whole analysis for both the nodal orderings. However, in ANSYS, a 12×1 mesh of the SHELL181 element cannot conduct the analysis even using a very small increment of load step, while a 24×2 mesh of the SHELL181 element cannot get convergence using only 10 equal load steps. When the initial load step is set to 10, 39 program-chosen load steps and 263 iterations are needed to complete the analysis using the SHELL181 element in ANSYS. Note that the SCRQ4 element adopts the symmetrized geometric stiffness matrix by default in this example, while the SCRQ4 element is more efficient when using the unsymmetrical geometric stiffness matrix, with only 5 equal load steps and 28 iterations in total. This is because the wrapping effect makes the SCRQ4 element using symmetrized geometric stiffness matrix need more iterations, but it is still more accurate and efficient than the SHELL181 element in this example.

7.1.8 Cylindrical shell segment under a concentrated force

Figure 7.20 depicts that a cylindrical shell segment is subjected to a concentrated force at the centre, while its two sides are hinged and the other two are free. This is a well-known problem used to check the ability of a shell element against instability behaviour, whose equilibrium path exhibits a snap-through response with two limit points. The material properties are given below.

Elastic modulus E=3.10275 kN/mm^2, Poisson's ratio v=0.3.

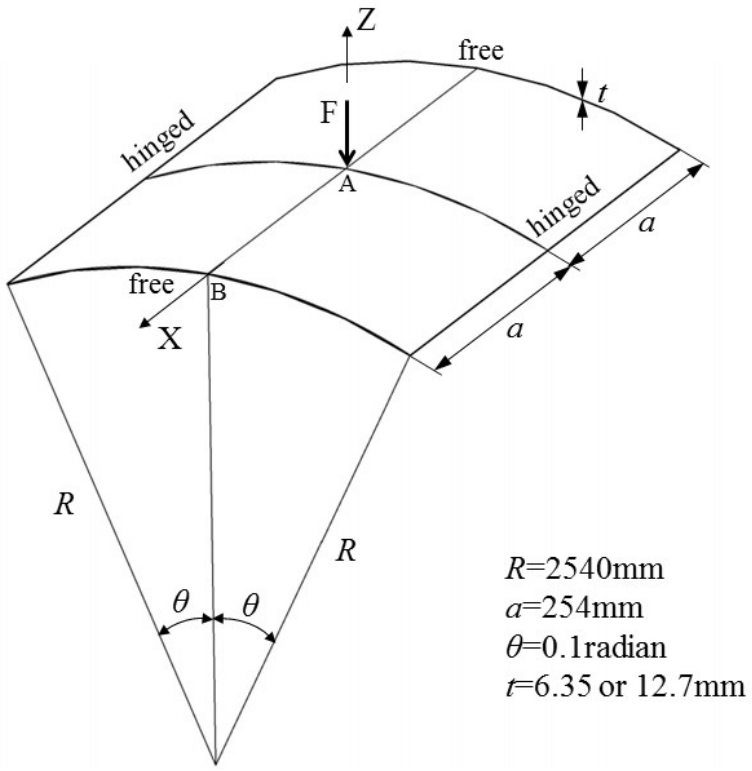

Figure 7.20 Cylindrical shell segment under a concentrated load

In this example, two different thicknesses (i.e. 6.35 mm and 12.7 mm) are considered. Due to the symmetry, a quarter part of the cylindrical shell segment is modelled with a 4×4 mesh of the proposed shell elements, while the vertical concentrated force is applied to the point A, as shown in Figure 7.21.

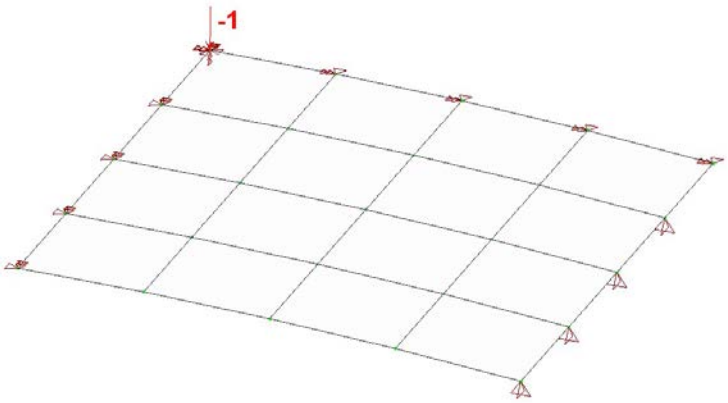

(a) SCRQ4

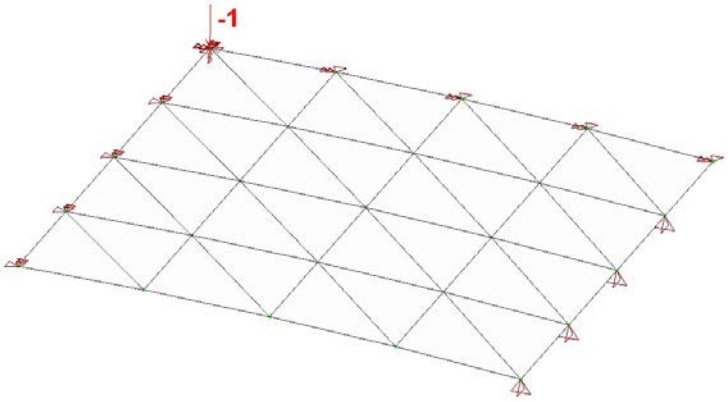

(b) SCRT3

Figure 7.21 Meshing details of cylindrical shell

In the program NIDA, the combined arc-length with minimum residual displacement method is adopted to trace the whole equilibrium paths of these models. The vertical displacements at the points A and B obtained by the proposed shell elements are

plotted in Figure 7.22, while the solutions obtained by the SHELL181 element in ANSYS are taken as reference. The results obtained by these different shell elements are close to each other. Thus, the proposed shell elements can accurately describe the instability behaviour of shell structures.

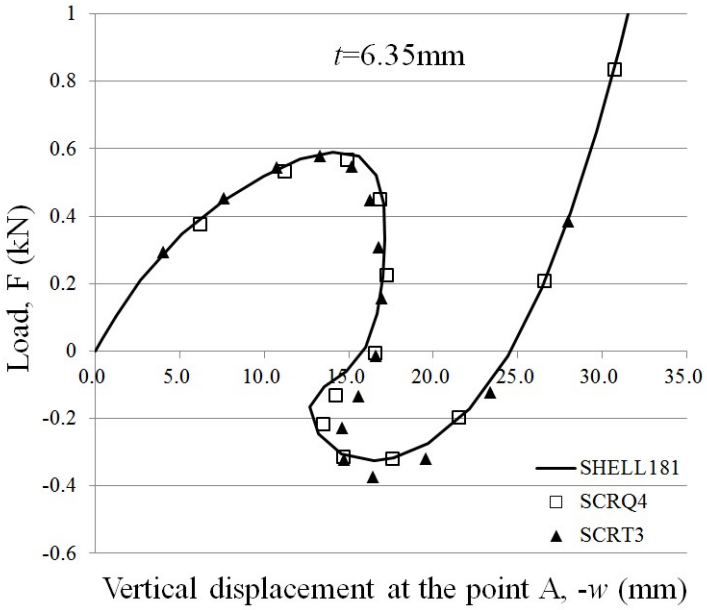

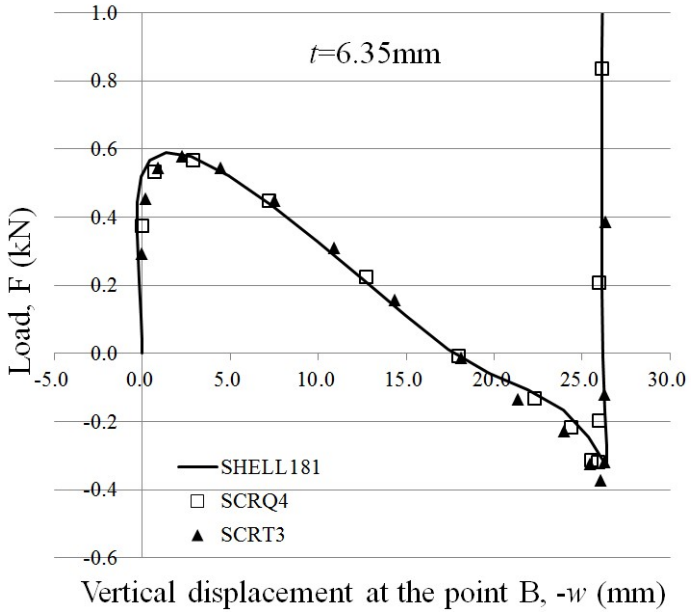

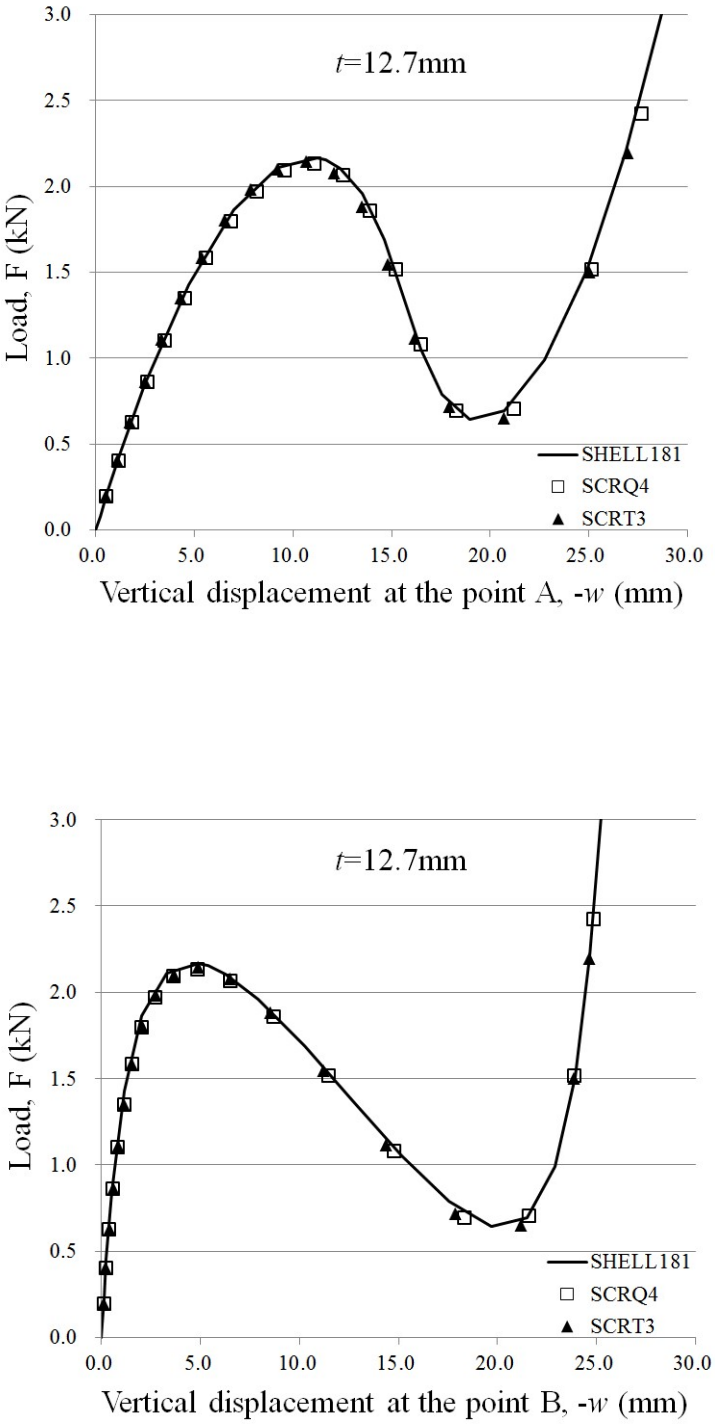

Figure 7.22 Load-displacement curves of cylindrical shell segment under a concentrated force

7.1.9 Clamped right-angle frame under an in-plane load

Figure 7.23 shows that a right-angle frame is clamped on one end and subjected to an in-plane force at the other free end. The geometric properties are given in Figure 7.23. The material properties are given below.

Elastic modulus E is 71240 N/mm^2 and Poisson's ratio v is 0.3.

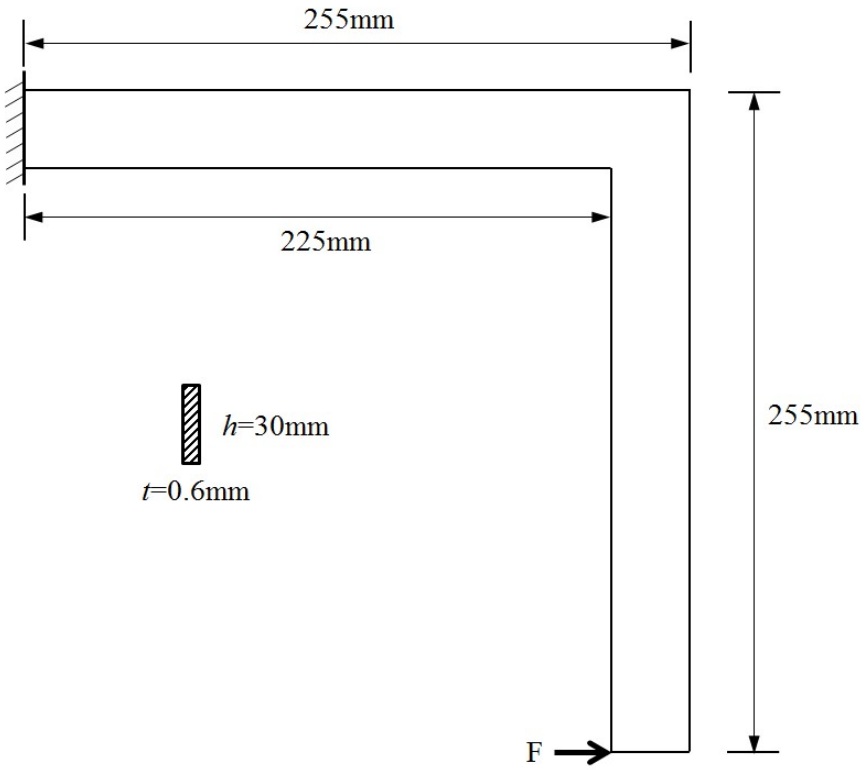

Figure 7.23 Right angle frame under an in-plane force

The frame is modelled by a 2×30 mesh of the proposed shell elements in the program NIDA, as shown in Figure 7.24. In addition, the right-angle frame is analysed using the identical mesh of the SHELL181 element in ANSYS for comparison. In the

simulation, an out-plane imperfect load equal to one thousandth of the in-plane force is applied at the point of the in-plane force to initiate the lateral buckling of the frame.

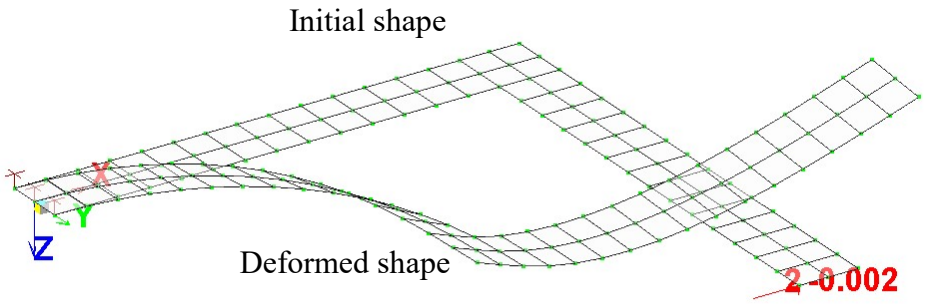

(a) SCRQ4

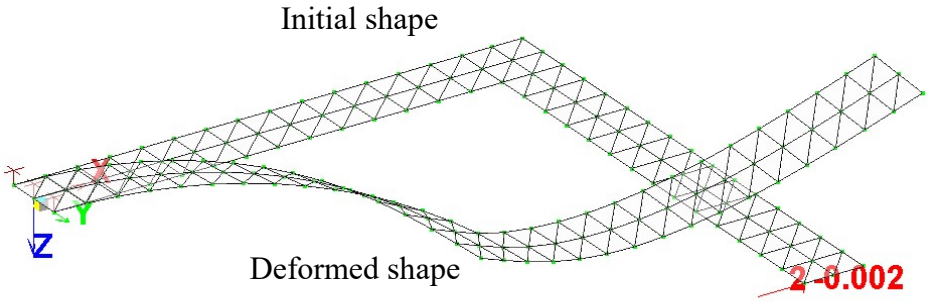

(b) SCRT3

Figure 7.24 Meshes and deformed shapes of right angle frame

To trace the whole equilibrium path, the program NIDA adopts the combined arc-length with minimum residual displacement method and the load-displacement curves at the point applied loads are plotted in Figure 7.25. These different shell elements are in good agreement with each other. Also, the deformed shapes obtained

by the SCRT3 and the SCRQ4 elements in the program NIDA are shown in Figure 7.24, when the in-plane force F=2N.

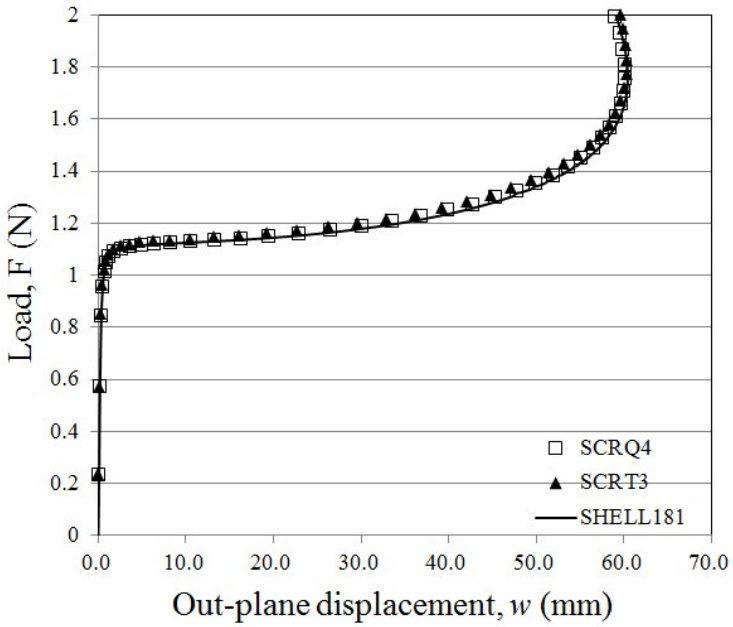

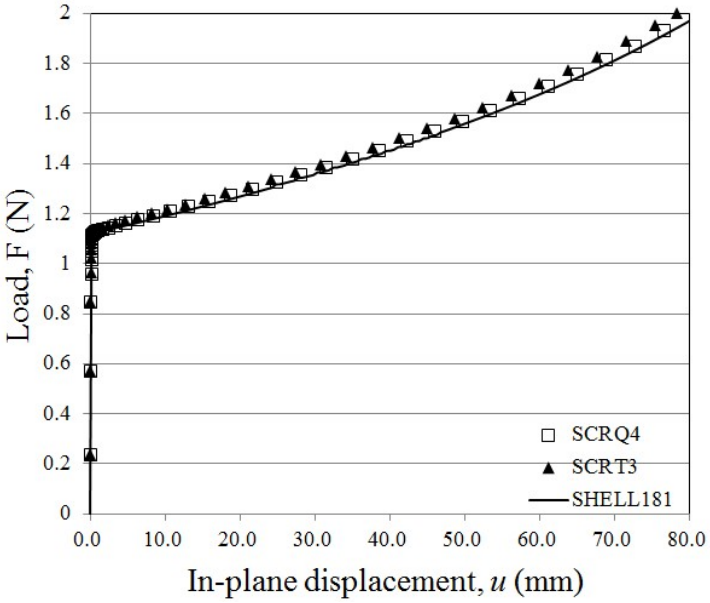

Figure 7.25 Load-displacement curves of right angle frame under an in-plane force

7.1.10 Channel section beam under compression

Figure 7.26 depicts that a channel section beam is subjected to an axial compressed load uniformly applied at the end sections. In addition, two small forces are applied at the midsection (x=550) to introduce torsional imperfections. The values of the two small forces are set to λ, while the compressed load is set to 125λ. The boundary conditions are $u(550,0,0)=0$, $v(0,0,0)=v(1100,0,0)=0$, $w(0,y,0)=w(1100,y,0)=0$. A (3+8+3)×56 mesh is used to model this example, as shown in Figure 7.27. The material properties are given below.

Elastic modulus E is 2.1×10^6 and Poisson's ratio v is 0.3.

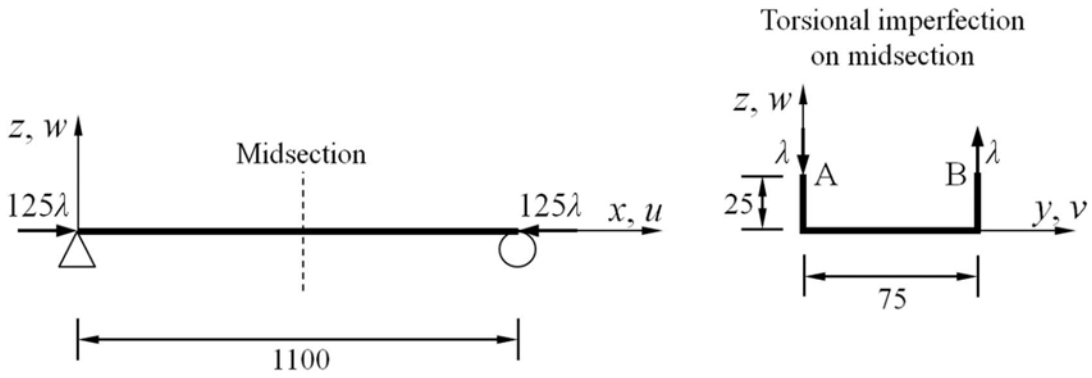

Figure 7.26 Channel section beam under compression

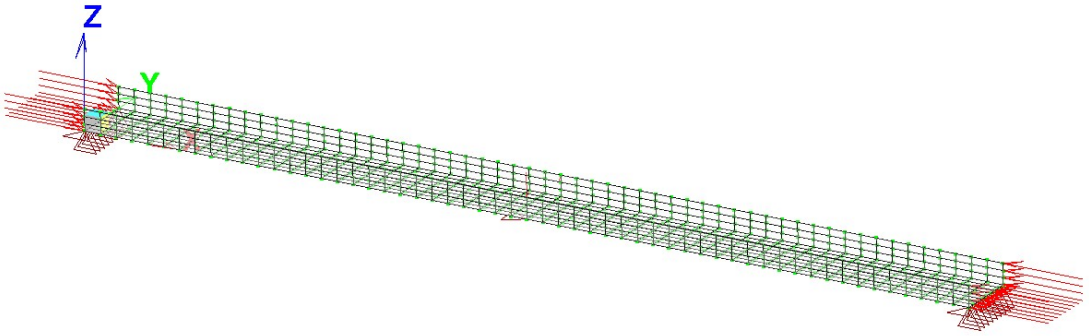

(a) SCRQ4

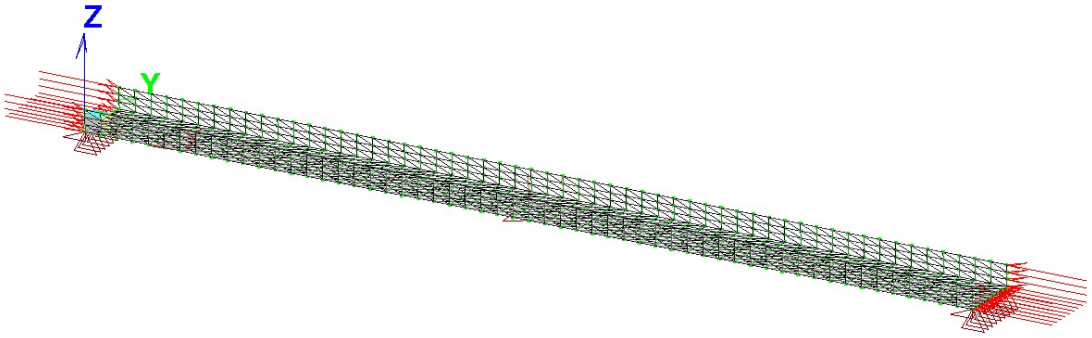

(b) SCRT3

Figure 7.27 Meshing details of channel section beam

The results of the vertical displacements at the points A and B, obtained by the proposed shell elements in NIDA, are plotted in Figure 7.28 and compared with the results obtained by the SHELL181 element in ANSYS. Also, the values of λ at the limit point are given in Table 7.10 which shows that the results obtained by these different elements are close to each other.

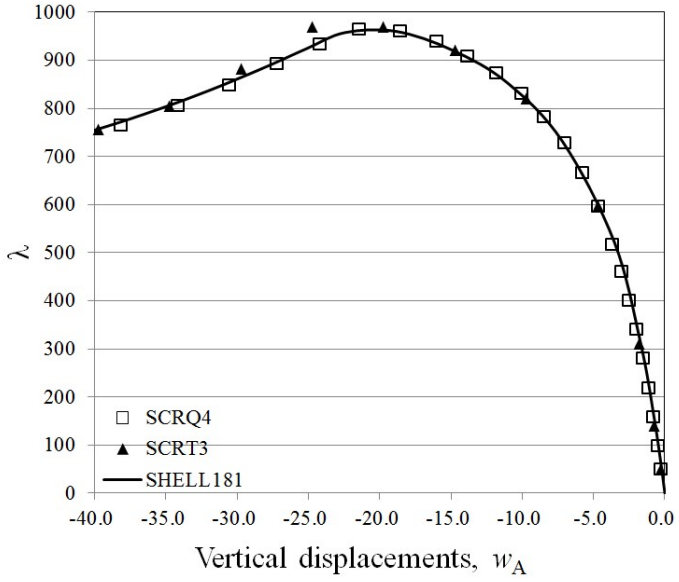

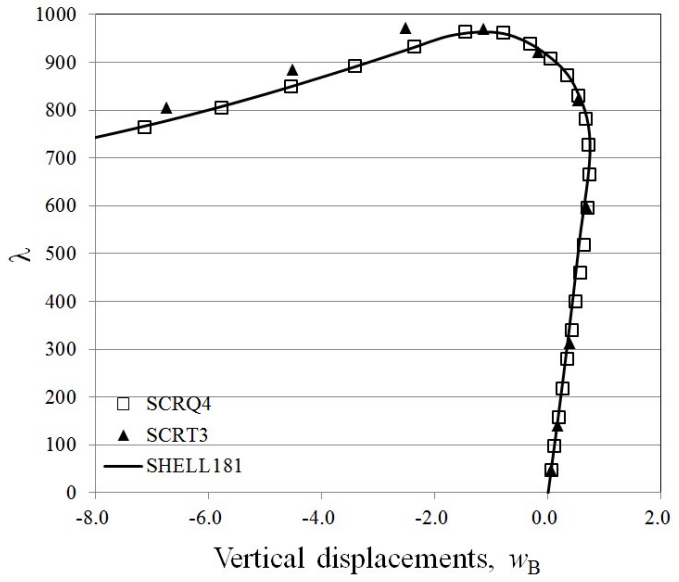

Figure 7.28 Load-displacement curves of channel section beam under compression

Table 7.10 Values of λ at the limit point

	SCRT3	SCRQ4	SHELL181
λ	971.2	964.8	960.2

7.2 Geometrically nonlinear elastoplastic analysis of shell structures

Several elastoplastic shell problems involved with large displacements and large rotations are analysed using the proposed SCRT3 and SCRQ4 elements considering elastoplasticity by layered approach. The obtained results are compared with those available in the existing literature. For all examples, the thickness of shell element is equally divided into 10 layers, and only the von Mises yield criterion with the associated flow rule and the isotropic hardening is taken into account.

7.2.1 Cantilever beam under bending

A cantilever beam subjected to a shear force at its free end for four different length/thickness ratios of L/t=10/3, 10, 100 and 1000, respectively, is analysed using the proposed shell elements, while a 10×1 mesh of the SCRQ4 and SCRT3 shell elements in the program NIDA are shown in Figure 7.29. The geometric and material properties are given below.

Length L=10, width b=1.

Young's modulus E=1.2×10^7, Poisson's ratio ν=0.

Initial yield stress σ_y=1.2×10^6, hardening parameter H=1.2×10^5.

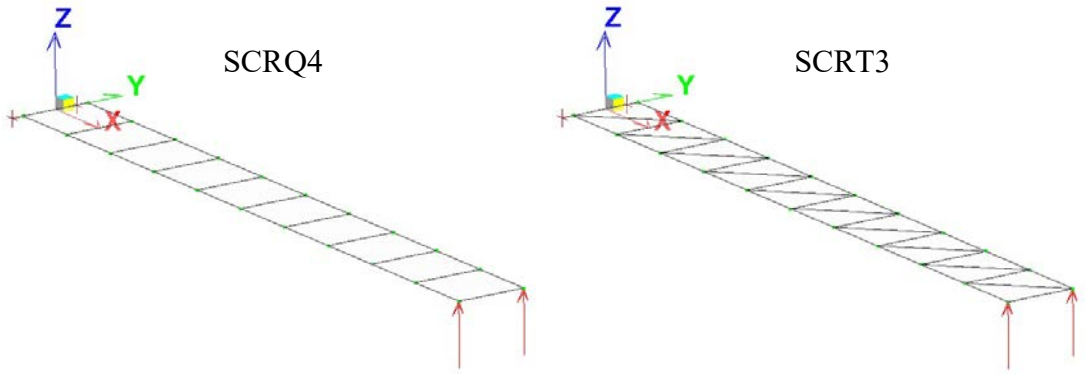

Figure 7.29 Meshing details of cantilever beam

The load-displacement curves at the free ends obtained by the proposed shell elements in the program NIDA are plotted in Figure 7.30, while the results obtained by Eberlein and Wriggers (1999) using 20 five-parameter quadrilateral 4-node shell elements are taken as reference.

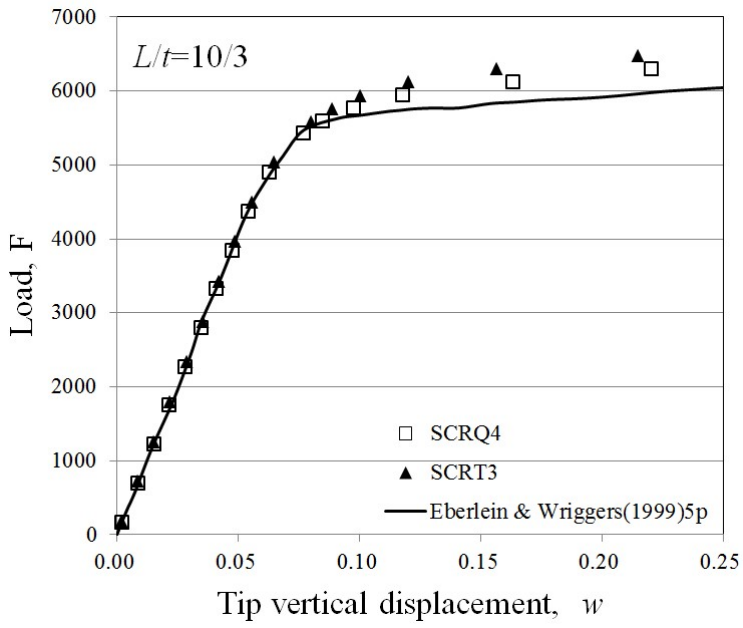

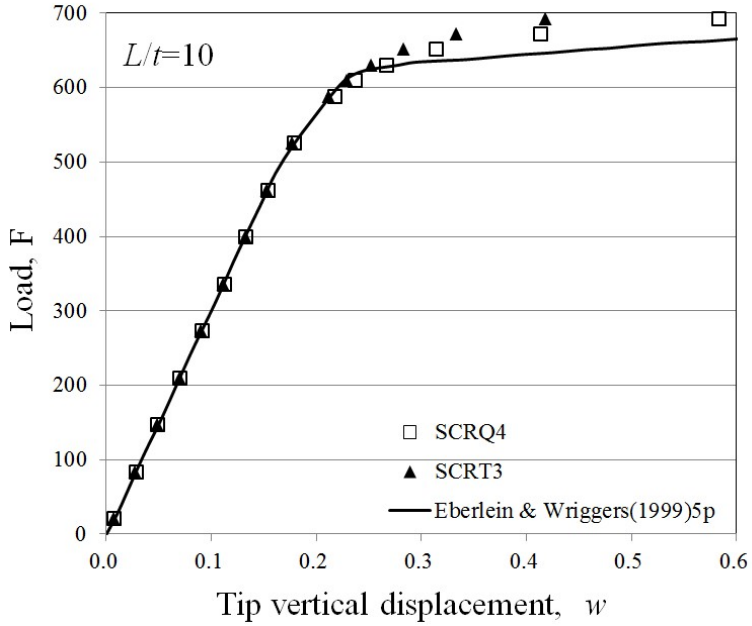
L/t=10
Load, F
Tip vertical displacement, w
SCRQ4
SCRT3
Eberlein & Wriggers(1999)5p
0
100
200
300
400
500
600
700
0.0
0.1
0.2
0.3
0.4
0.5
0.6

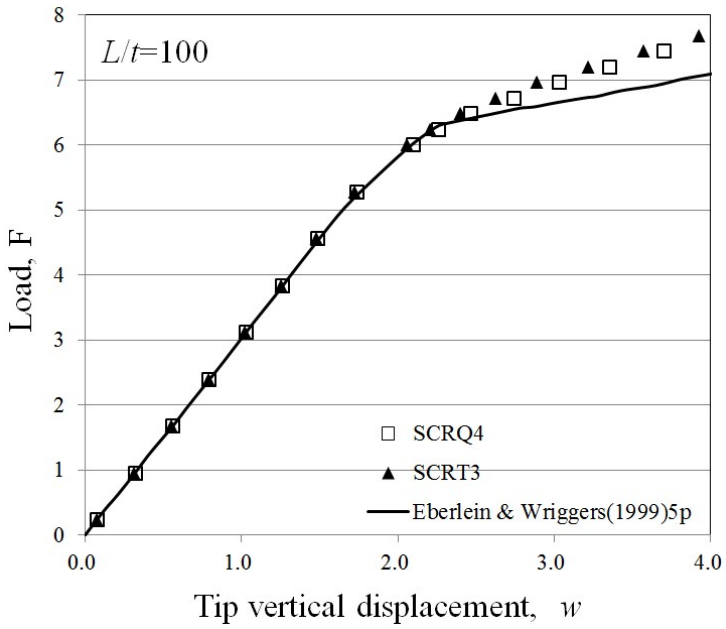
L/t=100
Load, F
Tip vertical displacement, w
SCRQ4
SCRT3
Eberlein & Wriggers(1999)5p
0
1
2
3
4
5
6
7
8
0.0
1.0
2.0
3.0
4.0

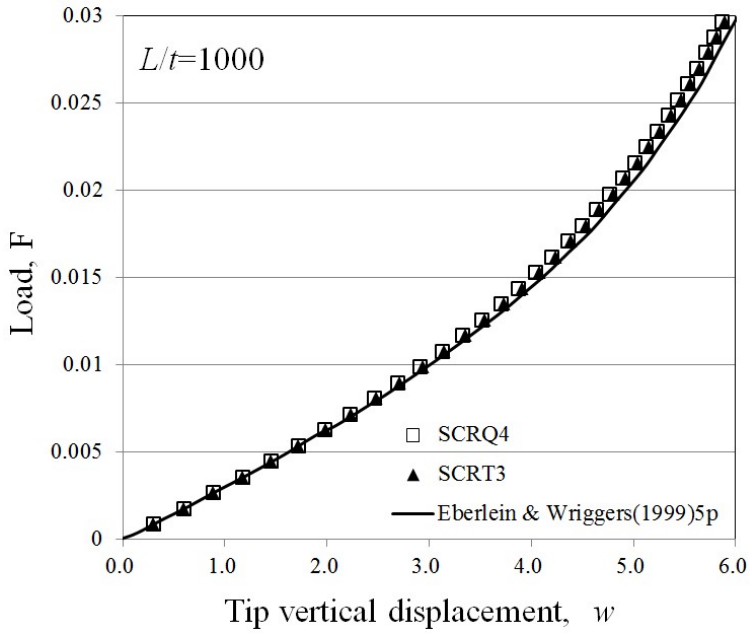

Figure 7.30 Load-displacement curves of cantilever beam subjected to a shear force for different length/thickness ratios

It can be seen that the results obtained by the proposed shell elements are close to each other, but they are slightly stiffer than those by Eberlein and Wriggers (1999) when the cantilever beam is in the hardening phase. This is because the proposed shell elements use a method different from the literature to conduct the elastoplastic analysis. However, the yield points obtained by the proposed shell elements are very close to those in literature.

7.2.2 Pinched cylinder under a pair of point loads

This example investigates a short cylindrical shell under a pair of point load at the midsection for large displacements, large rotations and elastoplastic behaviour. Its

two ends are supported by two rigid diaphragms, where only the displacements along the longitudinal axis are allowed. It is a classical benchmark problem in shell element researches, firstly presented Simo and Kennedy (1992) and then followed by many researchers (Brank *et al.*, 1997; Eberlein and Wriggers, 1999; Fontes Valente *et al.*, 2005; Miehe, 1998; Sansour and Kollmann, 2000; Sorić *et al.*, 1997; Wriggers *et al.*, 1996). The geometric properties and the material properties are listed below.

Length L=600, radius R=300, thickness t=3.

Young's modulus E=3000, Poisson's ratio v=0.3.

Initial yield stress σ_y=24.3 and hardening parameter H=50.

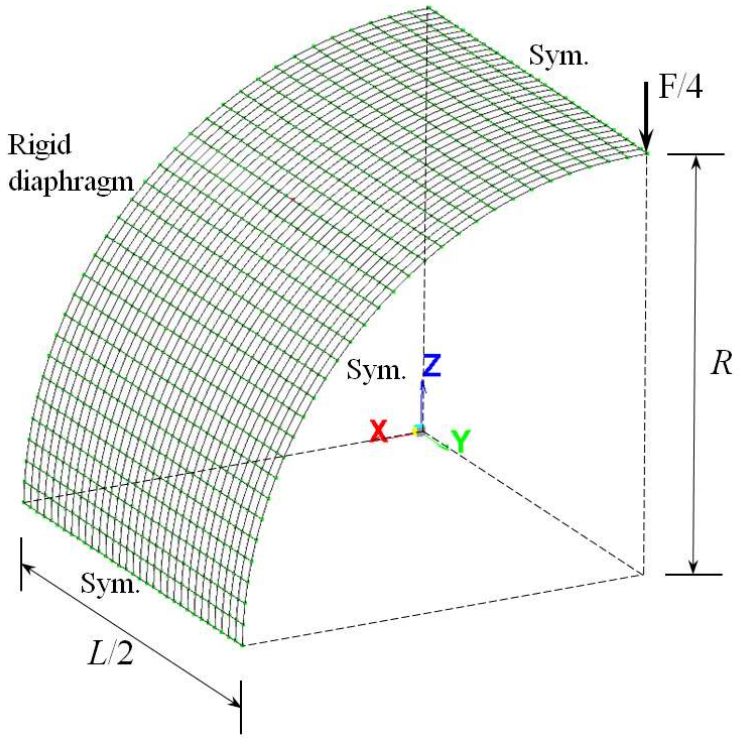

Figure 7.31 Pinched cylinder under a pair of point loads

Due to symmetry, only one eighth of the cylinder is analysed with a regular mesh of 32×32 elements, as depicted in Figure 7.31. The results of vertical displacements under the point load obtained by the proposed shell elements are plotted in Figure 7.32, compared with those obtained by Brank et al. (1997) where the same mesh of a nonlinear 4-node isoparametric quadrilateral shell element was used to model the pinched cylinder.

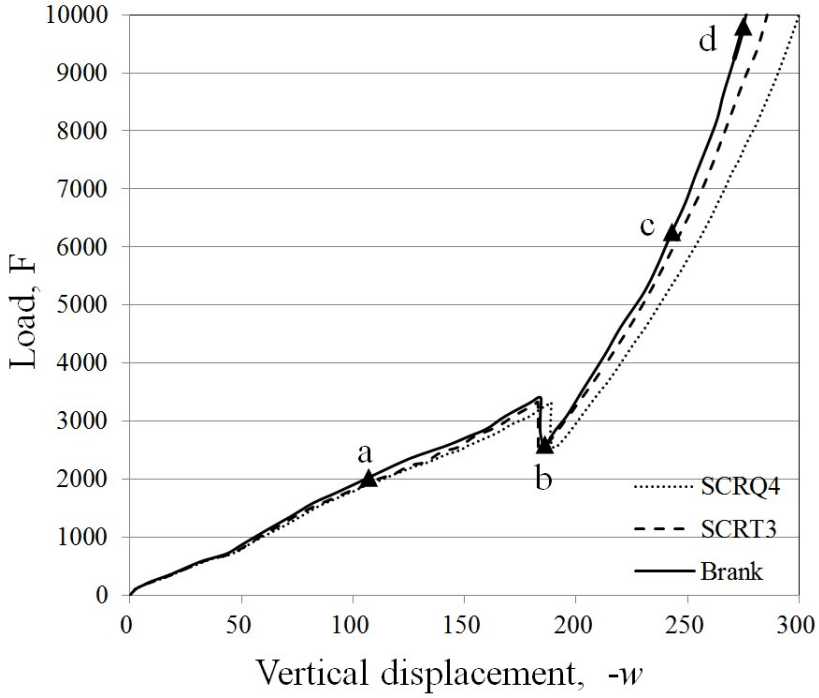

Figure 7.32 Load-displacement curves of pinched cylinder

The result obtained by the SCRT3 element is close to those observed by Brank et al., while the SCRQ4 element is slightly softer. However, the snap-through response of the cylinder can be accurately observed by these shell elements with the similar limit points and stiffening behaviour. The deformed shapes obtained by the SCRT3

element in the program NIDA at the Points a, b, c and d and the corresponding values of the vertical displacements are shown in Figure 7.33 respectively.

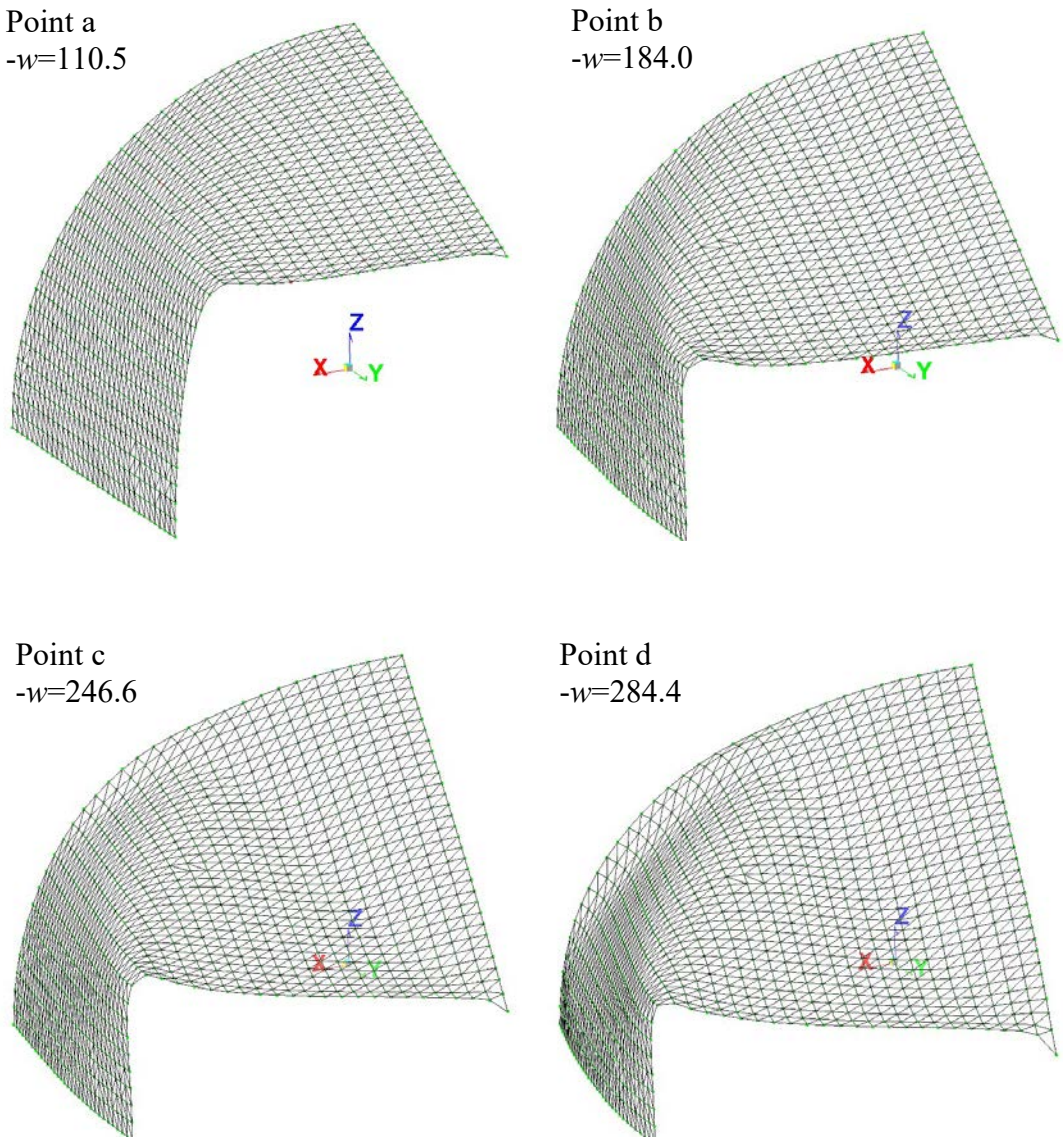

Figure 7.33 Deformed shapes of pinched cylinder

7.2.3 Scordelis-Lo roof under a gravity load

The Scordelis-Lo roof subjected to a uniform gravity load is a classical benchmark problem for testing geometrically nonlinear elastoplastic shell elements, with performed by many researchers (Argyris et al., 2002b; Battini and Pacoste, 2006; Brank et al., 1997; Kim and Lomboy, 2006; Peric and Owen, 1991; Roehl and Ramm, 1996). The roof has a half-length of L=7.6m, radius of R=7.6m, thickness of t=0.076m and half-angle of θ=40˚. It is subjected to a uniform gravity load on the roof with a reference value p_0 = 4.0kN/m^2 and supported by rigid diaphragms at its ends. The material properties are listed below.

Length L=600, radius R=300, thickness t=3.

Young's modulus E=2.1×10^{4}kN/m^2, Poisson's ratio v=0.

Initial yield stress σ_y=4.2kN/m^2, hardening parameter H=0.

Due to symmetry, only one quarter of the roof is modelled with the proposed shell elements using a 16×16 mesh in the program NIDA and the symmetric boundary conditions are applied along the lines X=0 and Y=0, while the mesh of the SCRQ4 element in NIDA is shown in Figure 7.34.

The gravity load versus vertical displacement curves at the point A obtained by the proposed shell elements are plotted in Figure 7.35. For comparison, the results from a 50×50 mesh of a quadrilateral shell element by Brank et al. (1997), a 12×12 mesh of a seven-parameter shell element by Roehl and Ramm (1996) and a 32×32 mesh of a co-rotational quasi-conforming 4-node shell element with 7 stress points by Kim and Lomboy (2006) are also shown in Figure 7.35.

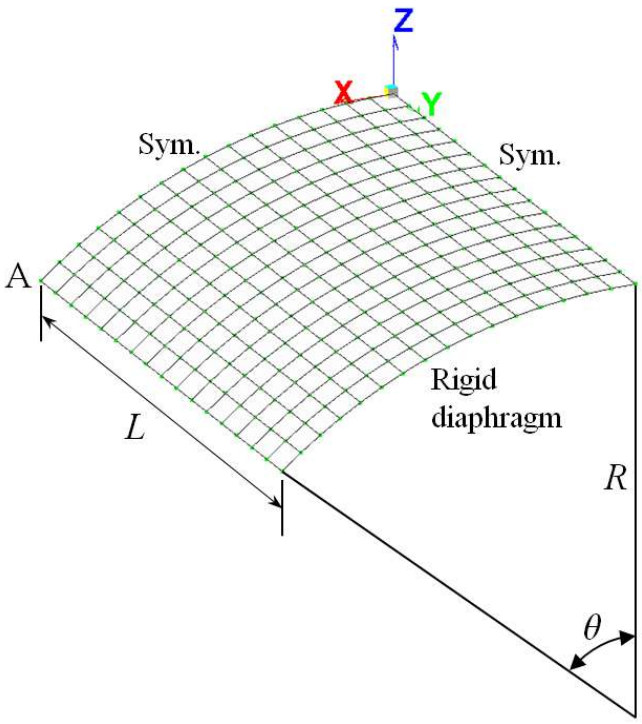

Figure 7.34 Scordelis-Lo roof

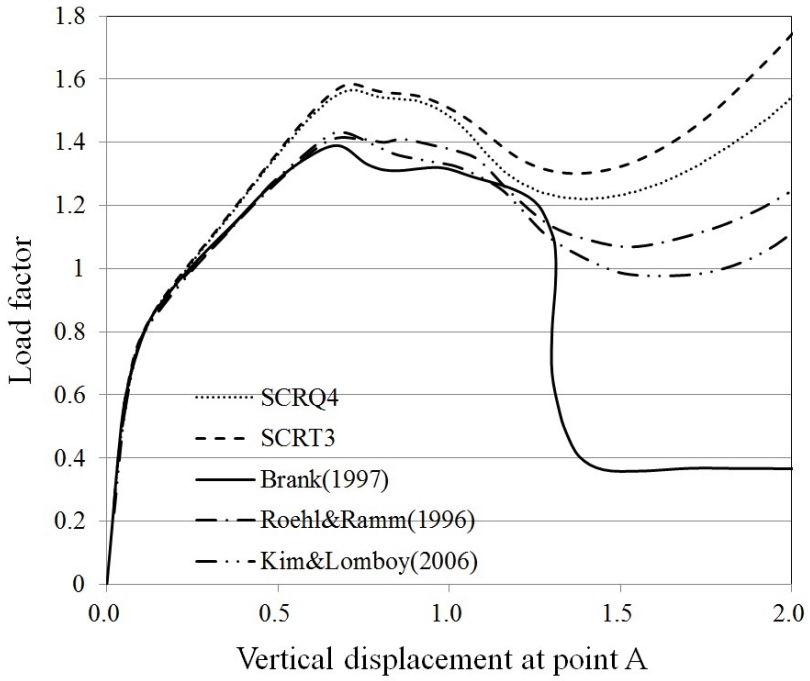

Figure 7.35 Load-displacement curves of Scordelis-Lo roof

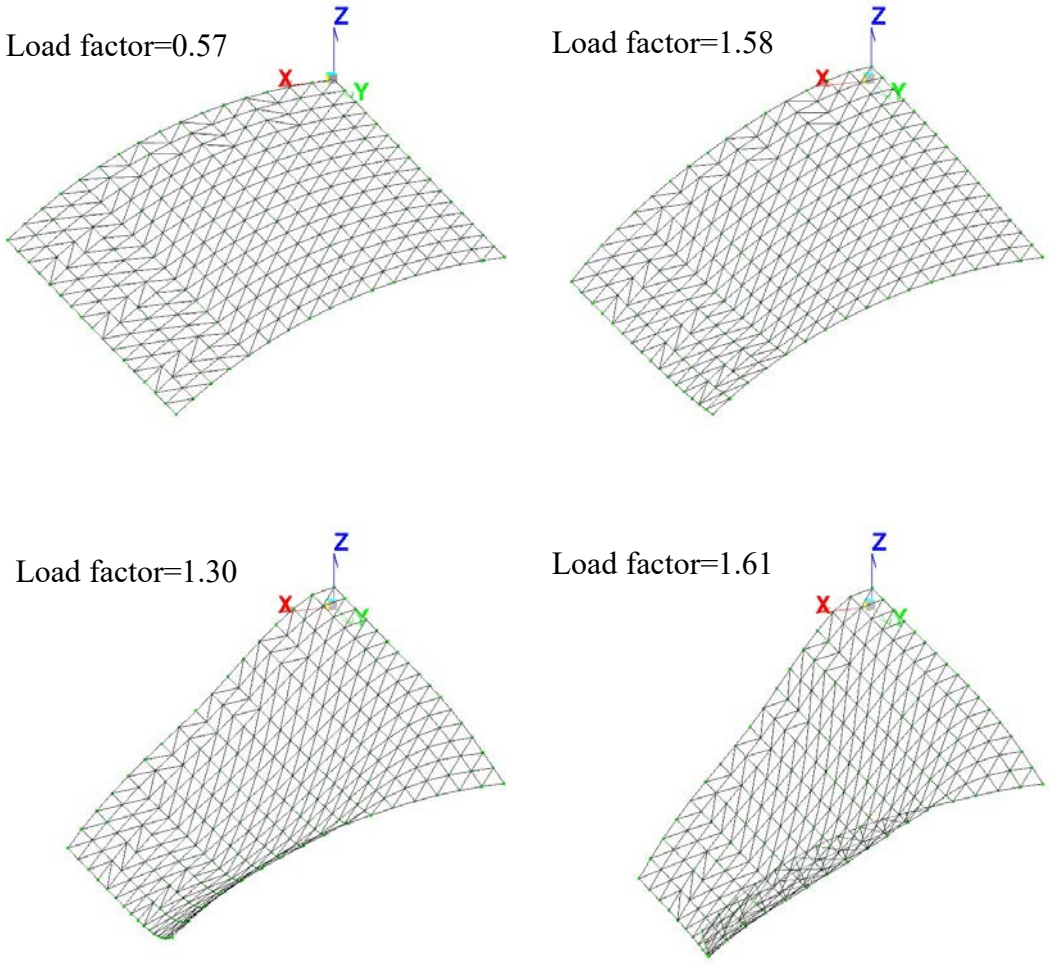

Figure 7.36 Deformed shapes of Scordelis-Lo roof

Actually, it has been found by many researchers that this problem has two solution trends. One has a sudden drop in load carrying capacity, such as the results obtained by Brank *et al.* (1997). The other one has a less drastic loss capacity with a gain in stability as the deflection increases. The results obtained by the proposed shell elements in NIDA are the latter solution type, as well as those obtained by Roehl and Ramm (1996) and Kim and Lomboy (2006). This example is sensitive to meshing size, element type, number of integration points through the thickness, etc. In any case, the limit points of load factor obtained by these different elements are close, while

both proposed shell elements have the similar limit points of load factor slightly larger than others. This may be due to the coarse mesh or the stiffness of drill rotations considered. The deformed shapes of the Scordelis-Lo roof at different load steps obtained by the SCRT3 element in the program NIDA are shown in Figure 7.36.

7.2.4 Shallow cylindrical shell under a point load

The geometrically nonlinear elastoplastic analysis of a shallow cylindrical shell under a concentrated vertical load F=1kN is performed in this example. As shown in Figure 7.37, the curved edges of the shell are free in all directions, while the longitudinal edges are hinged. The geometric properties and the material properties are listed below.

Length L=254mm, radius R=2450mm, thickness t=6.35mm and half-angle of θ=5.729578°.

Young's modulus E=3.103kN/mm^2 and Poisson's ratio v=0.3.

Initial yield stress σ_y=0.001kN/mm^2 and hardening parameter H=0.

Due to symmetry, only one quarter of the shell is modelled with a 20×20 mesh of the proposed shell elements, as shown in Figure 7.37. The results obtained by the proposed shell elements in the program NIDA are compared with those from the same mesh of a quadrilateral shell element by Montag et al. (1999). The load-displacement curves at the centre of the shell are plotted in Figure 7.38 which shows that the solutions obtained by these elements are close to each other.

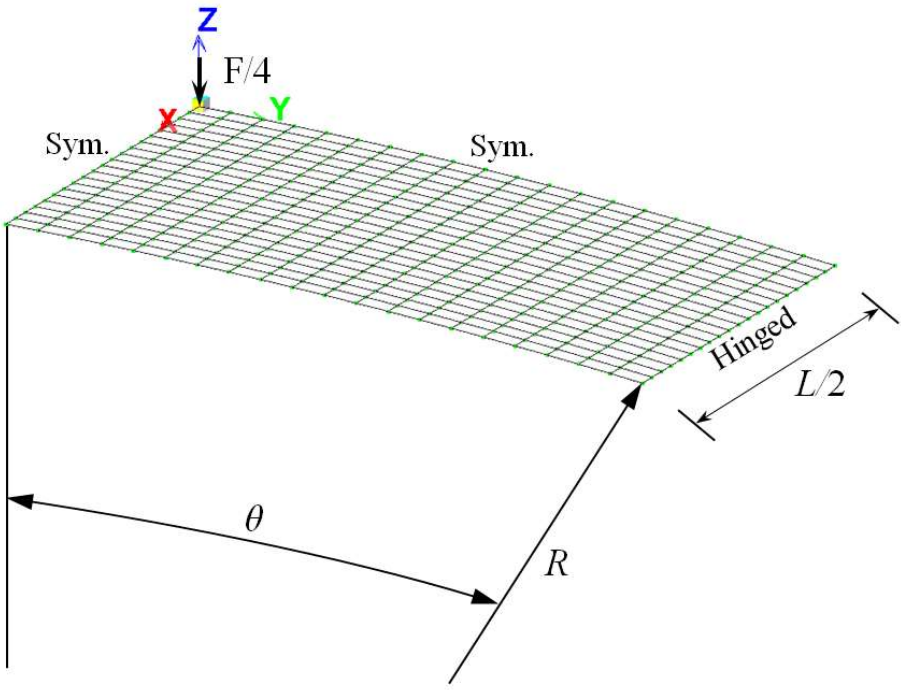

Figure 7.37 Shallow cylindrical shell under a point load

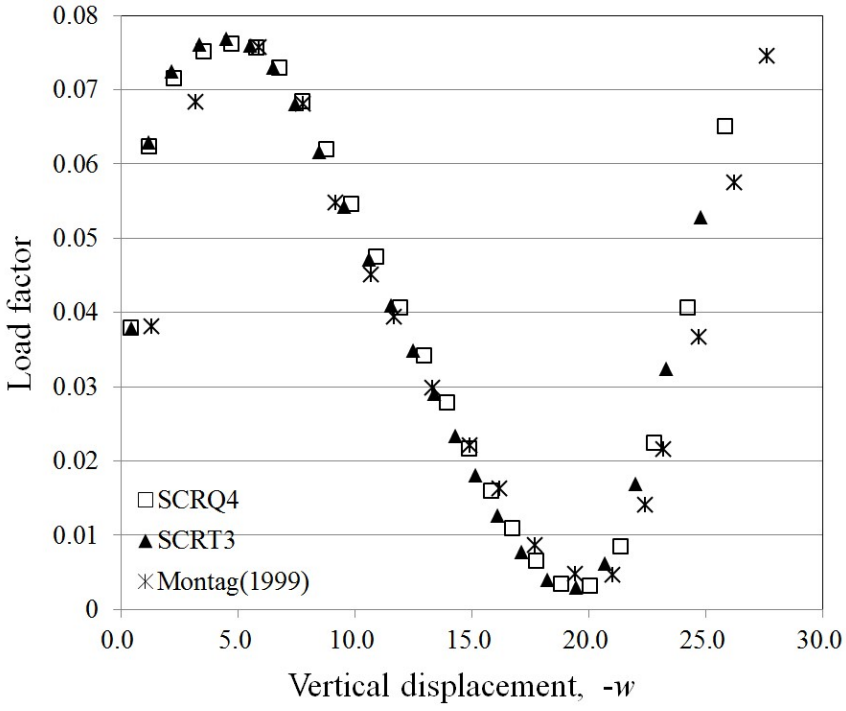

Figure 7.38 Load-displacement curves of shallow cylindrical shell

7.2.5 Square plate under pressure

A simply-supported square plate under uniform pressure load is analysed in this example. It is pinned along all four edges, while the pressure load with a reference value $p_0 = 0.01$ is deformation independent. Only a quarter of the plate is modelled with a 16×16 mesh of the proposed shell elements in the program NIDA due to symmetry. Figure 7.39 depicts the mesh of the SCRQ4 element and boundary conditions. The load factor versus the vertical displacement at the centre of the square plate is plotted in Figure 7.40, and the presented results in NIDA are compared with those from a 24×24 mesh of an eight-node C^0 shell element by Schieck *et al.* (1999). The geometric properties and the material properties are listed below.

Length of the plate $2L$=508, thickness t=2.54.

Young's modulus E=6.9×10^4 and Poisson's ratio ν=0.3.

Initial yield stress σ_y=248 and hardening parameter H=0.

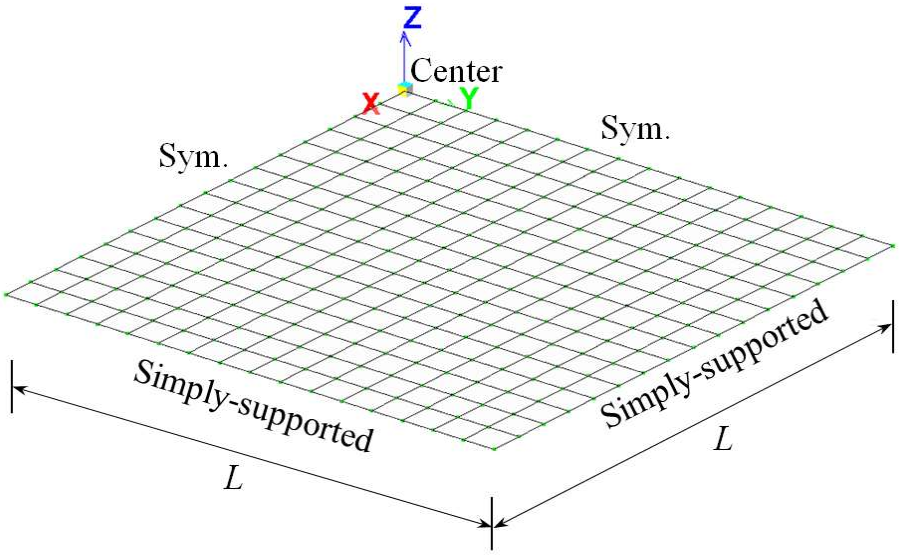

Figure 7.39 Simply-supported square plate under pressure

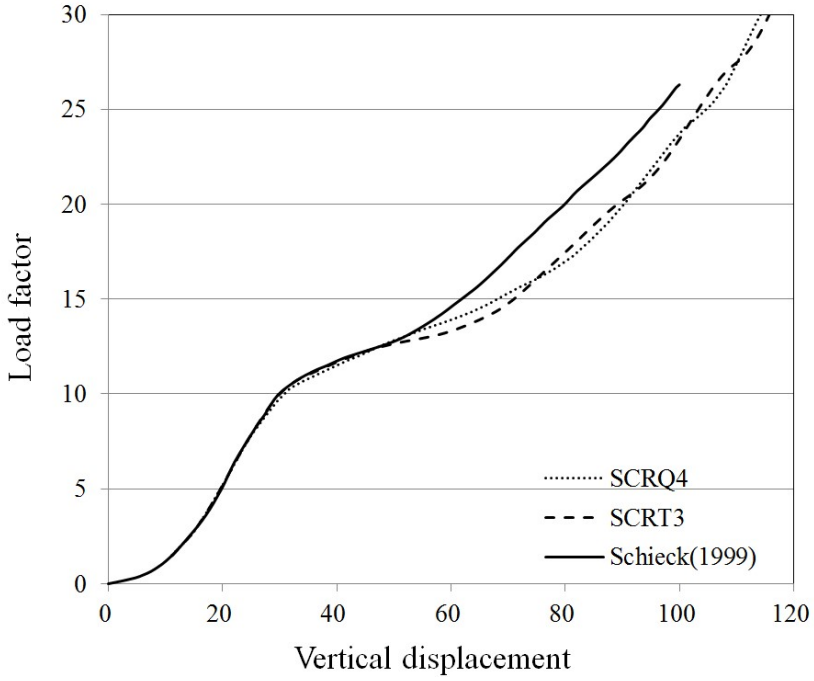

Figure 7.40 Load-deflection curve of simply-supported square plate

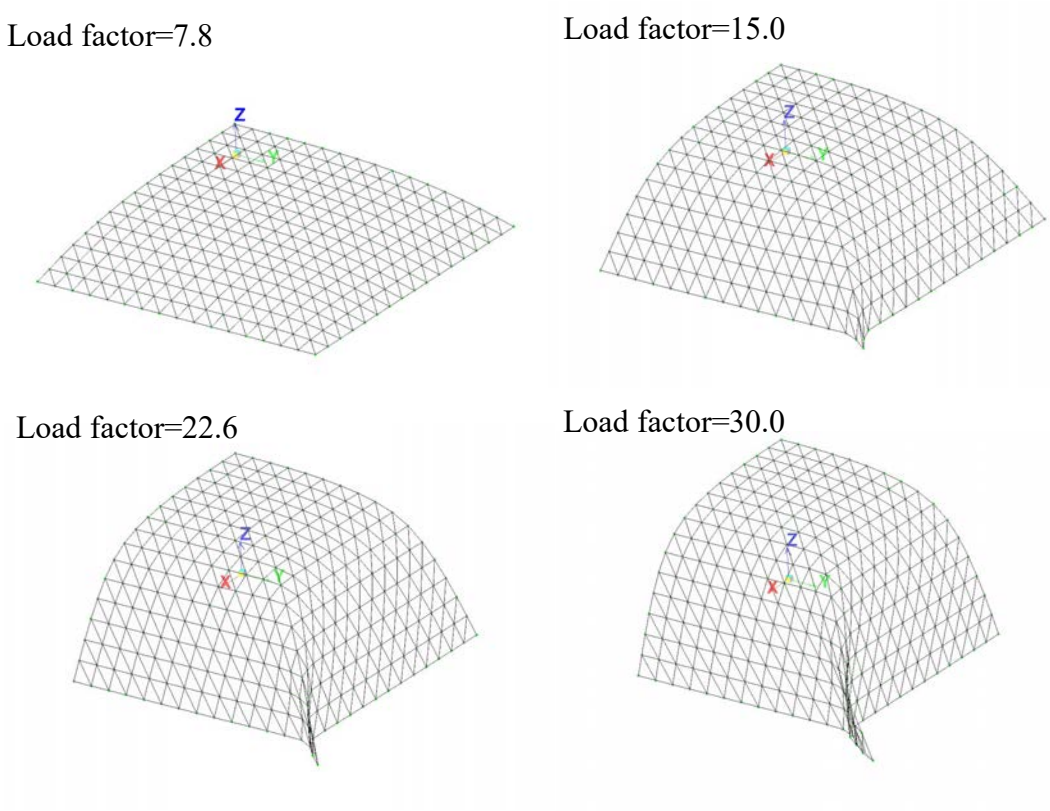

Figure 7.41 Deformed shapes of simply-supported square plate

7.2.6 Pinched hemispherical shell

A hemispherical shell subjected to two pairs of inward and outward forces at the quarter points of its open edge is analysed in this example. The two applied loads have a reference value of F=0.001. The geometric properties and the material properties are listed below.

Radius R=10, thickness t=0.5.

Young's modulus E=10.0 and Poisson's ratio ν=0.2.

Initial yield stress σ_y=0.2 and hardening parameter H=9.0.

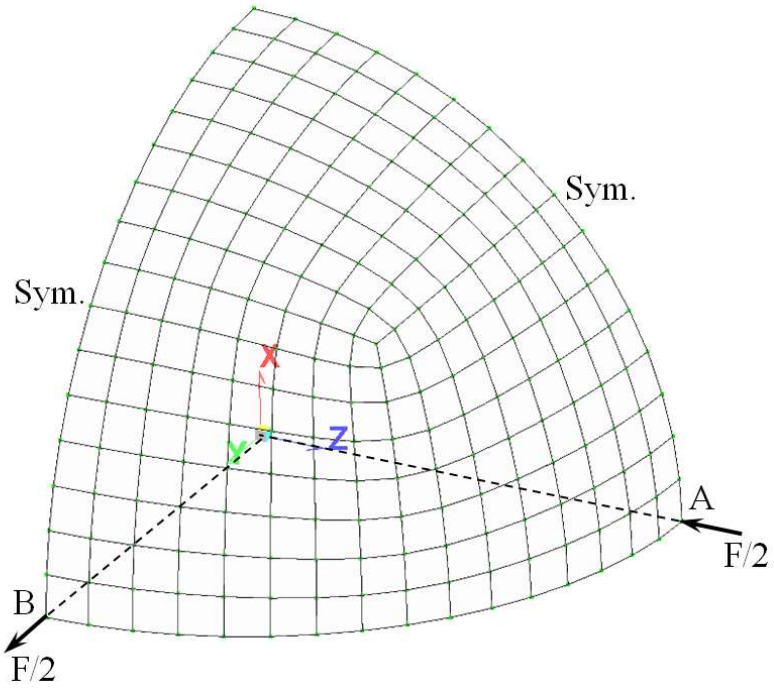

Figure 7.42 Pinched hemispherical shell

Due to symmetry, only one quarter of the hemispherical shell is modelled with a 12×12 mesh of the proposed shell element in the program NIDA, as shown in Figure

7.42. The load factors versus the normal displacements at the pinching points A and B are plotted in Figure 7.43. The results obtained by the proposed shell elements are compared with those from a 12×12 mesh of a 3-node flat triangular shell element by Argyris et al. (2002b). And Figure 7.43 shows that these different shell elements are in good agreement with each other.

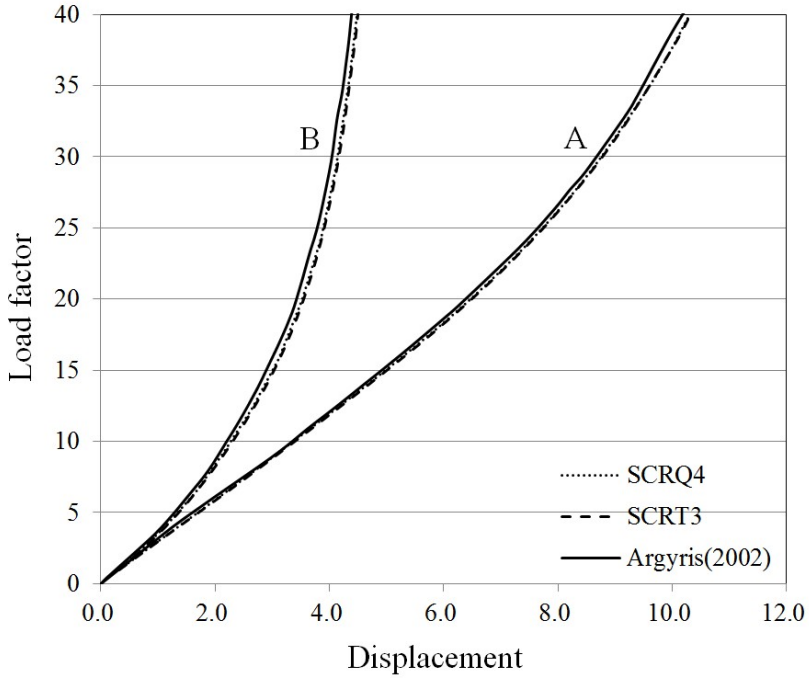

Figure 7.43 Load-displacement curves of pinched hemispherical shell

7.2.7 Angle section beam under compression

The elastic and elastoplastic buckling analyses of angle section beam are performed in this example. As shown in Figure 7.44, the angle section beam is fixed at one end and

free at the other end, and a compression load **P** is applied to the point A at the free end section. The material properties are listed below.

Young's modulus E=2.1×10^6 and Poisson's ratio v=0.3.

Initial yield stress σ_y=500 and hardening parameter H=48325.

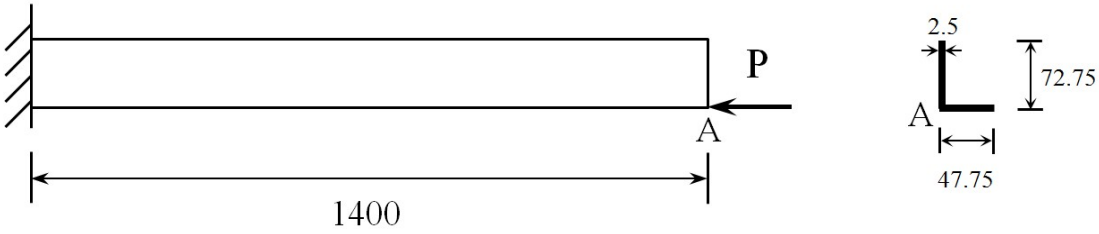

Figure 7.44 Angle section beam

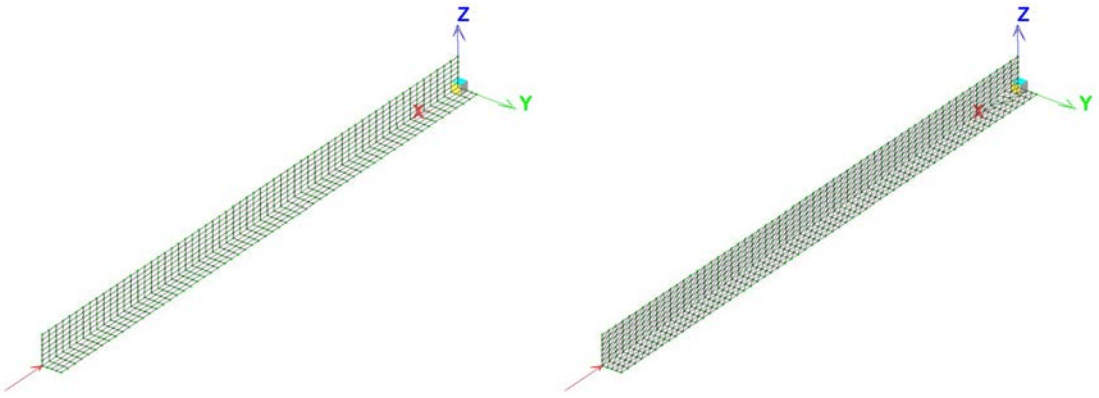

(a) SCRQ4 (b) SCRT3

Figure 7.45 Meshes of angle section beam

In the program NIDA, the angle section beam is modelled with a (4+6)×60 mesh of the proposed shell elements, as shown in Figure 7.45. The compression load versus

the axial displacement at the point A for elastic and elastoplastic analyses are depicted in Figure 7.46 and compared with the results obtained by Battini and Pacoste (2006) where a nonlinear flat triangular shell element, consisting of the OPT membrane element with drilling rotations (Felippa, 2003) and the DKT plate element (Batoz et al., 1980a), was proposed based on the general EICR formulation.

Figure 7.46 shows that the results obtained by the SCRQ4 element are slightly softer than those in the reference, while the results obtained by the SCRT3 element are slightly stiffer. This problem is a membrane-dominated case, so that the difference between these shell elements may be mainly due to the membrane elements. It also can be noticed that considering of the elastoplastic behaviour decreases the limit point of the compression load in this example.

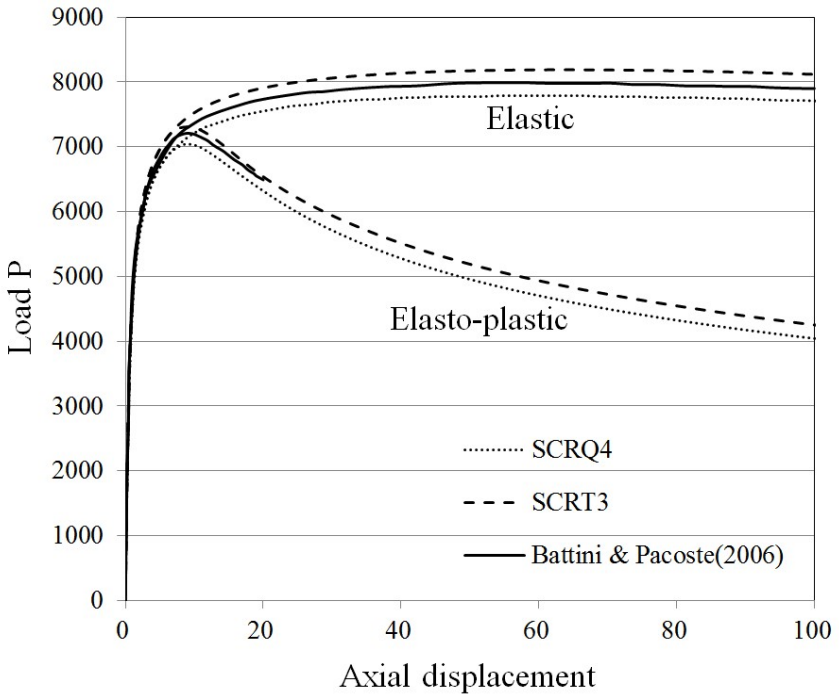

Figure 7.46 Load-displacement curves of angle section beam

7.3 Summary

In this chapter, the proposed SCRT3 and SCRQ4 shell elements are extensively verified by many numerical examples. It is shown that the proposed simplified EICR formulations with the proposed triangular and quadrilateral shell elements are not only concise but also accurate and efficient.

Although the simplified EICR formulations lead to unsymmetrical geometric stiffness matrices which cannot be used in the conventional solvers only allowing for symmetric matrices, the numerical examples demonstrate that the unsymmetrical part of geometric stiffness has insignificant impacts on the accuracy and efficiency of most problems, except for the problem of a cantilever beam rolling up to a circle using large load steps. In this example, the proposed shell elements using the symmetrized geometric stiffness matrices cannot complete the whole analysis due to large load steps. However, when smaller load steps are used, the difference between the unsymmetrical geometric stiffness matrices and the symmetrized ones can be decreased or removed. Moreover, for some elastic numerical examples, the proposed shell elements with the symmetrized geometric stiffness matrices perform better than the SHELL181 element in ANSYS in terms of accuracy and efficiency.

As mentioned in the previous chapter, the proposed simplified co-rotational method is element-independent. Particularly, its geometric stiffness matrix is independent of the local shell element formulation. This is very different from the conventional geometrically nonlinear analysis based on the total and updated Lagrangian formulations with Green-Lagrangian strains. Thus, when transverse shear deformation

or material nonlinearity is taken into account based on the EICR formulations, it merely needs to modify the local shell element formulation. In addition, the numerical examples show that the proposed shell elements can accurately and efficiently solve the problems allowing for transverse shear deformation and elastoplastic behaviour.

This chapter covers membrane-dominated, bending-dominated and mixed shell problems. All these problems can be solved by the proposed shell elements accurately, although there are small differences between the SCRQ4 and SCRT3 shell elements in some cases which mainly are membrane-dominated and mixed problems. This is because the membrane elements adopted in the SCRQ4 and SCRT3 shell elements are derived based on different methods, especially for the problems in which the drilling stiffness plays an important role. Thus, it is important to select accurate local shell elements for the EICR formulations.

CHAPTER 8

CONCLUSIONS AND RECOMMENDATIONS

8.1 Conclusions

This thesis focuses on the development of shell elements and the formulations for nonlinear analysis. Specifically, this research is devoted to: (1) propose a novel pure deformational method for shell elements which is element-independent and consistent with the co-rotational formulation; (2) formulate a novel element-independent co-rotational formulation based on the presented pure deformational method, whose derivation is much simpler than the traditional method; (3) simplify the co-rotational formulation based on the physical interpretation and the small strains assumption and therefore proposing a simplified co-rotational formulation; (4) develop a 3-node geometrically nonlinear triangular shell element allowing for drilling rotations and transverse shear deformation based on the simplified co-rotational formulation, which is named as SCRT3 and further simplified by using the proposed pure deformational method; (5) derive a 4-node geometrically nonlinear quadrilateral shell element based on the simplified co-rotational formulation, which is named as SCRQ4 and allows for drilling rotations, transverse shear deformation, invariance to nodal ordering and insensitivity to irregular meshes; (6) consider material nonlinearity in the SCRT3 and SCRQ4 shell elements through the layered method; (7) code the proposed shell elements into the program NIDA to realize geometrically nonlinear elastic and elastoplastic analyses of shell structures and verifying their accuracy and efficiency

through a number of benchmark problems. The main contributions and conclusions of this dissertation are summarized as follows.

1. A novel pure deformational method for 3-node triangular and 4-node quadrilateral shell elements based on the first-edge definition of the local coordinate system, in which the *x*-axis is aligned with one side, is proposed. The new method is different from the traditional natural mode method by Argyris *et al.* (1979). The local displacements of a shell element can be regarded as pure deformations through the first-edge definition of the local coordinate system. This is because there are six degrees of freedom of a shell element are restrained and the corresponding local displacements are zero. Compared with the conventional isoparametric finite element formulation, the pure deformational method separates the pure deformations from the rigid body movements of an element and then decreases the element quantities, so the local element formulation based on the basic coordinate system with fewer qualities is simpler and has substantial computational advantages, especially for the elements requiring numerical integration and having complicated formulations. Also, the new pure deformational method for shell elements is element-independent and can be applied for any 3-node triangular and 4-node quadrilateral shell elements. However, compared with the method used for beam-column elements, the derivation of the proposed method is more complicated, since a beam-column element can be simplified as a 2D problem while a shell element is a 3D problem.

2. A novel co-rotational method with element-independence for geometrically nonlinear analysis is proposed, which is consistent with the proposed pure deformational method. Different from the traditional co-rotational method firstly introduced by Rankin and Brogan (1986) with a strict and complete derivation, the

proposed one is derived from the physical interpretations based on the local coordinate system of a shell element. The geometric stiffness of a triangular shell element has three parts. They are due to the rigid body movements of the shell element, the changes of dimensions of the membrane and plate element, respectively. The geometric stiffness of a quadrilateral shell element has one more part due to the change of warping. The proposed co-rotational method has clear physical meanings and is simpler and easier to visualize than the traditional one. It is also consistent with the proposed pure deformational method. Compared with the total and updated Lagrangian formulations based on Green-Lagrangian strains, the co-rotational formulation is easier to be integrated with many existing linear elements to extend them to conduct geometrically nonlinear analysis as the local element formulations and the geometrically nonlinear procedure are separated. The geometric stiffness in the element-independent co-rotational formulation is explicit and formulated by the nodal internal forces of the element rather than the stresses at the integration points used in the TL and UL formulations. Also, material nonlinearity only need to be considered in the local element formulation and treated separately from geometrical nonlinearity in the element-independent co-rotational formulation. Thus, simplifying the co-rotational formulation is vital to finite element nonlinear analysis.

3. Based on the former proposed co-rotational method, a simplified co-rotational method inheriting the property of element-independence is proposed. The simplified one neglects the change of dimensions of the membrane and plate elements in the derivation of the geometric stiffness according to the small strain assumption, which makes its formulation simpler again. Finally, in the simplified co-rotational formulation, triangular shell elements merely need the geometric stiffness due to the

rigid body movements, while the geometric stiffness of quadrilateral shell elements is contributed by rigid body movements and warping.

4. A 3-node triangular shell element is developed for geometrically nonlinear analysis based on the simplified EICR formulation, named as SCRT3 shell element. The new shell element consists of the optimal triangular (OPT) membrane element with drilling rotations by Felippa (2003) and the refined triangular (RDKT) Mindlin-Reissner plate element allowing for transverse shear deformation by Chen and Cheung (2001). Both the membrane and the plate elements have good performances and were usually extended into nonlinear analysis for shell structures by many researchers. Further, these elements are simplified using the proposed pure deformational method. It is clear to see the effect of simplification through the comparison in Chapter 5.

5. A 4-node quadrilateral shell element is developed for geometrically nonlinear analysis based on the simplified EICR formulation, named as SCRQ4 shell element. The membrane part of SCRQ4 with drilling rotations was proposed by Ibrahimbegovic et al. (1990) based on a mixed variational formulation with independent rotation fields. The plate part of SCRQ4 allowing for transverse shear deformation was developed by Chen and Cheung (2000) based on the Mindlin-Reissner plate theory, in which the exact displacement function of the Timoshenko's beam is used to derive the displacement interpolations of the plate element. For the SCRQ4 shell element, the bisector definition of the local coordinate system is used. Although the variations of the rigid body rotations are more complicated than the one for the first-edge definition of the local coordinate system,

the bisector definition makes the SCRQ4 shell element invariant to the nodal ordering and more accurate for coarse-mesh models.

6. The proposed geometrically nonlinear shell elements based on the simplified co-rotational formulation are extended to geometrically nonlinear elastoplastic analysis. In the computational procedure, material and geometrical nonlinearities can be separated. The elastoplastic behaviour only needs to be considered in the local element formulation. Specifically, the layered approach is used to simulate the elastoplastic behaviour through the thickness, in which the thickness is divided into several layers and each layer uses the plane stress description. For the elastoplastic constitutive model, the von Mises yield criterion, the associated flow rule and the linear isotropic hardening are assumed. An implicit backward Euler return-mapping integration algorithm is used to update stresses in plastic deformation. To avoid the spurious unloading phenomenon, the incremental displacements rather than the iterative displacements should be used in the procedure of updating internal forces.

7. The proposed shell elements for geometrically nonlinear elastic and elastoplastic analysis were implemented in the NIDA software. To comply with the solver for symmetric matrices in most programs like NIDA and improve computational efficiency, the unsymmetrical geometric stiffness matrix derived by the simplified co-rotational formulation is symmetrized. A number of numerical examples are performed to verify the efficiency and accuracy of the proposed shell elements. It is proved that the symmetrized geometric stiffness matrix has insignificant effects on the results and the numbers of load steps for most problems. The presented benchmark problems contain membrane-dominated, bending-dominated and mixed shell situations. All of them can be solved by the proposed shell elements with efficiency

and accuracy in NIDA. Some of these examples have very large displacements and large rotations, far beyond the requirements of civil engineering structures. Thus, the proposed nonlinear shell elements are fully suitable for civil engineering structures. Most importantly, the proposed simplified co-rotational formulation with acceptable accuracy is much simpler than the traditional formulations for geometrically nonlinear analysis, and therefore it can improve the efficiency of nonlinear analysis and design for plate and shell structures in civil engineering.

8.2 Recommendations for future work

Although some unique works and improvements for nonlinear analysis of shell structures have been made in this thesis, there are several important issues requiring future studies.

1. The novel pure deformational technique has been successfully applied in the triangular and quadrilateral shell elements and it contributes to a novel derivation of the element-independent co-rotational algorithm. However, it only can be used in the elements using the first-edge definition of the local coordinate system where one axis is aligned with one element side, and the first-edge definition often makes the element sensitive to the nodal ordering in some cases. The other definitions of the local coordinate system cannot restrain the displacements and rotations of the element, as a result, the element quantities cannot be reduced. However, the derivation by the proposed pure deformational method can be used to find the relationship between these element quantities. In a word, more works are needed to extend the pure

deformational method into the other definitions of local coordinate system and make the element invariant to the nodal ordering.

2. The proposed simplified co-rotational algorithm is much simpler than the conventional one and keeps element-independence, efficiency and accuracy. However, it produces unsymmetrical geometric stiffness like the conventional method. This is not good for matrix computation. Although the symmetrized geometric stiffness has little influence on results and convergence, it cannot be eliminated completely. This problem needs more discussions.

3. The local triangular and quadrilateral shell elements are flat, and the warping phenomenon in the quadrilateral shell element is regarded as eccentricities at nodes. Thus, for the flat shell structures with large curvature, refined meshes of the proposed shell elements should be used to obtain acceptable results. To improve their performance in the simulations of shell structures with large curvature, the total Lagrangian formulation based on the degenerated Green-Lagrangian strains, known as the shallowly curved shell theory, can be used to establish the local shell element formulation and then consider moderate strains. Although the local material stiffness matrix becomes complicated and nonlinear, it does not affect the geometric stiffness derived based on the simplified co-rotational method.

4. To consider material nonlinearity in the proposed shell elements, this thesis adopts the layered approach. The relevant computational procedure is easily extended to that for composite shell elements. The main difference is that layers of a composite shell element may have different thicknesses and material properties.

5. In addition to the layered approach to consider material nonlinearity, an alternative method is the non-layered approach which use stress resultants to take into account the elastoplastic behaviour and does not need the division of shell element thickness. Thus, the non-layered approach which is more efficient can be integrated with the simplified co-rotational formulation.

6. For the elastoplastic constitutive model, this thesis adopts the von Mises yield function, the associated flow rule and the linear isotropic hardening. Actually, more formulations and theories about nonlinear constitutive modelling can be used here, such as the Mohr-Coulomb failure criterion describing the response of concrete, the non-associated flow rule, kinematic hardening, multilinear hardening, etc. Moreover, even damage constitutive equations can be used with the proposed simplified co-rotational method.

7. The proposed simplified co-rotational formulation can be extended to the dynamic nonlinear analysis.

8. Design methods such as shear wall design can be integrated into the proposed geometrically nonlinear elastoplastic analysis procedure.

REFERENCES

Aalto, J. (1988). From Kirchhoff to Mindlin plate elements. *Communications in applied numerical methods, 4*(2), 231-241.

Ahmad, S., Irons, B. M., & Zienkiewicz, O. C. (1970). Analysis of thick and thin shell structures by curved finite elements. *International Journal for Numerical Methods in Engineering, 2*(3), 419-451.

Allman, D. J. (1984). A compatible triangular element including vertex rotations for plane elasticity analysis. *Computers & Structures, 19*(1), 1-8.

Allman, D. J. (1987). The constant strain triangle with drilling rotations: a simple prospect for shell analysis. *Mathematics of Finite Elements and Applications VI,* 233-240: Academic Press.

Allman, D. J. (1988a). A quadrilateral finite element including vertex rotations for plane elasticity analysis. *International Journal for Numerical Methods in Engineering, 26*(3), 717-730.

Allman, D. J. (1988b). Evaluation of the constant strain triangle with drilling rotations. *International Journal for Numerical Methods in Engineering, 26*(12), 2645-2655.

Almeida, F., & Awruch, A. (2011). Corotational nonlinear dynamic analysis of laminated composite shells. *Finite Elements in Analysis and Design, 47*(10), 1131-1145.

Alves de Sousa, R., Natal Jorge, R., Fontes Valente, R., & César de Sá, J. (2003). A new volumetric and shear locking-free 3D enhanced strain element. *Engineering computations, 20*(7), 896-925.

Alves de Sousa, R. J., Cardoso, R. P., Fontes Valente, R. A., Yoon, J. W., Grácio, J. J., & Natal Jorge, R. M. (2006). A new one-point quadrature enhanced assumed

strain (EAS) solid-shell element with multiple integration points along thickness:part II: nonlinear applications. *International Journal for Numerical Methods in Engineering, 67*(2), 160-188.

Alvin, K., Horacio, M., Haugen, B., & Felippa, C. A. (1992). Membrane triangles with corner drilling freedoms:I. The EFF element. *Finite Elements in Analysis and Design, 12*(3-4), 163-187.

Andelfinger, U., & Ramm, E. (1993). EAS-elements for two-dimensional, three-dimensional, plate and shell structures and their equivalence to HR-elements. *International Journal for Numerical Methods in Engineering, 36*(8), 1311-1337.

ANSYS® Academic Research, Release 16.2.

Arciniega, A., & Roman, A. (2006). *On a tensor-based finite element model for the analysis of shell structures*: Texas A&M University.

Arciniega, R., & Reddy, J. (2007). Tensor-based finite element formulation for geometrically nonlinear analysis of shell structures. *Computer Methods in Applied Mechanics and Engineering, 196*(4), 1048-1073.

Areias, P., César de Sá, J., António, C., & Fernandes, A. (2003). Analysis of 3D problems using a new enhanced strain hexahedral element. *International Journal for Numerical Methods in Engineering, 58*(11), 1637-1682.

Areias, P., Garção, J., Pires, E., & Barbosa, J. I. (2011). Exact corotational shell for finite strains and fracture. *Computational Mechanics, 48*(4), 385-406.

Argyris, J. H. (1982). An excursion into large rotations. *Computer Methods in Applied Mechanics and Engineering, 32*(1), 85-155.

Argyris, J. H., Papadrakakis, M., Apostolopoulou, C., & Koutsourelakis, S. (2000a). The TRIC shell element: theoretical and numerical investigation. *Computer Methods in Applied Mechanics and Engineering, 182*(1), 217-245.

Argyris, J. H., Papadrakakis, M., & Mouroutis, Z. S. (2003). Nonlinear dynamic analysis of shells with the triangular element TRIC. *Computer Methods in Applied Mechanics and Engineering, 192*(26), 3005-3038.

Argyris, J. H., Papadrakakis, M., & Stefanou, G. (2002a). Stochastic finite element analysis of shells. *Computer Methods in Applied Mechanics and Engineering, 191*(41), 4781-4804.

Argyris, J. H., Tenek, L., & Olofsson, L. (1997). TRIC: a simple but sophisticated 3-node triangular element based on 6 rigid-body and 12 straining modes for fast computational simulations of arbitrary isotropic and laminated composite shells. *Computer Methods in Applied Mechanics and Engineering, 145*(1-2), 11-85.

Argyris, J. H., Tenek, L., Papadrakakis, M., & Apostolopoulou, C. (1998). Postbuckling performance of the TRIC natural mode triangular element for isotropic and laminated composite shells. Computer Methods in Applied Mechanics and Engineering, 166(3-4), 211-231.

Argyris, J. H., Balmer, H., Doltsinis, J. S., Dunne, P. C., Haase, M., Kleiber, M., . . . Scharpf, D. W. (1979). Finite element method-the natural approach. Computer Methods in Applied Mechanics and Engineering, 17, 1-106.

Argyris, J. H., Papadrakakis, M., Apostolopoulou, C., & Koutsourelakis, S. (2000b). The TRIC shell element: theoretical and numerical investigation. Computer Methods in Applied Mechanics and Engineering, 182(1), 217-245.

Argyris, J. H., Papadrakakis, M., & Karapitta, L. (2002b). Elasto-plastic analysis of shells with the triangular element TRIC. Computer Methods in Applied Mechanics and Engineering, 191(33), 3613-3636.

Baecklund, J. (1973). Finite element analysis of nonlinear structures.

Başar, Y., & Ding, Y. (1992). Finite-rotation shell elements for the analysis of finite-rotation shell problems. International Journal for Numerical Methods in Engineering, 34(1), 165-169.

Bathe, K. J. (2006). Finite element procedures: Klaus-Jurgen Bathe.

Bathe, K. J. (2016). Finite element procedures (2nd ed.): United States of America.

Bathe, K. J., & Bolourchi, S. (1980). A geometric and material nonlinear plate and shell element. Computers & Structures, 11(1), 23-48.

Bathe, K. J., Brezzi, F., & Cho, S. W. (1989). The MITC7 and MITC9 plate bending elements. Computers & Structures, 32(3), 797-814.

Bathe, K. J., & Ho, L. W. (1981). A simple and effective element for analysis of general shell structures. Computers & Structures, 13(5-6), 673-681.

Bathe, K. J., Iosilevich, A., & Chapelle, D. (2000a). An evaluation of the MITC shell elements. Computers & Structures, 75(1), 1-30.

Bathe, K. J., Iosilevich, A., & Chapelle, D. (2000b). An inf-sup test for shell finite elements. Computers & Structures, 75(5), 439-456.

Bathe, K. J., Lee, P. S., & Hiller, J. F. (2003). Towards improving the MITC9 shell element. Computers & Structures, 81(8), 477-489.

Bathe, K. J., & Bolourchi, S. (1979). Large displacement analysis of three-dimensional beam structures. International Journal for Numerical Methods in Engineering, 14(7), 961-986.

Bathe, K. J., Dvorkin, E., & Ho, L. W. (1983). Our discrete-Kirchhoff and isoparametric shell elements for nonlinear analysis: an assessment. Computers & Structures, 16(1-4), 89-98.

Bathe, K. J., & Dvorkin, E. N. (1985). A four-node plate bending element based on Mindlin/Reissner plate theory and a mixed interpolation. International Journal for Numerical Methods in Engineering, 21(2), 367-383.

Bathe, K. J., & Dvorkin, E. N. (1986). A formulation of general shell elements: the use of mixed interpolation of tensorial components. International Journal for Numerical Methods in Engineering, 22(3), 697-722.

Batoz, J. L., & Lardeur, P. (1989). A discrete shear triangular nine dof element for the analysis of thick to very thin plates. International Journal for Numerical Methods in Engineering, 28(3), 533-560.

Batoz, J. L. (1982). An explicit formulation for an efficient triangular plate-bending element. International Journal for Numerical Methods in Engineering, 18(7), 1077-1089.

Batoz, J. L., Bathe, K. J., & Ho, L. W. (1980a). A study of three-node triangular plate bending elements. International Journal for Numerical Methods in Engineering, 15(12), 1771-1812.

Batoz, J. L., & Katili, I. (1992). On a simple triangular Reissner/Mindlin plate element based on incompatible modes and discrete constraints. International Journal for Numerical Methods in Engineering, 35(8), 1603-1632.

Batoz, J. L., & Tahar, M. B. (1982). Evaluation of a new quadrilateral thin plate bending element. International Journal for Numerical Methods in Engineering, 18(11), 1655-1677.

Battini, J. M. (2007). A modified corotational framework for triangular shell elements. Computer Methods in Applied Mechanics and Engineering, 196(13), 1905-1914.

Battini, J. M. (2008). A non-linear corotational 4-node plane element. Mechanics research communications, 35(6), 408-413.

Battini, J. M., & Pacoste, C. (2006). On the choice of the linear element for corotational triangular shells. Computer Methods in Applied Mechanics and Engineering, 195(44), 6362-6377.

Battini, J. M., & Pacoste, C. (2004). On the choice of local element frame for corotational triangular shell elements. Communications in numerical methods in engineering, 20(10), 819-825.

Bazeley, G., Cheung, Y. K., Irons, B. M., & Zienkiewicz, O. C. (1966). Triangular elements in plate bending-conforming and non-conforming solutions: Stiffness

characteristics of triangular plate elements in bending, and solutions. 1966., 547-576.

Belytschko, T., & Hsieh, B. (1973). Non-linear transient finite element analysis with convected co-ordinates. International Journal for Numerical Methods in Engineering, 7(3), 255-271.

Belytschko, T., Ong, J. S. J., & Liu, W. K. (1984). A consistent control of spurious singular modes in the 9-node Lagrange element for the Laplace and Mindlin plate equations. Computer Methods in Applied Mechanics and Engineering, 44(3), 269-295.

Belytschko, T., Schwer, L., & Klein, M. (1977). Large displacement, transient analysis of space frames. International Journal for Numerical Methods in Engineering, 11(1), 65-84.

Belytschko, T., Tsay, C., & Liu, W. (1981). A stabilization matrix for the bilinear Mindlin plate element. Computer Methods in Applied Mechanics and Engineering, 29(3), 313-327.

Belytschko, T., & Tsay, C. S. (1983). A stabilization procedure for the quadrilateral plate element with one-point quadrature. International Journal for Numerical Methods in Engineering, 19(3), 405-419.

Bergan, P., & Felippa, C. (1985). A triangular membrane element with rotational degrees of freedom. Computer Methods in Applied Mechanics and Engineering, 50(1), 25-69.

Betsch, P., Gruttmann, F., & Stein, E. (1996). A 4-node finite shell element for the implementation of general hyperelastic 3D-elasticity at finite strains. Computer Methods in Applied Mechanics and Engineering, 130(1-2), 57-79.

Betsch, P., & Stein, E. (1995). An assumed strain approach avoiding artificial thickness straining for a non-linear 4-node shell element. International Journal for Numerical Methods in Biomedical Engineering, 11(11), 899-909.

Bieniek, M., & Funaro, J. (1976). Elasto-plastic behavior of plates and shells: Retrieved from New York

Bischoff, M., & Ramm, E. (1997). Shear deformable shell elements for large strains and rotations. International Journal for Numerical Methods in Engineering, 40(23), 4427-4449.

Brank, B., Perić, D., & Damjanić, F. B. (1997). On large deformations of thin elasto-plastic shells: implementation of a finite rotation model for quadrilateral shell element. International Journal for Numerical Methods in Engineering, 40(4), 689-726.

Brannon, R. (2002). A review of useful theorems involving proper orthogonal matrices referenced to three dimensional physical space: Sandia National Laboratories.

Brezzi, F., Bathe, K. J., & Fortin, M. (1989). Mixed-interpolated elements for Reissner-Mindlin plates. International Journal for Numerical Methods in Engineering, 28(8), 1787-1801.

Bucalem, M. L., & Bathe, K. J. (1997). Finite element analysis of shell structures. Archives of Computational Methods in Engineering, 4(1), 3-61.

Bucalem, M. L., & Bathe, K. J. (1993). Higher-order MITC general shell elements. International Journal for Numerical Methods in Engineering, 36(21), 3729-3754.

Bucalem, M. L., & da Nóbrega, S. H. S. (2000). A mixed formulation for general triangular isoparametric shell elements based on the degenerated solid approach. Computers & Structures, 78(1), 35-44.

Buechter, N., & Ramm, E. (1992). Shell theory versus degeneration: a comparison in large rotation finite element analysis. International Journal for Numerical Methods in Engineering, 34(1), 39-59.

Cai, Y., Tian, L., & Atluri, S. (2011). A simple locking-free discrete shear triangular plate element. Computer Modeling in Engineering & Sciences(CMES), 77(3-4), 221-238.

Cardoso, R. P., Yoon, J. W., Mahardika, M., Choudhry, S., Alves de Sousa, R., & Fontes Valente, R. (2008). Enhanced assumed strain (EAS) and assumed natural strain (ANS) methods for one-point quadrature solid-shell elements. International Journal for Numerical Methods in Engineering, 75(2), 156-187.

Carpenter, N., Stolarski, H., & Belytschko, T. (1985). A flat triangular shell element with improved membrane interpolation. Communications in applied numerical methods, 1(4), 161-168.

Cen, S., & Shang, Y. (2015). Developments of Mindlin-Reissner plate elements. Mathematical Problems in Engineering, 2015.

Chan, S. L., & Gu, J. X. (2000). Exact tangent stiffness for imperfect beam-column members. Journal of Structural Engineering, 126(9), 1094-1102.

Chan, S. L. (1992). Large deflection kinematic formulations for three-dimensional framed structures. Computer Methods in Applied Mechanics and Engineering, 95(1), 17-36.

Chan, S. L., & Chui, P. T. (2000). Non-linear static and cyclic analysis of steel frames with semi-rigid connections: Elsevier.

Chan, S. L., & Zhou, Z. H. (1994). Pointwise equilibrating polynomial element for nonlinear analysis of frames. Journal of Structural Engineering, 120(6), 1703-1717.

Chapelle, D., & Bathe, K. J. (2010). The finite element analysis of shells-Fundamentals: Springer Science & Business Media.

Chen, W. F., & Lui, E. M. (Eds.). (2005). Handbook of structural engineering: CRC press.

Chen, W. J. & Cheung, Y. (1998). Refined triangular discrete Kirchhoff plate element for thin plate bending, vibration and buckling analysis. International journal for numerical methods in engineering, 41(8), 1507-1525.

Chen, W. J., & Cheung, Y. K. (2000). Refined quadrilateral element based on Mindlin/Reissner plate theory. International Journal for Numerical Methods in Engineering, 47(1-3), 605-627.

Chen, W. J., & Cheung, Y. K. (2001). Refined 9-Dof triangular Mindlin plate elements. International Journal for Numerical Methods in Engineering, 51(11), 1259-1281.

Cho, H., Shin, S., & Yoh, J. J. (2017). Geometrically nonlinear quadratic solid/solid-shell element based on consistent corotational approach for structural analysis under prescribed motion. International Journal for Numerical Methods in Engineering.

Cinefra, M., & Carrera, E. (2013). Shell finite elements with different through-the-thickness kinematics for the linear analysis of cylindrical multilayered structures. International Journal for Numerical Methods in Engineering, 93(2), 160-182.

Cook, R. D. (1986). On the Allman triangle and a related quadrilateral element. Computers & Structures, 22(6), 1065-1067.

Cook, R. D. (1987). A plane hybrid element with rotational dof and adjustable stiffness. International Journal for Numerical Methods in Engineering, 24(8), 1499-1508.

Coulomb, C. A. (1773). Essai sur une application des règles de maximis et minimis à quelques problèmes de statique relatifs à l'architecture: Mem. Div. Sav. Acad.

Crisfield, M. (1981). Finite element analysis for combined material and geometric nonlinearities Nonlinear finite element analysis in structural mechanics: Springer, Berlin, Heidelberg.

Crisfield, M. (1991). Nonlinear finite element analysis of solids and structures: Volume 1: Essentials: John Wiley & Sons.

Crisfield, M., & Ciampi, V. (1997). Non-linear Finite Element Analysis of Solids and Structures Vol. 1. Meccanica, 32(6), 586-587.

Crisfield, M., Moita, G., Lyons, L., & Jelenić, G. (1995). Enhanced lower-order element formulations for large strains. Computational mechanics, 17(1-2), 62-73.

Crisfield, M. A., & Moita, G. F. (1996). A unified co-rotational framework for solids, shells and beams. International Journal of Solids and Structures, 33(20), 2969-2992.

da Veiga, L. B., Chapelle, D., & Suarez, I. P. (2007). Towards improving the MITC6 triangular shell element. Computers & Structures, 85(21), 1589-1610.

Dal Cortivo, N., Felippa, C. A., Bavestrello, H., & Silva, W. T. (2009). Plastic buckling and collapse of thin shell structures, using layered plastic modeling and co-rotational ANDES finite elements. Computer Methods in Applied Mechanics and Engineering, 198(5), 785-798.

Drucker, D. C., & Prager, W. (1952). Soil mechanics and plastic analysis or limit design. Quarterly of applied mathematics, 10(2), 157-165.

Dvorkin, E. N., & Bathe, K. J. (1984). A continuum mechanics based four-node shell element for general non-linear analysis. Engineering computations, 1(1), 77-88.

Dvorkin, E. N., Pantuso, D., & Repetto, E. A. (1995). A formulation of the MITC4 shell element for finite strain elasto-plastic analysis. Computer Methods in Applied Mechanics and Engineering, 125(1-4), 17-40.

Dvorkin, E. N., & Toscano, R. G. (2013). Shell Element Formulations for General Nonlinear Analysis. Modeling Techniques Finite Element Analysis of the Collapse and Post-Collapse Behavior of Steel Pipes: Applications to the Oil Industry.

Eberlein, R., & Wriggers, P. (1999). Finite element concepts for finite elastoplastic strains and isotropic stress response in shells: theoretical and computational analysis. Computer Methods in Applied Mechanics and Engineering, 171(3-4), 243-279.

Eriksson, A., & Pacoste, C. (2002). Element formulation and numerical techniques for stability problems in shells. Computer Methods in Applied Mechanics and Engineering, 191(35), 3775-3810.

Farshad, M. (2013). Design and analysis of shell structures (Vol. 16): Springer Science & Business Media.

Felippa, C. A, & Haugen, B. (2005). A unified formulation of small-strain corotational finite elements: I. Theory. Computer Methods in Applied Mechanics and Engineering, 194(21), 2285-2335.

Felippa, C. A. (2003). A study of optimal membrane triangles with drilling freedoms. Computer Methods in Applied Mechanics and Engineering, 192(16), 2125-2168.

Felippa, C. A., & Alexander, S. (1992). Membrane triangles with corner drilling freedoms: III. Implementation and performance evaluation. Finite Elements in Analysis and Design, 12(3-4), 203-239.

Felippa, C. A., & Militello, C. (1992). Membrane triangles with corner drilling freedoms: II. The ANDES element. Finite Elements in Analysis and Design, 12(3-4), 189-201.

Ferreira, A., Carrera, E., Cinefra, M., Roque, C., & Polit, O. (2011). Analysis of laminated shells by a sinusoidal shear deformation theory and radial basis functions collocation, accounting for through-the-thickness deformations. Composites Part B: Engineering, 42(5), 1276-1284.

Flores, F. G. (2016). A simple reduced integration hexahedral solid-shell element for large strains. Computer Methods in Applied Mechanics and Engineering, 303, 260-287.

Fontes Valente, R., Parente, M., Natal Jorge, R., César de Sá, J., & Grácio, J. (2005). Enhanced transverse shear strain shell formulation applied to large elasto-plastic deformation problems. International Journal for Numerical Methods in Engineering, 62(10), 1360-1398.

Gal, E., & Levy, R. (2005). The geometric stiffness of triangular composite-materials shell elements. Computers & Structures, 83(28), 2318-2333.

Gal, E., & Levy, R. (2006). Geometrically nonlinear analysis of shell structures using a flat triangular shell finite element. Archives of Computational Methods in Engineering, 13(3), 331-388.

Goldstein, H. (1950). Classical mechanics. Addison-Wesley World Student Series, Reading, Mass: Addison-Wesley.

Gruttmann, F., & Wagner, W. (2006). Structural analysis of composite laminates using a mixed hybrid shell element. Computational Mechanics, 37(6), 479-497.

Han, S. C., Tabiei, A., & Park, W. T. (2008). Geometrically nonlinear analysis of laminated composite thin shells using a modified first-order shear deformable element-based Lagrangian shell element. Composite Structures, 82(3), 465-474.

Hauptmann, R., & Schweizerhof, K. (1998). A systematic development of 'solid-shell' element formulations for linear and non-linear analyses employing only displacement degrees of freedom. International Journal for Numerical Methods in Engineering, 42(1), 49-69.

Hauptmann, R., Schweizerhof, K., & Doll, S. (2000). Extension of the 'solid-shell' concept for application to large elastic and large elastoplastic deformations. International Journal for Numerical Methods in Engineering, 49(9), 1121-1141.

Herrmann, L. R. (1967). Finite-element bending analysis for plates. Journal of the Engineering Mechanics Division, 93(5), 13-26.

Hossain, S., Sinha, P., & Sheikh, A. (2004). A finite element formulation for the analysis of laminated composite shells. Computers & Structures, 82(20), 1623-1638.

Hrabok, M., & Hrudey, T. (1984). A review and catalogue of plate bending finite elements. Computers & Structures, 19(3), 479-495.

Hsiao, K. M., & Hung, H. C. (1989). Large-deflection analysis of shell structure by using corotational total lagrangian formulation. Computer Methods in Applied Mechanics and Engineering, 73(2), 209-225.

Hsiao, K. M. (1987). Nonlinear analysis of general shell structures by flat triangular shell element. Computers & Structures, 25(5), 665-675.

Hughes, T., Masud, A., & Harari, I. (1995a). Numerical assessment of some membrane elements with drilling degrees of freedom. Computers & Structures, 55(2), 297-314.

Hughes, T. J., & Brezzi, F. (1989). On drilling degrees of freedom. Computer methods in applied mechanics and engineering, 72(1), 105-121.

Hughes, T. J., Cohen, M., & Haroun, M. (1978). Reduced and selective integration techniques in the finite element analysis of plates. Nuclear Engineering and Design, 46(1), 203-222.

Hughes, T. J., Masud, A., & Harari, I. (1995b). Dynamic analysis and drilling degrees of freedom. International Journal for Numerical Methods in Engineering, 38(19), 3193-3210.

Hughes, T. J., & Tezduyar, T. (1981). Finite elements based upon Mindlin plate theory with particular reference to the four-node bilinear isoparametric element. Journal of applied mechanics, 48(3), 587-596.

Ibrahimbegovic, A. (1997). On the choice of finite rotation parameters. Computer Methods in Applied Mechanics and Engineering, 149(1-4), 49-71.

Ibrahimbegović, A. (1993). Quadrilateral finite elements for analysis of thick and thin plates. Computer Methods in Applied Mechanics and Engineering, 110(3-4), 195-209.

Ibrahimbegović, A. (1994). Stress resultant geometrically nonlinear shell theory with drilling rotations: Part I. A consistent formulation. Computer Methods in Applied Mechanics and Engineering, 118(3-4), 265-284.

Ibrahimbegović, A., & Frey, F. (1994a). Stress resultant geometrically non-linear shell theory with drilling rotations: Part III: Linearized kinematics. International Journal for Numerical Methods in Engineering, 37(21), 3659-3683.

Ibrahimbegović, A., & Frey, F. (1994b). Stress resultant geometrically nonlinear shell theory with drilling rotations: Part II. Computational aspects. Computer Methods in Applied Mechanics and Engineering, 118(3-4), 285-308.

Ibrahimbegović, A., Frey, F., & Kožar, I. (1995). Computational aspects of vector-like parametrization of three-dimensional finite rotations. International Journal for Numerical Methods in Engineering, 38(21), 3653-3673.

Ibrahimbegovic, A., Taylor, R. L., & Wilson, E. L. (1990). A robust quadrilateral membrane finite element with drilling degrees of freedom. International Journal for Numerical Methods in Engineering, 30(3), 445-457.

Ilyushin, A. A. (1956). Plasticité: Editions Eyrolles

Irons, B. M, & Zienkiewicz, O. C. (1969). The Isoparametric Finite Element System: A New Concept in Finite Element Analysis: Royal Aeronautical Society.

Irons, B. M. (1971). Numerical integration applied to finite element methods: Department of Civil Engineering, University College of Swansea.

Irons, B. M., & Razzaque, A. (1972). Experience with the patch test for convergence of finite elements. The mathematical foundations of the finite element method with applications to partial differential equations, 557-587.

Izzuddin, B. A. (2005). An enhanced co-rotational approach for large displacement analysis of plates. International Journal for Numerical Methods in Engineering, 64(10), 1350-1374.

Izzuddin, B. A., & Liang, Y. (2016). Bisector and zero-macrospin co-rotational systems for shell elements. International Journal for Numerical Methods in Engineering, 105(4), 286-320.

Jeon, H. M., Lee, Y., Lee, P. S., & Bathe, K. J. (2015). The MITC3+ shell element in geometric nonlinear analysis. Computers & Structures, 146, 91-104.

Jiang, L., Chernuka, M. W., & Pegg, N. G. (1994). A co-rotational, updated Lagrangian formulation for geometrically nonlinear finite element analysis of shell structures. Finite Elements in Analysis and Design, 18(1-3), 129-140.

Kansara, K. (2004). Development of Membrane, Plate and Flat Shell Elements in Java: Virginia Tech.

Katili, I. (1993a). A new discrete Kirchhoff-Mindlin element based on Mindlin-Reissner plate theory and assumed shear strain fields: part I: An extended DKT element for thick-plate bending analysis. International Journal for Numerical Methods in Engineering, 36(11), 1859-1883.

Katili, I. (1993b). A new discrete Kirchhoff-Mindlin element based on Mindlin-Reissner plate theory and assumed shear strain fields: part II: An extended DKQ element for thick-plate bending analysis. International Journal for Numerical Methods in Engineering, 36(11), 1885-1908.

Kebari, H., & Cassell, A. (1992). A stabilized 9-node non-linear shell element. International Journal for Numerical Methods in Engineering, 35(1), 37-61.

Khosravi, P., Ganesan, R., & Sedaghati, R. (2007). Corotational non-linear analysis of thin plates and shells using a new shell element. International Journal for Numerical Methods in Engineering, 69(4), 859-885.

Khosravi, P., Ganesan, R., & Sedaghati, R. (2008). An efficient facet shell element for corotational nonlinear analysis of thin and moderately thick laminated composite structures. Computers & Structures, 86(9), 850-858.

Kim, D. N., & Bathe, K. J. (2009). A triangular six-node shell element. Computers & Structures, 87(23), 1451-1460.

Kim, K. D., Han, S. C., & Suthasupradit, S. (2007). Geometrically non-linear analysis of laminated composite structures using a 4-node co-rotational shell element with enhanced strains. International Journal of Non-Linear Mechanics, 42(6), 864-881.

Kim, K., Liu, G., & Han, S. (2005). A resultant 8-node solid-shell element for geometrically nonlinear analysis. Computational Mechanics, 35(5), 315-331.

Kim, K., & Lomboy, G. (2006). A co-rotational quasi-conforming 4-node resultant shell element for large deformation elasto-plastic analysis. Computer Methods in Applied Mechanics and Engineering, 195(44), 6502-6522.

Kim, K., Lomboy, G., & Han, S. (2003). A co-rotational 8-node assumed strain shell element for postbuckling analysis of laminated composite plates and shells. Computational Mechanics, 30(4), 330-342.

Knight, N. (1997). Raasch challenge for shell elements. AIAA journal, 35(2), 375-381.

Ko, Y., Lee, P. S., & Bathe, K. J. (2016). The MITC4+ shell element and its performance. Computers & Structures, 169, 57-68.

Ko, Y., Lee, P. S., & Bathe, K. J. (2017). The MITC4+ shell element in geometric nonlinear analysis. Computers & Structures, 185, 1-14.

Kolahi, A., & Crisfield, M. (2001). A large-strain elasto-plastic shell formulation using the Morley triangle. International Journal for Numerical Methods in Engineering, 52(8), 829-849.

Krabbenhøft, K. (2002). Basic computational plasticity. Lecture Notes.

Krakeland, B. (1978). Nonlinear analysis of shells using degenerate isoparametric elements. Finite Elements in Nonlinear Mechanics, 1, 265-284.

Chen, K. K. (1979). A triangular plate finite element for large-displacement elastic-plastic analysis of automobile structural components. Computers & Structures, 10(1), 203-215.

Lee, P. S., & Bathe, K. J. (2004). Development of MITC isotropic triangular shell finite elements. Computers & Structures, 82(11), 945-962.

Lee, Y., Jeon, H. M., Lee, P. S., & Bathe, K. J. (2015). The modal behavior of the MITC3+ triangular shell element. Computers & Structures, 153, 148-164.

Lee, Y., Lee, P. S., & Bathe, K. J. (2014). The MITC3+ shell element and its performance. Computers & Structures, 138, 12-23.

Levy, R., & Gal, E. (2001). Geometrically nonlinear three-noded flat triangular shell elements. Computers & Structures, 79(26), 2349-2355.

Levy, R., & Gal, E. (2003). Triangular shell element for large rotations analysis. AIAA journal, 41(12), 2505-2508.

Levy, R., & Gal, E. (2006). The geometric stiffness of thick shell triangular finite elements for large rotations. International Journal for Numerical Methods in Engineering, 65(9), 1378-1402.

Levy, R., & Spillers, W. (2003). Analysis of Geometrically Nonlinear Structures. 2nd edition. Dordtrecht: Kluwer Academic Publishers.

Levy, R., & Spillers, W. R. (2013). Analysis of geometrically nonlinear structures: Springer Science & Business Media.

Li, Z. X., Izzuddin, B., & Vu-Quoc, L. (2008). A 9-node co-rotational quadrilateral shell element. Computational mechanics, 42(6), 873-884.

Li, Z. X., Liu, Y., Izzuddin, B., & Vu-Quoc, L. (2011a). A stabilized co-rotational curved quadrilateral composite shell element. International Journal for Numerical Methods in Engineering, 86(8), 975-999.

Li, Z. X., & Vu-Quoc, L. (2007). An efficient co-rotational formulation for curved triangular shell element. International Journal for Numerical Methods in Engineering, 72(9), 1029-1062.

Li, Z. X., Zheng, T., Vu-Quoc, L., & Izzuddin, B. (2015). A 4-Node Co-Rotational Quadrilateral Composite Shell Element. International Journal of Structural Stability and Dynamics, 1550053.

Li, Z. X., Zhuo, X., Vu-Quoc, L., Izzuddin, B., & Wei, H. (2013). A four-node corotational quadrilateral elastoplastic shell element using vectorial rotational variables. International Journal for Numerical Methods in Engineering, 95(3), 181-211.

Li, Z. X., Liu, Y. F., Izzuddin, B. A., & Vu-Quoc, L. (2011b). A stabilized co-rotational curved quadrilateral composite shell element. International Journal for Numerical Methods in Engineering, 86(8), 975-999.

Li, Z. X., & Vu-Quoc, L. (2007). An efficient co-rotational formulation for curved triangular shell element. International Journal for Numerical Methods in Engineering, 72(9), 1029-1062.

Liang, Y., & Izzuddin, B. A. (2015). Nonlinear analysis of laminated shells with alternating stiff/soft lay-up. Composite Structures, 133, 1220-1236.

Liang, Y., & Izzuddin, B. A. (2016). Large displacement analysis of sandwich plates and shells with symmetric/asymmetric lamination. Computers & Structures, 166, 11-32.

Macneal, R. H. (1987a). A theorem regarding the locking of tapered four-noded membrane elements. International Journal for Numerical Methods in Engineering, 24(9), 1793-1799.

MacNeal, R. H. (1987b). Zen and the art of finite element design. Finite Elements in Analysis and Design, 3(2), 85-91.

Macneal, R. H., & Harder, R. L. (1988). A refined four-noded membrane element with rotational degrees of freedom. Computers & Structures, 28(1), 75-84.

Madeo, A., Casciaro, R., Zagari, G., Zinno, R., & Zucco, G. (2014). A mixed isostatic 16 dof quadrilateral membrane element with drilling rotations, based on Airy stresses. Finite Elements in Analysis and Design, 89, 52-66.

Malkus, D. S., & Hughes, T. J. (1978). Mixed finite element methods: reduced and selective integration techniques: a unification of concepts. Computer Methods in Applied Mechanics and Engineering, 15(1), 63-81.

Marques, J. (1984). Stress computation in elastoplasticity. Engineering computations, 1(1), 42-51.

Masud, A., Tham, C. L., & Liu, W. K. (2000). A stabilized 3-D co-rotational formulation for geometrically nonlinear analysis of multi-layered composite shells. Computational mechanics, 26(1), 1-12.

Meek, J. L., & Tan, H. S. (1983). Large deflection and post-buckling analysis of two and three dimensional elastic spatial frames.

Melosh, R. J. (1961). A stiffness matrix for the analysis of thin plates in bending. Journal of the Aerospace Sciences, 28(1), 34-42.

Miehe, C. (1998). A theoretical and computational model for isotropic elastoplastic stress analysis in shells at large strains. Computer Methods in Applied Mechanics and Engineering, 155(3-4), 193-233.

Militello, C., & Felippa, C. A. (1991). The first ANDES elements: 9-dof plate bending triangles. Computer Methods in Applied Mechanics and Engineering, 93(2), 217-246.

Mindlin, R. (1951). Influence of rotary inertia and shear on flexural motions of isotropic elastic plates. Journal of Applied Mechanics, Transaction of American Society of Mechanical Engineers, 18(1), 31-38.

Mises, R. v. (1913). Mechanik der festen Körper im plastisch-deformablen Zustand. Nachrichten von der Gesellschaft der Wissenschaften zu Göttingen, Mathematisch-Physikalische Klasse, 1913(4), 582-592.

Mohr, O. (1900). Welche Umstände bedingen die Elastizitätsgrenze und den Bruch eines Materials. Zeitschrift des Vereins Deutscher Ingenieure, 46(1524-1530), 1572-1577.

Montag, U., Krätzig, W. B., & Soric, J. (1999). Increasing solution stability for finite-element modeling of elasto-plastic shell response. Advances in Engineering Software, 30(9), 607-619.

Morley, L. (1971). The constant-moment plate-bending element. The Journal of Strain Analysis for Engineering Design, 6(1), 20-24.

Mostafa, M. (2016). An improved solid-shell element based on ANS and EAS concepts. International Journal for Numerical Methods in Engineering, 108(11), 1362-1380.

Mostafa, M., Sivaselvan, M., & Felippa, C. (2013). A solid-shell corotational element based on ANDES, ANS and EAS for geometrically nonlinear structural analysis. International Journal for Numerical Methods in Engineering, 95(2), 145-180.

NIDA. (2015). User's Manual, Nonlinear Integrated Design and Analysis: NIDA 9.0 HTML Online Documentation, http://www.nidacse.com.

Norachan, P., Suthasupradit, S., & Kim, K. D. (2012). A co-rotational 8-node degenerated thin-walled element with assumed natural strain and enhanced assumed strain. Finite Elements in Analysis and Design, 50, 70-85.

Nour-Omid, B., & Rankin, C. (1991). Finite rotation analysis and consistent linearization using projectors. Computer Methods in Applied Mechanics and Engineering, 93(3), 353-384.

Pacoste, C. (1998). Co-rotational flat facet triangular elements for shell instability analyses. Computer Methods in Applied Mechanics and Engineering, 156(1), 75-110.

Pajot, J. M., & Maute, K. (2006). Analytical sensitivity analysis of geometrically nonlinear structures based on the co-rotational finite element method. Finite Elements in Analysis and Design, 42(10), 900-913.

Parisch, H. (1981). Large displacements of shells including material nonlinearities. Computer Methods in Applied Mechanics and Engineering, 27(2), 183-214.

Parisch, H. (1995). A continuum-based shell theory for non-linear applications. International Journal for Numerical Methods in Engineering, 38(11), 1855-1883.

Pawsey, S. F., & Clough, R. W. (1971). Improved numerical integration of thick shell finite elements. International Journal for Numerical Methods in Engineering, 3(4), 575-586.

Peng, X., & Crisfield, M. (1992). A consistent co-rotational formulation for shells using the constant stress/constant moment triangle. International Journal for Numerical Methods in Engineering, 35(9), 1829-1847.

Peric, D., & Owen, D. (1991). The Morley thin shell finite element for large deformation problems: simplicity versus sophistication. Paper presented at the Proceedings of the International Conference on Nonlinear Engineering Computations.

Providas, E., & Kattis, M. (1999). A simple finite element model for the geometrically nonlinear analysis of thin shells. Computational Mechanics, 24(2), 127-137.

Pugh, E., Hinton, E., & Zienkiewicz, O. (1978). A study of quadrilateral plate bending elements with 'reduced'integration. International Journal for Numerical Methods in Engineering, 12(7), 1059-1079.

Ramm, E. (1977). A plate/shell element for large deflections and rotations. Formulations and computational algorithms in finite element analysis, 264-293.

Rankin, C. C., & Brogan, F. (1986). An element independent corotational procedure for the treatment of large rotations. Journal of pressure vessel technology, 108(2), 165-174.

Rankin, C. C., & Nour-Omid, B. (1988). The use of projectors to improve finite element performance. Computers & Structures, 30(1), 257-267.

Reissner, E. (1965). A note on variational principles in elasticity. International Journal of Solids and Structures, 1(1), 93-95.

Robinson, M. (1971). A comparison of yield surfaces for thin shells. International Journal of Mechanical Sciences, 13(4), 345-354.

Roehl, D., & Ramm, E. (1996). Large elasto-plastic finite element analysis of solids and shells with the enhanced assumed strain concept. International Journal of Solids and Structures, 33(20-22), 3215-3237.

Sansour, C., & Kollmann, F. (2000). Families of 4-node and 9-node finite elements for a finite deformation shell theory. An assesment of hybrid stress, hybrid strain and enhanced strain elements. Computational Mechanics, 24(6), 435-447.

Schieck, B., Smoleński, W., & Stumpf, H. (1999). A shell finite element for large strain elastoplasticity with anisotropies: Part II: Constitutive equations and numerical applications. International Journal of Solids and Structures, 36(35), 5425-5451.

Schwarze, M., & Reese, S. (2009). A reduced integration solid-shell finite element based on the EAS and the ANS concept: Geometrically linear problems. International Journal for Numerical Methods in Engineering, 80(10), 1322-1355.

Sessa, S., Serpieri, R., & Rosati, L. (2017). A continuum theory of through-the-thickness jacketed shells for the elasto-plastic analysis of confined composite structures: Theory and numerical assessment. Composites Part B: Engineering, 113, 225-242.

Shi, G., & Voyiadjis, G. Z. (1992). A simple non-layered finite element for the elasto-plastic analysis of shear flexible plates. International Journal for Numerical Methods in Engineering, 33(1), 85-99.

Simo, J. C., & Armero, F. (1992). Geometrically non-linear enhanced strain mixed methods and the method of incompatible modes. International Journal for Numerical Methods in Engineering, 33(7), 1413-1449.

Simo, J. C. (1993). On a stress resultant geometrically exact shell model: part VII: Shell intersections with 5, 6-dof finite element formulations. Computer Methods in Applied Mechanics and Engineering, 108(3-4), 319-339.

Simo, J. C., Armero, F., & Taylor, R. (1993). Improved versions of assumed enhanced strain tri-linear elements for 3D finite deformation problems. Computer Methods in Applied Mechanics and Engineering, 110(3-4), 359-386.

Simo, J. C., Fox, D., & Hughes, T. (1992a). Formulations of finite elasticity with independent rotations. Computer Methods in Applied Mechanics and Engineering, 95(2), 277-288.

Simo, J. C., Fox, D., & Rifai, M. (1989). On a stress resultant geometrically exact shell model. Part II: The linear theory; computational aspects. Computer Methods in Applied Mechanics and Engineering, 73(1), 53-92.

Simo, J. C., Rifai, M., & Fox, D. (1990a). On a stress resultant geometrically exact shell model: Part IV: Variable thickness shells with through-the-thickness stretching. Computer Methods in Applied Mechanics and Engineering, 81(1), 91-126.

Simo, J. C., Rifai, M., & Fox, D. (1992b). On a stress resultant geometrically exact shell model: Part VI: Conserving algorithms for non-linear dynamics. International Journal for Numerical Methods in Engineering, 34(1), 117-164.

Simo, J. C., & Fox, D. D. (1989). On a stress resultant geometrically exact shell model. Part I: Formulation and optimal parametrization. Computer Methods in Applied Mechanics and Engineering, 72(3), 267-304.

Simo, J. C., Fox, D. D., & Rifai, M. S. (1990b). On a stress resultant geometrically exact shell model: Part III: Computational aspects of the nonlinear theory. Computer Methods in Applied Mechanics and Engineering, 79(1), 21-70.

Simo, J. C., & Kennedy, J. G. (1992). On a stress resultant geometrically exact shell model: Part V. Nonlinear plasticity: formulation and integration algorithms. Computer Methods in Applied Mechanics and Engineering, 96(2), 133-171.

Simo, J. C., & Rifai, M. (1990). A class of mixed assumed strain methods and the method of incompatible modes. International Journal for Numerical Methods in Engineering, 29(8), 1595-1638.

Skallerud, B., & Haugen, B. (1999). Collapse of thin shell structures: stress resultant plasticity modelling within a co-rotated ANDES finite element formulation. International Journal for Numerical Methods in Engineering, 46(12), 1961-1986.

Sorić, J., Montag, U., & Krätzig, W. (1997). An efficient formulation of integration algorithms for elastoplastic shell analysis based on layered finite element approach. Computer Methods in Applied Mechanics and Engineering, 148(3-4), 315-328.

Surana, K. S. (1983). Geometrically nonlinear formulation for the curved shell elements. International Journal for Numerical Methods in Engineering, 19(4), 581-615.

Sze, K., & Yao, L. (2000). A hybrid stress ANS solid-shell element and its generalization for smart structure modelling: Part I: solid-shell element formulation. International Journal for Numerical Methods in Engineering, 48(4), 545-564.

Sze, K., & Zhu, D. (1998). A quadratic assumed natural strain triangular element for plate bending analysis. International Journal for Numerical Methods in Biomedical Engineering, 14(11), 1013-1025.

Sze, K., Zhu, D., & CHEN, D. P. (1997). Quadratic triangular C0 plate bending element. International Journal for Numerical Methods in Engineering, 40(5), 937-951.

Tang, Y. Q., Zhou, Z. H., & Chan, S. L. (2015). Nonlinear beam-column element under consistent deformation. International Journal of Structural Stability and Dynamics, 15(05), 1450068.

Tang, Y. Q., Zhou, Z. H., & Chan, S. L. (2016). Geometrically nonlinear analysis of shells by quadrilateral flat shell element with drill, shear and warping. International Journal for Numerical Methods in Engineering, 108(10), 1248-1272.

Taylor, R. L., & Simo, J. C. (1985). Bending and membrane elements for analysis of thick and thin shells. Paper presented at the Proc. of NUMETA Conference.

Taylor, R. L. (1987). Finite element analysis of linear shell problems. Paper presented at the Whiteman, JR (ed.), Proceedings of the Mathematics in Finite Elements and Applications.

Tessler, A., & Hughes, T. J. (1983). An improved treatment of transverse shear in the Mindlin-type four-node quadrilateral element. Computer Methods in Applied Mechanics and Engineering, 39(3), 311-335.

Tessler, A., & Hughes, T. J. (1985). A three-node Mindlin plate element with improved transverse shear. Computer Methods in Applied Mechanics and Engineering, 50(1), 71-101.

Timoshenko, S. P., & Woinowsky-Krieger, S. (1959). Theory of plates and shells: McGraw-hill.

Tresca, H. (1869). Mémoires sur l'écoulement des corps solides: Imprimerie impériale.

Valente, R. F., Sousa, R. A. d., & Jorge, R. N. (2004). An enhanced strain 3D element for large deformation elastoplastic thin-shell applications. Computational Mechanics, 34(1), 38-52.

Van Keulen, F., Bout, A., & Ernst, L. J. (1993). Nonlinear thin shell analysis using a curved triangular element. Computer Methods in Applied Mechanics and Engineering, 103(1), 315-343.

Wempner, G. (1969). Finite elements, finite rotations and small strains of flexible shells. International Journal of Solids and Structures, 5(2), 117-153.

Wilson, E. L., Taylor, R., Doherty, W., & Ghaboussi, J. (1973). Incompatible displacement models. Numerical and computer methods in structural mechanics, 43.

Wilson, E. L. (1996). Three-dimensional static and dynamic analysis of structures. Computers and Structures, Inc., Berkeley, CA.

Wriggers, P., Eberlein, R., & Reese, S. (1996). A comparison of three-dimensional continuum and shell elements for finite plasticity. International Journal of Solids and Structures, 33(20-22), 3309-3326.

Yang, H. T., Saigal, S., Masud, A., & Kapania, R. (2000). A survey of recent shell finite elements. International Journal for Numerical Methods in Engineering, 47(1-3), 101-127.

Zallo, A., & Gaudenzi, P. (2003). Finite element models for laminated shells with actuation capability. Computers & Structures, 81(8), 1059-1069.

Zhou, Y., Li, Y. Q., Shen, Z. Y., & Zhang, Y. Y. (2016). Corotational Formulation for Geometric Nonlinear Analysis of Shell Structures by ANDES Elements. International Journal of Structural Stability and Dynamics, 16(03), 1450103.

Zienkiewicz, O. C., Taylor, R., & Too, J. (1971). Reduced integration technique in general analysis of plates and shells. International Journal for Numerical Methods in Engineering, 3(2), 275-290.

Zienkiewicz, O. C. (1971). The finite element method in engineering science: McGraw-Hill.

Zienkiewicz, O. C., Parekh, C. J. & King, I. P. (1967). Arch Dams Analysed by a Linear Finite Element Shell Solution Program: School of Engineering, University College of Swansea.

Zienkiewicz, O. C., & Taylor, R. L. (2000). The finite element method: solid mechanics (Vol. 2): Butterworth-heinemann.

Zienkiewicz, O. C., Taylor, R. L., & Taylor, R. L. (1977). The finite element method (Vol. 3): McGraw-hill London.

Zienkiewicz, O. C., Taylor, R. L., & Zhu, J. Z. (2013). The finite element method: its basis and fundamentals (Seventh Edition): Elsevier.

Zouari, W., Hammadi, F., & Ayad, R. (2016). Quadrilateral membrane finite elements with rotational DOFs for the analysis of geometrically linear and nonlinear plane problems. Computers & Structures, 173, 139-149.